AN INVESTIGATION OF LINKED PHYSICAL AND BIOGEOCHEMICAL PROCESSES IN HETEROGENEOUS SOILS IN THE VADOSE ZONE

A Dissertation

by

DAVID JOSEPH HANSEN

Submitted to the Office of Graduate Studies of
Texas A&M University
in partial fulfillment of the requirements for the degree of

DOCTOR OF PHILOSOPHY

August 2011

Major Subject: Geology

AN INVESTIGATION OF LINKED PHYSICAL AND BIOGEOCHEMICAL PROCESSES IN HETEROGENEOUS SOILS IN THE VADOSE ZONE

A Dissertation

by

DAVID JOSEPH HANSEN

Submitted to the Office of Graduate Studies of
Texas A&M University
in partial fulfillment of the requirements for the degree of

DOCTOR OF PHILOSOPHY

Approved by:

Co-Chairs of Committee,	Jennifer T. McGuire
	Binayak P. Mohanty
Committee Members,	Robin L. Autenrieth
	Anthony M. Filippi
	Ethan L. Grossman
Head of Department,	Andreas K Kronenberg

August 2011

Major Subject: Geology

ABSTRACT

An Investigation of Linked Physical and Biogeochemical Processes in Heterogeneous Soils in the Vadose Zone. (August 2011)

David Joseph Hansen, B.S., Brigham Young University - Idaho

Co-Chairs of Advisory Committee: Dr. Jennifer T. McGuire
Dr. Binayak P. Mohanty

Chemical dynamics in the vadose zone are poorly understood due to the transient nature of chemical and hydrologic conditions, but are nonetheless critical to understanding contaminant fate and transport. This dissertation explored the effects of soil structure (i.e. layers, lenses) on linked geochemical, hydrological, and microbiological processes under changing hydrologic conditions (e.g. rainfall, introduction of groundwater, and fluctuating water table heights). A homogenized medium-grained sand, homogenized organic-rich loam and a sand-over-loam layered column were constructed for the first series of experiments. The second series of experiments employed two soil columns with lenses that were packed identically with sterilized and untreated sediments. Each column consisted of two lenses of organic-rich loam in a medium-grained sand matrix. Lenses were located at different vertical depths and were horizontally offset. *In-situ* collocated probes collected soil hydrologic and chemical data.

In the layered column, enhanced biogeochemical cycling was observed over the texturally homogeneous soil columns. Enumerations of Fe(III) and SO_4^{2-} reducing microorganisms also show 1-2 orders of magnitude greater community numbers in the layered column. The greatest concentrations of aqueous FeS clusters (FeS_{aq}) were observed in close proximity to the soil interface. To our knowledge, this was the first documentation of FeS_{aq} in partially saturated sediments. Mineral and soil aggregate composite layers were also most abundant near the soil layer interface; the presence of which, likely contributed to an order of magnitude decrease of hydraulic conductivity.

In the live lens column, Fe-oxide bands formed at the fringes of the lenses that retarded water flow rates by an order of magnitude compared to the sterilized column. Microbial activity also produced insoluble gases and that led to the creation of a separate gas phase that reduced hydraulic conductivity. This limited the interaction between groundwater with soil-pore waters that led to the formation of geochemically distinct water masses in relatively close proximity to one another. No such changes were observed in the sterilized column.

When compared to homogenous columns, the presence of soil heterogeneities altered biogeochemical and hydrologic processes considerably which highlights the need to consider soil heterogeneity in contaminant fate and transport models. These findings suggest that quantifying coupled hydrologic-biogeochemical processes occurring at small scale soil interfaces is critical to accurately describing and predicting chemical changes at the larger system scale.

DEDICATION

To my lovely wife who deserves this degree as much I do. You've been my biggest fan and loyal beyond all expectations. You have my complete adoration. Thank you for everything.

ACKNOWLEDGEMENTS

I would like to thank my committee co-chairs for their patience, the many manuscripts they edited, and the get-togethers at their homes. They worked tirelessly to secure funding for my project and coached me along the way. My family and I are indebted to them for their generosity in supporting me.

I am grateful for Dr. McGuire who granted me a spot in her research group even though I knew she was not accepting any more students. She gave me the direction and the means to start and finish this degree. I always felt she was "in my corner" and wanted me to succeed no matter what it took. She believed in me, even when I doubted myself.

My thanks go to Dr. Mohanty for his support as well. He helped me keep a level-headed attitude about problems in the lab and supported my technology needs in the lab. I also felt his support and desire for my success.

I acknowledge my committee members: Dr. Autenrieth, Dr. Filippi, and Dr Grossman for their time and instruction during my time at Texas A&M. I express gratitude to Erik Smith (and his tools) who taught me how to build it better and stronger. I also thank David Zuberer and Anette Fincher for their instruction on and help with microbial enumerations. Their experience was invaluable. I would also like to thank Dr. Kronenberg for his assistance in getting through the last year of my Ph.D. Also Max Kohne for getting me started on the right foot. I also acknowledge those professors at BYU-Idaho that encouraged my academic growth and gave me opportunities for

undergraduate research. So many teachers have been instrumental in my life. I owe much more than I could ever pay back to everyone in academia; a group which is grossly underappreciated, but is so critical.

I appreciate other students that helped me along the way. Notably those were my officemates: Susan Baez-Cazull and Tara Kneeshaw. They taught me how to work in the lab, gave me feedback, and even helped with my experiments. Thanks also to Bhavna Arora who was always patient when helping me run numerical simulations. Lastly, thanks to my undergraduate employee, Nakita Luckett, who stumbled alongside me as we tried new laboratory methods. These students were a key ingredient in my success. I realized the importance of collaboration from my relationship with them.

I also want to extend my gratitude to the National Science Foundation and the Texas Water Resources Institute for research funding. I also thank ConocoPhillips, the East Texas Communities Foundation, Noble Energy, the Society of Independent Professional Earth Scientists, and the Association of Former Students at Texas A&M for their generous scholarship donations. Thanks also go to the staff of the Geology and Geophysics and Biological and Agricultural Engineering departments for their assistance. Thanks to the Nuclear Science Center here at Texas A&M for their donation of radiation services.

Last, but certainly not least, I express the deep appreciation to my family. My wife was a “dissertation widow,” but didn’t complain. Thanks to my children, who didn’t cry too much when I wasn’t there to tuck them into bed. To my parents, thank you for the weekly phone calls and encouragement. To my dad, you encouraged me not

to pursue a career in science and it goes to show that children never do what their parents tell them to. Thanks for your advice and encouragement. It meant more to me than anyone else's words. Thanks to my siblings who offered encouragement to their spoiled little brother. Thanks to Grandpa Hansen who passed away during my studies, but passed on his power tools that helped me build my research equipment.

TABLE OF CONTENTS

CHAPTER Page

LIST OF FIGURES

Page

Page

Page

Page

LIST OF TABLES

Page

CHAPTER I

INTRODUCTION

A fundamental issue in understanding the biogeochemical transformations that occur in the vadose zone is quantifying the mechanisms controlling linked hydrologic, geochemical, and microbiological processes in variably saturated heterogeneous environments. One property unique to the vadose zone, is that it is confined by two vastly different hydraulic conditions on its lower (i.e. groundwater table, capillary fringe) and upper (i.e. precipitation, evaporation) boundaries. Through either of these boundaries, waters that can affect redox cycling occurring within its sediments, may be introduced. Understanding redox potential is difficult because it is sensitive to changes in environmental conditions which are highly dynamic in the vadose zone

Redox potential in subsurface systems is dependent on several factors that include: microbial activity, geochemisty, and hydrologic conditions. The redox potential of a system is critical to the prediction of chemical fate and transport in subsurface systems because redox state affects the form, mobility, and toxicity of many chemical constituents. Thus, the characterization of redox distribution in the vadose zone is vital to understanding chemical fate and transport.

Of particular importance are the metabolic activities of microorganisms, which first consume oxygen and then a succession of alternate terminal electron acceptors to support their growth using a variety of carbon sources (Lovley and Goodwin 1988;

This dissertation follows the style of Vadose Zone Journal.

Lovley 1991; Stumm and Morgan 1996; Chapelle 2001). The sequence of pertinent terminal electron accepting processes (TEAPs) in order of decreasing redox potential and energy yield is generally aerobic respiration, denitrification, iron reduction, sulfate reduction, and methanogenesis. Within the vadose zone, reducing conditions can occur and include methanogenesis (Oliver et al. 2003; Smith et al. 2003; Bekins et al. 2005; Salminen et al. 2006) despite a sometimes close proximity to oxygen at the soil/atmosphere boundary.

Redox conditions depend on geochemistry (availability of terminal electron acceptors) and microbial activity, but are also controlled by hydrologic conditions. This linkage was demonstrated by Bekins et al. (2005) who observed an increase in methanogenic activity in areas that of more than 20% water content. For example, a rising groundwater table may introduce waters with higher chemical concentrations and replace partially-filled pore spaces with anaerobic waters where reducing redox conditions will develop. Conversely, rainwater, which may simultaneously enter the vadose zone from the top boundary may dilute pore-water chemical concentrations and introduce dissolved oxygen to pore waters thus promoting oxidizing redox conditions. Thus the vadose zone serves as a highly dynamic area where vastly different geochemical water masses are juxtaposed against one another.

An additional control on linked geochemical, microbial, and hydrologic process that is poorly understood is the effects of soil heterogeneity (layers, lenses, and macropores) in the vadose zone. These structures have the capability to influence water flow, microbial activity, and geochemistry. Consequently, the redox potential of a

system may be different than previously expected due to presence of soil structures. The soil textural interfaces, created between differing soil types in layers or lenses, have been shown to be populated by a greater number of microorganisms than in the soil matrix itself (Fredrickson et al., 1997a; Madigan et al., 1997a). Because soil type has been shown to be a control on the distribution of microorganisms, (Federle et al., 1986) the interface between two soils may create a sharp boundary between differing microbial populations and enhance overall microbial activity. Increased microbial biomass and corresponding activity between soil types could lead to biofilm formation and eventual bioclogging (Holden and Fierer, 2005, Bundt et al., 2001; Vinther et al., 1999) Soil structures also impact hydrologic flow rates and pathways within the vadose zone. For example layering of soils with different hydraulic conductivities may retard water flow, divert flowing to other areas of within the vadose zone, or increase residence time for both water and chemicals

The overall objective of this work was to quantify the effects of linked water flow, geochemical and microbiological processes in an unsaturated system using repacked soil columns. One aim of this work was to determine the effects of a soil structures (e. g. layers, lenses) on redox conditions, water flow, water chemistry, microbial activity, and transport processes. Another aim of this work was to determine how geochemical and microbial processes changed in response to changing hydrologic conditions such as: rainfall events, the introduction of groundwater of various chemical compositions, and fluctuations in water table height.

CHAPTER II

ENHANCED BIOGEOCHEMICAL CYCLING AND SUBSEQUENT REDUCTION OF HYDRAULIC CONDUCTIVITY ASSOCIATED WITH SOIL INTERFACES IN THE VADOSE ZONE

INTRODUCTION

The potential influence of the vadose zone on contaminant fate and transport is significant, but poorly understood due to the difficulty of characterizing linked, dynamic hydrologic and biogeochemical processes. In fact, many numerical models, focused on transport in the saturated zone, use rainwater chemistry as an upper boundary (Barry et al., 2002; Prommer et al., 2002). This assumption neglects chemical changes to the rainwater occurring in the vadose zone due to mineral-water interactions, sorption/desorption, or biogeochemical cycling. Maleki et al. (2002) demonstrated that subsurface water chemistry is determined more by processes and reactions occurring in the variably-saturated, vadose zone than in the saturated zone. They found that the average total dissolved solids values for rainwater changed from 30.2 mg L^{-1} in the vadose zone to 318 mg L^{-1} in the saturated zone. They also note the change from a SO_4^{2-}-Cl^--Ca^{2+}-NH_4^+ hydrochemical-type water to a HCO_3^--SO_4^{2-}-Ca^{2+}-Mg^{2+} type. Changes in reduction-oxidation (redox) state have also been identified within the vadose zone (Bekins et al., 2005; Oliver et al., 2003; Smith et al., 2003). The redox potential of a system is critical to the prediction of chemical fate and transport in subsurface systems because redox state affects the form, mobility, and toxicity of many chemical constituents. Despite its importance, it is poorly understood how linked hydrological,

microbiological, and geochemical processes affect redox state in the variably saturated subsurface.

Biogeochemical cycling of organic and inorganic contaminants is primarily controlled by changes in the redox potential of a system. Of particular importance in subsurface systems are the metabolic activities of microorganisms, which first consume oxygen and then a succession of alternate terminal electron acceptors to support their growth using a variety of carbon sources (Chapelle, 2001; Lovley, 1991; Lovley and Goodwin, 1988; Stumm and Morgan, 1996). In saturated systems, the sequence of terminal electron accepting processes in order of decreasing redox potential and energy yield is generally aerobic respiration, denitrification, iron reduction, sulfate reduction, and methanogenesis. Within the vadose zone, reducing conditions occur frequently and include methanogenesis (Bekins et al., 2005; Oliver et al., 2003; Salminen et al., 2006; Smith et al., 2003) despite unsaturated hydrologic conditions. However, the controls on the distribution of redox zones are not well known.

Within contaminant plumes, the most reduced conditions (e.g., methanogenesis) occur spatially near the contaminant source due to greater availability of electron donors, while less reducing conditions (e.g., nitrate reduction) dominate down gradient flow path. More reducing conditions are also observed at the interface between the saturated and unsaturated zones due to the accumulation of electron donor (such as hydrocarbons) in the capillary fringe. This results in both horizontal and vertical redox zonation (Chapelle et al., 1996; McGuire et al., 2000). In association with reducing conditions, are “secondary” redox reactions such as the re-oxidation of products derived from

terminal electron accepting processes (e.g. methane, ammonia, iron-sulfide minerals, and hydrogen sulfide gases) that often occur at system interfaces such as the boundaries of a contaminant plume. These reactions have been shown to be important in driving and maintaining biogeochemical cycling of nutrients and contaminants (Grossman et al., 2002; Hunter et al., 1998; Mayer et al., 2002). Although these secondary redox reactions have been primarily documented in saturated areas, this reoxidation likely occurs within the vadose zone but is not well documented in the literature. Thus, it is unclear how redox conditions are spatially distributed in unsaturated systems and how physical, biological, and geochemical processes control the development of aerobic/anaerobic zones.

Redox studies in soil systems can be especially difficult because of the dynamic nature of the vadose zone. Water content can change rapidly due to rainfall or evapotranspiration that may act to dilute or concentrate chemical species in water. Redox conditions may change from reducing environment to an oxidizing environment as rainwater transports electron acceptors such as dissolved oxygen deeper into the system. Additionally, chemically reactive, soil aggregates are frequently transported, formed, disbanded and transported again (Emerson and Greenland, 1990).

In addition to the dynamic nature of the vadose zone, complexity stems from structural heterogeneities in the subsurface including soil layers, lenses, fractures, and macropores (e.g. earthworm burrows, decayed root casts, etc.). In particular, soil layering has the potential to alter water flow and biogeochemical cycling significantly. These interfaces, created between soil layers, have been shown to be populated by a

greater number of microorganisms than in the soil matrix itself (Fredrickson et al., 1997a; Madigan et al., 1997a). Because soil type has been shown to be a control on the distribution of microorganisms, (Federle et al., 1986) the interface between two soils may create a sharp boundary between differing microbial populations and enhance overall microbial activity. Increased microbial biomass and corresponding activity between soil types could lead to biofilm formation and eventual bioclogging (Holden and Fierer, 2005, Bundt et al., 2001; Vinther et al., 1999)

Soil structures, most certainly, have an impact on hydrologic flow rates and pathways within the vadose zone. The layering of soils with different hydraulic conductivities may retard water flow and increase residence time for both water and chemicals. For example, if an underlying soil layer has a lower hydraulic conductivity, water flow may be impeded. However, the converse pattern may also have the same effect. Several studies have shown that an underlying layer with higher conductivity may create a capillary barrier that inhibits water flow under certain unsaturated conditions (Hillel, 2004; Iqbal, 2000; Walser et al., 1999). Thus, either soil layering scenario may lead to an increased residence time that may consequently lead to rapid consumption of dissolved oxygen and development of reducing conditions. The influence of water content on redox conditions was demonstrated by Bekins et al. (2005). They observed methanogenic degradation of crude oil in soils and noted that degradation rates in areas with greater than 20% water saturation were significantly greater than those with less water.

The overall objective of this study was to quantify the effects of linked water flow, geochemical and microbiological processes in an unsaturated system using repacked soil columns. Specifically, the evolution of aqueous geochemical species were evaluated in two texturally homogenous soil systems and a layered soil system to measure the effects of a soil interface on redox conditions, water flow, water chemistry, microbial activity, and transport processes.

MATERIALS AND METHODS

Three repacked soil columns, identical in size, were constructed for this study. The first column was packed with homogenized medium-sized sand while the second column was packed with homogenized loam. The third was packed in a layered configuration, wherein the bottom half of the column was packed with loam which was overlain by sand. Thus the homogenous sand and loam columns served as a control, to which results from layered column could be compared, in order to evaluate the biogeochemical and hydrologic effects of a soil layer.

Soil Physical Properties

Soils were collected near a closed and capped municipal landfill near the Canadian River in Norman, Oklahoma, USA. This landfill and surrounding area has been a research site for the U.S. Geologic Survey and other university research groups to study hydrologic and biogeochemical processes surrounding a leachate plume that has developed in the aquifer beneath the landfill (Báez-Cazull et al., 2007; Cozzarelli et al.,

2000; Kneeshaw et al., 2007). The first soil collected was an alluvial, medium-grained sand from the banks of the Canadian River and the second, an organic-rich loam from a wetland adjacent to the landfill. The loam soil was collected under saturated conditions from the wetland. Soils were air-dried, ground, and passed through a 0.8 mm mesh sieve. The particle size distribution of the soils were determined by hydrometer method (Gee and Bauder, 1986) and are shown in Table 2.1. Small aluminum rings (7.5 cm diameter and height) were packed with the loam from the wetland and the sand from the river bank in order to determine saturated hydraulic conductivity of each material (Klute and Dirksen, 1986). The results for saturated hydraulic conductivity are show in Table 2.2. These same packed soils in aluminum rings were used to determine the soil water retention curve (SWRC) in a ceramic plate tempe cell. The volume of effluent derived from the tempe cells were recorded after stepwise increases in pressure. The effluent was only recorded after sufficient time passed for the pressures to equilibrate. The pressure steps used in the analysis were: 0.0, 1.0, 2.0, 4.1, 5.1, 10.5, 11.2, 18.6, 30.1, 50.0, 100.0, 300.0, and 500.0 kPa. Pressure and water content were then plotted against one another to determine the shape of the SWRC. Inverse modeling of these data in HYDRUS-1D (Simunek et al., 2008) was then used to obtain the van Genuchten SWRC parameters (Table 2.2).

Soil Chemical Properties

Soil pH and electrical conductivity were determined in a 1:2 soil:water extract of the soil using deionized water. Samples were stirred and allowed to equilibrate for a

Table 2.1 - Soil textural (USDA classification), % organic carbon, bulk density, and porosity values of the sand and loam soils.

	Textural Properties (Percent Weight)						
Soil	0.5 – 0.2 mm (Medium Sand)	0.2 – 0.05 mm (Fine Sand)	0.05 – 0.002 mm (Silt)	<0.002 mm (Clay)	% Organic Carbon	Bulk Density ($Mg\ m^{-3}$)	% Porosity
Sand	33.6	62.9	2.2	1.3	0.02	1.5	43.4 %
Loam	46.5		39.5	12.5	1.5	1.1	58.5 %

Table 2.2 - Soil hydraulic parameters. θ_r and θ_s are the residual and saturated soil moisture content respectively, α is the inverse of the bubbling pressure, n is pore size distribution shape parameter, and K_s is the saturated hydraulic conductivity.

Soil	θ_r ($m^3\ m^{-3}$)	θ_s ($m^3\ m^{-3}$)	α ($1\ m^{-1}$)	n	K_s* ($m\ s^{-1}$)
Sand	0.027	0.321	3.18	1.60	1.06×10^{-4}
Loam	0.015	0.385	2.02	1.86	2.35×10^{-5}

minimum of 30 minutes after adding the water and then measured for pH and conductivity (Rhoades, 1982; Schofield and Taylor, 1955). Nitrate-nitrogen (NO_3^--N) was extracted from soils using a 1 N KCl solution. Nitrate was reduced to nitrite using a cadmium column followed by spectrophotometric measurement (Keeny and Nelson, 1982). Phosphorus, K, Ca, Mg, Na and S were extracted using the Mehlich III extractant and determined by inductively coupled plasma (ICP) atomic spectrometry (Mehlich, 1978; Mehlich, 1984). Iron and Mn were extracted using a diethylene triamine pentaacetic acid method and determined by ICP (Lindsay and Norvell, 1978). The results of these analyses are generally interpreted as plant-available concentrations and are listed in Table 2.3.

Physical Setup

Prior to packing soils in the experimental columns, soils were sieved which resulted in the large-sized (> 8 mm) organic matter (sticks, leaves, snail shells) being discarded. This organic matter was separated from the soils to ensure consistency of the soil-water properties. However, because the large organic matter was excluded from the packed soils, the bulk density of the packed soils and soils from the collection site were slightly different. Soils were packed into columns made of clear acrylic pipe (15 cm in diameter and 40 cm in height) and were packed with a piston compactor in 3 cm increments to achieve a constant bulk density.

At the bottom of the column, a nylon fabric mesh was glued to a densely perforated (one 0.19 cm diameter hole per 1.16 cm^2) polyvinyl chloride (PVC) plate that

Table 2.3 - Results of chemical analyses of the sand and loam soils. Concentrations are generally expressed in plant available values.

Soil	pH	Cond ($uS\ cm^{-1}$)	NO_3^--N ($mg\ L^{-1}$)	P ($mg\ L^{-1}$)	K ($mg\ L^{-1}$)	Ca ($mg\ L^{-1}$)	Mg ($mg\ L^{-1}$)	S ($mg\ L^{-1}$)	Na ($mg\ L^{-1}$)	Fe ($mg\ L^{-1}$)	Mn ($mg\ L^{-1}$)
Sand	8.5	106	4	4	19	1,688	56	40	154	2.83	1.28
Loam	7.9	1,030	2	5	86	24,833	802	694	374	88.35	19.27

was attached to the base of the column cylinder to prevent soil loss and allow for water flow. The column was drained by a funnel shaped cap that directed water into a single 1.9 cm outer diameter vinyl tube. Thus, the nylon fabric mesh at the bottom was open to the atmosphere via the vinyl tubing (Figure 2.1). Only glues/epoxys that did not leach chemicals (e.g. acetate, formaldehyde, etc) after soaking in deionized water for 48 hours were used in column construction.

The top of the column was open to the atmosphere which allowed water to be introduced through a rainfall simulator made of a PVC reservoir and 18 gauge needles. A digitally controlled peristaltic pump (Cole-Parmer, Vernon Hills, IL) delivered water to the rainfall simulator from a sealed nalgene carboy. Experiments were conducted in a lab with an ambient air temperature of 22º ± 2º C.

Feed Solution Chemistry

The chemistry of input solution was designed to emulate the chemistry of rainwater in the environment. The pH of Nanopure water (18.2 MΩ resistance) was lowered with ultra pure HCl to approximately 5 to mimic the drop in pH caused by reaction of CO_2 with H_2O to form carbonic acid. On occasion, rainwater was spiked with either 25 mg L^{-1} or 50 mg L^{-1} NO_3^- and SO_4^{2-} to simulate effects of pollution (see Figure 2.2). On all other occasions, the pH adjusted Nanopure was used for input water. A total of 10 L (approximately 3 pore volumes) of water was applied during each rainfall event to flush out any residual water from previous events.

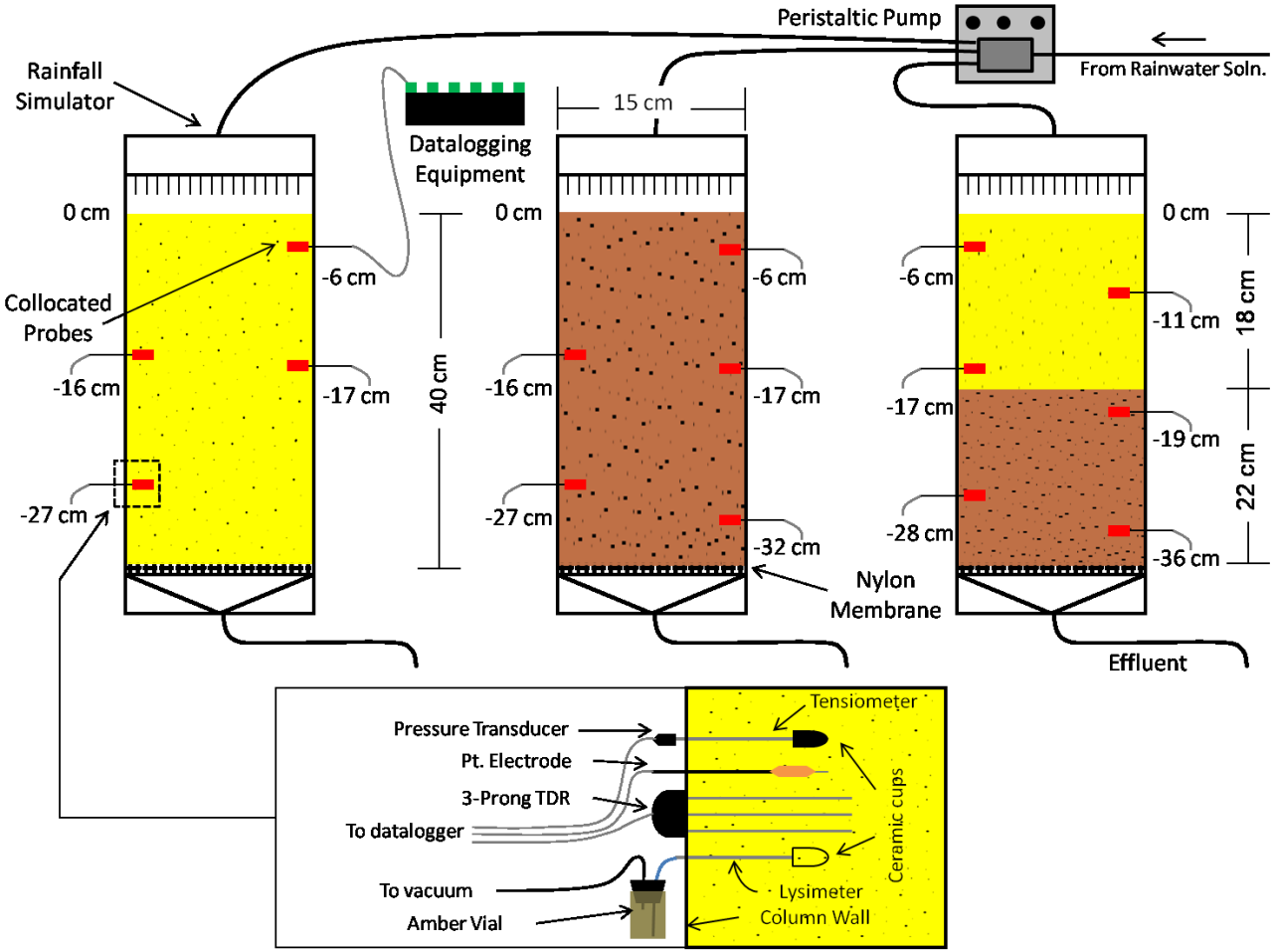

Figure 2.1 - Physical experimental setup. From left to right, the homogenous sand, homogenous loam, and layered columns and the location of sampling ports and probes.

Experimental Period

Before starting experiments, each column was wetted up from the bottom to prevent any air pockets from being trapped in the columns that would artificially alter water flow. Studies on the homogenous sand column were conducted prior to the experiments on the homogenous loam and layered column, which were conducted simultaneously.

In total, four rainfall events were applied to the homogeneous sand column. These rainfall events occurred on the days: 15, 16, 18, and 19 of September, 2007. The concentration of each rainwater solution was 25 mg L^{-1} NO_3^- and SO_4^{2-}. During each rainfall event, 20 L of rainwater solution was applied at the top of the column at a pumping rate of 105 cm^3 min^{-1} for approximately 3 hours.

For the homogenous loam and layered columns, the experimental period was divided into two major phases that took place over an eight-month timeframe. The first phase (Phase I) was characterized by rainfall events that occurred every one to two weeks for 1.5 months. Rainfall event durations were typically 12 hours. Between rainfall events, the columns were gravity drained. The second phase (Phase II) lasted for two months and was characterized by short intervals (4-5 days) between rainfall events with rainfall durations of up to 18 hours. A dry period of 4 months, wherein no rainfall events occurred, separated the two phases. Figure 2.2 shows a timescale of rainfall events, as well as flow rates, boundary conditions, and water chemistry for the loam and layered experiment.

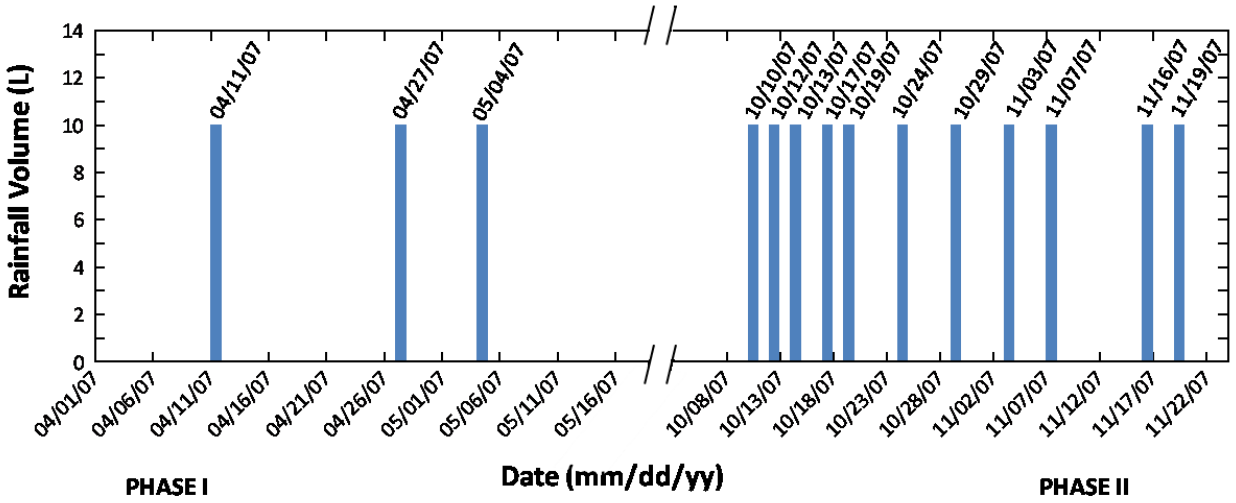

Date	Event - Time Duration	Aqueous Solution Chemistry	Sampling Schedule	Top Boundary
03/30/07 - 04/06/07	Wetting Up - 8 days	25 mg L^{-1} NO_3^- and SO_4^{2-}	On 8th day of saturation	Atmospheric
04/11/07	Rainfall - 12 hours Rain every other 10 min	50 mg L^{-1} NO_3^- and SO_4^{2-} 100 mg L^{-1} Br- - pH = 5.0	After 16 days	Flux Rate: 52 ml min^{-1} (73.6 cm min^{-1})
04/27/07	Rainfall - 12 hours continuously	25 mg L^{-1} NO_3^- and SO_4^{2-} 50 mg L^{-1} Cl^- - pH = 5.0	During rainfall	Flux Rate: 52 ml min^{-1} (73.6 cm min^{-1})
05/04/07	Rainfall - 12 hours continuously	100 mg L^{-1} NO_3^- and SO_4^{2-} - pH = 5.0.	Before rainfall, 8 days after previous rainfall	Flux Rate: 2.1 ml min^{-1} (2.97 cm min^{-1})
10/10/07 – 11/19/07	Rainfall - 6 – 18 Hours	NanopureWater – pH = 5.0	During rainfall	Flux Rate: 0.8 ml min^{-1} (1.13 cm min^{-1})

Figure 2.2 - Experimental time table and conditions.

Physical Measurements

Columns were equipped with collocated sets of measurement probes (tensiometers, and time domain reflectometry) installed at various depths. Three-pronged time domain reflectometry (TDR) probes (8 cm long, 1.1 cm spacing between rods) were used to measure soil water content. Tensiometers with 6 mm diameter ceramic cups (SDEC 220, SDEC France) were equipped with pressure transducers (Microswitch, Soil Measurement System, Tucson, AZ) for automated soil water pressure monitoring. Data from pressure transducers were monitored using equipment from Campbell Scientific, Inc. (Logan, UT), consisting of a CR10X data logger with an AM 16/32A multiplexer. TDR probe data were collected using a TDR100 with SDMX50 multiplexers and a CR10X.

Inverse Modeling

Inverse estimation of soil hydraulic parameters using water content and soil water pressure data with HYDRUS -1D model (Simunek et al., 2008) was performed on experimental data. The values for residual water content (θ_r), saturated water content (θ_s), and van Geunchten coefficients (α and n) were obtained from the inverse parameter estimation. Measured saturated hydraulic conductivity was used as an input parameter for inverse modeling of 27 April and 4 May 2007 data. For the other inverse modeling exercise (data from 12 October 2007), the θ_r value was held constant and the saturated hydraulic conductivity value was estimated in the layered column as the change in saturated hydraulic conductivity was not equal in the sand and the loam soil. Although

we measured an effective saturated hydraulic conductivity value for the entire column, this did not reveal the hydraulic conductivity changes in each soil, thus this parameter was estimated via inverse modeling.

The top boundary condition (with the exception of the 12th October 2007 layered column data) was pressure values from the uppermost tensiometer data (-6 cm depth). Thus the top 6 cm of the soil profile were truncated in the modeling. Questionable tensiometer data in the layered column on 12 October 2007 required the use of rainfall water flux rate data for the top boundary condition. The bottom boundary condition for the columns was a seepage face condition which is applied to laboratory soil columns when the bottom of the soil column is exposed to the atmosphere (gravity drainage of a finite soil column). "The condition assumes that the boundary flux will remain zero as long as the pressure head is negative. However, when the lower end of the soil profile becomes saturated, a zero pressure head is imposed at the lower boundary and the outflow calculated accordingly" (Hydrus-1D User's Manual).

For the layered-column bottom boundary conditions, the threshold pressure for outflow was set to 10 cm while the pressure threshold in the loam column was left at 0 cm. The need to impose different pressure thresholds to match experimental observations, despite an identical physical setup, suggests that the presence of a soil layer impacts the bottom boundary conditions differently from the homogenous soil profile. This phenomenon will be discussed in further detail in the Results and Discussion section. Only inverse model runs with R^2 values of at least 0.95 were considered acceptable.

Geochemical Analyses

One challenge with water sampling in the vadose zone is that only very small sample volumes can be collected without altering flow paths and hydrologic conditions. This creates geochemical analysis limitations. To minimize disruptions of hydrologic conditions in the soil columns during sample collection, less than a total of 7 ml was collected at each sample location for all geochemical analyses. Lysimeters made from 6-mm diameter ceramic cups (SDEC 220, SDEC France), aluminum tubing, and amber catchment vials were used for *in situ* sampling and were controlled by two Campbell Scientific A6-REL12 relay drivers. Due to low sample volume requirements (Goettlein and Blasek, 1996), capillary electrophoresis (CE) was used for the determination of anions (SO_4^{2-}, NO_3^-), and NH_4^+ (Báez-Cazull et al., 2007). Each sample analysis consumed ~1 nL. Approximately 250 µL solution samples were collected to ensure sufficient volume for replicate runs. Anions samples were preserved with formaldehyde while NH_4^+ samples were flash frozen immediately upon collection. Alkalinity (determined by Gran plot (Gran, 1952) and pH were measured simultaneously.

The lysimeter-drawn water samples were also analyzed for reduced species of S and Fe, which were quantified voltammetrically using a hanging drop mercury electrode (Metrohm, Switzerland). The voltage range scanned was from 0 mV to -2100 mV using square wave voltammetry with the following parameters: pulse height 15 mV, step increment 4 mV, frequency 100 mHz, and scan rate 80 mV s^{-1}. Platinum electrodes manufactured after Patrick et al. (1996) and Wafer et al. (2004) were used in conjunction with a Ag/AgCl reference electrode from Fisher Scientific (Hampton, NH) to measure

Eh. Electrodes were connected to a CR10X datalogger coupled with an AM 16/32A multiplexer through a interface suggested by van Bochove et al. (2002) and calibrated as outlined in Owens et al. (2005).

Post-Mortem Mineralogical and Microbiological Analyses

Post-mortem analyses of the soil columns were performed on sediment cores (3.8 cm diameter x 40 cm length) taken from the experimental soil columns. Cores were split in two longitudinally and then halved into sections that were used for microbial enumeration analysis and imaging. Most probable number enumerations (MPN) were prepared in 1 mL, 96 well, microtiter plates. Samples were extracted every 2-3 cm along the depth profile. Each sample was serially diluted in tenfold increments up to a ratio of $1{:}10^9$ with 5 replicates for each increment. An Fe-reducing bacteria growth medium was produced after Lovely and Phillips (1986). Also Postgate's Medium B (Postgate, 1984) was prepared for SO_4^{2-} reducing bacteria. Both Fe and SO_4^{2-} reducing MPNs were allowed to incubate for 8 weeks at which time they were quantified.

The halved cores used for imaging were oven dried (60º C) for 24 hours. The dried sediment was saturated by matric and gravity induced flow with a low viscosity Buehler epoxy (Lake Bluff, IL). The sediments were cut, attached to a glass slide (1.3 x 3.8 cm), thin sectioned, and polished. Soil aggregate volume fraction was measured in small (3.8 x 1.3 cm) thin sections extracted from the loam and layered columns. Samples were then scanned on a Canon Coolscan scanner (Lake Success, NY) that produced high resolution (4000 dpi) images. Image analyses of soil aggregates were

performed using ImageJ software (National Institutes of Health). Samples were also imaged using a Cameca SX50 (Cameca, Courbevoie, France) microprobe to investigate the composition of individual aggregates. Scanning electron microscope (SEM) was used for imaging and Energy Dispersive Spectrometry for elemental analysis.

RESULTS AND DISCUSSION

Geochemistry of Homogenous Loam and Sand Columns

Detailed results from the homogenous sand column are not reported here because in general, chemical concentrations were very dilute due to the low chemical reactivity of the sand material (mostly quartz). However, the low chemical concentrations observed in the sand provide baseline values against which results from the loam and layered columns were compared. The chemical concentrations evolved were generally greater in the loam than in the sand column. This was expected due to the higher fraction of clays, organic matter, and diversity of minerals (smectite, calcite, illite, and SO_4^{2-} bearing minerals such as: anhydrite, gypsum, and barite) present in the loam than in the sand.

The pH of the percolating water changed from an initial value of 5 to an approximate value of 8 in the upper few centimeters of the sediments of both homogeneous columns during rainfall events (data not shown) as carbonate minerals reacted with the acidic rainwater. There was relatively little change in pH from the top to the bottom of the column as values generally ranged from 7.5 to 8.7 and did not change considerably during the experiment. During rainfall, alkalinity values from the

homogenous column were low (30-97 mg L^{-1}) due to low carbonate content of the sand. In the homogenous loam column alkalinity values were much higher (283-606 mg L^{-1}) than in the sand column, but as the experiment progressed and as a greater amount of rainwater was applied to the sediments, the alkalinity values in the upper centimeters of the column decreased to near zero (15.1 mg L^{-1} by the 242nd day of the experiment) suggesting that the soil had lost its ability to buffer the acidic rainwater.

Nitrogen Cycling

Differences in nitrogen cycling were observed between the two homogenous soil columns. Nitrate (NO_3^-) concentrations in the sand column averaged 25 mg L^{-1} (std dev = 2.5 mg L^{-1}) with depth. In the loam column however, NO_3^- was consistently consumed within the first 15 cm. This rapid removal was likely due to microbial denitrification (Tiedje et al., 1984) and created conditions for microbial utilization of lower potential terminal electron acceptors such as iron oxides and sulfate. Ammonium was below detection limits in the homogeneous sand column but was detected in the loam column and showed some variability with depth as shown in Figure 2.3a. The exact mechanism producing NH_4^+ is unknown although it likely includes microbial mineralization of organic matter (Báez-Cazull et al., 2007) and desorption of NH_4^+ from clays (Rosenfeld, 1979). Mineralization, via active microbial cycling of organic material, is consistent with the observation of denitrification.

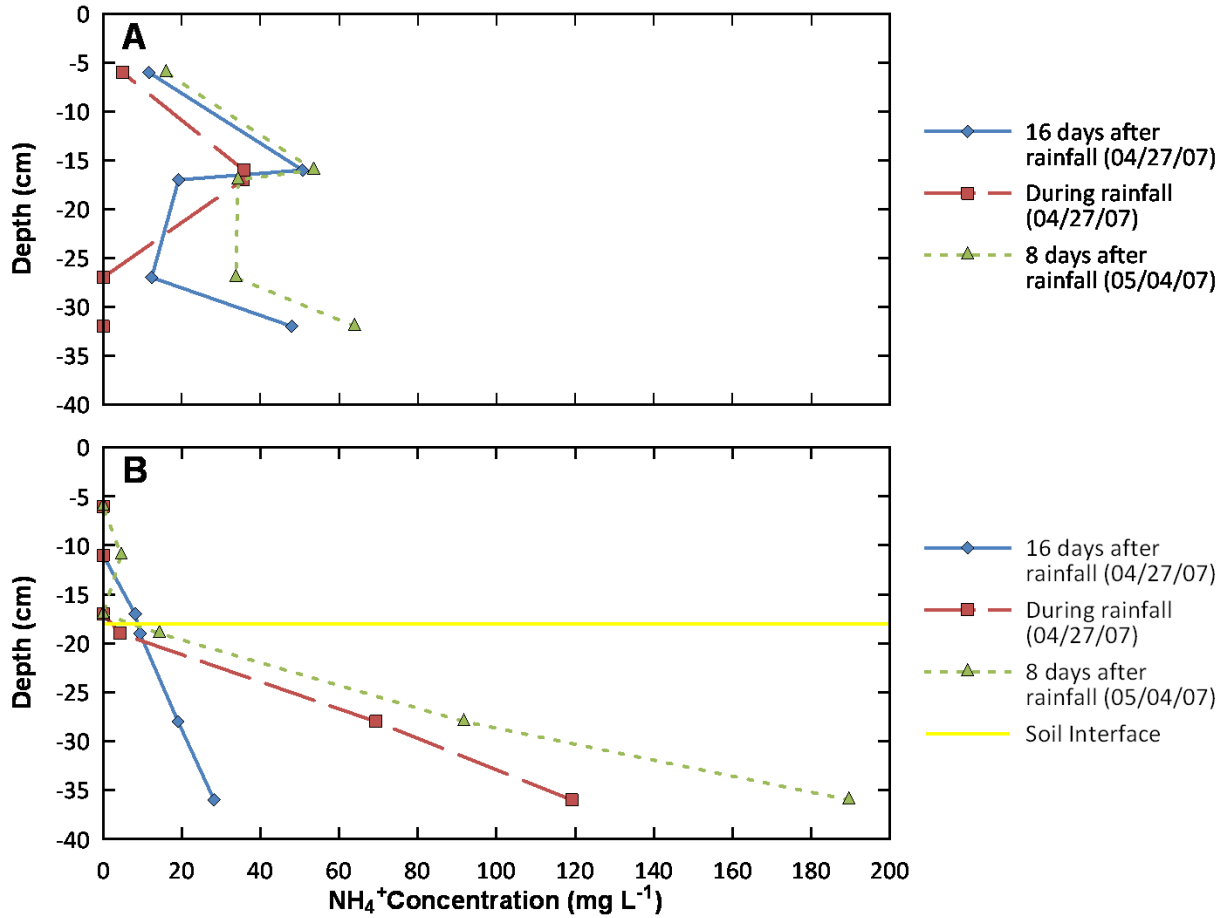

Figure 2.3 - Ammonium concentrations in the loam and layered columns. A - during and after rainfall in the homogenous loam and B – in the layered column. Peak NH_4^+ concentration in the layered column was nearly 4 times greater than in the homogenous loam column.

Iron-Sulfur Cycling

Average SO_4^{2-} concentrations throughout the experiment remained nearly constant in the homogenous sand column (mean of 29.3 mg L^{-1}, standard deviation of 7.6; Figure 2.4a). In the loam column, SO_4^{2-} concentrations were roughly 30 times higher than in the sand column and had a mean of 1059.0 mg L^{-1} (standard deviation of 286.0) over this 16-day time frame (see Figure 2.4b). Sulfate likely originated from either dissolution of SO_4^{2-} minerals (e.g. gypsum, barite) and/or from the oxidation of iron-sulfide minerals (Ulrich et al., 2003).

Similar to SO_4^{2-} trends, the loam material was iron-rich compared to the sand (Table 2.3). Consistent with these observations, reduced species of Fe or S were never observed in the sand column but were prevalent in the homogeneous loam column. Once the loam column was wetted up, the system became anaerobic quickly (less than 48 hours) and Fe(III) and SO_4^{2-}reduction began as evidenced by the presence of blackened sediment (indicative of the reaction between Fe^{2+} and S(-II)). Episodes of near-saturated or saturated conditions lead to a decline in oxygen and a shift in microbial metabolism to alternate electron acceptors such as NO_3^-, Fe(III), and SO_4^{2-}. Microbial reduction of Fe(III) and SO_4^{2-} would have lead to the creation of thermodynamically favorable iron-sulfide minerals (Rickard and Luther, 2007).

Concentration and distribution of reduced Fe and S species in the loam column were variable throughout both phases of experiment. Greatest concentrations occurred at different sampling locations; and at times, Fe^{2+} was not observed at all. Concentrations of Fe^{2+} ranged from 0.6 to 1.2 mg L^{-1}. Likewise, sulfide concentrations

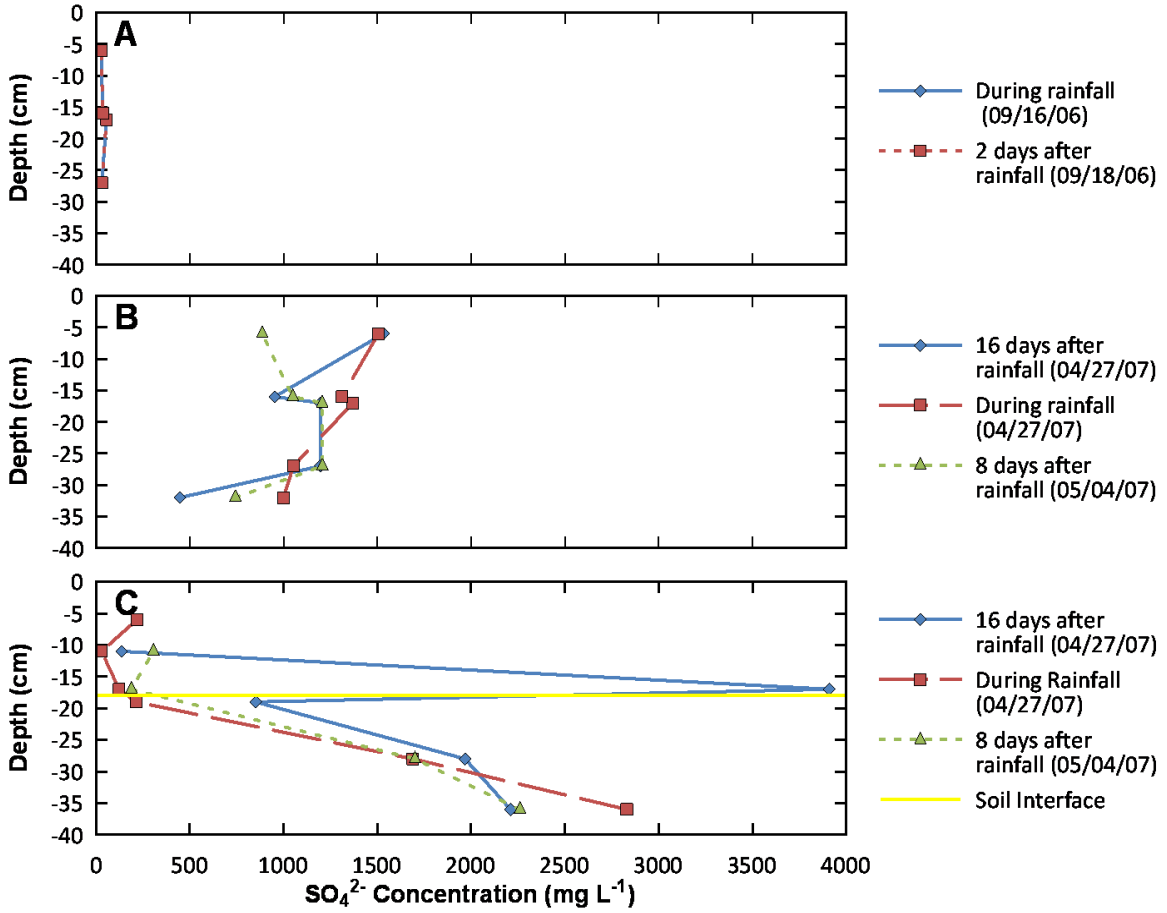

Figure 2.4 - Sulfate concentrations in the loam and layered columns. A - during and after rainfall in the homogenous sand, B - in the homogenous loam, and C in the layered column. Greater concentrations of SO_4^{2-} in the layered column were due to increased reduction/oxidation reactions. The spike in SO_4^{2-} concentration 16 days after rainfall was likely caused by oxidation of an FeS containing mineral crust.

did not exhibit any consistent concentration or distribution trends. Concentrations over the extent of the experiment ranged from 1.4 to 16.4 μg L^{-1}. The loam column produced significant FeS minerals as evidenced by the black colored effluent water. Classical redox theory would predict that vertically distributed zones of varying energy yielding electron accepting zones would develop in the column. Thus, the greatest energy yielding zones would be located near the top of the column transitioning to decreasing energy yield zones with increasing depth. The irregular distribution of Fe^{2+} and S(-II) suggests that there were dynamic pockets or zones of reducing conditions within the loam column. The development of microenvironments can be responsible for the simultaneous production of Fe^{2+} and S(-II) and explain the irregular distribution of these same chemical species. Although the Eh data (Figure 2.5) from the loam column were not consistent with Fe(III) reduction or SO_4^{2-} reduction, the distance between Pt electrodes (up to 10 cm) prevented small-scale dynamic pockets from being identified.

Geochemistry of Sand-over-Loam Layered Column

Similar to the two homogeneous columns, pH values generally ranged from 7.4 to 8.6 from the top of the column to the bottom and remained consistent throughout the experiment. Similar to the loam column, carbonate minerals were depleted after reacting with the acidic rainwater and thus the alkalinity values in the upper centimeters of the column also decreased to zero by the 242nd day of the experiment. Throughout the duration of the experiment, alkalinity values in the lower loam half of the column were

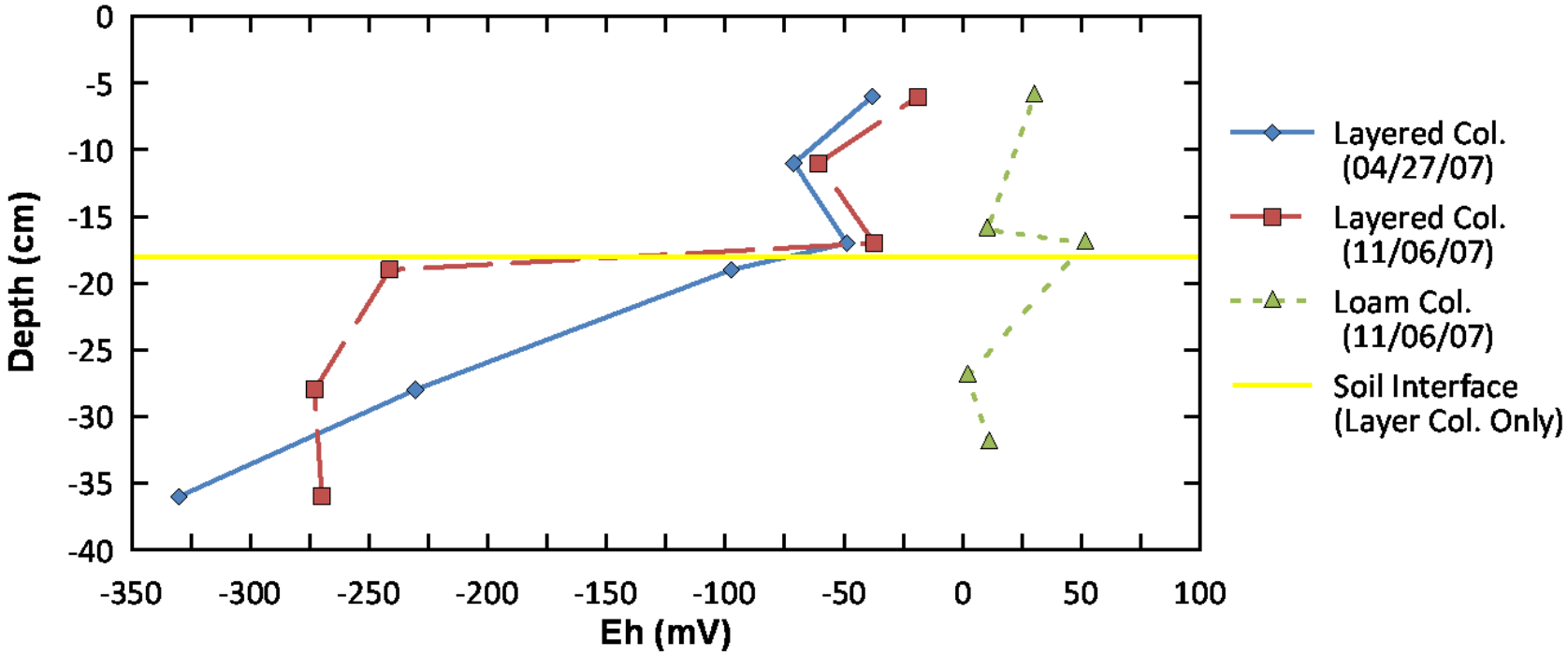

Figure 2.5 - Eh measurements during the experiment. Eh in the layered column below the interface shifted to more negative Eh during phase II. Note - Eh values for phase I are not available in the loam column due to a probe malfunction.

4-10 times greater compared to those in the upper sand half. This increase was due to the greater geochemical reactivity of the loam.

Sharp changes in the aqueous chemistry of soil solutions were observed in many constituents (SO_4^{2-}, NH_4^+, Eh) at the interface between the sand and loam in the layered column (Figures 2.4, 2.3, and 2.5 respectively). These steep geochemical gradients illustrate the influence of soil structure/layering on the evolution of aqueous geochemical species when compared to the geochemical profiles from the homogenous columns.

Iron and Sulfur Cycling

Figure 2.4c shows SO_4^{2-} concentrations in the layered column. Concentration trends in the top half were similar to those in the homogenous sand column; showing low SO_4^{2-} concentrations and little variability. However, concentration trends in the bottom half deviated from those observed in the homogenous loam column. Not only did SO_4^{2-} in the layered column increase markedly just below the soil interface, but the peak concentration was nearly two times the highest concentration in the homogeneous loam column.

As in the homogenous loam column, SO_4^{2-} was likely generated from the dissolution of sulfate-bearing minerals (e.g. $CaSO_4$ and $BaSO_4$) and from the oxidation of iron-sulfide minerals. Because both soils used in the experiment were ground, and thus homogenized with respect to mineralogy, it was unlikely that any sulfur-bearing minerals preferentially accumulated during the packing of the column. Consequentially, mineral heterogeneity, at least at the commencement of the experiment, could not

explain the high concentrations of SO_4^{2-} near the interface. Therefore, high SO_4^{2-} concentrations in the layered column were consistent with oxidation of iron-sulfide minerals originating from biogeochemical cycling occurring near the sand-loam interface.

Peak concentrations of reduced Fe and S near the sand-loam interface (Figure 2.6) supported an interpretation of enhanced biogeochemical cycling at the interface; this was especially true for sulfide where the greatest concentrations were observed. Peak concentrations of Fe^{2+}, located slightly below the interface, were double those observed in the homogeneous loam column (2.9 mg L^{-1} and 1.2 mg L^{-1} respectively). The vertically offset depth of peak Fe^{2+} concentrations from the sand-loam interface was likely due to vertical transport due to gravity flow as well as removal via precipitation of FeS minerals. Concentrations of reduced Fe and S in close proximity to one another support the likelihood of the formation of iron-sulfide minerals. The greater concentrations of these reduced species compared to those in the homogeneous loam column are consistent with higher microbial activity in the layered column.

Once hydrological conditions changed from wetting to drying, oxygen was allowed to return to areas once dominated by reducing conditions. In a secondary redox reaction, the minerals precipitated under reducing conditions were then oxidized. Specifically, the oxidation of iron sulfide minerals produced insoluble iron oxide minerals while releasing SO_4^{2-} into solution. This phenomenon can be observed during the rainfall event on 4 May 2006 in Figure 2.7. The Eh data show a shift from reducing conditions to conditions consistent with oxidation.

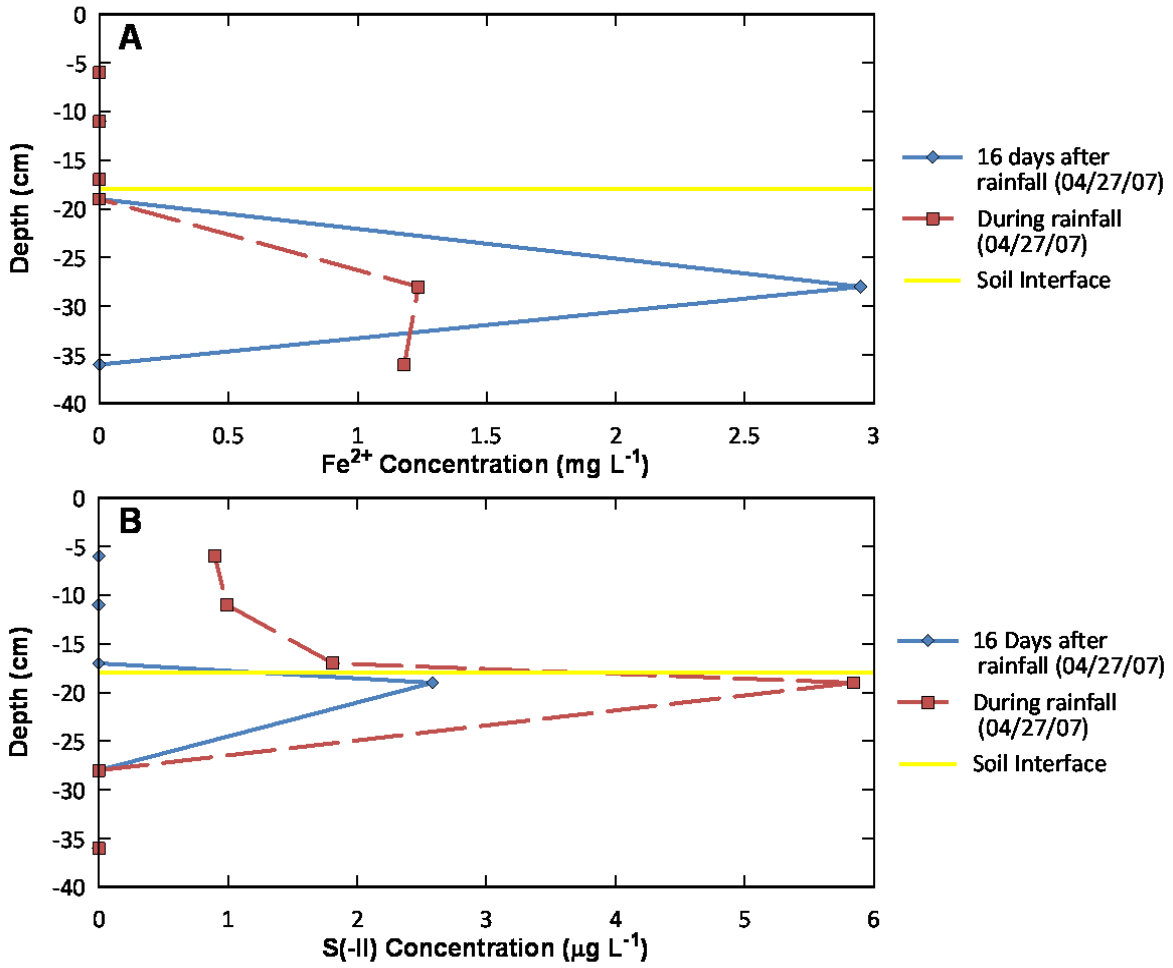

Figure 2.6 - Reduced iron and sulfide measurements in the layered column during a rainfall event and 16 days after a rainfall event.

Above the soil-layer interface, a large SO_4^{2-} concentration spike of nearly 4000 mg L^{-1} was observed on 27 April 2006 (Figure 2.4c). Below the soil-layer interface, SO_4^{2-} concentrations consistently increased (up to ~3000 mg L^{-1}) with depth during the first experimental phase (Figure 2.4b). These large SO_4^{2-} concentrations coupled with observations of iron oxide bands near the interface suggested that microbial activity was greatest near the soil-layer interface and produced a relatively large quantity of iron-sulfide minerals that were later oxidized. However, it is possible that the elevated SO_4^{2-} concentrations were a product of increased residence time as greater amounts of SO_4^{2-} bearing minerals were dissolved into the porewater solution. Ultimately, microbial enumeration data and the observation of Fe^{2+} and S(-II) suggest that the dominant process in SO_4^{2-} production within the layered column was iron-sulfide mineral oxidation.

The observed high SO_4^{2-} concentrations and observations of Fe oxides were consistent with recent studies (Hunter et al., 1998; Mayer et al., 2002) that demonstrated the importance of "secondary" redox reactions such as the re-oxidation of products from dominant TEAPs (e.g. methane, ammonia, and hydrogen sulfide gases) in driving and maintaining biogeochemical cycling of nutrients and contaminants.

Nitrogen Cycling

Ammonium concentrations in the layered column displayed similar patterns to SO_4^{2-} and are shown in Figure 2.3b. Ammonium concentrations were near zero in the upper (sandy) half of the layered column, but increased sharply below the soil interface.

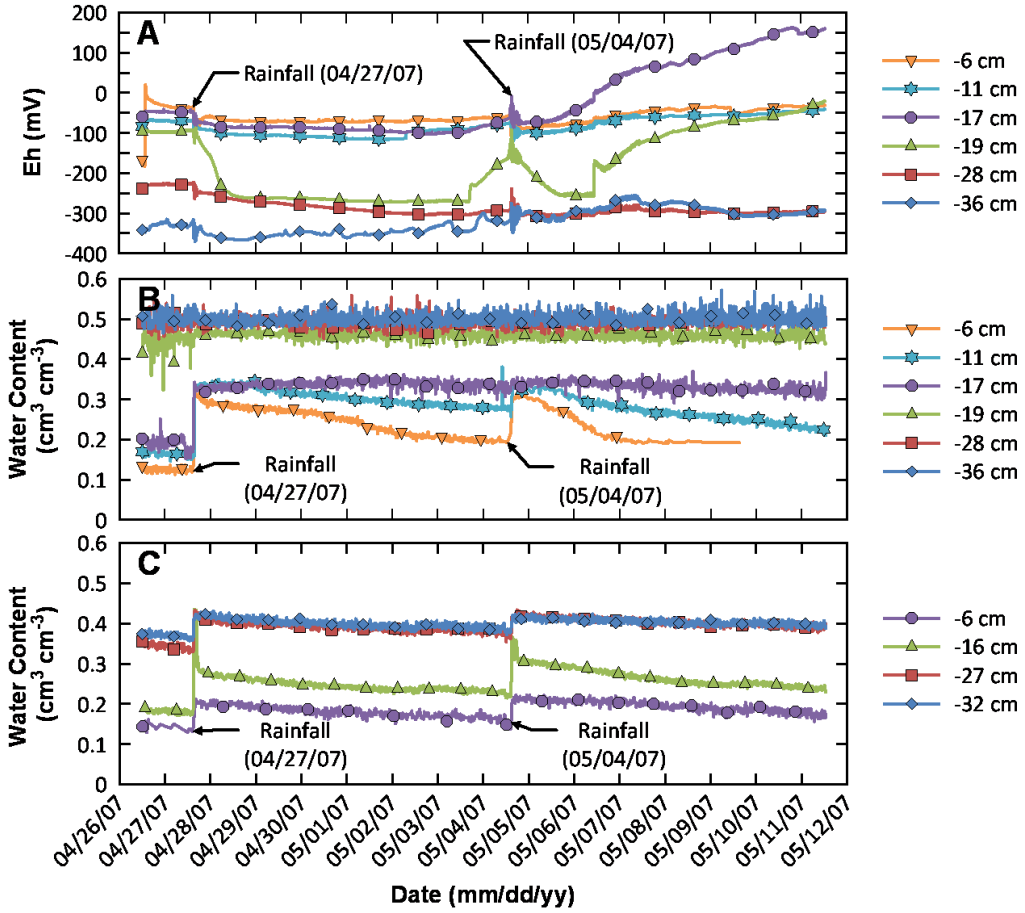

Figure 2.7 – Eh and water content results. Eh values from the layered column during Phase I of the experiment (A). Water content values from the layered column (B); soil textural interface is located at -18 cm depth. Water content from the homogenous loam column (C). Note – Eh data from the loam column during this period are unavailable due to probe malfunction.

The highest concentration of NH_4^+ in the layered column was nearly three times that of the highest concentration in the homogeneous loam column. Ammonification may proceed via microbial metabolism, desorption of NH_4^+ from clay, or by organic material oxidation involved in iron-redox cycling. In this instance, the higher concentrations of NH_4^+ in the layered column were consistent with enhanced microbial cycling (Báez-Cazull et al., 2007; Bally et al., 2004).

Unlike SO_4^{2-} concentrations, which did not greatly vary over time, NH_4^+ concentrations changed substantially over relatively short time periods consistent with microbial growth and decay (Figure 2.3b). During rainfall, NH_4^+ concentrations reached 140 mg L^{-1}, with the highest observed concentration, 200 mg L^{-1}, on the 8th day after the rainfall event started. After 16 days, NH_4^+ concentration had dropped below 50 mg L^{-1} probably due to microbial uptake.

Redox Potential

Eh in the layered column decreased sharply below the soil interface consistent with the trends of iron-sulfur cycling and NH_4^+ concentrations (microbial growth and decay). Figure 2.5 shows Eh values at the beginning and near the end of the experiment. The presence of reduced species of Fe and S agreed with negative Eh values that further decrease with depth. Although Eh decreased below the interface during phase I, the values during phase II demonstrated an even sharper contrast of Eh (~250 mV) across the soil interface. As the experiment proceeded, Eh values at the interface further decreased and added to the striking biogeochemical contrasts near the soil interface.

The aforementioned results demonstrate that areas near the soil interface were "hotspots" of biogeochemical activity which led to greater geochemical variation compared to the homogenous soil columns and illustrate the broader implications of redox dynamics in partially saturated soil systems.

Influence of a Soil Textural Interface in Geochemical Cycling

Our geochemical results demonstrate that conclusions drawn from indiscriminately combining results from experiments with single homogenous materials to simulate a layered soil system would not accurately predict the geochemical changes observed. Sulfate and NH_4^+ concentrations were fairly consistent for each soil type, but a simple layer cake model application to a layered soil system would underestimate actual concentrations by 2-3 times. Clearly, textural interfaces between soils must be taken into account for accurate geochemical characterization of subsurface systems.

Microbial Enumeration

Geochemical changes in the layered column were probably caused by the combination of several processes that included linked microbial activity and water flow. MPN analyses to determine iron and sulfate reducing bacteria cell counts were performed on the loam and layered columns post-mortem. Sulfate reducing bacteria (SRB) counts were approximately 2-3 orders of magnitude lower than iron reducing bacteria (IRB) in both columns. It is unclear why this difference exists, but a possible

reason could be that IRB outcompeted SRB for electron donor which limited their community size (Achtnich et al., 1995).

Geochemical data suggested that the soil interface within the layered column became a hotspot of biological activity. Consistent with an increase in microbial activity, were the distinct geochemical trends observed in the layered column. MPN enumerations of the layered and loam columns show that Fe and SO_4^{2-} reducer populations were greatest directly below the soil interface (Figure 2.8) consistent with geochemical trends and interpretations of enhanced iron and sulfate reduction in this zone. Iron and SO_4^{2-} oxidizer populations were not enumerated, however they have been observed in high abundance together with Fe and SO_4^{2-} reducers in mine tailings (Kock and Schippers, 2008) and may also be prevalent beneath the soil interface as well. These greater microbial population counts at the interface compared to the soil matrix is consistent with other similar studies in saturated systems (Fredrickson et al., 1997a; Madigan et al., 1997a).

In the layered column, SRB and IRB counts increased by 2-3 orders of magnitude across the soil interface from the top sand layer to the bottom loam layer. To some extent, this variance could be explained by differences in soil type. A study by Federle et al. (1986) showed that soil type is a control on the magnitude of microbial population and activity. The organic-rich loam, rich in nutrients, likely had higher cell counts than the sand to begin with. However, microbial cell counts for both IRB and SRB in the lower part of the layered column were significantly higher than in the homogeneous loam column. This difference was most dramatic in the SRB numbers

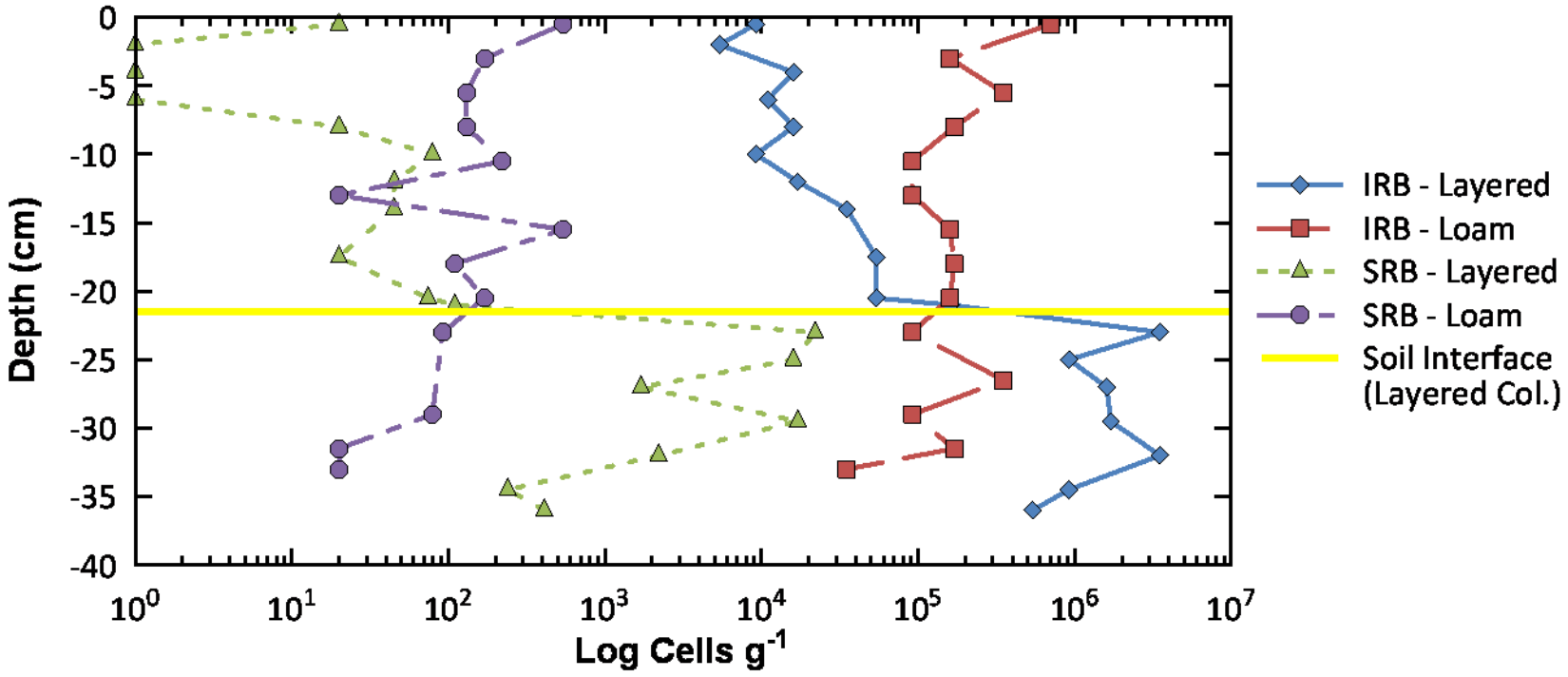

Figure 2.8 - Most probable number (MPN) analysis. MPN enumerations show a significant increase in both Fe(III) and SO_4^{2-} reducing bacteria near the soil interface. Compaction of sediment during sampling accounts for a different interface depth.

which showed a two orders of magnitude increase while the IRB showed an order of magnitude increase over corresponding counts in the homogeneous loam column.

Similar to the chemical data, the microbial enumerations demonstrate the importance of soil type, but cannot alone account for elevated numbers associated within the layered system. A layer-cake approach that doesn't consider the soil-layer interface cannot account for the increased numbers of microorganisms in the layered columns.

Soil Structure

Microorganisms not only influence geochemistry, but also affect small-scale soil structure through the development of biofilms that consist of: glue-like excretions, filamentous hyphae and/or colonies that bind mineral particles and organic material together into soil aggregates (Tisdall and Oades, 1982). Although the formation of these aggregates are complex and involve many agents, microorganisms have been demonstrated to play a significant and widespread role in aggregate genesis (Six et al., 2004). Furthermore, increased microbial activity has been shown to increase the number as well as the stability of soil aggregates (Bronick and Lal, 2005).

Samples for soil aggregate volume fraction (aggregate cross sectional area / total cross sectional area) analysis for the loam column was sampled at a 10 cm depth while the layered column sample came from 20 cm depth (2 cm below the interface). Thin sections were scanned using a high resolution (4000 dpi) reflected light scanner. Imaging software isolated the dark areas in the thin sections, measured their maximum diameter, and cross sectional area. These dark areas were chosen because SEM analyses

revealed that the vast majority of dark colored areas were soil aggregates. The sum of all aggregate cross sectional areas was divided by the total cross sectional area of the thin section to calculate the aggregate volume fraction. The thin sections with aggregates outlined in yellow are shown in Figure 2.9.

Although this method was not exact and the input variable, the results support the visual analysis that there was greater volume fraction of aggregates in the layered column than in the homogenous column. The cross sectional analyses showed a greater volume fraction of aggregates in the layered column (0.0640 cm^2 cm^{-2}) than in the loam column (0.0195 cm^2 cm^{-2}). This greater aggregate volume fraction also supported an interpretation of escalated microbial activity near the soil interface.

Iron oxide mineral crusts were often observed in association with soil aggregates in both homogeneous loam and layered columns during the post-mortem analysis. It is unclear what relationship existed between the two; however these mineral crusts may have influenced geochemistry as well as microbial colonization and activity. During saturated conditions, black Fe-S mineral crusts formed within a matter of days. During unsaturated conditions, these black mineral crusts oxidized to Fe-oxide. The crust may have led to blocked pore spaces that trapped soil aggregates. Increased microbial activity near the crust may have also contributed to aggregate formation. For example, during the wetting up phase, a black crust was formed at the top of the homogeneous loam column, directly below the sediment water interface. This crusts may explain why SRB and IRB counts were the highest at the top of the homogeneous loam column (See

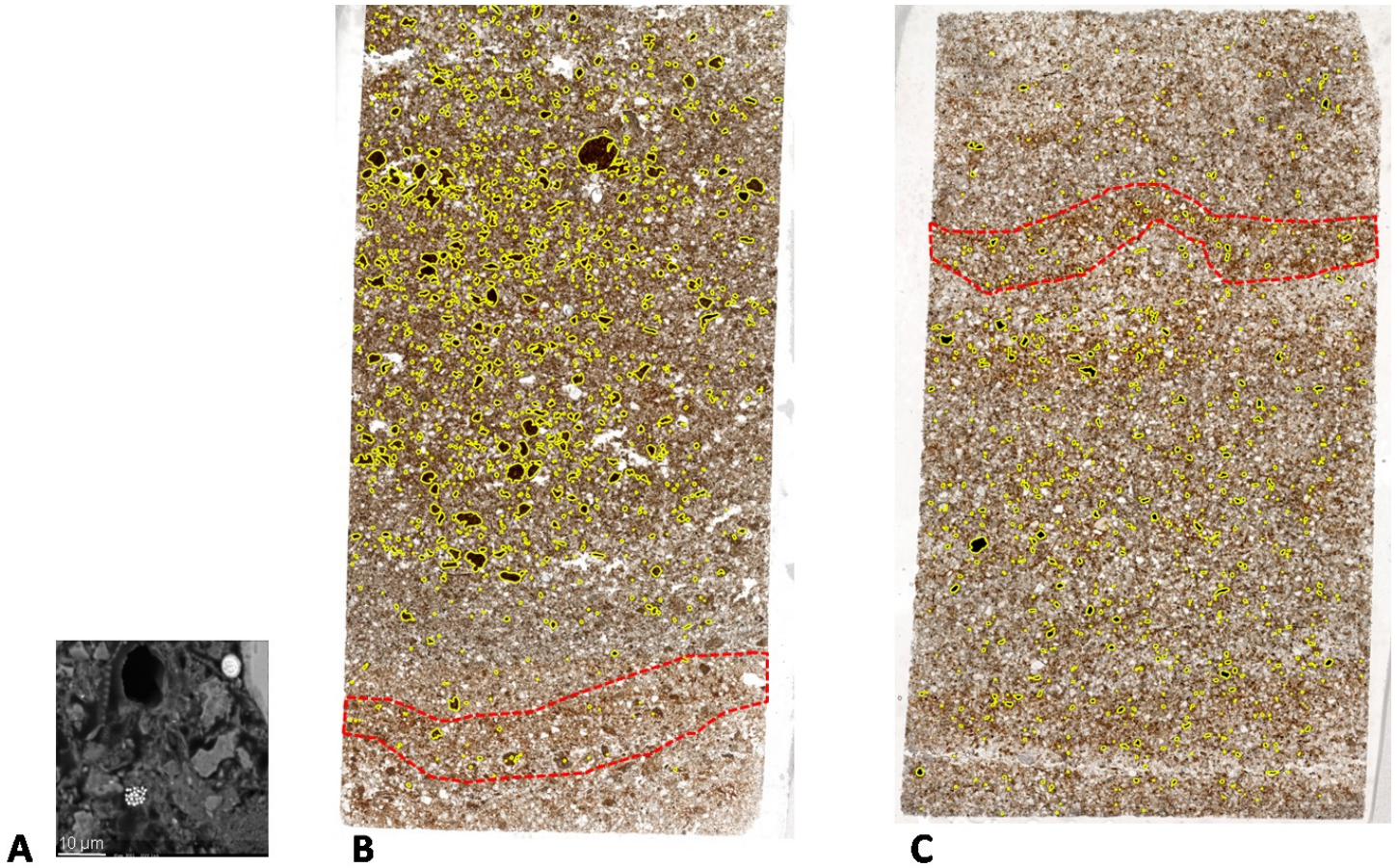

Figure 2.9 - Soil aggregate analysis. A magnified aggregate is shown in the feature A. This aggregate is typical of other aggregates and consists of organic matter, pyrite framboids, micro skeletal material, and other minerals. Vertically sliced thin sections (4 × 1.5 cm) of loam material from the layered column and homogenous column are shown in B and C respectively. Yellow outlines were drawn around aggregates (dark spots) larger than 256 µm in diameter. Red dashed lines highlight bands high in iron oxides.

Figure 2.10) as well as why SO_4^{2-} concentrations were also the greatest at the top of the column.

Soil Hydrology and Temporal Dynamics

The formation of crusts and soil aggregates within the study columns may help to explain the observed decrease in hydraulic conductivity throughout the experiment (e.g., Figures 2.9 and 2.10). For example, the saturated hydraulic conductivity changed from 2.35×10^{-5} m s^{-1} to 6.9×10^{-7} m s^{-1}. Initially the difference in unsaturated hydraulic conductivity ($K(\psi)$) between the overlaying sand (high $K(\psi)$) and loam (low $K(\psi)$) likely caused water to "pond" at the soil interface. This increase in the residence time of water allowed for an intensification of microbial activity which subsequently led to consumption of dissolved oxygen and use of alternate terminal electron acceptors such as NO_3^-, Fe(III), and SO_4^{2-}.

This increase in microbial activity and water residence time would have produced reduced minerals and increased soil aggregation, both of which likely contributed to reduction of porosity and/or permeability. The formation of reduced FeS minerals and subsequent oxidation would have created Fe oxide mineral crusts. An example of these mineral crust/soil aggregate composites is shown in Figure 2.9. These mineral crust/soil aggregate composites generally consisted of several small layers with 1-2 cm spacings between layers rather than one thick layer, but nonetheless contributed to the modification of the soil hydraulic properties.

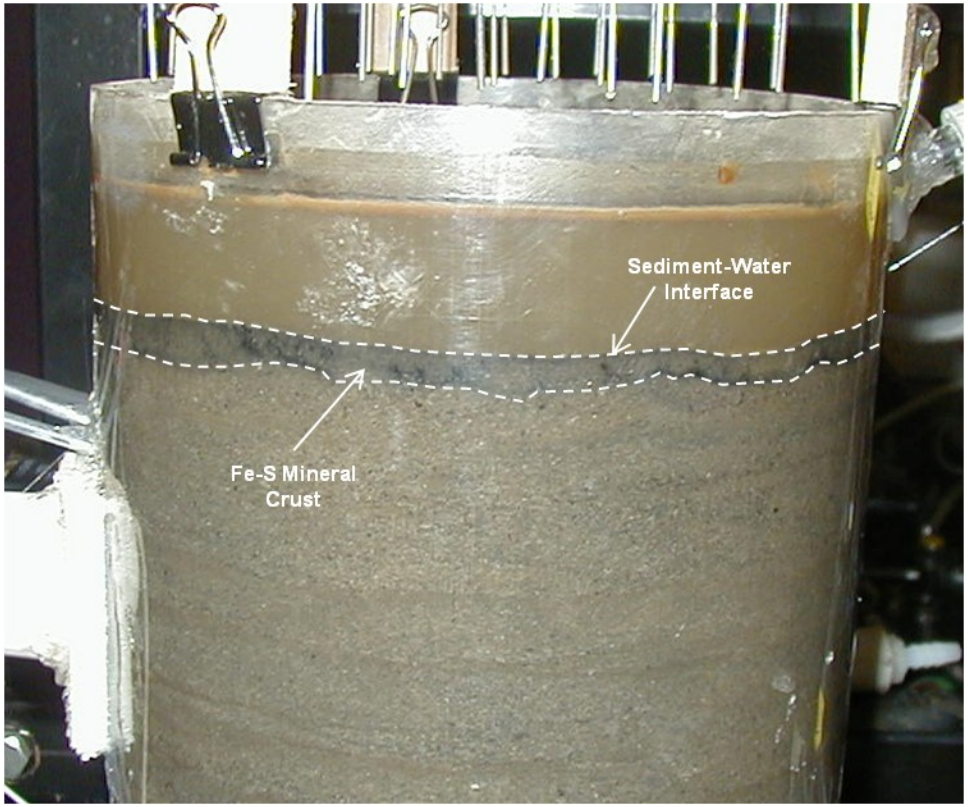

Figure 2.10 - Photograph of the homogenous loam column during wetting up. Note the dark Fe-S mineral crust that formed at the sediment-water interface.

Microbiological processes may also play a role in directly altering hydrological conditions through the development of biofilims. It was unclear how bioclogging (Bundt et al., 2001; Holden and Fierer, 2005; Vinther et al., 1999), as a result of increased microbial activity, may have influenced the development of these mineral crust/soil aggregate composites.

The development of crusts and aggregates would cause a reduction of flow leading to a positive feedback relationship between water residence time and microbial activity coupled to redox cycling. Reduced hydraulic conductivity at the soil interface would lead to longer residence times of water which would allow increased microbial activity and the further spatial development of reducing conditions and soil aggregation.

This positive feedback cycling led to an extensive decrease of hydraulic conductivity of the soil system. Temporal declines in $K(\psi)$ in the homogeneous and layered soil column are shown in Figure 2.11. Although both the homogenous loam and layered columns showed decreases in hydraulic conductivity, the change was most drastic in the layered column where the decline was more than an order of magnitude. Note that this decrease was so drastic that the "shoulders" of the 10 December 2007 curves are not resolved in Figure 2.11 and appear to be flat lines. The reduction of hydraulic conductivity in the homogeneous loam column was probably caused by similar small-scale positive feedback relationships that occurred in the layered column, but at a lesser rate/magnitude.

These linkages between biogeochemical cycling and water movement in the vadose zone may ultimately lead to a greater potential in layered systems to naturally

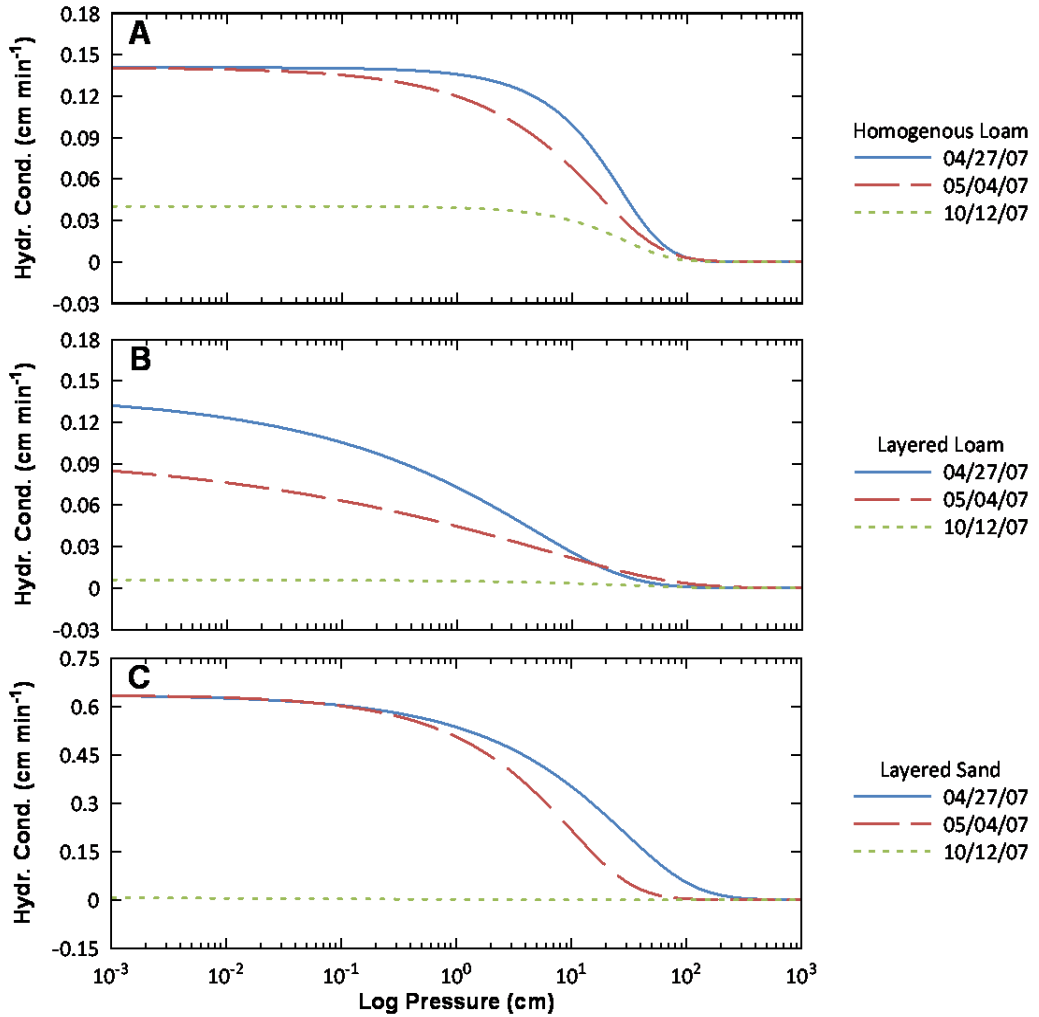

Figure 2.11 - Unsaturated hydraulic conductivity decreases in both columns over time.

remediate contaminants than homogenous systems. This is not only due to enhanced biogeochemical cycling but also due to longer contaminant residence times caused by mineral crust/soil aggregate composite development that reduce hydraulic conductivity.

Redox State Considerations

Changes in the hydrologic framework had implications for the longer-term redox state of the vadose zone. Iron mineral crusts/soil aggregate composites in the layered column retarded evaporation as well as drainage. As a result, after 4 months without a rainfall event, moisture content in the lower half (18 – 40 cm depth) of the layered column remained much higher than in the homogenous column as shown in Figure 2.12. The average water content in the loam column increased to 0.41 cm^3 cm^{-3} from 0.15 cm^3 cm^{-3} (difference of 0.26 cm^3 cm^{-3}) compared to an increase to 0.49 cm^3 cm^{-3} from 0.41 cm^3 cm^{-3} in the layered column (difference of 0.08 cm^3 cm^{-3}).

However, water-content values in the bottom loam sediments of the layered column were higher than those at similar depths in the homogeneous sand or loam columns (Figure 2.13) from the onset of the experiment. The presence of the sand soil on top of the loam soil created a capillary barrier effect, wherein the smaller capillaries of the loam could not connect to the larger capillaries of the sand. Because of the capillary barrier, water near the bottom of the column could not be drawn as far a distance upward as compared to the homogenous column. Thus water at the bottom of column tended not to be distributed upward and this resulted in elevated water content values in the layered column compared to the homogenous loam column. This phenomenon has been

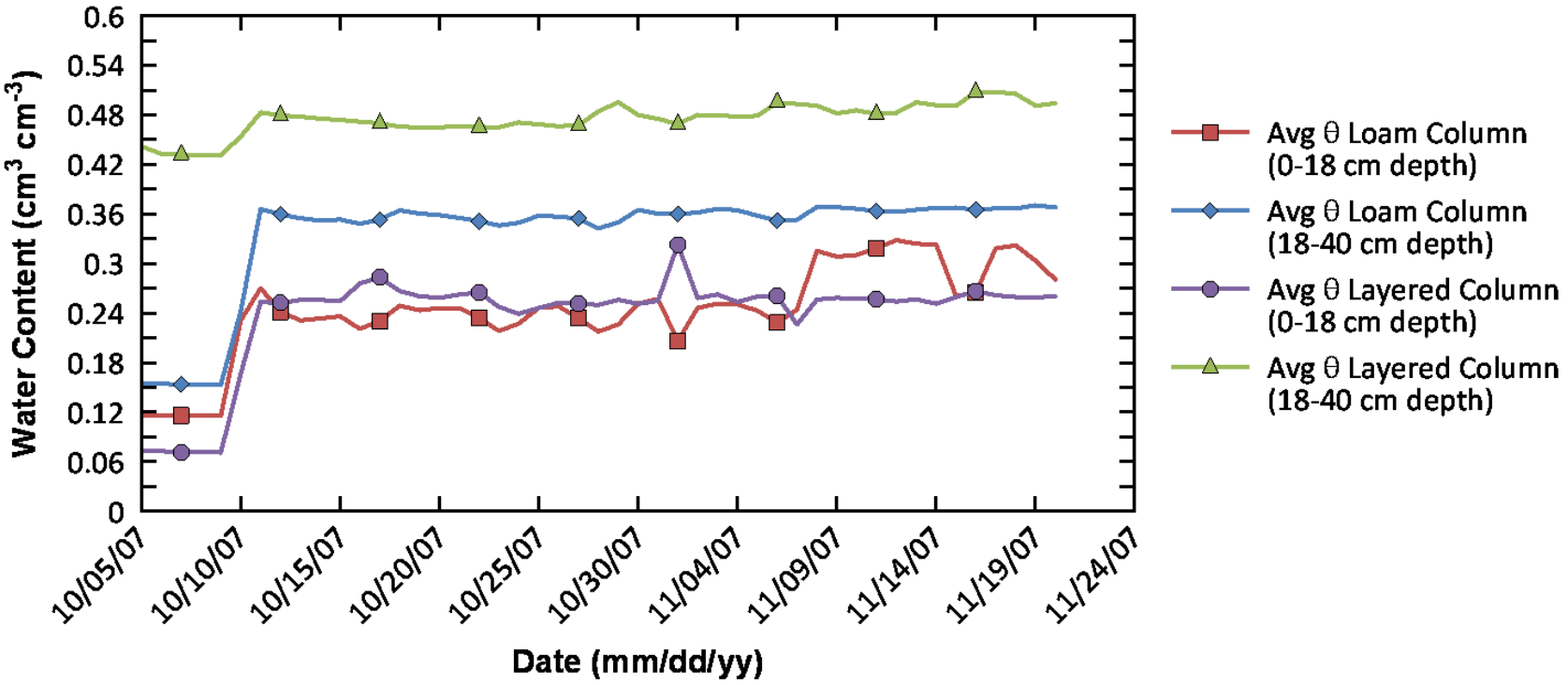

Figure 2.12 - Average water content from phase I through the end of the phase II. The beginning of phase II is marked by the large spike in water content in early October. Water content was higher in the lower loam material in than the homogenous loam column. This difference in water content is magnified during the dry interval that separated the phases.

documented in studies by Ines and Mohanty (2008) and Zhu and Mohanty (2002; 2003) that demonstrated how the effective hydraulic properties of soils change as the distance from the water table was increased or decreased which is analogous to the thickness of the loam layers.

Regardless of the various factors that led to increased water content in the lower half of the layered column, elevated water content, the presence of mineral crusts and aggregates, and microbial respiration acted to prevent the introduction of oxygen which allowed for reducing conditions to be maintained through relatively long periods of time without rainfall.

In addition to limiting evaporation, minerals formed near the soil-layer interface during periods of saturation also contribute to the sustaining of reducing conditions. As oxygen-rich rainwater percolated from the top of the column, it came in contact with these reduced minerals that consumed oxygen as they were oxidized. Generally, Eh became more positive in response to rainfall events but redox conditions were typically restored to previous background levels within a day (Figure 2.6).

Sustained anaerobic conditions observed primarily in the layered column may be important in remediation of some contaminants, such as chlorinated compounds, that degrade exclusively under reducing conditions. The limiting of oxygen diffusion, coupled with removal of dissolved oxygen by reduced minerals via oxidation, lead to anaerobic conditions generally not thought to exist in the vadose zone. Thus there exists a considerable potential for anaerobic degradation of contaminants in the vadose zone.

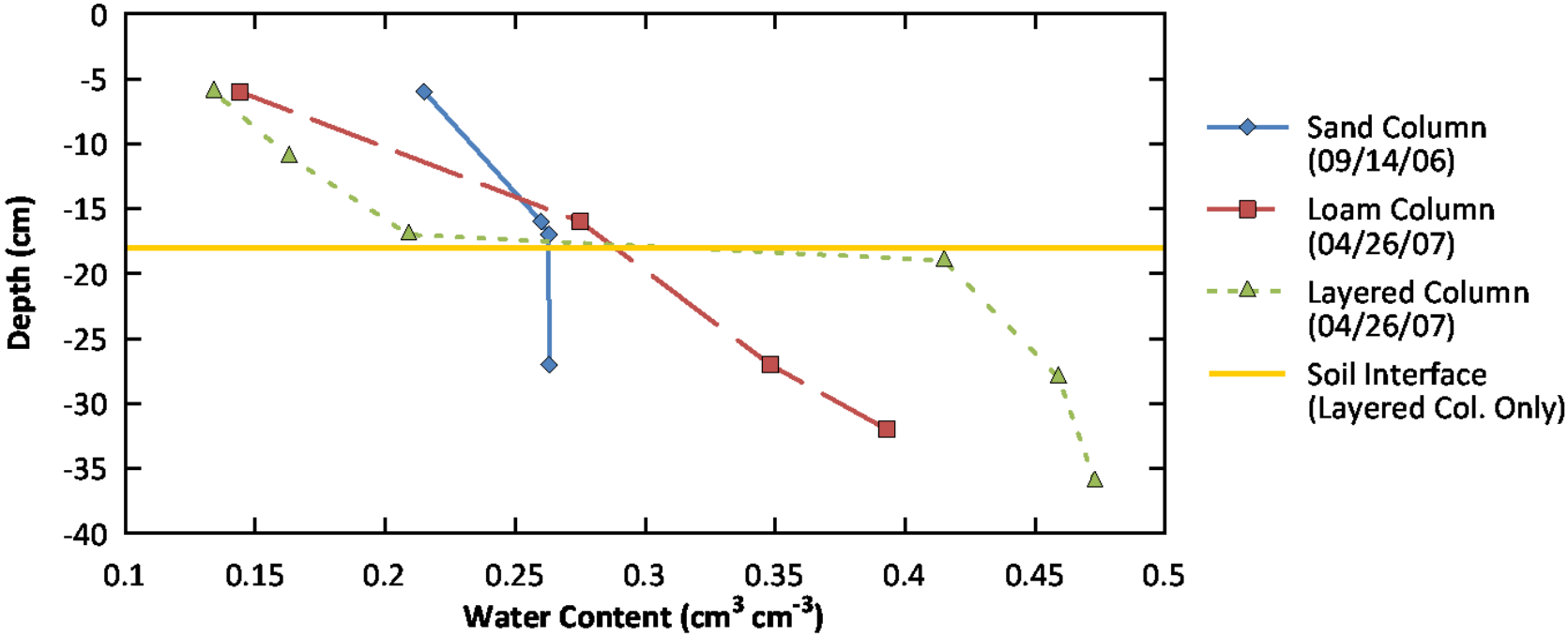

Figure 2.13 - Water content profiles for the homogenous sand, homogenous loam, and layered columns.

CONCLUSIONS

The results of this study demonstrate the need to consider the effects of soil layers on biogeochemistry and hydrology in variably saturated subsurface systems. A layer-cake model that treats soil layers as independent entities that do not interact with one another will significantly underestimate hydrologic, chemical, and microbiological conditions in layered systems.

The unique combination of hydrologic, geologic, and microbial process occurring at soil interfaces created areas of enhanced biogeochemical cycling that are critical to understanding and predicting water and chemical migration in the unsaturated zone. Consideration of soil interfaces yield more representative results that are crucial to the successful application of contaminant fate and transport models to natural systems.

Geochemical data show there is a greater potential for a layered soil system to deliver higher concentrations of terminal electron acceptors to a contaminated aquifer than homogenous soil systems. These higher concentrations can affect rates of degradation as well as cause a shift in the active (dominant) terminal electron accepting processes.

In addition to contributing greater concentrations of electron acceptors to groundwater systems, layered soil systems have greater potential for enhanced biodegradation under unsaturated conditions. Microbial enumerations suggest that contaminants transported through a layered system have a greater chance of being degraded before reaching the saturated zone due to higher activity not only in the system as a whole, but especially near the soil textural interface. Thus the majority of

biodegradation in the vadose zone may occur in close proximity to soil textural interfaces.

CHAPTER III

EVIDENCE OF AQUEOUS FES CLUSTERS IN THE VADOSE ZONE

INTRODUCTION

The ubiquity and abundance of iron in the environment causes it to play a major role in abiotic and biotic reactions including redox reactions, precipitation, and sorption in soils. Recently, there have been numerous field and laboratory studies that have polargraphically identified an aqueous iron-sulfide species (Davison et al., 1998; de Vitre et al., 1988; Theberge and Luther, 1997) in the environment. This specie can form from the direct combination of Fe^{2+} and S(-II) at low concentrations (Luther et al., 1996) or from dissolution of poorly crystalline mackinawite (Rickard, 2006). The aqueous species form clusters which are defined as polynuclear complexes of Fe and S (Rickard and Luther, 2005). The presence of such an aqueous specie would not only have significance in metal sequestration but also on overall iron-sulfide cycling as well as its transport.

Iron-sulfide minerals are considered particularly important in toxic metal sequestration because of their high insolubility and the ease with which toxic metals such as silver, cadmium, mercury, or lead are incorporated into the mineral structure. This high insolubility is advantageous because it minimizes the transport and release of toxic metals into the environment. An aqueous iron-sulfide specie can also incorporate these toxic metals (Rozan et al., 2000b) but in this case, the aqueous nature means that any associated or incorporated toxic metals become subject to transport. As a result,

these metals may be transferred to uncontaminated or sensitive environments. Thus, documenting the presence of an aqueous FeS specie (FeS_{aq}) has great implications for understanding and predicting contaminant fate and transport. These aqueous species have been observed in numerous environmental settings but, to our knowledge, have not been studied or documented in partially saturated medium in the vadose zone and thus are not currently considered in current environmental models.

The first published account of an aqueous FeS species was voltammetrically measured in anoxic, hypolimnetic lake waters (Davison, 1977). Although the exact nature of the polargraphic peak was unknown, the authors noted that this peak was "only observable when both ferrous iron and sulfide were present" and suggested the peak may be "a soluble, electroactive ferrous sulfide complex". Since the first mention of this peak, many studies have worked to verify the identity of this substance; most commonly through titration of Fe^{2+} and S(-II). Regardless of the titrant used (either Fe^{2+} or S(-II)), all results indicated the formation of an aqueous iron-sulfide complex (Davison et al., 1998; de Vitre et al., 1988; Theberge and Luther, 1997).

The combination of Fe^{2+} and S(-II) produces several thermodynamically favorable iron-sulfide minerals including mackinawite (FeS), Griegite, (Fe_3S_4), and Pyrite (FeS_2). Initial iron-sulfide mineral precipitation favors mackinawite (referred to as FeS_m hereafter) over other iron-sulfide minerals due to its low solubility product (K_{sp}) (Davison, 1991; Rickard, 2006). For example, the K_{sp} of FeS_m is $10^{-2.95}$ compared to pyrite at $10^{-16.4}$. Thus, the formation of more thermodynamically favorable iron-sulfide minerals occurs in a stepwise progression with the lowest soluble iron-sulfide specie

being the common intermediate (Luther and Rickard, 2005). The discovery of aqueous FeS clusters (FeS_{aq}) fits well with observations that low solubility products are formed first. This suggests FeS_{aq} may be the common intermediate from which other iron-sulfide minerals are formed.

Supporting studies have shown that FeS_{aq} clusters act as a key intermediate in pyrite formation (Rickard and Luther, 1997) and that pyrite formation was inhibited by FeS_{aq} suppression (Rickard et al., 2001). The existence of an aqueous iron-sulfide phase is not currently included in traditionally accepted conceptual models of iron-sulfur dynamics in natural systems. However, the inclusion of FeS_{aq} may lead to improved prediction of Fe and S distribution and reactivity as well as a better understanding of heavy metal fate and transport in natural systems.

The calculation of equilibrium constants involving FeS_{aq} formation depend on the stoichiometry of the clusters, which is currently unknown. In attempts to discover the stoichiometery of FeS_{aq} the structure of FeS_{aq} has been studied, and although it has not been conclusively determined, several studies have successfully characterized aspects of its makeup. Rickard (1995) proposed that FeS_{aq} was not a complex with a central atom to which other ligands were bound, but rather a molecular cluster that formed a multinuclear complex. These multinuclear complexes are called clusters to which FeS_{aq} will often be referred to in this paper. Another study showed that these FeS_{aq} clusters are arranged in a tetrahedral geometry (Theberge and Luther, 1997). These observations were confirmed by a study characterizing nanoparticulate (~2 nm) amorphous FeS (Wolthers et al., 2003) in which they determined that amorphous FeS

was not truly amorphous but rather displayed a disordered tetragonal mackinawite structure. This suggests that FeS_{aq} clusters may easily transform into the more crystalline mackinawite and are an intermediate for more thermodynamically stable iron-sulfide minerals.

If FeS_{aq} is an intermediate, then they should be readily observed in nature, and indeed, FeS_{aq} clusters have been documented in lakes (Buffle et al., 1988; de Vitre et al., 1988; Luther et al., 2003) , river waters (Rozan et al., 2000b), estuary sediments (Rickard et al., 1999), marine sediments (Luther et al., 1999; Luther et al., 1998), deep ocean hydrothermal vents (Luther et al., 2001), in flooded underground mines (Roesler et al., 2007) and even in sewage treatment effluent (Rozan et al., 2000b). The seemingly ubiquitous nature of FeS_{aq} clusters suggests their potential importance in the environment which range from inorganic biochemistry to transport of Fe and other associated metals to biogeochemical cycling. If these clusters are truly ubiquitous, they should be present in soils, although they have not yet been documented, and may have profound implications for chemical fate and transport in the vadose zone.

We observed differences in FeS_{aq} production in layered and unlayered soil systems. Layers in soils systems are interesting from a chemical fate and transport perspective because the interface created by layering of soils may retard water flow and increase residence time for both water and chemicals (D. J. Hansen et al., Enhanced biogeochemical cycling and subsequent reduction of hydraulic conductivity associated with soil interfaces in the vadose zone, submitted to Journal of Environmental Quality, 2010) (hereinafter referred to as Hansen et al., Submitted, 2011a). This increased

residence time may consequently lead to rapid consumption of dissolved oxygen and development of reducing conditions. Correspondingly, these soil interfaces have been shown to be populated by a greater number of microorganisms than in the soil matrix itself (Fredrickson et al., 1997b; Madigan et al., 1997b). The dynamic and rapidly changing nature of the vadose zone make it an ideal location to look at processes occurring rapidly or out of equilibrium.

The purpose of this paper is to present observations of FeS_{aq} in unsaturated soil systems and the conditions in which these clusters were observed. To our knowledge, this is the first investigation of the occurrence of FeS_{aq} cluster in variably-saturated soil environments. In addition to presenting observations of FeS_{aq}, we discuss the potential implications of the presence of FeS_{aq} on the linkages between iron-sulfur cycling and hydrologic flow in the vadose zone.

MATERIALS AND METHODS

Two homogenous soil columns containing loam and sand respectively were characterized to evaluate geochemical transformations during fluid migration in a variably saturated system. Results from the homogeneous columns were then compared with a layered system (constructed of the same materials) to evaluate the effects of a soil interface.

Soil Materials

Two soil types were collected near the Norman, OK landfill (Breit et al., 2005; Kneeshaw et al., 2007); the first, an alluvial medium-grained sand from the banks of the

Canadian River and the second, an organic-rich loam from a wetland adjoining the capped landfill. Three repacked soil columns were constructed: a homogenized medium-grained sand, homogenized organic-rich loam, and a sand-over-loam layered column. The textural properties of the sand and loam soils are listed in Table 3.1.

Preceding the packing of the soils in the experimental columns, soils were sieved and the large-sized (> 8 mm) organic matter (sticks, leaves, snail shells) was discarded. These large organic constituents were separated from the soils to guarantee the soil-water properties would be consistent. However, because the large organic components were excluded from the packed soils, the bulk density of the packed soils and soils from the collection site were not identical. Soils were packed into columns with a piston compactor in 3 cm increments to achieve a constant bulk density.

Soil pH and electrical conductivity were measure in a 1:2 soil:deionized water mixture. Samples were stirred and measured for pH and conductivity after the mixture was allowed to equilibrate for a minimum of 30 (Rhoades, 1982; Schofield and Taylor, 1955). Nitrate-nitrogen (NO_3^--N) was extracted from soils using a solution of 1 N KCl. Nitrate was reduced to nitrite using a cadmium column and was then spectrophotometrically measured (Keeny and Nelson, 1982). Phosphorus, K, Ca, Mg, Na and S were extracted using a Mehlich III extractant and measured by inductively coupled plasma (ICP) atomic spectrometry (Mehlich, 1978; Mehlich, 1984). Iron and Mn were extracted using a diethylene triamine pentaacetic acid and then measured by ICP (Lindsay and Norvell, 1978). The results of these analyses are listed in Table 3.2 and are generally interpreted as plant-available concentrations.

Table 3.1 - Soil textural (USDA classification), organic carbon, bulk density, and hydraulic conductivity values of the two soil types collected from Norman, OK and used in soil columns

	Textural Properties (Percent Weight)							
Soil	0.5 – 0.2 mm (Medium Sand)	0.2 – 0.05 mm (Fine Sand)	0.05 – 0.002 mm (Silt)	<0.002 mm (Clay)	% Organic Carbon	Bulk Density (g/cm^3)	% Porosity	Saturated Hyd. Cond. (cm/hr)
Sand	33.6	62.9	2.2	1.3	0.02	1.5	43.4 %	38.1
Loam	46.5		39.5	12.5	1.5	1.1	58.5 %	8.4

Table 3.2 - Chemical analyses results of the two soil types used in the experiments. Concentrations are generally expressed in plant available values.

Soil	pH	Cond (uS/cm)	NO3-N (mg/L)	P (mg/L)	K (mg/L)	Ca (mg/L)	Mg (mg/L)	S (mg/L)	Na (mg/L)	Fe (mg/L)	Mn (mg/L)
Sand	8.5	106	4	4	19	1,688	56	40	154	2.83	1.28
Loam	7.9	1,030	2	5	86	24,833	802	694	374	88.35	19.27

Experimental Column Setup

The soil columns were constructed from clear acrylic pipe (15 cm in diameter and 40 cm in height). At the bottom of the acrylic pipe, a mesh fabric made of nylon was glued to a densely perforated (one 0.19 cm diameter hole per 1.16 cm^2) polyvinyl chloride (PVC) plate that was attached to the base of the column cylinder to allow for water flow and prevent soil loss. A funnel-shaped cap that directed water into a single 1.9 cm outer diameter vinyl tube drained the column. Thus, the nylon mesh fabric at the bottom was open to the atmosphere via the vinyl tubing. Only glues/epoxys that did not leach chemicals (e.g. acetate, formaldehyde, etc) after soaking in deionized water for 48 hours were used in column construction.

The top of the column was open to atmosphere which allowed water to be introduced through a rainfall simulator made of a PVC reservoir and 18 gauge needles. Water, delivered from a sealed nalgene carboy, was delivered to the rainfall simulator through a digitally controlled peristaltic pump (Cole-Parmer, Vernon Hills, IL). The temperature in the lab where experiments were conducted was maintained at 22º ± 2º C.

Columns were equipped with collocated sets of measurement probes installed at selected depths to measure water content and collect water samples as shown in Figures 3.1 & 3.2. Time domain reflectometry (TDR) three-prong probes (8 cm long, 1.1 cm spacing between rods) were used to measure water content. Data from TDR probes were automatically collected using a TDR100 (Campbell Scientific, Logan, UT) attached to a CR10X data logger (Campbell Scientific, Logan, UT).

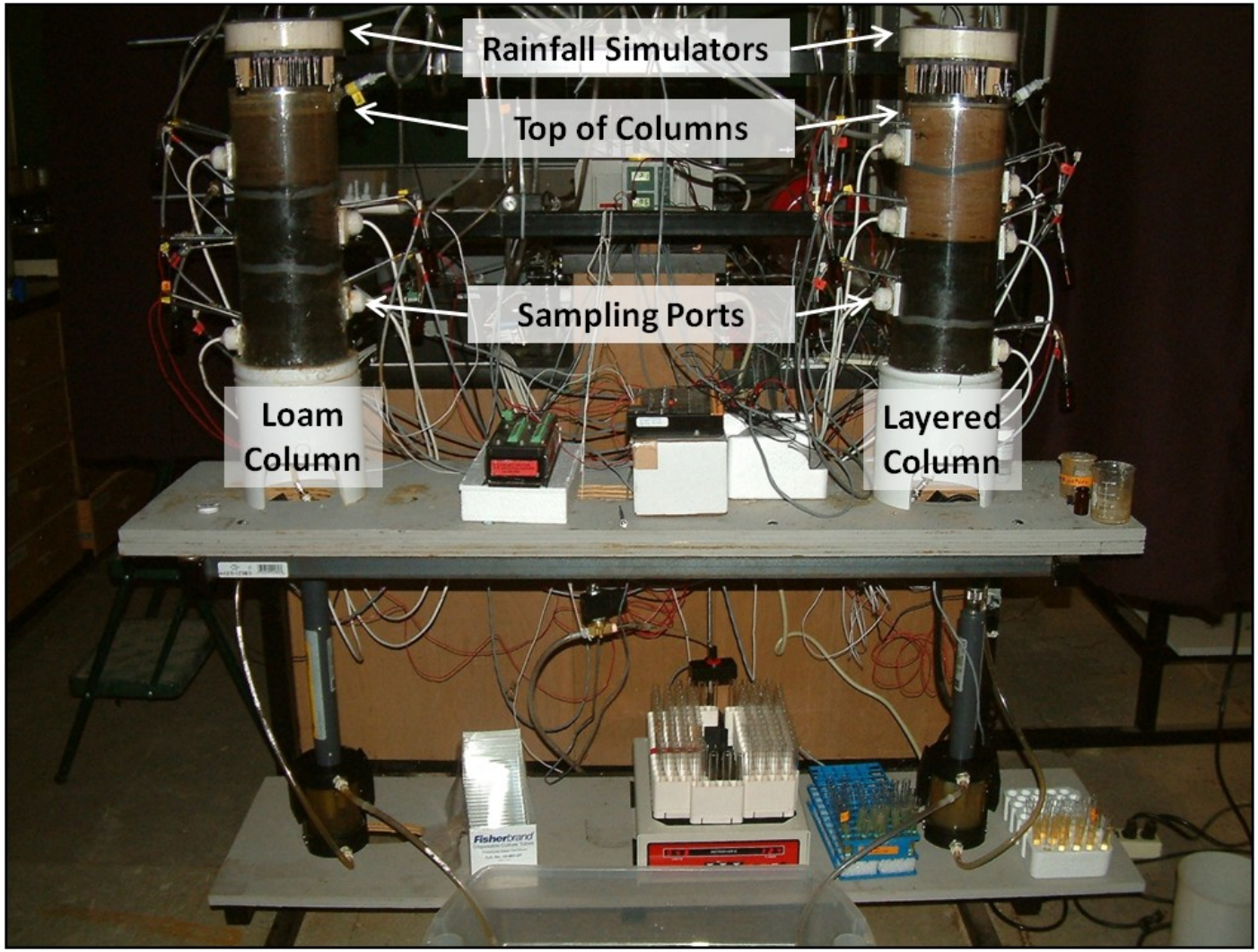

Figure 3.1 – Photograph of experimental setup of homogenous loam (left) and layered (right) columns.

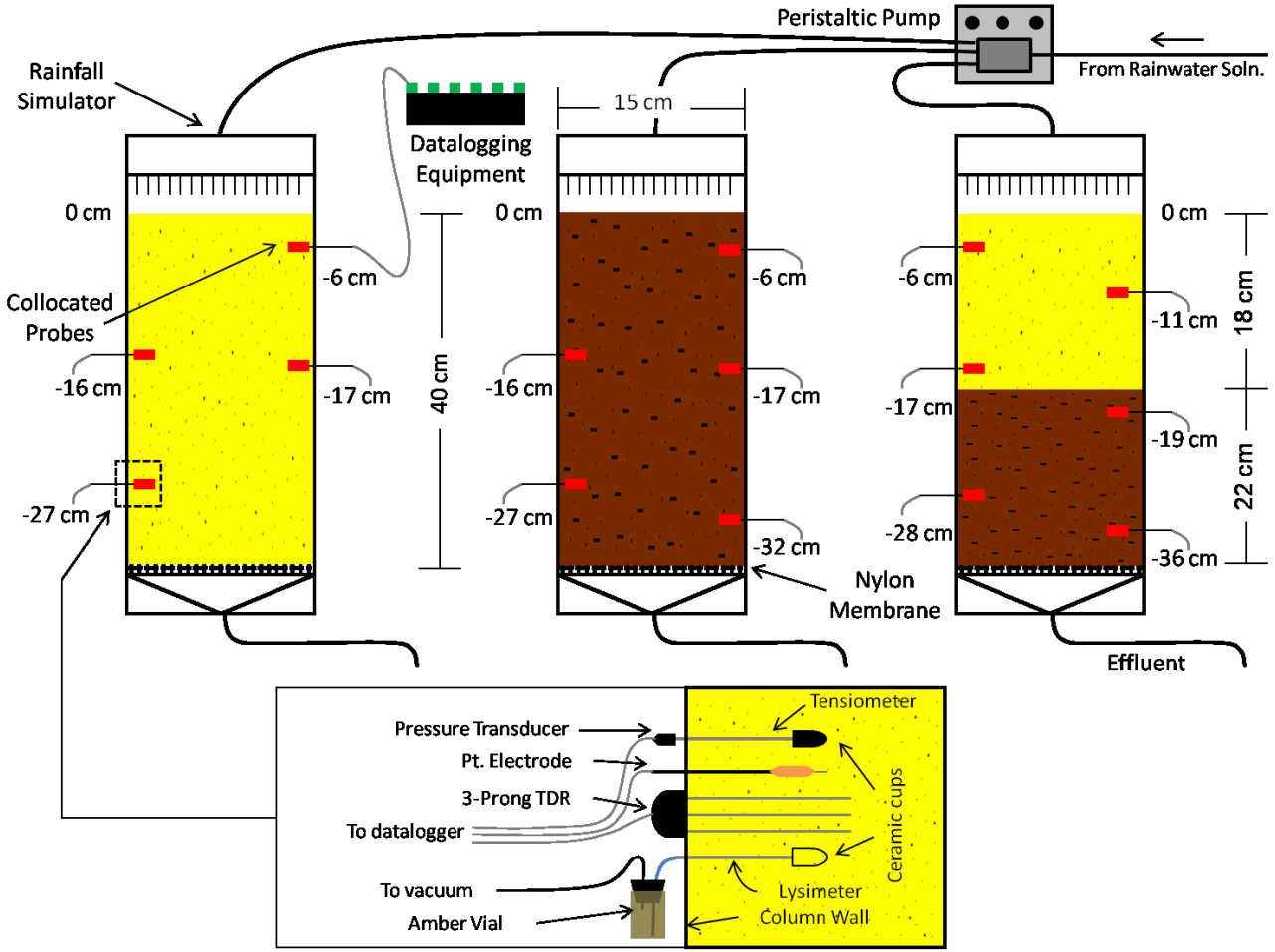

Figure 3.2 - Physical experimental setup showing (from left to right) the homogenous sand, homogenous loam, and layered columns and the location of sampling ports and probes.

Geochemical Sampling and Analysis

Small suction lysimeters, used for aqueous geochemical sampling, were positioned with the collocated probe sets. Lysimeters were made from 6-mm diameter ceramic cups (SDEC 220, SDEC France), aluminum tubing, and amber catchment vial connected to a vacuum. Approximately 16 kPa of vacuum was applied to lysimeters for five minutes to recover a sufficient volume (7 ml) of water for geochemical analyses. Water samples were immediately divided for various analyses. The pH was measured and then reduced species of S and Fe were quantified voltammetrically using a hanging-drop mercury electrode (Metrohm, Switzerland). Samples were purged for 4 minutes with ultra-high-purity nitrogen gas before being measured with square-wave voltammetry. The parameters used in the voltammetric analysis were: scanning range - 0 mV to -2100 mV, pulse height - 15 mV, step increment - 4 mV, frequency - 100 mHz, and scan rate - 80 mV/s. The balance of the water was allocated for cation and anion analyses using capillary electrophoreses (data not shown).

Rainwater Solution

Rainwater solutions were made with Nanopure water and reagent grade chemicals. The pH of the water was adjusted to approximately 5, with HCl , to imitate the pH of natural rainwater. During some rainfall events, NO_3^- and SO_4^{2-} were added (as sodium salts) to rainwater solutions to simulate the effects of polluted waters entering into the system. The concentrations of NO_3^- and SO_4^{2-} ranged from 25-100 mg/L. Bromide and Cl^- were also added (as sodium salts) to rainwater solutions as a chemical

tracer during some rainfall events. The dates in which NO_3^-, SO_4^{2-}, Br^-, and Cl^- were added to rainwater are listed in the "Experimental Period" section and Figure 3.3.

Experimental Period

Experiments on the homogenous sand column were conducted before the set of experiments on the homogenous loam and layered column, which were conducted simultaneously. Before any of the experiments were started, columns were wetted up from the bottom to prevent any air pockets from being trapped in the sediments that would artificially alter water flow.

Four rainfall events were applied to the homogenous sand column on the following days: the 15th, 16th, 18th, and 19th of September, 2006. Twenty liters, or approximately 6 pore volumes of rainwater solution, with concentrations of 25 mg/L NO_3^- and SO_4^{2-} and 50 mg/L Br^- were applied to the column during each rainfall.

The duration of the experiment on the loam and layered column was approximately eight months. Figure 3.3 shows the frequency, chemistry, and pumping rate of the rainwater applications. During the first month (04/11/07-05/04/07) of the experiment, rainwater; amended with NO_3^-, SO_4^{2-}, Br^-, and Cl^-; was used for the rainfall events. After this first month of the experiment, the column was exposed to a five month dry period (where no rainfall was applied) that mimicked drought conditions in nature. This dry period was followed by two more months of rainfall (10/10/07-11/19/07) during which time rainwater consisted of pH adjusted Nanopure water. It was during this post-drought time that the results presented in this study were collected.

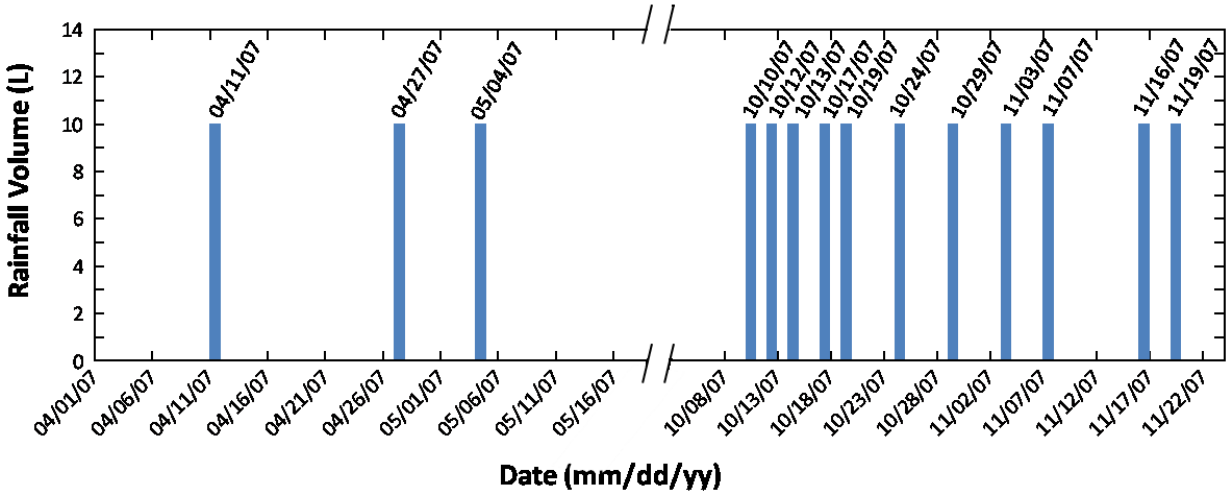

Date	Event - Time Duration	Aqueous Solution Chemistry	Sampling Schedule	Top Boundary
03/30/07 - 04/06/07	Wetting Up - 8 days	25 mg/L NO_3^- and SO_4^{2-}	On 8th day of saturation	Atmospheric
04/11/07	Rainfall - 12 hours Rain every other 10 min	50 mg/L NO_3^- and SO_4^{2-} 100 mg/L Br- - pH = 5.0	After 16 days	Flux Rate: 52 ml/min (73.6 cm/min)
04/27/07	Rainfall - 12 hours continuously	25 mg/L NO_3^- and SO_4^{2-} 50 mg/L Cl^- - pH = 5.0	During rainfall	Flux Rate: 52 ml/min (73.6 cm/min)
05/04/07	Rainfall - 12 hours continuously	100 mg/L NO_3^- and SO_4^{2-} - pH = 5.0.	Before rainfall, 8 days after previous rainfall	Flux Rate: 2.1 ml/min (2.97 cm/min)
10/10/07 – 11/19/07	Rainfall - 6 – 18 Hours	NanopureWater – pH = 5.0	During rainfall	Flux Rate: 0.8 ml/min (1.13 cm/min)

Figure. 3.3 - Experimental time table and conditions.

Post Mortem Analysis

Sediment cores (3.8 cm diameter x 40 cm length) taken from the soil columns were used for post-mortem analyses. Cores were longitudinally split in two and the halved sections were used for microbial enumeration analysis and imaging. Before the halved cores were imaged, the sediments were oven dried (60º C) for 24 hours. The dried sediment was saturated by matric and gravity-induced flow with a low viscosity Buehler epoxy (Lake Bluff, IL). After the epoxy cured, the bonded sediments were cut, attached to a glass slide (1.3 x 3.8 cm), and polished. A Cameca microprobe equipped with an energy dispersive system (EDS) was used to obtain back scattered electron (BSE) and x-ray mapping images.

RESULTS AND DISCUSSION

Evidence of FeS_{aq} Clusters

Of the three columns used in this study, FeS_{aq} was observed in the homogenous loam and layered columns but not in the homogenous sand column. Reduced species, Fe^{2+} or S(-II), were also not observed in the sand column study. The absence of any reduced species was likely due to a combination of short residence times of the water and limited carbon substrate for microbial growth. Figure 3.4 shows Eh and water content from the sand column for the period of 3 days (09/16/06 – 09/19/06). Eh values increased in response to rainfall events but the data range is narrowly constrained from 0 to 80 mV. Water content values showed a response to rainfall as well, but also fall within a narrow range of 0.2 to 0.36 cm^3/cm^3. Due to the lack of observations of FeS_{aq} in

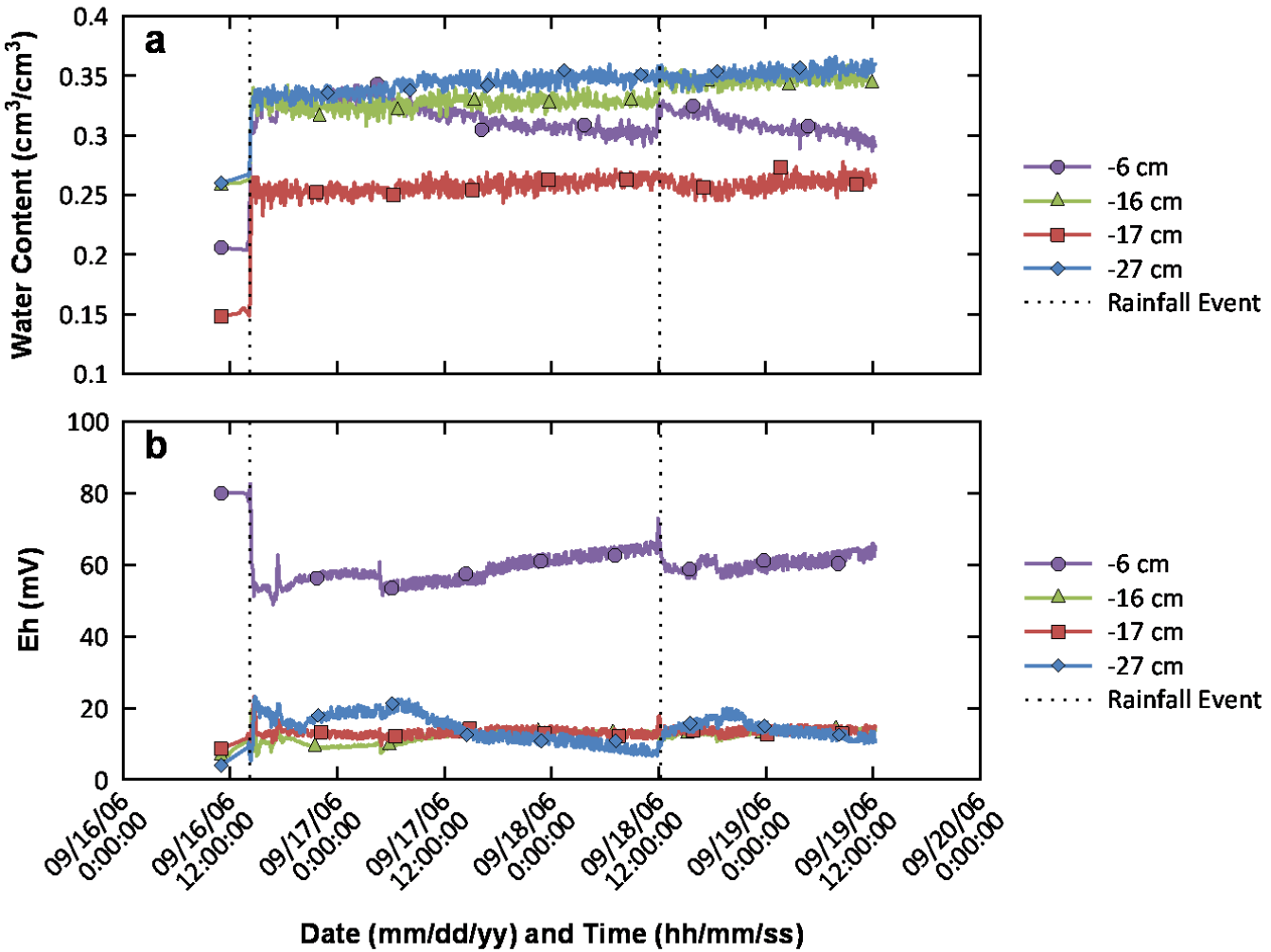

Figure 3.4 - Water content (a) and Eh (b) in the homogenous sand column over a two-day period.

this column, any further discussion of these results will be limited, but are given here as baseline values for comparisons with the other two columns.

In the loam and layered columns, FeS_{aq} was manifest on voltagrams as a single or double peak at -1.2 V (vs Ag/AgCl) (Luther et al., 2003) and are shown in Figure 3.5. Complexities in reactive particle size and a lack of complete chemical characterization prevent determination of FeS_{aq} concentration (Luther and Rickard, 2005). Instead current (A) from FeS_{aq} peaks height are reported as a semi-quantitative representation of concentration. The greatest peak heights for FeS_{aq} measured during the experiment were observed at the soil-layer interface in the layered column. Furthermore, the, the maximum peak heights, from the layered column were nearly double than those from the homogenous loam column.

It has been noted that caution should be exercised when interpreting the FeS_{aq} voltammetric signal in complex natural systems because other metal sulfide clusters (particularly copper-sulfide clusters) have displayed similar signals (Bura-Nakic et al., 2007). However, observations of sulfide, Fe^{2+}, and pryrite oxidation to SO_4^{2-} in the columns (Hansen et al., Submitted, 2011a), support the assumption that these peaks indeed represent FeS_{aq}. In addition, microprobe analyses also revealed an abundance of Fe and a lack of any other cluster forming metals (e.g. copper). Titanium was present in appreciable amounts, but has not been shown form an electroactive sulfide cluster.

In this study, the majority of FeS_{aq} peaks were single peaked. Double peaked signals were only detected in the homogenous (loam) column and are thought to represent aged (hours) FeS_{aq} (Bura-Nakic et al., 2007). The voltagram from the layered

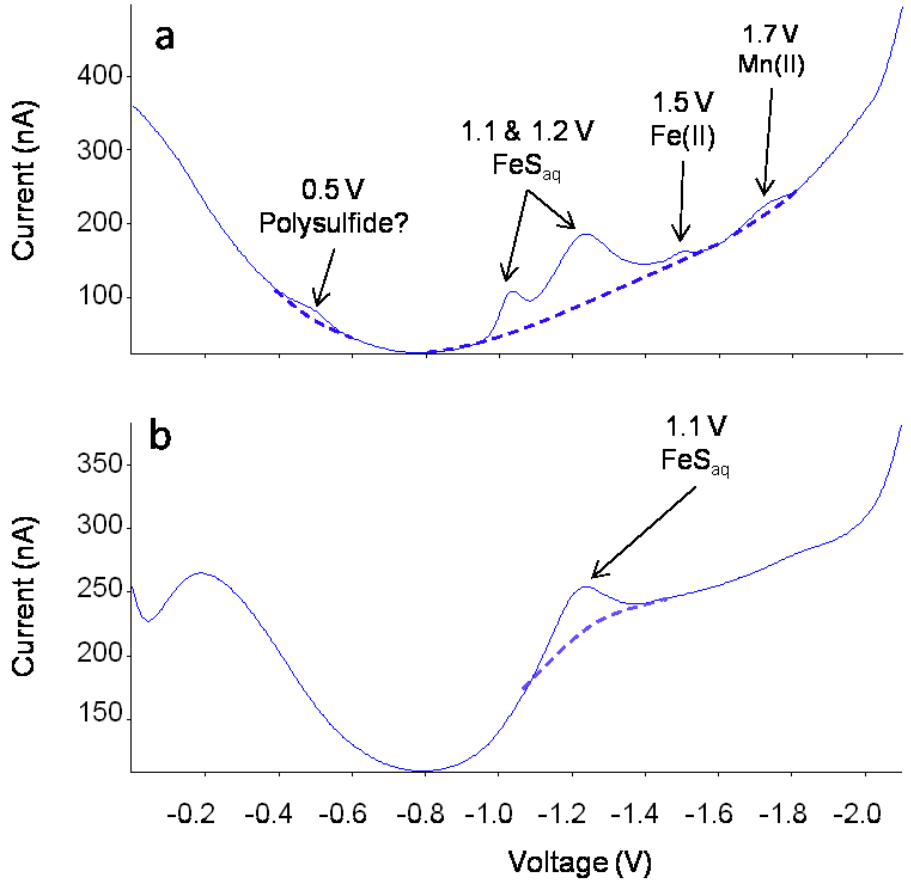

Figure 3.5 – Voltagrams of FeS clusters (vs Ag/AgCl). Voltagram (a) shows a double peak expression of FeS_{aq} centered at -1.2 V measured in the loam column. (b) shows a single peak expression of FeS_{aq} at -1.2 V measured in the layered column. Dashed line shows baseline.

column exhibits a single FeS_{aq} peak at -1.2 V (Figure 3.5a) while the voltagram from the loam column has a FeS_{aq} peak at -1.2 V, an Fe^{2+} peak at -1.5 V and Mn(II) at -1.7 V and an unknown peak at -0.5 V (Figure 3.5b). The unknown peak at -0.5V is likely a polysulfide complex (Luther et al., 2001). Assuming the system is in equilibrium, it would be expected that S(-II) and Fe^{2+}would be present in both the layered and loam columns where FeS_{aq} is observed. However, both $Fe^{2+}$and S(-II) are notably absent from the layered column (Figure 3.5a). Previous work (Hansen et al., Submitted, 2011a), has documented enhanced Fe and S reduction within the layered system. This suggests that S(-II) and Fe^{2+}were produced but were removed by precipitation or sequestered by another mechanism before detection. In fact, FeS_{aq} was only observed sporadically throughout the experiments, consistent with the interpretation that this phase may be a fleeting intermediate central to other iron-sulfur reactions.

Timing

FeS_{aq} was only observed in the last two months of the eight month long experiment. Figure 3.6 shows FeS_{aq} peak heights with time at selected sampling points from both columns as well as the occurrence of rainfall events. The difference between the early and later portions of the experiment was the frequency of rainfall events (days versus weeks). Results show that FeS_{aq} was observed when the frequency of rainfall was much higher (i.e., in the second half of the experiment). A greater regularity of water may have allowed for higher microbial activity leading to different redox conditions than was observed in the first half of the experiment. Although increased frequency of rainfall maintained high water content values, the water content alone could not explain

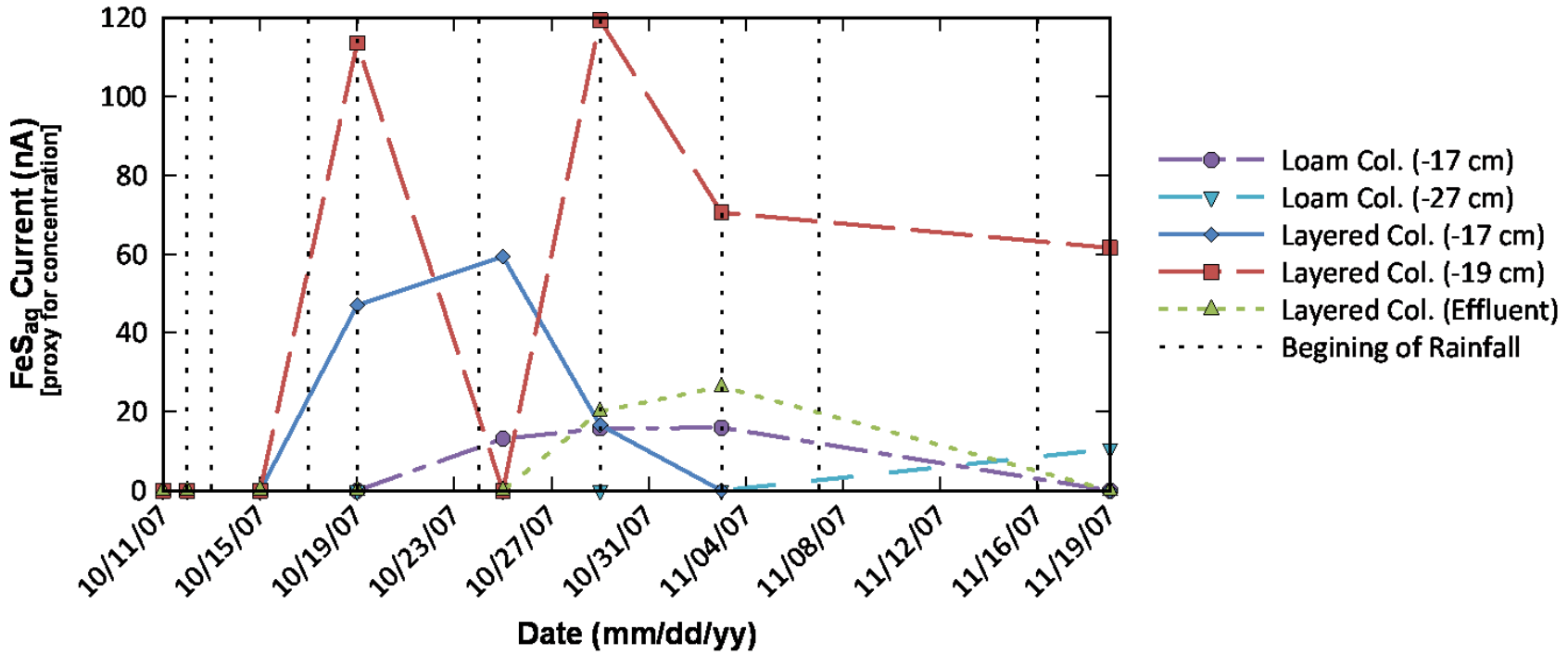

Figure 3.6 – FeS_{aq} peak currents in selected locations in the loam and layered columns. Dotted lines denote rainfall events.

the formation of FeS_{aq} as these clusters were observed at lower (~0.25 cm^3 cm^{-3}) and higher (~0.47 cm^3 cm^{-3}) saturation levels. This demonstrates that FeS_{aq} forms in unsaturated conditions and is not confined to saturated systems.

pH Effects

Another potential controlling factor on the formation of FeS_{aq} may be pH. Davison et al. (1998) showed that the FeS_{aq} signal increased with increasing pH suggesting that concentration depends on pH. However, the actual stoichiometry would control the degree to which FeS_{aq} formation is dependent on pH. The determination of a stoichiometeric value has been undertaken in many studies, but none have conclusively determined the actual value. Suggestions have ranged from Fe_2S_2 (Buffle et al., 1988), $Fe_x(HS)_{2x}$ ($x \geq 2$)(Davison et al., 1999), Fe_2SH^{3+} Luther et al. (2003), and Fe_xS_x (Luther and Rickard, 2005).

In our experiments, the range of the pH of soil pore waters in the layered column were higher (approximately 7-10) compared to the pH in the loam column (approximately 7-8.5) (Figure 3.7). Although FeS_{aq} was measured more frequently in and peak heights were greater from the layered column, there didn't appear to be any definitive correlation between the occurrence of FeS_{aq} with pH. However the pH ranges from the sediment pore waters observed in the experiment was limited and any concrete conclusions cannot be drawn from these data.

Distribution of FeS_{aq}

FeS_{aq} was most frequently observed at the soil-texture interface as shown in Figure 3.8 from 10/19/07 to 11/19/2007. In addition to the constant presence of FeS_{aq},

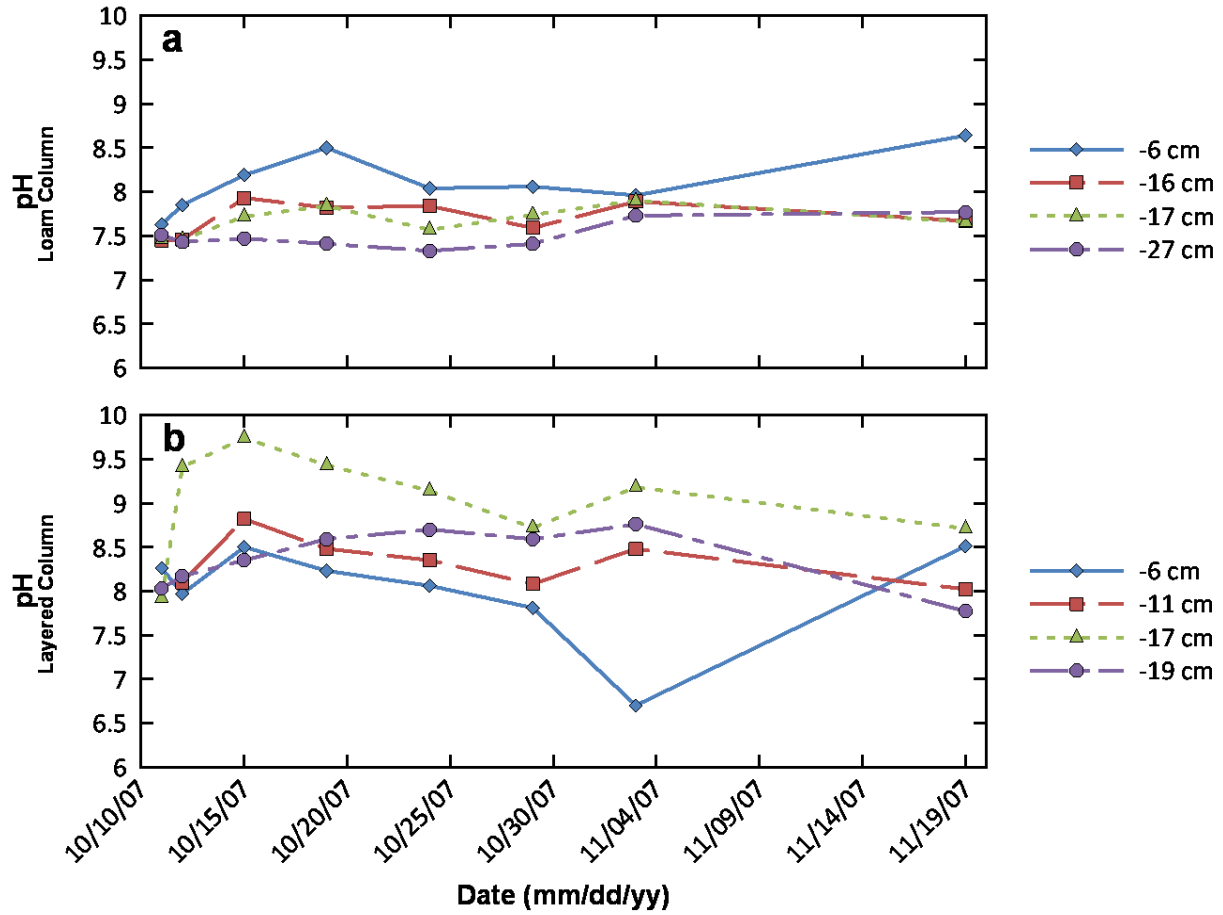

Figure 3.7 – pH in the layered and loams columns. Due to blocked sampling ports, there is no data below for locations below -19 cm in. in the layered column and none for the location at -32 cm in the loam column.

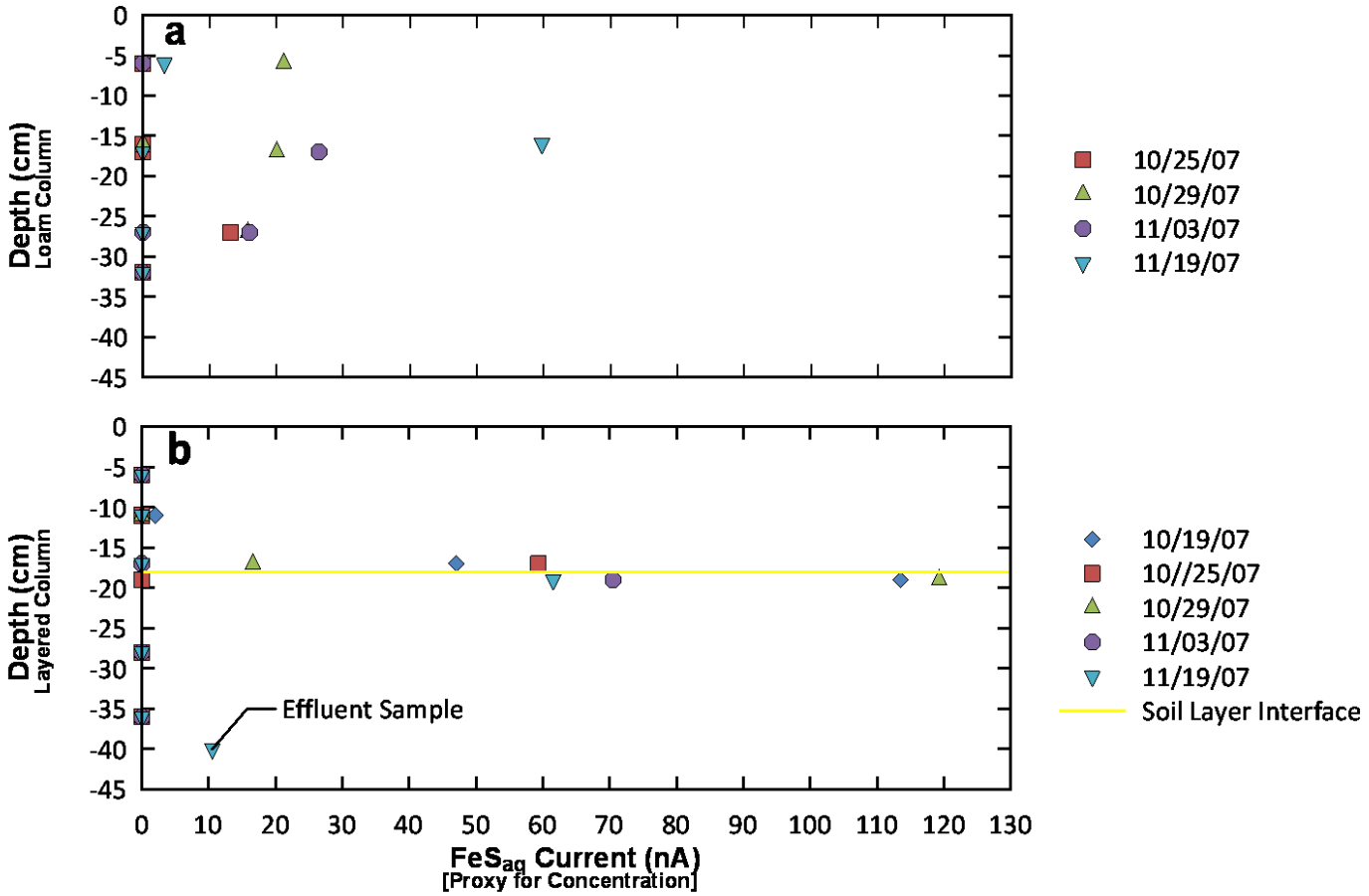

Figure 3.8 – Observed peak height currents of voltammetrically measured FeS_{aq} from the layered and loam columns. The point at -40 cm denotes samples from the column effluent.

the peak currents near the soil interface were more than double than any other FeS_{aq} measurements in the loam column. The frequent observation of larger magnitude of FeS_{aq} peaks near the soil interface corresponds well with observations of enhanced biogeochemical cycling at this same soil interface. With the exclusion of the fairly constant presence at the soil interface, the behavior of FeS_{aq} is transient and was rarely detected in the same location consecutively. Similarly, FeS_{aq} is seldom observable at multiple locations during concurrent sampling. This transient behavior is consistent with that of a fleeting intermediate and agrees well with observations that FeS_{aq} is an intermediate in pyrite formation (Rickard and Luther, 1997).

Redox Potential

Eh data from the layered column support other observations of enhanced geochemical cycling at the soil-layer interface. The data from the two lowest probes at -28 and -36 cm show that reducing conditions (negative Eh values) were fairly consistent during this half of the experiment (Figure 3.9). The data also show an increase of the Eh values by up to 80 mV each time a rainfall event occured. As the rainwater percolated through the soils, it transported dissolved O_2 with it that caused oxidation to occur and consequently the Eh increased. However, this increase only lasted several hours before the O_2 was depleted; through either chemical oxidation of reduced minerals or biologic activity which consumed the dissolved O_2 causing the Eh to decrease to pre rainfall levels.

The Eh data from the sampling location just below the soil interface (-19 cm), where the greatest concentrations of FeS_{aq} were observed provide the greatest insight on

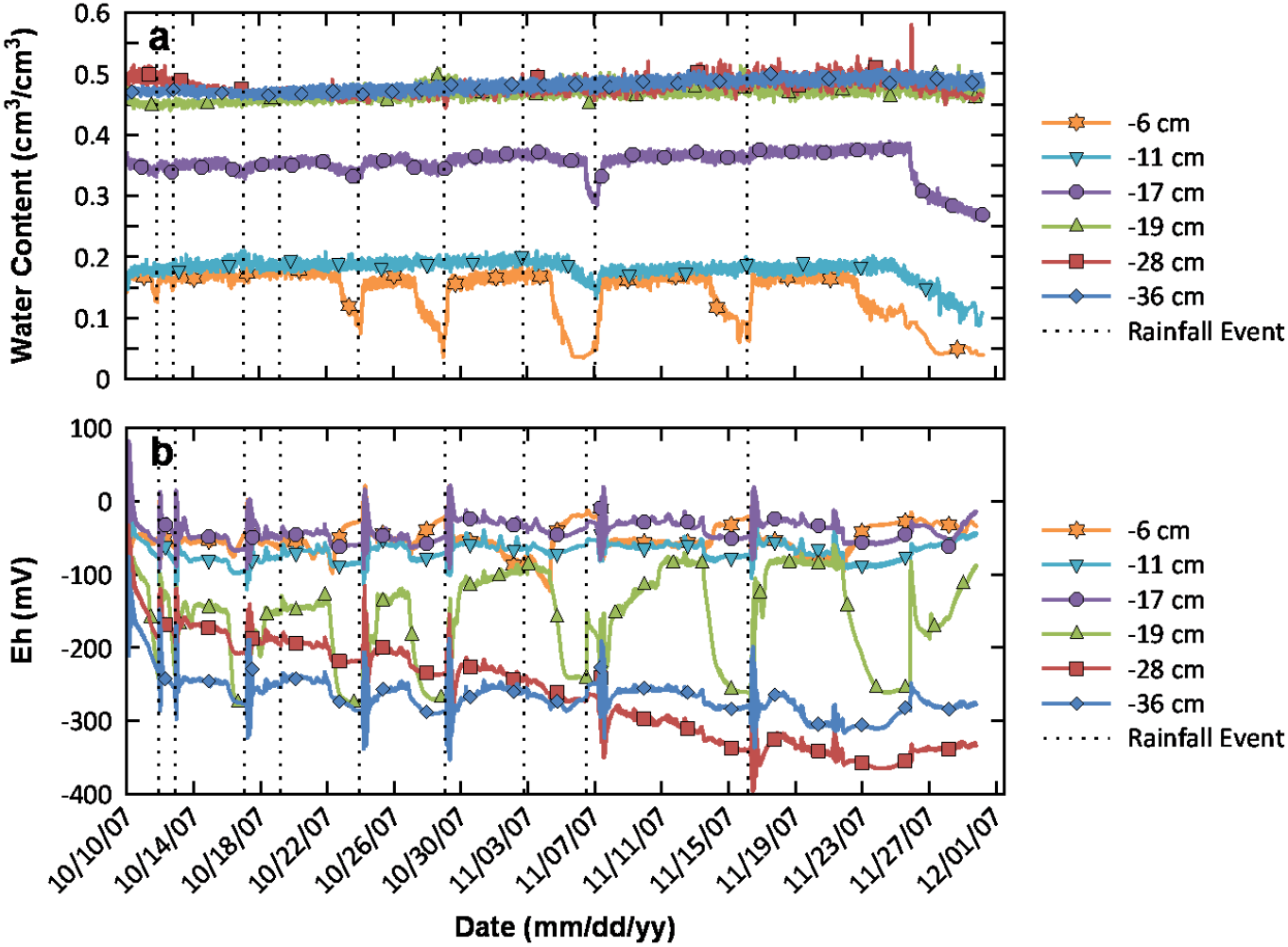

Figure 3.9 – Water content (a) and Eh (b) in the layered column.

FeS_{aq} development in soils. Similar to the data from the lower probes, the Eh values are negative which suggest reducing conditions are prevalent. However, unlike the data from the lower probes, the Eh response to rainfall is much more dramatic. The greatest observed change in Eh was a change of nearly 200 mV in response to the rainfall on 11/19/07. The amount of time that it took for the Eh to drop to the pre-rainfall values was on the order of days to a week. For example, after the rainfall event on 11/7/07, Eh values stabilized at approximately -80 mV after several days. On 11/14/07, the Eh dropped from -96 mV to -230 mV within 24 hours. This pattern of stabilization after rainfall followed by rapid drop in Eh was repeated throughout the experiment.

Although Eh is not a certain indicator of which terminal electron accepting process (TEAP) is active, the sharp drop of Eh suggests that Fe(III) and SO_4^{2-} reduction operated within a short period of time. A quick succession from Fe(III) reduction to SO_4^{2-} reduction would have supplied the Fe^{2+} and S(-II) necessary to form FeS_{aq}. The observations of greatest FeS_{aq} concentrations at the sampling location below the soil-layer interface (-19 cm) suggest that the rapid redox cycling created ideal conditions for the formation of FeS_{aq}. Ultimately, the presence of an interface between soils, wherein this behavior was observed, may have contributed to enhanced redox cycling.

In contrast to the Eh data from the layered column, Eh data from the loam column, with the exception of the -6 cm sampling location, did not vary greatly through time (Figure 3.10). Some minor fluctuation of Eh values were observed, associated with rainfall, as observed in the layered column, but the magnitude of Eh change was not nearly as great. The Eh data at -6 cm, show that Eh dropped dramatically compared to

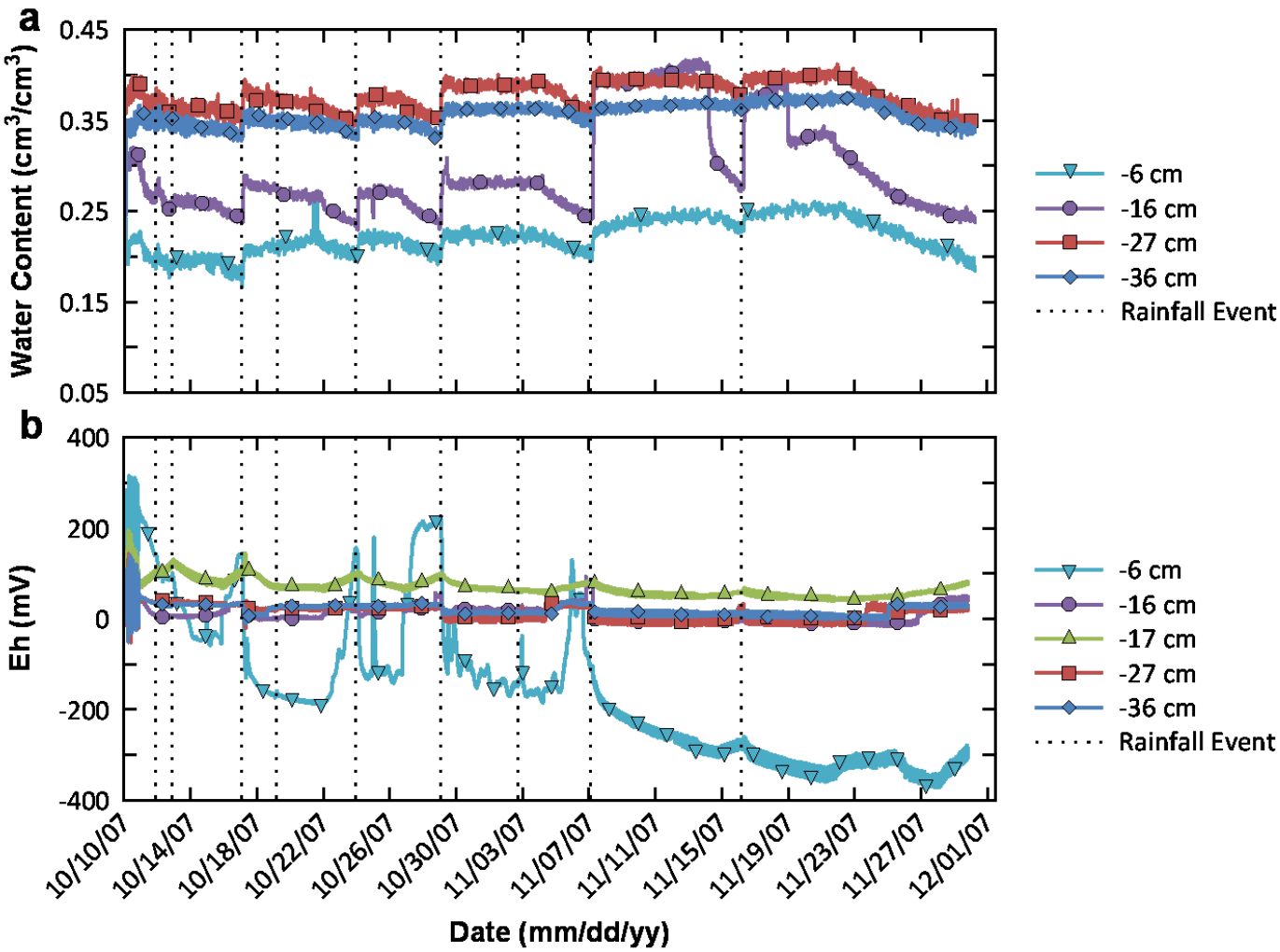

Figure 3.10 – Water content (a) and Eh (b) in the loam column.

the other sampling points in the loam column. It seemed unlikely that such negative Eh values would be associated with an area so close to the top of the column where oxygen could more readily penetration into the sediment. This suggests that the sampling location at -6 cm was located in a microenvironment where the redox environment was limited to a localized area that likely ranged in size, from the μm to cm scale. FeS_{aq} observed in the loam column likely originated from microenvironments, such as this one located at -6 cm.

Ultimately, the presence of a soil-layer interface, where frequent redox cycling of sulfur and iron occurred, created conditions suitable for the consistent production of and greatest peak heights (proxy for concentration) of FeS_{aq}. The formation of FeS_{aq} at the interface implied that instead of precipitation of an insoluble mineral in this zone, percolating water would have transported FeS_{aq} from the interface into lower areas of the soil column. FeS_{aq} was probably mineralized in the lower sections of the column as it was generally absent from the column effluent. However, Figures 3.6 and 3.8, show FeS_{aq} in the effluent and demonstrate its ability to be transported away from the vadose zone. In this study, this distance could have been as great as 40 cm, but another study has shown FeS_{aq} clusters that had been transported up to several kilometers (Rozan et al., 2000b). These results suggest that current conceptual models of iron-sulfide cycling may need to be adapted to include the possibility that Fe^{2+} and S(-II) may not rapidly precipitate as an insoluble mineral but may in fact be present in an aqueous phase subject to transport; making iron-sulfur cycling more dynamic than previously believed.

FeS_{aq} Linkages

The presence of FeS_{aq} in soils may influence soil structure which in turn may have a measured effect on the hydrologic properties of the vadose zone. In addition to the greatest peak concentration of FeS_{aq} (as manifested by largest peaks in electric current) being observed at the soil-layer interface, a greater density of soil aggregation was observed near the soil interface in the layered column than in the loam column (Hansen et al., Submitted, 2011a) and may have contributed to a decrease in hydraulic conductivity. This increase in aggregate density, at the interface correlates with the observation of the greatest concentrations of FeS_{aq} also at the soil-layer interface and suggests a relationship between the two.

Aggregates are "secondary particles formed through the combination of mineral particles with organic and inorganic substances" (Bronick and Lal, 2005). Oades and Waters (1991) found that aggregates initially form as fragments of plant material that are encrusted by inorganic materials (i.e. metal bearing minerals) which protect them from rapid decomposition. It is this initial step, wherein inorganic materials bind to the organic matter is when FeS_{aq} may play a role in aggregate stabilization. Because FeS_{aq} is reactive with organic matter (Rickard et al., 2001), it would be the first inorganic material to begin to bind to the organic matter that would eventually become the core of the aggregate. The organically bound FeS_{aq} would then facilitate further mineralization of other Fe-S minerals around the organic matter. As the thickness of inorganic minerals increased, the aggregate would then stabilize and the organic material would become

totally encrusted. In this manner, FeS_{aq} could perform a decisive role in facilitating the binding of two discordant hard and soft (Lewis) acids and bases (HSAB) species.

Microprobe analyses of soil aggregates from both columns were performed to determine their composition. Soil aggregates were largely composed of clays; organic material that ranged from microfossils to plant material; fine grained quartz and various other minerals that included: pyrite, illmanite, iron-oxides, calcite, barite, anhydrite, and apatite. Aggregates near the soil interface contained higher proportions of Fe than aggregates further away from the interface or in the loam column. This was consistent with Fe-S cycling observed at the soil-layer interface, as shown in Figure 3.9. An example of an aggregate near the soil-layer interface is shown in Figure 3.11. The first image (a) is a BSE image while the second (b) is a false-colored composite where the elements Fe, S, and Si are represented by red, green, and blue respectively. Thus blue represents quartz or feldspar; green corresponds to S, generally incorporated into organic material; yellow is iron-sulfide minerals (mostly pyrite) and red is Fe oxide or Fe carbonate. The presence of yellow (red + green = yellow) indicated that Fe and S were associated one with another in an iron-sulfur mineral. (If any two elements are present at the same location, color additive mixing would produce secondary colors.) Thus, the yellow was interpreted to be pyrite because of its thermodynamic stability and the abundance of pyrite framboids observed at higher magnification.

The false-colored image shows the preferential accumulation of Fe within an aggregate. It is not clear whether the accumulation was caused by a reaction of organic material with the FeS_{aq} clusters or whether the FeS_{aq} clusters were formed at the

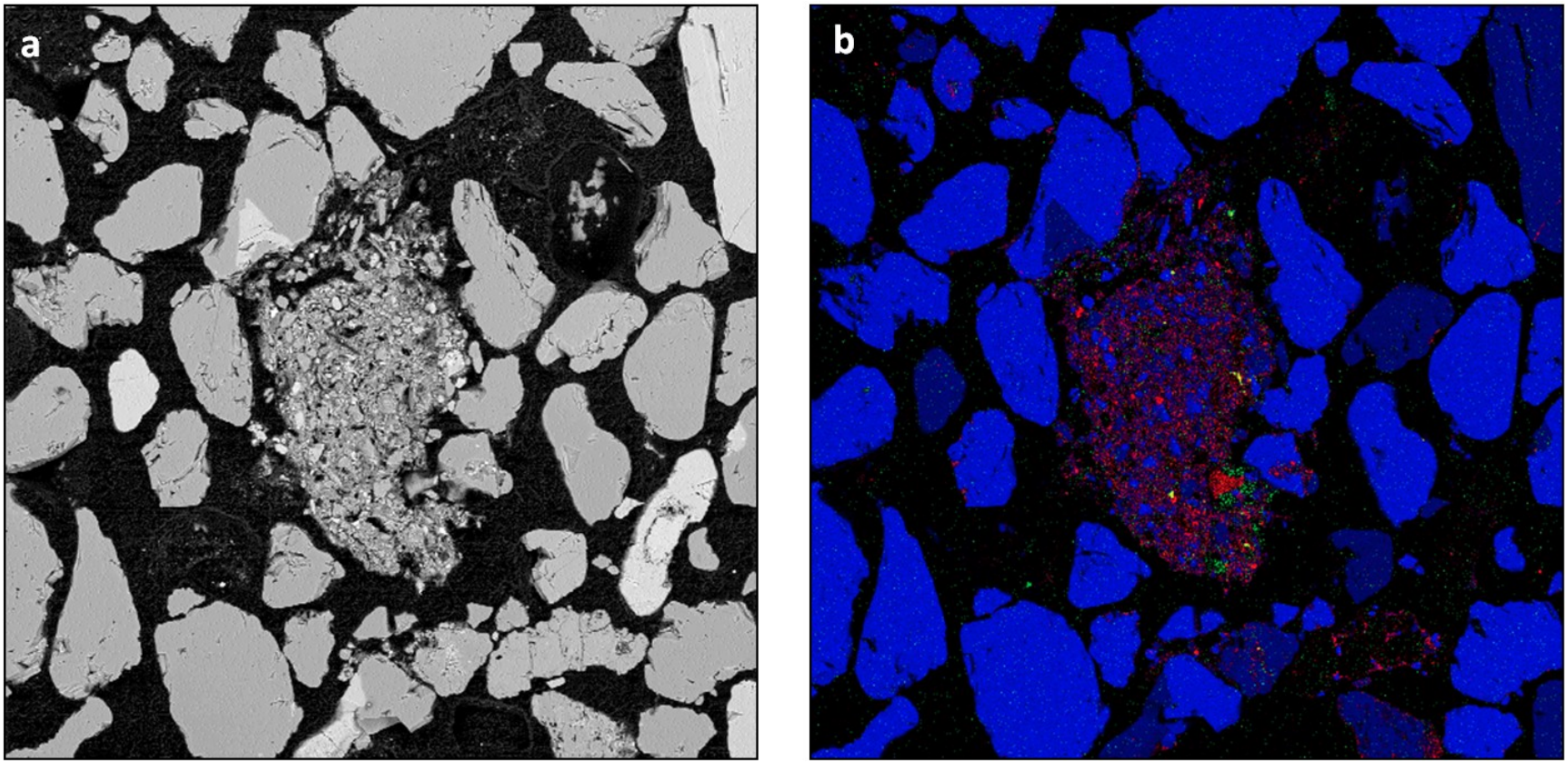

Figure 3.11 – (a) Backscattered electron image (1 mm x 1 mm) of a soil aggregate. (b) RGB false color composite of the same soil aggregate where red represents iron, green is sulfur, yellow is iron-sulfur minerals, and blue is silicon.

aggregates from the reduction of preexisting Fe or S. Furthermore, the role of Fe oxides in the formation of aggregates is unclear. The high accumulations of Fe could also have meant that Fe oxides have played an active role in creating these aggregates. If Fe oxides played a large role in aggregate formation, it does not necessarily nullify the role that FeS_{aq} played as a bridge between the organic matter and inorganic material (such as Fe-oxides).

From a hydrologic perspective, the greatest concentration of FeS_{aq} was observed at the soil interface which acted as a barrier to flow as water flowed from the sand (higher hydraulic conductivity) into the loam (lower hydraulic conductivity). As a result, iron-sulfide minerals may have precipitated near hydrologic barriers due to an accumulation of FeS_{aq} (a pyrite intermediate). Likewise these clusters were observed where soil aggregates were most densely accumulated, which could indicate they play a role in soil aggregate formation or stabilization. Ultimately, precipitation of Fe-S minerals or aggregate formation decreases hydraulic conductivity in the sediment.

Implications of FeS_{aq} in Contaminant Fate and Transport

While not enough is known about FeS_{aq} clusters to draw a definitive conclusion about the exact nature of the relationship between FeS_{aq} and soil aggregates, the observation of FeS_{aq} in the vadose zone is significant and has implications for contaminant fate and transport. In particular, the presence of a soil interface caused some unique biogeochemical and hydrologic conditions to form. From a geochemical perspective, the observation of the greatest concentrations of FeS_{aq} at the soil layer was accompanied by dramatic shifts in redox potential. This association suggests that FeS_{aq}

is not only an indicator of systems that are frequently in redox disequilibrium, but their formation is favored in these conditions. Certainly, observations of FeS_{aq} in environments such as tidal flats (Taillefert et al., 2007), estuaries (Rickard et al., 1999), and deep ocean hydrothermal vents (Luther et al., 2001) where redox conditions are out of equilibrium, are consistent with observations from this study.

FeS_{aq} have been shown to be stable in the absence of FeS_m (Rickard, 2006) and O_2, which allows for their transport from their source (Luther et al., 2003) as was observed in this study. Iron (II), often thought to be immediately precipitated in sulfide rich areas, may be instead transported via FeS_{aq} clusters through such regions. Toxic metals may be substituted into FeS_{aq} clusters (Rozan et al., 2000b) and modify predictions of chemical fate and transport which may alter perceived ecologic risks in the environment.

Up to this point in time, the existence of an aqueous iron-sulfide specie has not been integrated into current conceptual models. However, as this study has shown, there may be many roles that these clusters play in the environment. They may be indicators of redox disequilibrium or enhanced biogeochemical cycling, predictors of decreased hydraulic conductivity, or may help to more accurately predict the fate and transport toxic metals and contaminants in not only in the vadose zone but all other environments. As our knowledge of FeS_{aq} increases, revising contaminant fate and transport models to include FeS_{aq} may prove vital to increase the accuracy of and benefits derived from these models.

CONCLUSIONS

Evidence for aqueous iron-sulfide clusters was, to our knowledge, observed for the first time in a vadose zone system. FeS_{aq} peaks were centered at -1.2 V (vs. Ag/AgCl) and both double and single peaks were observed. FeS_{aq} was observed in both a homogenous loam column and a layered sand-over-loam column. However, the greatest FeS_{aq} peak heights (semi-quantitative proxy for concentration) were detected near the soil interface which is consistent with observations of enhanced biogeochemical cycling occurring at soil boundaries.

The soil-layer interface was also zone of frequent and large magnitude fluctuations in Eh. At a minimum, the presence of FeS_{aq} was indicative of areas that were frequently in disequilibrium with respect to redox conditions and geochemical cycling. Thus FeS_{aq} in unsaturated sediments may serve as indicator of these types of systems that are frequently out of equilibrium. Consequently, this knowledge can be used in characterization of a soil system where contaminant fate and transport is of concern.

This study also demonstrated the ability of the FeS_{aq} to be transported through and out of the vadose zone. This observation is especially pertinent when coupled with results from Rozan et al. (2000b) that discovered that toxic metals such as silver, cadmium, mercury, or lead can be incorporated in FeS_{aq} clusters and may subsequently transported beyond the vadose zone. Thus the incorporation of an aqueous iron-sulfide specie into current conceptual models should be considered to account for complexities not presently taken into account especially in contaminant fate and transport.

Observations of FeS_{aq} also have implications for hydrologic fluxes in the vadose zone. FeS_{aq} was also observed in association with soil aggregates containing high amounts of Fe. Because FeS_{aq} has been shown to be reactive with organics (Rickard et al., 2001), it is likely that FeS_{aq} was attracted to the organic constituents within soil aggregates and further cemented and stabilized these aggregates. The nature of the relationship between FeS_{aq} and soil aggregates is unclear, but FeS_{aq} may affect the formation of soil aggregates that may ultimately change the hydraulic properties of the soil. This suggests that the presence of FeS_{aq} impacts not only biogoechemical cycling, but also the physical and flow properties of sediments, which has broader implications for the fate and transport of all chemical constituents in the system.

CHAPTER IV

BIOGEOCHEMICAL CYCLING IN HETEROGENEOUS UNSATURATED SOILS: A COMPARISON BETWEEN LIVE AND STERILIZED SEDIMENTS

INTRODUCTION

In subsurface systems, the vadose zone may act as a buffer to mitigate contamination of groundwater through biodegradation of contaminants as they seep into the subsurface (McCarthy and Zachara, 1989). However, the dynamic nature and unique combination of physical, hydrologic, and biogeochemical conditions in the vadose zone make it difficult to predict contaminant fate and transport in these systems (Malecki and Matyjasik, 2002). In particular, the rapidly changing hydrologic conditions of the vadose zone suggest that these systems are often in a state of redox disequilibrium (Marshall et al., 2009). This disequilibrium is critical to the prediction of chemical fate and transport in subsurface systems because redox state affects the form, mobility, and toxicity of many chemical constituents.

A controlling factor on the redox state is the metabolic activities of microorganisms, which first consume oxygen and then a succession of alternate terminal electron acceptors to support their growth using a variety of carbon sources (Chapelle, 2001; Lovley, 1991; Lovley and Goodwin, 1988; Stumm and Morgan, 1996). The sequence of pertinent terminal electron accepting processes (TEAPs) in order of decreasing redox potential and energy yield is generally aerobic respiration, denitrification, iron reduction, sulfate reduction, and methanogenesis. Within the vadose

zone, reducing conditions can occur and include methanogenesis (Bekins et al., 2005; Oliver et al., 2003; Salminen et al., 2006; Smith et al., 2003) despite an intermittently close proximity to oxygen at the soil/atmosphere boundary. However, what controls the distribution of TEAPs in the vadose zone is not fully understood.

Redox conditions within the vadose zone depend on geochemistry (e.g.., pH, availability of terminal electron acceptors and donors) and microbial activity, but are also controlled by hydrologic conditions. This physical-chemical process linkage was demonstrated by Bekins et al. (2005) who observed an increase in methanogenic activity in the areas with more than 20% volumetric water content. Higher water content in the sediment likely impedes oxygen diffusion and causes microorganisms to shift to different TEAPs. Furthermore, these linkages can be altered by soil heterogeneity (layers, lenses, and macropores) in the vadose zone because these structures have the capability to influence water flow through sediment (e.g. funnel flow) and water distribution (e.g. perched water table). Consequently, TEAPs in heterogeneous systems may be different than homogenous systems due to the presence of soil structures and rapidly changing hydrologic conditions.

A study by Hansen et al. (see D.J. Hansen et al., Enhanced biogeochemical cycling and subsequent reduction of hydraulic conductivity associated with soil-layer interfaces in the vadose zone, Submitted to Journal of Environmental Quality, 2011)(Hereafter referred to as Submitted, 2011a) evaluated the effects of a soil layer by comparing homogenous sand and loam columns to a sand-over-loam layered column and found considerably greater biogeochemical activity in the layered column than in either

of the homogeneous columns. For example, the greatest concentrations of SO_4^{2-}, NH_4^+, Fe^{2+} and the highest numbers of Fe(III) and SO_4^{2-} reducing bacteria were observed near the textural interface between the sand and loam layers. This enhanced biogeochemical activity over time led to a decline in hydraulic conductivity in the layered column.

The importance of soil lenses in unsaturated flow has been documented through both field and laboratory studies (Bradford et al., 2003; Ward et al., 1997). The hydraulic properties of the lens material, regardless of whether or not it has higher or lower permeability than the surrounding matrix, will alter flow paths and fluxes through the subsurface. The alteration of flow occurs because of the textural interface between soil materials, which results in differences of pore-size distribution and/or wettability characteristics, creates capillary barriers (Bradford et al., 2004). Low permeable lenses may act as barriers to vertical flow which may change water flow direction as well as accumulate water in areas of the vadose zone (Gwo et al., 1996).

Because lenses affect water flow in the soil medium, they also affect contaminant transport. At the Hanford nuclear production site, soil lenses ranging from a few millimeters thick to a few cm thick, were shown to alter fluid flow and cause a significant horizontal spread of fluids. In response to this finding, these fine-grained lenses have been targeted as optimal sampling points to locate contaminants (Ward et al., 1997). Similarly, modeling studies observed ponded water above clay lenses and noted that lenses tend to dilute chemical concentrations delivered to the water table by spreading out the delivery rate (Bosch et al., 2001). Furthermore, lenses in the subsurface contribute to the challenge of the successful application of in-situ

bioremediation efforts because the lenses redirect application of electron acceptor treatments (e.g. nitrate solutions or air sparging) away from their intended target (McCray and Falta, 1996).

Clearly, lenses in the vadose zone have considerable potential to influence contaminant transport. However, many studies have solely focused on fluid flow dynamics caused by lenses, but have neglected the potential for biodegradation. For example, many studies assume or have observed ponded water overlying soil lenses, but only a few have considered the redox implications of this ponded water in such a scenario (Fendorf and Jardine 2003). Although, there is a sense of the microbial distribution surrounding lenses (Holden and Fierer, 2005), it is unknown how microbial activity may influence geochemical or hydrologic condition near the lenses. A better understanding of the links between microbial, geochemical, and water flow processes in the vicinity of soil lenses will provide improved insight on the critical mechanisms affecting contaminant fate and transport in the vadose zone. Ultimately, the understanding of these major coupled biogeochemical mechanisms can be applied such that remediation strategies can be improved upon because they account for the effects of soil heterogeneity in a contaminated system.

The primary objectives of this study were to (a) evaluate the effects of microbial activity on geochemistry and hydrology in heterogeneous soil system by comparison between a microbially-live and a killed-control column and (b) characterize the linked biogeochemical and hydrologic process occurring in the presence of soil lenses under a

range of hydrologic top boundary conditions (i.e. rainfall, evaporation) and bottom boundary conditions (i.e. free drainage, various water table heights).

MATERIAL AND METHODS

Soil Physical and Chemical Properties

Soils were collected adjacent to a capped municipal landfill on the floodplain of Canadian River in Norman, Oklahoma, USA. A leachate plume has developed over years in the aquifer beneath the landfill which has caused the landfill and surrounding areas to be studied extensively (Cozzarelli et al., 2000). Two soil types were collected from this site: an alluvial, fine-grained sand from the banks of the Canadian River and an organic-rich loam, from a wetland flanking the landfill, which has been intermittently exposed to the leachate plume. Soils were air-dried, ground, and sieved (0.8 mm mesh) before use in the experiments. Result from physical analyses of the soils are located in Table 4.1.

Soil pH and electrical conductivity were determined in a 1:2 soil:deionized water extract. After water was added, samples were stirred and allowed to equilibrate for a minimum of 30 minutes and then measured for pH and conductivity (Rhoades, 1982; Schofield and Taylor, 1955). A 1 N KCl solution was employed to extract nitrate-nitrogen (NO_3^--N) from soils. The nitrate was reduced to nitrite using a cadmium column before being measured using spectrophotometry (Keeny and Nelson, 1982). Mehlich III extractant was used to extract P, K, Ca, Mg, Na and S from the soils and were subsequently measure by inductively coupled plasma (ICP) atomic spectrometry

Table 4.1 - Soil textural (USDA classification), organic carbon, bulk density, and hydraulic conductivity values of the two soil types collected from Norman, OK and used in soil columns.

	Textural Properties (Percent Weight)								SWRC Van Genuchten Parameters			
Soil	0.5 – 0.2 mm (Medium Sand)	0.2 – 0.05 mm (Fine Sand)	0.05 – 0.002 mm (Silt)	<0.002 mm (Clay)	% Organic Carbon	Bulk Density (g/cm^3)	Porosity (%)	Saturated Hyd. Cond. (cm/min)	θr (cm3/cm3)	θs (cm3/cm3)	α (1/cm)	n (unitless)
Sand	33.6	62.9	2.2	1.3	0.02	1.4	43.4 %	0.636	0.027	0.321	0.0318	1.60
Loam	46.5		39.5	12.5	1.5	1.0	58.5 %	0.141	0.015	0.385	0.0202	1.86

Table 4.2 - Chemical analyses results of the two soil types used in the experiments. Concentrations are generally expressed in plant available values.

Soil	pH	Cond (uS/cm)	NO3-N (mg/L)	P (mg/L)	K (mg/L)	Ca (mg/L)	Mg (mg/L)	S (mg/L)	Na (mg/L)	Fe (mg/L)	Mn (mg/L)
Sand	8.5	106	4	4	19	1,688	56	40	154	2.83	1.28
Loam	7.9	1,030	2	5	86	24,833	802	694	374	88.35	19.27

(Mehlich, 1978; Mehlich, 1984). Iron and Mn were extracted using a diethylene triamine pentaacetic acid method and then measured by ICP (Lindsay and Norvell, 1978). The results of these analyses are on the whole, interpreted as plant-available concentrations and are listed in Table 4.2.

Column Setup

Before the soils were packed into the experimental columns, the large-sized (> 8 mm) organic matter (sticks, leaves, snail shells) was separated from the sediment and discarded. This separation of organic matter from sediment was performed to ensure consistency of the soil-water properties. However, this absence of the large organic matter from the packed soils slightly altered the bulk density of the packed soils compared to the soils from the collection site. In order to maintain a constant bulk density, the ground soils were packed with a piston compactor in 3 cm increments into columns made of clear acrylic pipe (15 cm in diameter and 60 cm in height).

The two soil columns were constructed and identically packed to create horizontally offset lenses of an organic-rich loam within a matrix of sand (Figure 4.1). The upper lens was centered at -19 cm depth and the lower lens was centered at -42 cm. Lenses were approximately 7.5 cm thick. Although the two columns were packed in an identical manner and with identical materials, the sediment placed in the second column was γ-irradiated to eliminate microbial life within the soils. Thus the second column acted as a killed-control lens column (KLC) in contrast to the other live lens column (LC).

At the bottom of the column, a nylon mesh fabric was glued to a densely perforated (one 0.19 cm diameter hole per 1.16 cm^2) polyvinyl chloride (PVC) plate to prevent the loss of soil while also permitting water to drain from the column. This plate was then fastened to the base of the column cylinder. The column was drained by a cone-shaped cap that funneled water into a single vinyl tube (1.9 cm outer diameter). Thus, the bottom sediment was exposed to the atmosphere via the vinyl tubing and the nylon mesh (Figure 4.1). From a hydraulic standpoint, this bottom boundary was considered to be a seepage face wherein water flowed across the nylon mesh once the overlying sediment became saturated. The glues/epoxies (hot melt adhesive, Adhesive Technologies Inc., Hampton, NH and Silvertip Gel Magic Adhesive, System Three, Auburn, WA) employed in the column construction were used only after it was determined that they did not leach chemicals (e.g. acetate, formaldehyde, etc) in solution after being soaked in deionized water for 48 hours after they had cured.

The top of the column was open to atmosphere. Rainfall simulators, constructed of a PVC reservoir and 18 gauge needles, were placed above the columns to introduction precipitation to the sediment. A digitally-controlled peristaltic pump (Cole-Parmer, Vernon Hills, IL) distributed rain-water solution from a sealed nalgene carboy to the rainfall simulators. Fabric drapes were mounted above the columns and were only removed during sampling. These drapes prevented light from entering the column and thus limited the growth of photoautotrophic microorganisms. The temperature of the lab where experiments were conducted was kept at 22º ± 2º C.

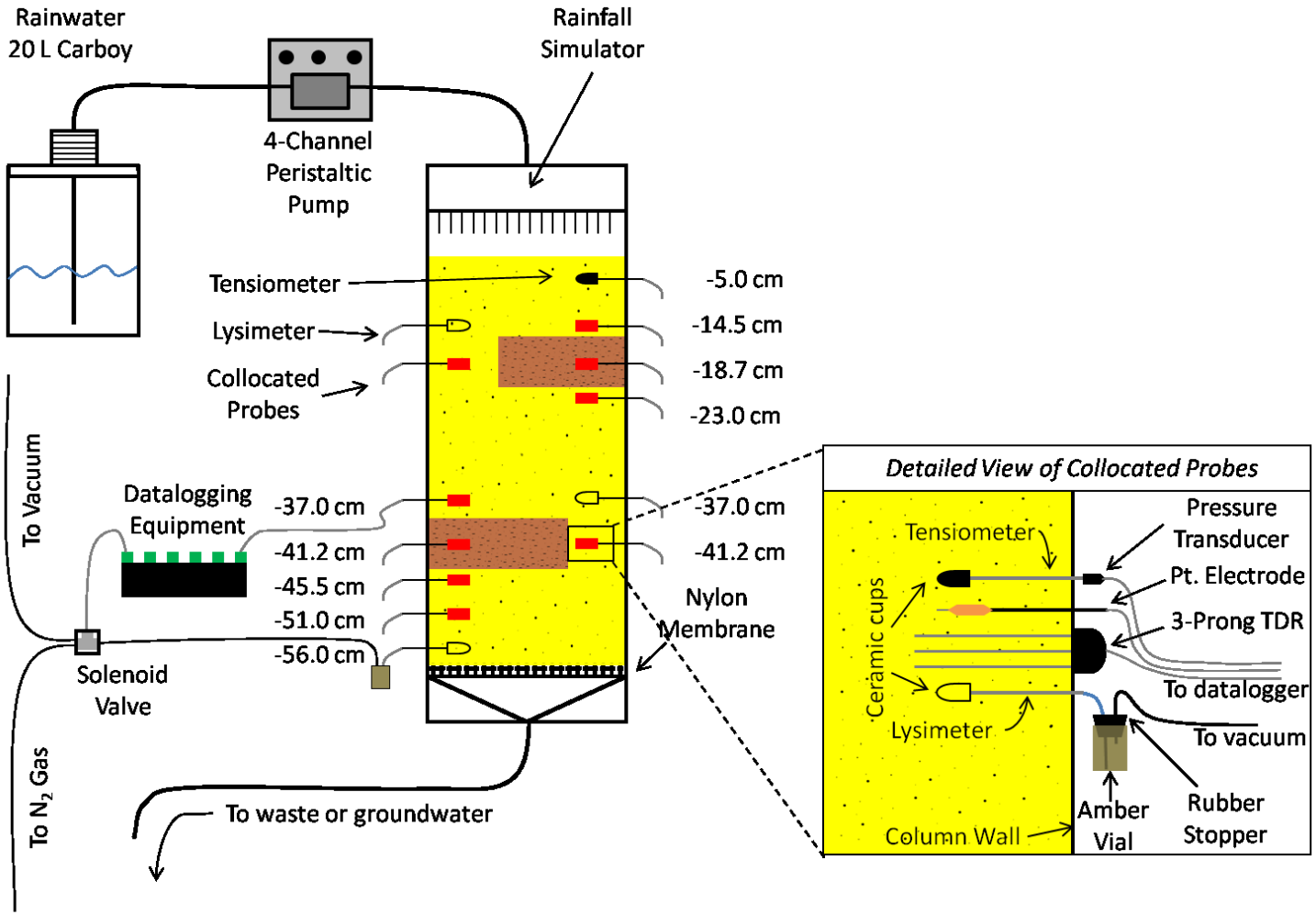

Figure 4.1 – Experimental column setup.

Soil Sterilization

Sediment used in the killed-control column was γ-irradiated at the Nuclear Science Center at Texas A&M University. Before sterilization, the soils were dried, ground, and sieved and placed into gallon-sized, freezer, zip-top plastic bags. These soil-filled bags were triple bagged to prevent contamination after sterilization. Sediment was irradiated with a cumulative dose of 2.687 Mega Rad over a three day period using a 1 MW TRIGA research reactor. After irradiation, sediment was stored in a chest freezer at a temperature of -15 ºC. Before the column was packed, any column materials (e.g. acrylic pipe, probes, etc) that would come in contact with the sterilized sediments were soaked in 3% hydrogen peroxide and/or were exposed to a germocidial lamp (UV-C light) to kill any microorganism. During column packing, the sterile column was surrounded by an enclosure composed of plastic sheets to prevent airborne contamination. As an additional safeguard, a germocidial lamp was placed within the enclosure to maintain sterile conditions.

Experimental Conditions

One of the goals of the study was to analyze the response of the columns to a range of hydrologic conditions that are common to the vadose zone. A frequent and rigorous sampling regimen was implemented to capture geochemical responses to hydrologic variations. The experiments took place from 11/2008 to 03/2009. The first analysis investigated the geochemical response to rainfall. The second analysis examined the response of an introduction of oxygenated groundwater to the columns. The third

analysis assessed the geochemical response to the introduction of a deoxygenated SO_4^{2-} rich groundwater. Finally, the last analysis examined the effects of raising of the elevation of the water table. A figure of groundwater heights and rainfall events over time are shown in Figure 4.2 and a table of experimental conditions are listed in Table 4.3.

Measurements and Automation in Data Collection

Columns were equipped with collocated sets of measurement probes installed at various depths. Three-pronged time domain reflectometry (TDR) probes (5 and 8 cm long, 1.1 cm spacing between rods) were used to measure soil water content. Tensiometers with 6 mm diameter ceramic cups (SDEC 220, SDEC France) were equipped with pressure transducers (Microswitch, Soil Measurement System, Tucson, AZ) for automated soil-water pressure monitoring. Data from pressure transducers were monitored using equipment from Campbell Scientific, Inc. (Logan, UT), consisting of a CR10X data logger with an AM 16/32A multiplexer. TDR probe data were collected using a TDR100 with SDMX50 multiplexers and a CR10X.

To prevent the introduction of oxygen into the sediments through lysimeter sampling ports, the ports were flushed with N_2 gas for 5 seconds every 20 minutes when not sampling. Two-way solenoid valves (Granzow, Charlotte, NC) connected to a manifold regulated the introduction of N_2 gas and vacuum to lysimeters. A three-way solenoid valve switched the manifold between the N_2 gas and vacuum. Solenoid valves

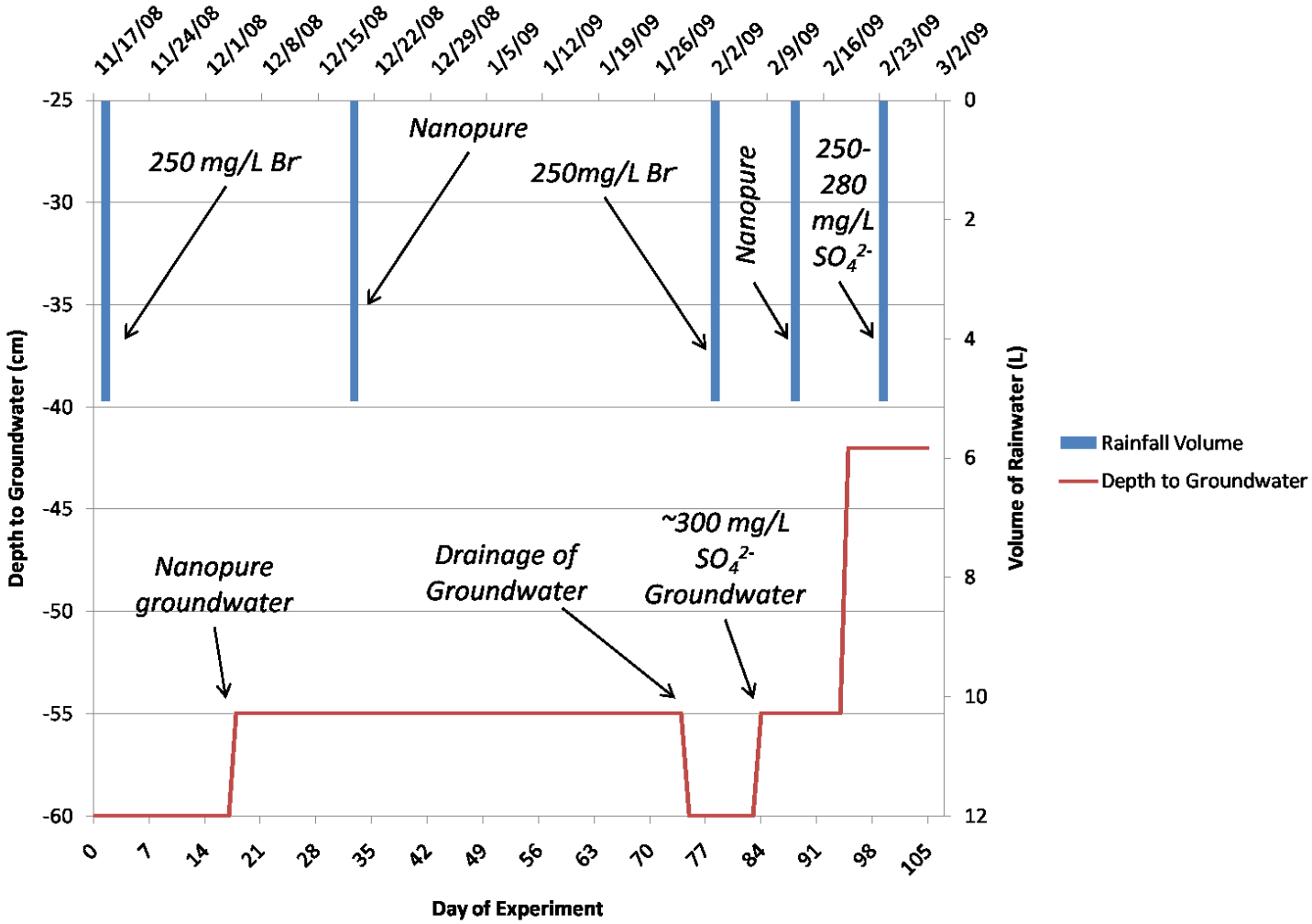

Figure 4.2 - Graph of rainfall events and groundwater heights over time.

Table 4.3 - Column experimental conditions for each sampling round. Abbreviations used in table: B.C. – boundary condition, W.T. – water table.

Sampling Round	Date (Day of Experiment)	General Description	Top Flow B.C.	Top Chemical Transport B.C.	Bottom Flow B.C.	Bottom Chemical Transport B.C.
001	11/18/2008 (1)	Rainfall	39.7 cm^3/min Flux	Nanopure pH ~ 5 125 mg/L Br,	Free Drainage	N/A
002	11/25/2008 (8)	Day 7 response to rainfall	Atmospheric	N/A	Free Drainage	N/A
003	12/02/2008 (15)	Rainfall	10 mL/min Flux	Nanopure pH ~ 5	Free Drainage	N/A
004	12/05/2008 (18)	Day 1 after W. T. Intro	Atmospheric	N/A	W.T. @-55 cm	Oxygenated Nanopure
005	12/06/2008 (19)	Day 2 after W. T. Intro	Atmospheric	N/A	W.T. @-55 cm	Oxygenated Nanopure
006	12/07/2008 (20)	Day 3 after W. T. Intro	Atmospheric	N/A	W.T. @-55 cm	Oxygenated Nanopure
007	12/09/2008 (22)	Rainfall w/ water table	20 cm^3/min Flux	Nanopure pH ~ 5	W.T. @-55 cm	Oxygenated Nanopure
008	12/10/2009 (23)	Day 1 response to rainfall	Atmospheric	N/A	W.T. @-55 cm	Oxygenated Nanopure
009	12/16/2008 (29)	Day 7 response to rainfall	Atmospheric	N/A	W.T. @-55 cm	Oxygenated Nanopure
010	2/03/2009 (78)	Rainfall	20 cm^3/min Flux	Nanopure pH ~ 5 250 mg/L Br^-	Free Drainage	N/A
011	2/09/2009 (84)	Day 1 after W. T. Intro	Atmospheric	N/A	W.T. @-55 cm	N_2 purged Nanopure w/ ~ 350 mg/L SO_4^{2-}
012	2/10/2009 (85)	Day 2 after W. T. Intro	Atmospheric	N/A	W.T. @-55 cm	N_2 purged Nanopure w/ ~ 350 mg/L SO_4^{2-}

Table 4.3 – continued

Sampling Round	Date (Day of Experiment)	General Description	Top Flow B.C.	Top Chemical Transport B.C.	Bottom Flow B.C.	Bottom Chemical Transport B.C.
013	2/11/2009 (86)	Day 3 after W. T. Intro	Atmospheric	N/A	W.T. @-55 cm	N_2 purged Nanopure w/ ~ 350 mg/L SO_4^{2-}
014	2/12/2009 (87)	Rainfall with W. T.	10 cm^3/min Flux	Nanopure pH ~ 5	W.T. @-55 cm	N_2 purged Nanopure ~ 350 mg/L SO_4^{2-}
015	2/13/2009 (88)	Day 1 after rainfall	Atmospheric	N/A	W.T. @-55 cm	N_2 purged Nanopure ~ 200-250 mg/L SO_4^{2-}
016	2/19/2009 (94)	Day 7 after rainfall	Atmospheric	N/A	W.T. @-55 cm	N_2 purged Nanopure ~ 200-250 mg/L SO_4^{2-}
017	2/20/2009 (95)	Day 1 - Heightened W. T.	Atmospheric	N/A	W. T. @ -42 cm	N_2 purged Nanopure ~ 200-250 mg/L SO_4^{2-}
018	2/21/2009 (96)	Day 2 - Heightened W. T.	Atmospheric	N/A	W. T. @ -42 cm	N_2 purged Nanopure ~ 200-250 mg/L SO_4^{2-}
019	2/22/2009 (97)	Day 3 - Heightened W. T.	Atmospheric	N/A	W. T. @ -42 cm	N_2 purged Nanopure ~ 200-250 mg/L SO_4^{2-}
020	2/23/2009 (98)	Rainfall with Heightened W. T.	10 cm^3/min Flux	Nanopure pH ~ 5	W. T. @ -42 cm	N_2 purged Nanopure ~ 200-250 mg/L SO_4^{2-}
021	2/24/2009 (99)	Day 1 response to rainfall	Atmospheric	N/A	W. T. @ -42 cm	N_2 purged Nanopure ~ 170-230 mg/L SO_4^{2-}
022	3/2/2009 (105)	Day 7 response to Rainfall	Atmospheric	N/A	W. T. @ -42 cm	N_2 purged Nanopure ~ 170-230 mg/L SO_4^{2-}

were manually controlled during sampling, but were controlled by two relay drivers (SDM-CD16AC) attached to CR10X between sampling.

Geochemical Analyses

One challenge with water sampling in the vadose zone is that only very small sample volumes can be collected without altering flow paths and hydrologic conditions. This created geochemical analysis limitations. To minimize disruptions in hydrology in the soil columns during sample collection, less than 7 ml total was collected at each sample location for all geochemical analyses. Lysimeters made from 6-mm diameter ceramic cups (SDEC 220, SDEC France), aluminum tubing, and amber catchment vials were used for *in situ* sampling. Capillary electrophoresis (CE) was used for the determination of major anions (Cl^-, Br^-, SO_4^{2-}, and NO_3^-), and NH_4^+ (Báez-Cazull et al., 2007) due to low sample volume requirements (Goettlein and Blasek, 1996). Each sample analysis consumed ~1 nL. Approximately 250 μL solution samples were collected to ensure sufficient volume for replicate runs. Anion samples were preserved with formaldehyde while NH_4^+ samples were flash frozen immediately upon collection. Alkalinity (determined by Gran plot (Gran, 1952)) and pH were measured together.

Sulfide, and Fe^{2+} as well as FeS_{aq}, H_2O_2, and Fe(III) complexed with an organic ligand (Fe^{3+}-L) were quantified voltammetrically using a hanging drop mercury electrode (Metrohm, Switzerland). The voltage range scanned was from 0 mV to -2100 mV using square wave voltammetry with the following parameters: pulse height 15 mV, step increment 4 mV, frequency 100 mHz, and scan rate 80 mV/S.

Hydrologic Modeling

Forward hydrologic modeling of a rainfall event was performed using HYDRUS 2D/3D (Simunek et al., 2008). The top boundary condition was set as 0.11 cm/min. The bottom boundary was defined as seepage face that simulates outflow at the bottom of laboratory columns. The duration of the rainfall event was 18 hours. Sand and loam soil property values used to model water flow were: $\theta_r = 0.027$ cm^3/cm^3, $\theta_s = 0.321$ cm^3/cm^3, $\alpha = 0.0318$/cm, n = 1.60, $K_s = 0.636$ cm/min and $\theta_r = 0.015$ cm^3/cm^3, $\theta_s = 0.385$ cm^3/cm^3, $\alpha = 0.0202$/cm, n =1.86, $K_s = 0.141$ cm/min respectively. These parameters were obtained from laboratory analysis using tempe pressure cells for the soil-water characteristic curve parameters and a constant head permeameter for the saturated hydraulic conductivity.

Multivariate Statistical Analysis

Geochemical and hydrogical data were statistically analyzed in JMP software (Version 8, SAS Institute, 2008). Attempts to normalize data by several transformation methods (natural logarithm, square root, inverse, and power data transformations) were unsuccessful, therefore only nonparametric tests were utilized in the data analysis.

Factor analysis was chosen for data analysis because of its ability to reveal patterns in datasets consisting of multiple variables. In essence, it seeks to reduce the complexity of the dataset size by identifying a smaller number of variables, called factors, which reveal the interrelationships among the larger number of variables. These

factors are not directly observable, nor expressed in terms of the original variables, but serve to reveal links in seemingly unrelated data. The original variables used in the statistical evaluations were the geochemical parameters (Cl^-, Br^-, SO_4^{2-}, NO_3^-, Fe^{2+}, FeS_{aq}, H_2O_2, S^{2-}, Fe^{3+}-L), matric potential, and water content data.

The objective of using multivariate statistics was to identify the most important of these geochemical and physical parameters in live lens column (LC) and killed lens column (KLC). Principal component analysis (PCA) was the method used to discriminate the importance and correlations between the chemical and physical processes/properties. A PCA analysis creates reduced sets of variables (geochemical and physical parameters) that simplify interpretation of large datasets. The names applied to these sets are principal components or principal factors and are commonly interchanged. In this study, these sets will be referred to simply as factors; dropping the word principal for the sake of brevity. Each factor has a correlation matrix that reveals any associations between the variables. The values in this correlation matrix are called “loadings”.

However, these PCA-derived factor loadings (correlations) may fail to reveal the underlying structures with the dataset (Suk and Lee, 1999). To eliminate this concern, an orthogonal rotation of the PCA-derived factors can be executed to produce a new set of loadings that facilitate interpretation. The rotation method used in this study was a Varimax rotation. This rotation results in high loadings for a few variables while the remainder will be near zero in each factor. An examination of the loadings within each factor allows for the interpretation of dominant physical and chemical processes acting

in each factor. These factor analyses also allow for comparison of the major geochemical and physical processes occurring in LC and KLC.

RESULTS AND DISCUSSION

Visual Indications of Redox Differences Between Columns

Visual examination of the sediments over time within each column indicated considerable differences between redox processes. Figure 4.3 shows time-series photographs of the top lens in both columns. In the live lens column (LC), areas of blackened sediments, indicative of Fe and S redox cycling, were observed in the central regions of the lenses. Reddish iron oxide bands were also observed near the edges of the lenses. The bands were likely formed as Fe^{2+}, produced in the center of lenses, diffused toward the outer limits of the lenses and were oxidized and immobilized as Fe(III) minerals. As the experiment progressed through time, these Fe-oxide bands expanded in size and their color became more pronounced. Conversely, the killed-control column (KLC) was devoid of any visual indications (blackened sediment or Fe-oxide bands) of redox cycling throughout the duration of the experiment.

Careful inspection of the spatial arrangement of the iron oxide bands reveals that their shape parallels the shape of the textural interface between the sand and loam. Furthermore, the distance between the iron-oxide bands and the textural interfaces are generally constant. The band-to-interface spacing at the top of the upper lens is approximately 3 cm. These spacings on the side and bottom edges of the lens are 2 cm. Similar distances were also observed around the edges of the lower lens.

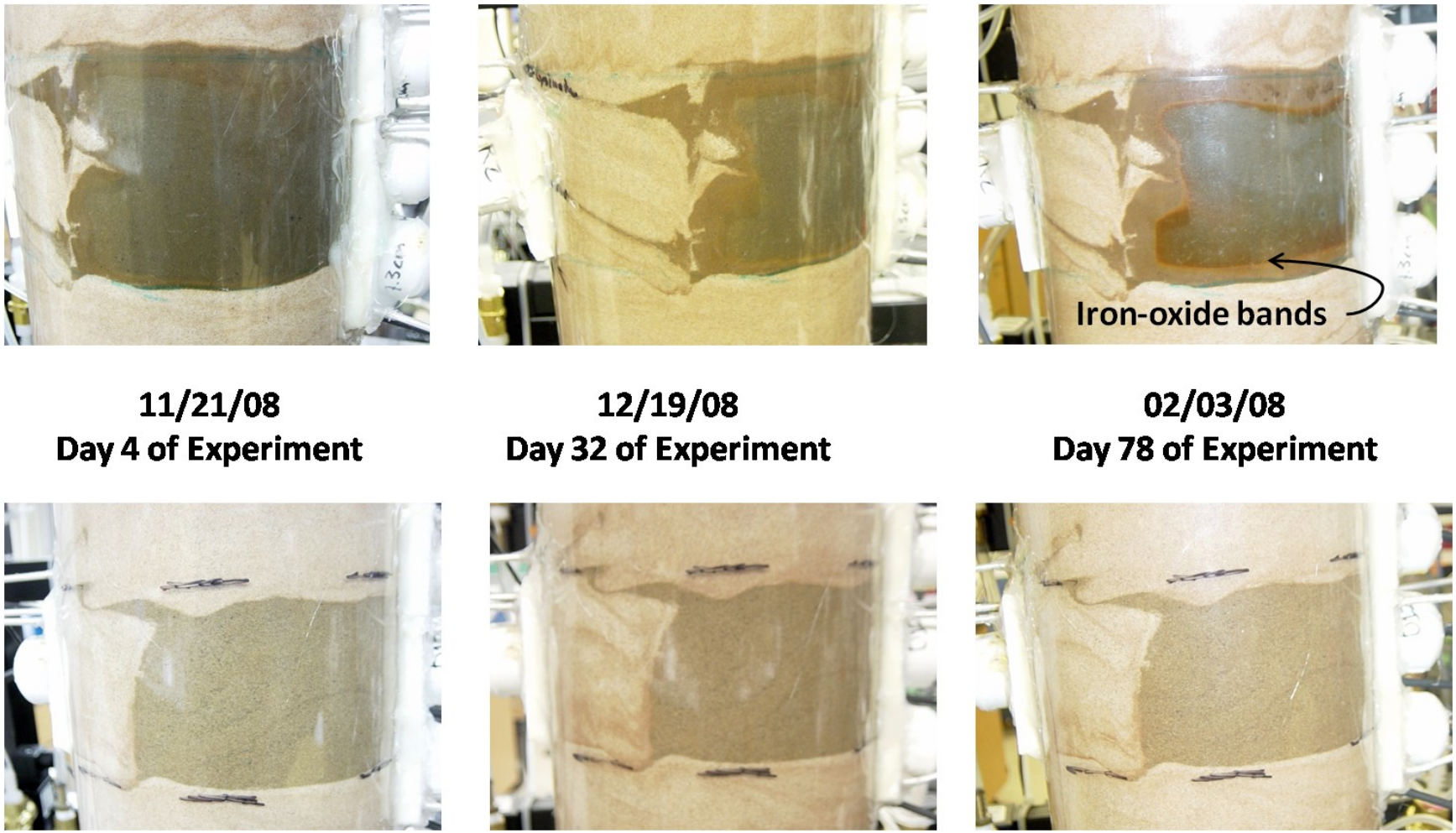

Figure 4.3 - Time series photographs of the upper lenses in the lens column (top) and the killed-controlled column (bottom). The progressive development of a sharp redox interface in the lens column is marked by reddish iron oxide bands.

Iron-oxide Band Formation

The regular spaced band-to-interface distances suggest there is a dominant process controlling this pattern. Diffusion of O_2 into the lens seems most probable considering the oxidization process that created the Fe-oxide bands. Unfortunately, accurately calculating diffusion in unsaturated sediment can be problematic due to charged soil particles (Gulliver, 2007), varying levels of water saturation (Porter et al., 1960), and tortuosity (Weerts et al., 2001). In this study, complexity is added by the presence of a capillary barrier created at the textural interface between the sand matrix and loam lens. This capillary barrier would have maintained high water content in the surrounding sediments (Yanful et al., 2003), which subsequently limited high concentrations of O_2 from diffusing into the lens. Concentrations of O_2 diffusing through water saturated sediment are 30 times less than O_2 in air (Mbonimpa et al., 2003). While O_2 diffusion was not calculated due to the aforementioned challenges, the location of iron-oxide bands was thought to represent an equilibrium point between O_2 entering into the lens and Fe^{2+} diffusing out from the central Fe(III) reducing areas in the lens.

There is a slight difference between the band-to-interface distance in top side of the lenses (3 cm) and the bottom and side of the lenses (2 cm). This difference may be attributed to water flow and dispersion and not to a variation in oxygen diffusion. As water flowed downward into the lens and would have retarded upward diffusion of Fe^{2+} and thus the distances at the top of the lenses are greater than the sides or bottom where the dominant process was more diffusion controlled than dispersion.

Effect of Lens on Hydrology and Geochemistry

Numerical forward modeling of vadose zone water flow through the columns at the onset of the experiment confirm the water flow around the lenses and slow flow through the lenses as shown in Figure 4.4. The flow velocity shows how water velocity increased as water was directed around the lenses. It also shows the low velocity of water that passed through the lenses.

Spatial trends of the geochemical measurements also agree with the water flow modeling. During rainfall, the chemical signatures below the lens demonstrate water had moved out of the lenses into the sand 1 cm below. Alkalinity (as reported as HCO_3^- concentrations) during rainfall was higher than what is normally observed at the sampling location in the sand. For example, in LC during rainfall, alkalinity in the lens was 421.4 mg/L (day 22 of experiment). At the same time, the alkalinity was much higher (317.3 mg/L) at the sampling port below the lens compared to the background levels of 207.6 mg/L (day 20 of experiment). This demonstrates that water was being flushed out of the lens downward, but that the concentrations had been diluted as the water mass exited the soil lens. Similar to the alkalinity trend, Fe^{2+} was observed below the lenses only during rainfall suggesting it was transported out of the lens where it was almost always present during measurement. Figure 4.5 shows the concentrations of these chemical constituents collected from a sampling port (located at -45.5 cm) below the lower lens - before, during, and after a rainfall event. An additional spike in Fe^{2+} concentration (day 29 of experiment) was also observed and likely originated from the groundwater below where Fe^{2+} was also present (data not shown).

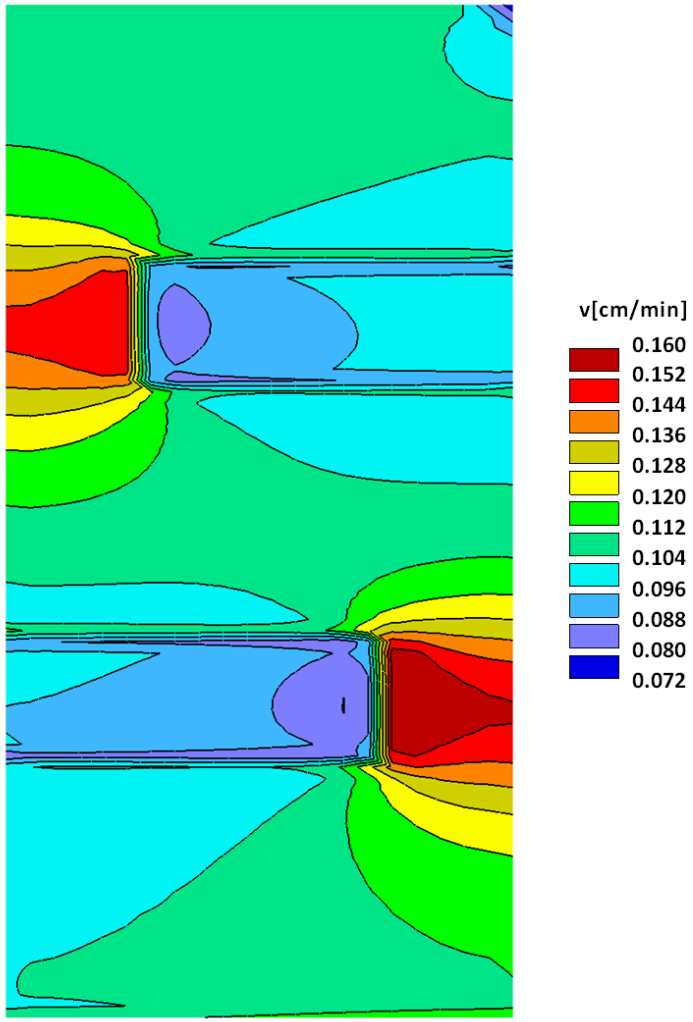

Figure 4.4 - Numerical forward modeling, flow velocity results, during rainfall with a rate of 0.11 cm/min.

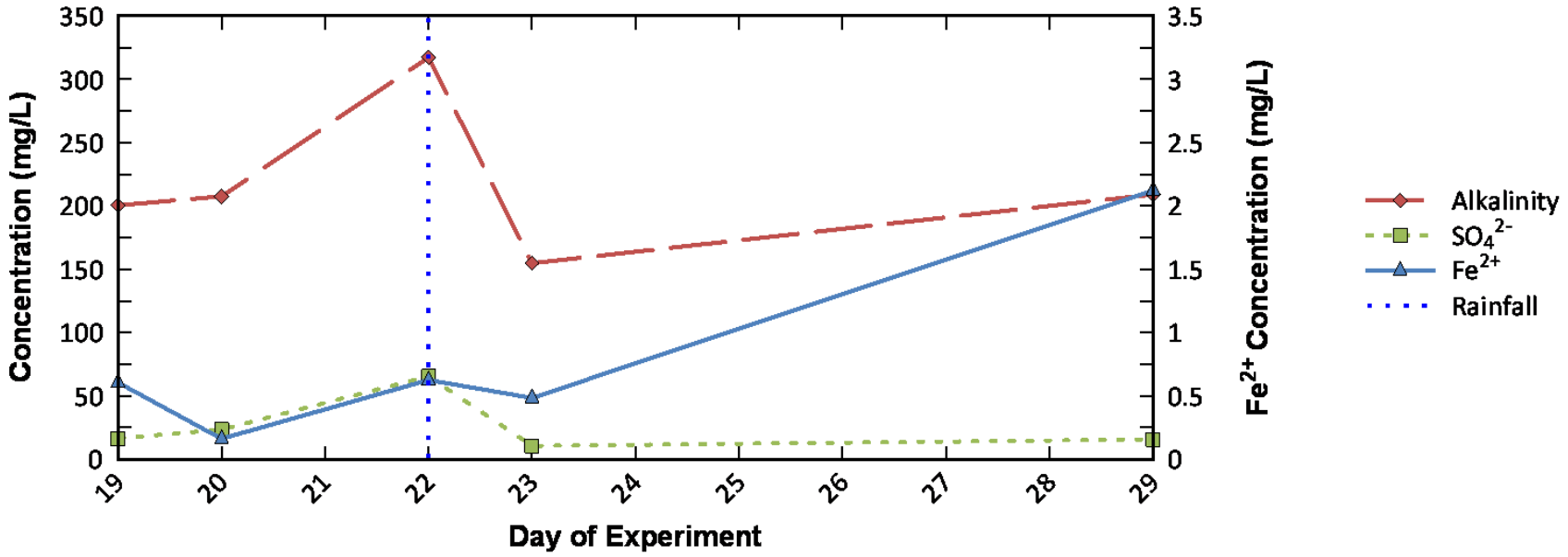

Figure 4.5 - The increase in Alkalinity, SO_4^{2-} and Fe^{2+} in response to rainfall.

Role of Interfaces on Microbiology

There are many types of interfaces, all of which may be important in natural systems and include water-sediment, sediment-sediment, redox, or chemical interfaces (Báez-Cazull et al., 2007). The development of the Fe-oxide bands created a geochemical interface that likely influenced the locations where microbial community numbers increased during the 4-month long column experiments. For example, the Fe-oxide bands in the soil lenses represent an interface between areas of contrasting textural and redox conditions and an abundance of electron acceptor (Fe(III)). It would thus be advantageous for Fe-reducing bacteria to colonize this area as it would provide conditions ideal for metabolism and growth. Other studies also confirm interfaces to be ideal localities for microbial prosperity with observed heightened microbial numbers (Brockman and Selker, 2004; Fredrickson et al., 1997b; Hansen et al., Submitted, 2011a; Madigan et al., 1997b).

Within LC, both chemical and physical interfaces were created. A redox interface was marked by the iron-oxide bands where reducing conditions prevailed within the limits of the bands and oxidized conditions prevailed outside of the bands. A physical interface was created by the juxtaposition of the sand and loam soils which created capillary barriers.. Microbial enumerations from Hansen et al. (Submitted, 2011a) showed the highest numbers of Fe(III) and SO_4^{2-} reducing bacteria at a textural interface between sand and loam within a layered soil system. For example, most probable number (MPN) analysis showed that numbers of SO_4^{2-} reducers at the interface between the sand and loam were 2.2×10^4 cells/g soil while numbers of SO_4^{2-} reducers in

homogenous sediments were 9.2×10^1 cells/g. Thus, these results suggest that the largest microbial community numbers were located in close proximity to the soil textural interface at the edges of the lens, and near the Fe-bands located at the outer bounds of the lens.

Statistical Analyses

The creation of Fe-oxide bands in LC and not KLC suggests that the geochemical processes in the columns were different. The dataset collected during the four month experimental timeframe contained 14 chemical and hydraulic parameters. Extracting data trends and understanding dominant processes proved difficult with a traditional graphical analysis. Multivariate statistical analyses, which have been valuable in analyzing in other complex systems (Baez-Cazull et al., 2008; McGuire et al., 2005; Suk and Lee, 1999), were employed to help identify and interpret the processes occurring in the two columns.

The initial investigative method to explore the dataset was to determine if any correlations existed between any of the variable pairs. A nonparametric test, Spearman's rank order correlation test was used. The test returns a correlation value (*rho*) between ±1 where the strongest correlations are nearest to ±1. Before this test was run, data were standardized using z-scores to avoid problems arising from different scales among the variables. The z-score is calculated by subtracting the individual raw score by the mean of the population which is then divided by the standard deviation of the population.

In analysis of small datasets, correlations that have $p < 0.0001$ would normally have been considered significant. However, large samples tend to produce low *p*-values when the actual correlations are low and not actually statistically significant (Baez-Cazull et al., 2008). Therefore, only pairs with Spearman's rank *rho* or correlative values greater than 0.5 and p-values < 0.0001 were considered significant. Under these criteria, there was a single significantly correlated pair in KLC; water content and matric potential (ρ=0.6326 and $p < 0.0001$). Likewise, only one variable pair was found to be significant in the LC; water content and Fe^{2+} (ρ=0.5270 and $p < 0.0001$). These correlations were not unexpected and agreed well with accepted principles, but failed to provide any further information about the significant processes occurring in the columns. Therefore supplementary statistical tests were used to derive more pertinent information.

Factor analysis (PCA) was used to identify and compare the dominant physical and chemical processes occurring in LC and KLC by assigning variables to factors. Factor selection was determined based on Eigenvalues greater than 1 according to the Kaiser Criterion (Kaiser, 1960). Factor loadings were orthogonally rotated before any analysis. Loadings that were greater than ±0.75 were considered to be strongly correlated within the factor. Loading values between ±0.5 and ±0.75 were considered moderately correlated. Values below ±0.5 were considered nonsignificant (Wayland et al., 2003). Sign designation indicates either a positive or a negative correlation to other variables within the same factor. Based on loadings, each factor was interpreted as a process that was likely to be associated with the significant variables in the factor.

Factor Analysis of the Lens Column (LC)

Principal component analysis and ensuing orthogonal factor rotation reduced the lens column dataset to five factors. Each of these factors from LC are numbered with Arabic numerals. Factors from KLC will be numbered with Roman numerals to differentiate between factors from LC. Two other variables (Fe^{3+}-L and H_2O_2) not observed in KLC were included in the PCA. In total, the five factors accounted for 75.1% of the dataset variability. These rotated factor patterns are listed in Table 4.4. Based on the loadings between variables, each factor was assigned a dominant geochemical or physical process.

Factor 1

Factor 1 (F_1^{LC}) was characterized by strong loadings on Cl^- (0.853), SO_4^{2-} (0.779), and Fe^{2+} (0.784). Matric potential (-0.695) and S^{2-} (0.617) showed moderate loadings in the factor 1 as well. This factor accounted for 28.6% of the variability of the dataset. The linked processes associated with this factor were water flow through the lenses, iron-sulfide mineral oxidation/SO_4^{2-} mineral dissolution and Fe(III) and SO_4^{2-} reduction. It is striking that greatest amount of variability of the dataset is associated with the lens which demonstrates the degree to which the lens is acting as biogeochemical hotspot. The variables (concentrations of Cl^-, SO_4^{2-}, Fe^{2+}, $S^{2-}$and matric potential) with strong and moderate loadings are shown over time Figure 4.6.

Visual and chemical analysis both show that Fe^{2+} and S^{2-} were being produced within the lenses. The stronger loading of Fe^{2+} compared to S^{2-} may have been related to the formation of FeS minerals. If more Fe^{2+} was being produced than S^{2-}, the sulfide

Table 4.4 - Live lens column factor analysis and interpretations. The five factors represented 75.1 % of total variability.

Parameter	Factor 1 (28.6 %)	Factor 2 (15.4 %)	Factor 3 (12.6 %)	Factor 4 (10.0 %)	Factor 5 (8.5 %)
Std Cl^-	**0.85**	0.24	0.02	0.01	0.12
Std Br^-	0.00	-0.07	-0.14	0.08	**0.78**
Std SO_4^{2-}	**0.78**	0.34	0.00	-0.04	0.21
Std NO_3^-	-0.08	0.06	**0.62**	-0.21	0.38
Std Fe^{2+}	**0.78**	0.32	-0.02	0.37	0.01
Std FeS_{aq} I	-0.04	-0.03	**0.88**	0.17	-0.10
Std FeS_{aq} II	0.01	-0.04	**0.87**	-0.14	-0.02
Std Fe^{3+}-L	**0.62**	-0.42	-0.04	-0.10	-0.25
Std S^{2-}	0.30	**0.88**	-0.01	0.02	0.00
Std H_2O_2	0.29	**0.88**	-0.02	0.09	0.01
Std pH	-0.20	-0.14	-0.29	0.02	**-0.72**
Std HCO_3^-	0.20	-0.01	-0.17	**0.69**	0.40
Std Matric Potential	**-0.70**	-0.27	0.12	0.40	-0.14
Std Water Content	-0.17	0.13	0.00	**0.88**	-0.11
Geochemical/ Hydrologic Interpretation	Fe(III) and SO_4^{2-} reduction, FeS Oxidation/SO_4^{2-} mineral dissolution, water flow through lenses	Fe^{2+} Oxidation / organic complexation	FeS_{aq} production and transportation	Water Flux / Carbonate dissolution	Rainwater Transportation

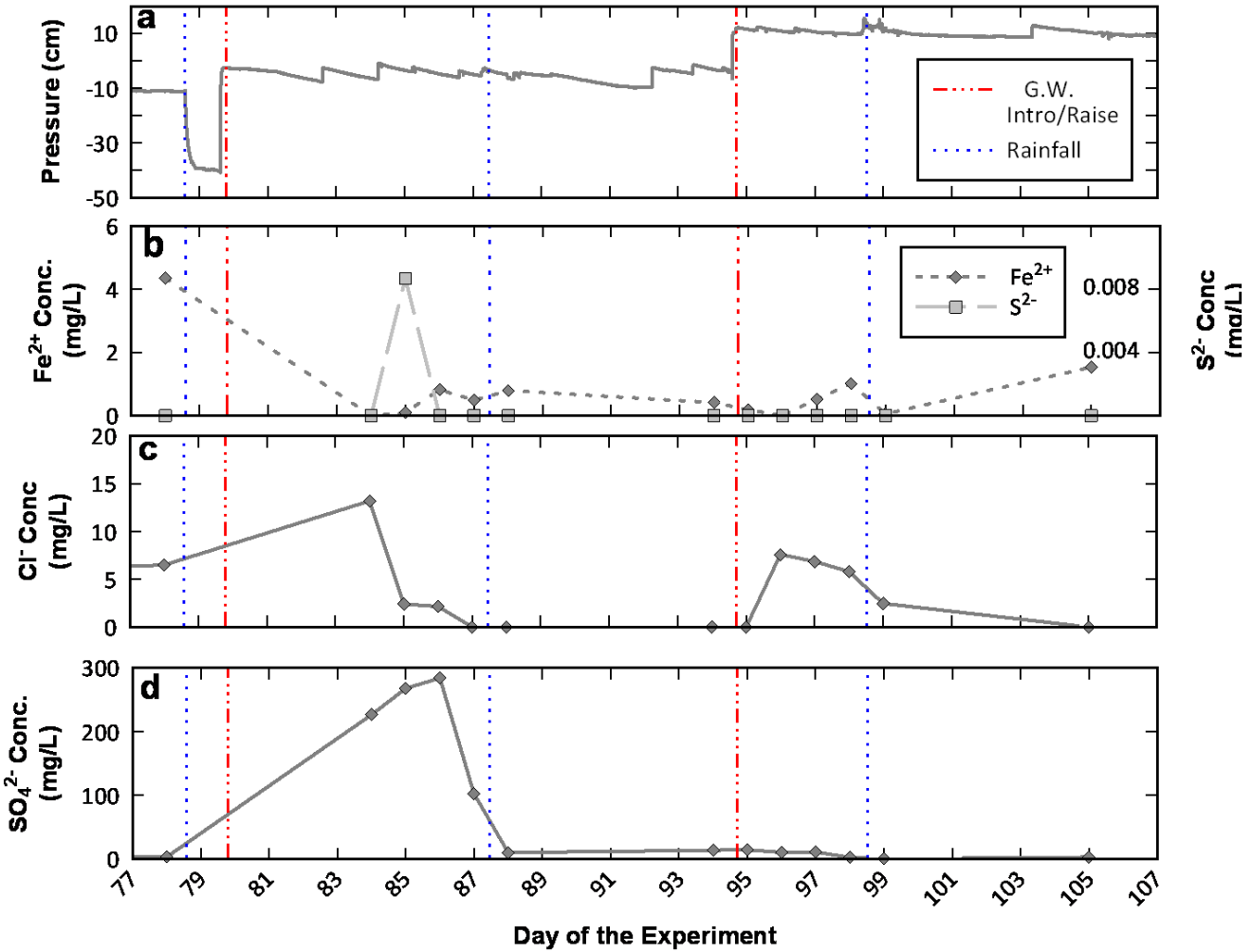

Figure 4.6 - Variables from Factor I of the lens column over time from the sampling location at -45.5 cm (directly below the lower lens).

would be the limiting factor in iron-sulfide mineral precipitation. This would also result in excess Fe^{2+} that would be measurable while there would be apparent absence of S^{2-}. Sulfide was also observed in the water table in the absence of Fe^{2+} which may have caused the correlation to be weakened somewhat.

The two principal sources of SO_4^{2-} in the system were believed to be oxidation of iron-sulfide minerals and dissolution of sulfate-bearing minerals ($CaSO_4$ and $BaSO_4$). Sulfate was evolved from oxidation of iron-sulfide minerals at the fringes of the lenses by the rainwater moving through the column. Although oxidation could be caused abiotically or biologically (Lowson, 1982; Moses and Herman, 1991; Moses et al., 1987), it is more probable that as the oxygen-rich rainwater entered the top of the lens it abiotically oxidized the Fe-sulfide minerals and produced Fe-oxide minerals and SO_4^{2-}. Evidence of this reaction can observed by presence of Fe-oxide minerals at the fringes of the lenses (Figure 4.3) and high SO_4^{2-} concentrations observed in the core or center of the lens transported from the lens fringe. Additional mechanisms of SO_4^{2-} production were dissolution of $CaSO_4$ and $BaSO_4$; both of which were observed during previous characterization of these sediments (Breit et al., 2005). The percentage of total SO_4^{2-} contributed from mineral dissolution was likely minimal because only a small portion of the mineral's surface area in the pore space was exposed (Kuechler et al., 2004) to flowing water. Any minerals that were exposed to flowing water would have been quickly depleted (Singh and Bajwa, 1990) in the early stages of the experiment and dissolution would become decreasingly important as the experiment progressed .

The source of Cl^- in the column was from residual Cl^- already present in the loam sediment. The loam was exposed to chloride-rich groundwater (landfill leachate) at the field site (Báez-Cazull et al., 2007) before it was collected for the column experiment. Thus when the dilute rainwater percolated through the sediment, the Cl^- entered into solution. The maximum observed concentration (226.8 mg/L) was measured at the beginning of the experiment. Thus, its correlative significance in the factor is linked to water flow (and dissolution) through the loam lenses, rather than being a causative factor in any geochemical processes.

There was a moderately negative loading (-0.695) of matric potential. It is unclear why the loading is negative and it is also unclear why an insignificant loading of water content was manifested in the factor as a correlation between water content and matric potential was expected. One reason for this may have been the influence of a gas phase in the column sediments (see D.J. Hansen et al., The Role of Microbial Activity and Soil Heterogeneity in the Partitioning of Geochemically Distinct Water Masses in the Vadose Zone, submitted to Water Resources Research, 2011) (Hereafter referred to as Hansen et al., Submitted, 2011c). Gas trapped in sediment pore spaces increased the pore pressure while simultaneously prevented water from filling the pore spaces which resulted in lower-than-expected water content values. These conditions caused matric potential and water content not to be correlated.

Factor 2

Factor 2 (F_2^{LC}) was characterized by strong loadings between organic complexed Fe (Fe^{3+} - L) (0.884) and H_2O_2 (0.876). This factor accounted for 15.4% of the variability of the dataset. The loadings of this factor were interpreted to be controlled by Fe^{2+} oxidation. Fe^{2+} reacts with dissolved O_2 and forms H_2O_2 with superoxide $(O_2^{\bullet})^-$ as an intermediate via a Haber-Weiss reaction mechanism.

$$Fe^{2+}(aq) + O_2 \rightarrow Fe^{3+}(aq) + (O_2^{\bullet})^- \quad (1)$$

$$Fe^{2+}(aq) + (O_2^{\bullet})^- + 2H^+ \rightarrow Fe^{3+}(aq) + H_2O_2 \quad (2)$$

This reaction mechanism producing reactive oxygen species (i.e., hydrogen peroxide and hydroxyl radicals) has been well documented, particularly with pyrite (Cohn et al., 2006a; Cohn et al., 2006b). Generally, the H_2O_2 formed in Equation 2 is consumed quickly in the Fenton reaction (best known for its use as in organic contaminant remediation) defined as:

$$Fe^{2+} + H_2O_2 \rightarrow Fe^{3+} + HO^- + HO^{\bullet} \quad (3)$$

Thus H_2O_2 is not commonly observed in natural systems. However, a recent study by Cohn et al. (2006b) found that in the presence of organic iron-chelating (complexing) molecules inhibit the hydrogen peroxide-to-hydroxyl radical conversion in the Fenton reaction, but does not inhibit the formation of H_2O_2 from the Haber-Weiss reaction.

Observations of organically complexed Fe(III) correlated with H_2O_2 confirm that Fe complexing organics were actively participating in biogeochemical cycling. This observation of complexing agents also explains why H_2O_2 was observed in the column. Because data were not collected on organic compounds in the system, little can be said

about their activity. However, the H_2O_2 present in the system may have reacted with organic matter (e.g., cellulose, lignins, proteins), which produces a variety of water-soluble compounds such as low molecular-weight organic acids (e.g., formic, acetic, oxalic, and malonic acid), phenols and benzene-carboxylic acids (Mikutta et al., 2005) that are capable of complexing with Fe (Szilas et al., 1998). It was thus very likely that the Fe(III) was a product of the oxidation of Fe^{2+} and was immediately complexed by organic compounds following oxidation. Iron oxidation processes, dominant in this factor, was associated with the Fe-oxide bands that developed near the fringes of the lenses.

Factor 3

Factor 3 (F_3^{LC}) is characterized by strong loadings between $FeS_{aq}I$ (0.867) and $FeS_{aq}II$ (0.876) and a weak loading of NO_3^- (0.615). This factor accounted for 12.6% of the variability of the dataset. The process associated with this factor is formation and transport of FeS_{aq}. Because FeS_{aq} is a relatively recent discovery, background information on it will be given in order to better understand the interpretation of this factor. FeS_{aq} are aqueous species that form clusters which are defined as polynuclear complexes of Fe and S (Rickard and Luther, 2005) and were first reported in 1988 (Buffle et al., 1988). Aqueous clusters may form *in situ* or by dissolution of FeS minerals (Rickard, 2006). They have been shown to be intermediates of pyrite formation as Fe^{2+} and S^{2-} react with one another under reducing conditions (Rickard and Luther, 1997). They have also been observed in oxidized environments which demonstrate an ability of FeS_{aq} to resist oxidation and be transported (Rozan et al., 2000b).

FeS_{aq} clusters are observed voltammetrically as one or two peaks centered around -1.1 V. For this study, each peak height (either single or split double peak) was quantified and classified as FeS_{aq}I (-1.0 V) and FeS_{aq}II (-1.1 V). The objective of classifying into two groups was to determine if one peak was associated with a certain variable and the other peak with a different variable. However, this was not the case and the strong loading with one another was not particularly unanticipated. From this point on, the two peaks will be referred to collectively as FeS_{aq}.

Observations of Fe^{2+} and S^{2-} in the lenses supply the ideal conditions for the formation of FeS_{aq}. However, the correlation of NO_3^- (which thermodynamics predict that Fe(III) and SO_4^{2-} reduction should not be occurring) with FeS_{aq}, suggests that FeS_{aq} was transported from the lens where it was formed. The highest concentration of NO_3^- (65.5 mg/L) was observed at the sampling point directly below the lower lens (-45.5 cm) during the introduction of groundwater from the bottom of the column (day 19 of experiment), although the groundwater did not contain NO_3^- (Figure 4.7). Thus, this NO_3^- was interpreted to produced by nitrification (Morrill and Dawson, 1967) as NH_4^+ was being transported out of the lens. Therefore the association of FeS_{aq} and NO_3^- developed as a result of chemical compounds (along with NH_4^+ oxidation) that were transported from the lens.

Alternatively, another explanation for the correlation between FeS_{aq} and NO_3^- may further our understanding of FeS_{aq}. Though there have been, Although no study has directly investigated FeS_{aq}-N biogeochemical interactions, several workers have studied Fe-N biogeochemical interactions. For instance, in one study, amorphous Fe-oxide was

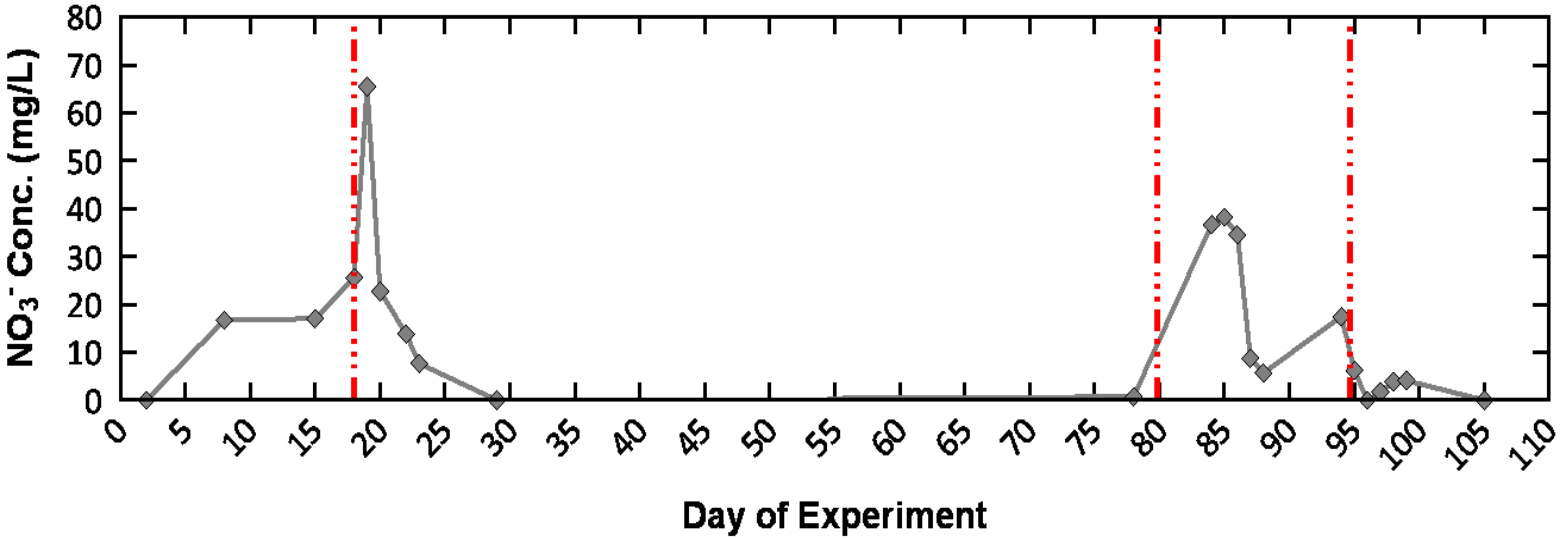

Figure 4.7 – Nitrate spikes just after the introduction or raising of the water table. Dotted/dashed lines indicate when groundwater tables were introduced (Days 18 and 79 of the experiment) or raised (Day 94 of the experiment).

reduced by the oxidation of NH_4^+ to NO_3^- under anaerobic conditions (Li et al., 1988). If free S^{2-} were available in the system, it could react with the reduced Fe and form FeS_{aq}, which would then be shown to be associated with NO_3^-. Nevertheless, correlation does not necessarily equate with causation and further study of the FeS_{aq}-N relationship may yield more concrete results.

Factor 4

Factor 4 (F_4^{LC}) is characterized by a strong loading of water content (0.880) and a moderate loading of alkalinity (as HCO_3^-) (0.694). This factor accounted for 10.0% of the variability of the dataset. The process assigned to this factor was flow through the lenses, where water content was generally high (Figure 4.8) and carbonate dissolution by rainwater. As acidic rainwater percolated through sediments, it dissolved carbonate material and increased alkalinity concentration. The greatest alkalinity concentrations were observed in the lense because there was a greater portion of calcium carbonate minerals in the loam material (Table 4.2) than in the sand. The mean alkalinity concentration in the lenses (471.0 mg/L) was double the mean concentration than in the sand (229.8).

Factor 5

Factor 5 (F_5^{LC}) is characterized by a strong loading of Br^- (0.781) and a moderate negative loading of pH (-0.716). This factor accounted for 8.5% of the variability of the dataset. The process associated with this factor was transport of rainwater (and its tracer Br-) through the column. Nevertheless, the loadings suggest that

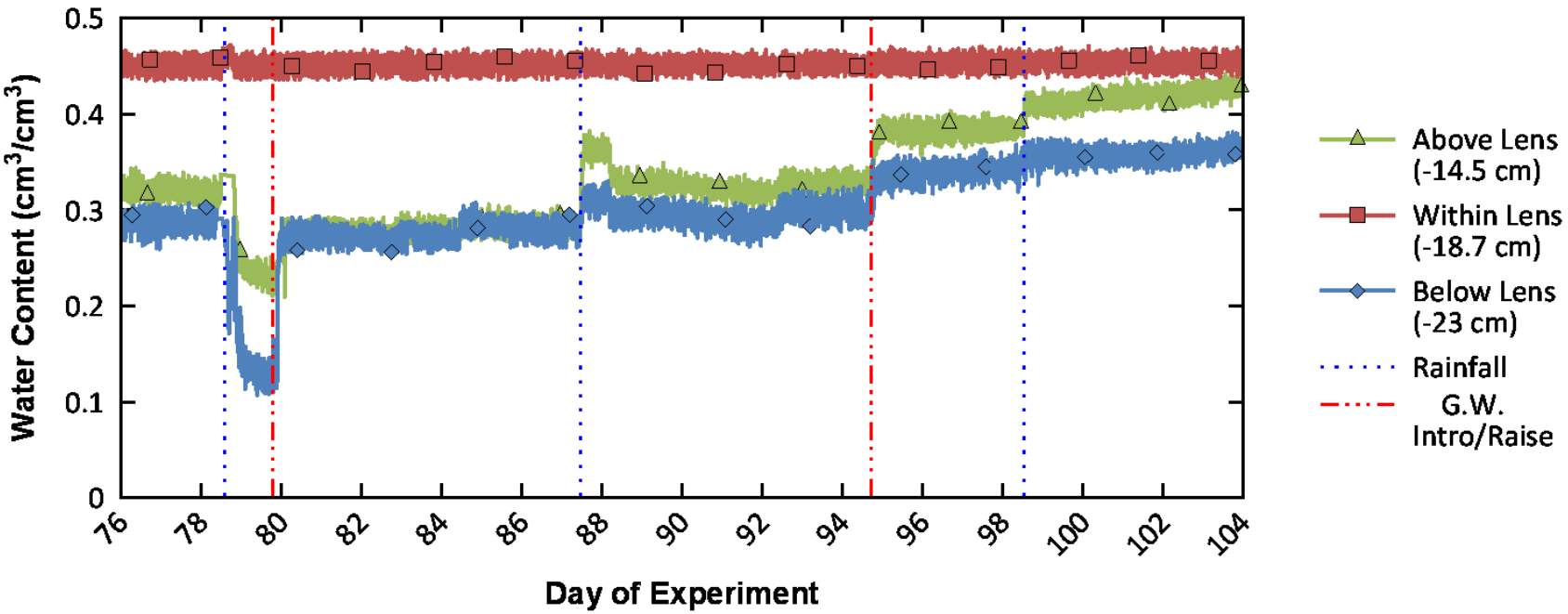

Figure 4.8 – TDR data shown above, in, and below the upper lens in the lens column (LC). The water content values from above the lens are generally higher than the below the lens.

the relationship between the Br^- tracer in the mildly acidic rainwater was the same in this column as in KLC.

Factor Analysis of the Killed Lens Column (KLC)

Principal component analysis and ensuing orthogonal factor rotation also reduced the lens column dataset to five factors (I-V). Note that the factors from analysis of KLC, will be labeled with Roman numerals to differentiate from them from the LC factors (Arabic numerals). Factor I explains the greatest amount of variability within the dataset, while factor V explains the least amount of variability. In total, the five factors account for 65.7% of the dataset variability. These rotated factor patterns are listed in Table 4.5. Based on the loadings between variables, an interpretation of a dominant geochemical or physical process was assigned to each factor.

Factor I

Factor I (F_I^{KLC}) was characterized by strong loadings of matric potential (0.853) and water content (0.780). Nitrate (0.634) and SO_4^{2-} (0.591) were also moderately loaded. This factor accounted for 21.3% of the variability of the dataset. The two processes associated with this factor were aqueous SO_4^{2-} dissolution and abiotic NH_4^+ oxidation. Figure 4.9 shows a time series plot of the factor constituent data (e.g. pressure, water content, concentration) from the sampling location at –45.5 cm. The positive correlation between water content and matric potential was not unanticipated as the two factors are generally related in the vadose zone as was discussed earlier.

Table 4.5 - Killed lens column factor analysis and interpretations. The five factors represented 65.6 % of total variability.

Parameter	Factor I (21.3 %)	Factor II (14.3 %)	Factor III (12.0 %)	Factor IV (9.6 %)	Factor V (8.6 %)
Std Cl^-	-0.39	0.26	-0.44	0.14	-0.53
Std Br^-	-0.23	-0.29	**-0.53**	0.19	0.00
Std SO_4^{2-}	**-0.59**	-0.09	-0.30	-0.23	0.28
Std NO_3^-	**-0.63**	-0.04	0.06	0.28	0.31
Std Fe^{2+}	0.03	0.17	-0.04	**0.71**	-0.16
Std FeS_{aq} I	-0.04	**0.80**	-0.16	0.07	-0.20
Std FeS_{aq} II	0.07	**0.81**	0.09	-0.07	0.22
Std S^0	-0.14	0.08	-0.17	0.06	**0.71**
Std pH	-0.07	-0.19	**0.83**	0.03	-0.14
Std HCO_3^-	-0.04	-0.25	-0.07	**0.75**	0.27
Std Matric Potential	**0.85**	0.03	0.27	-0.07	-0.01
Std Water Content	**0.78**	-0.04	-0.22	0.14	0.26
Geochemical/ Hydrologic Interpretation	(+)Water Flux (-)SO_4^{2-} Mineral Dissolution / abiotic NH_4^+ Oxidation	FeS_{aq} Dissolution	Rainwater Transportation	Abiotic Fe(III) reduction / carbonate dissolution	Pyrite Oxidation

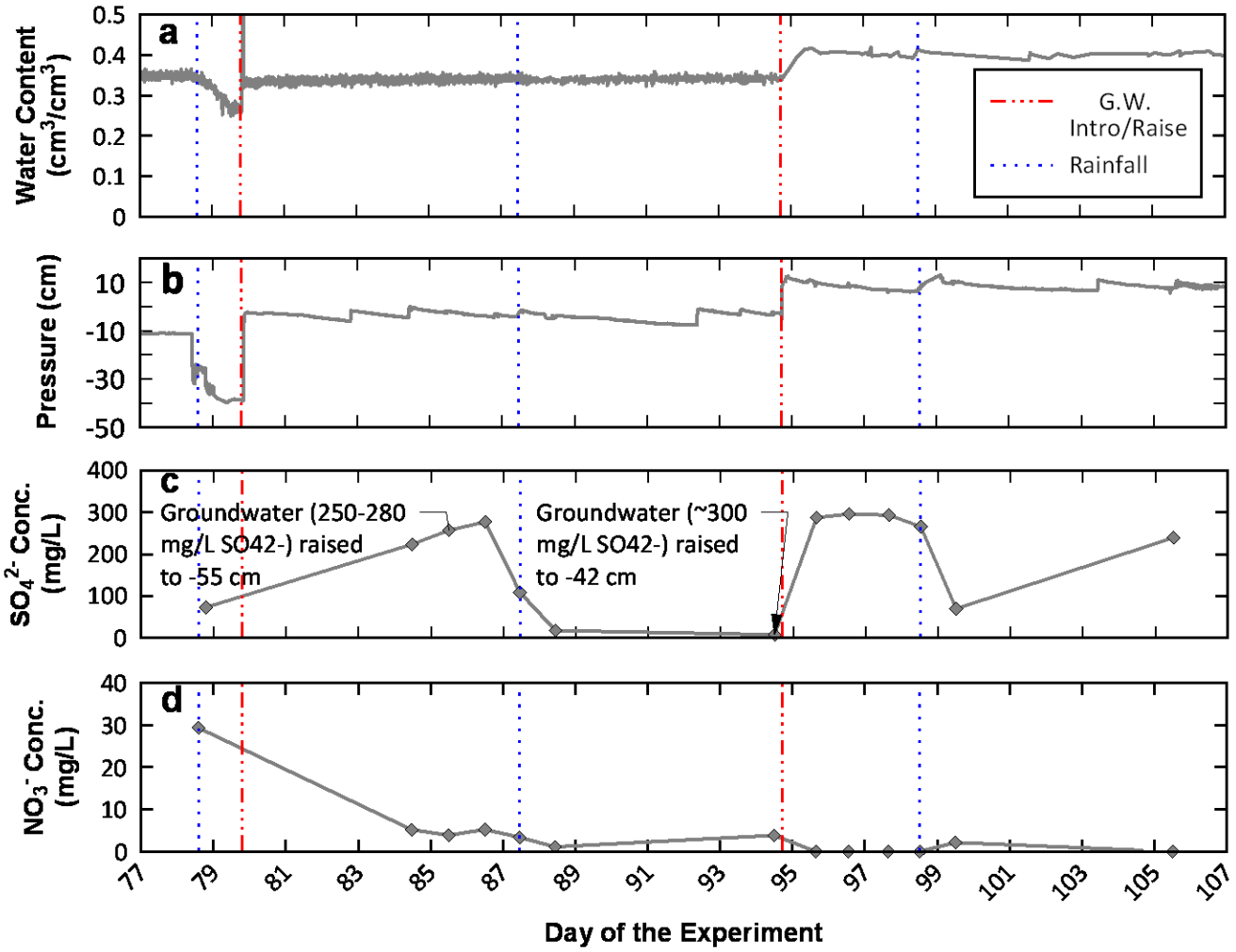

Figure 4.9 – Loadings of Factor 1 of the killed control column over time from sampling point at -45.5 cm (directly below the lower lens).

As in the lens column (LC), the two principal sources of SO_4^{2-} in the system were dissolution of SO_4^{2-} bearing minerals ($CaSO_4$ and $BaSO_4$) and oxidation of iron-sulfide minerals. Because the sediment was sterilized, the FeS mineral oxidation is thought to occur abiotically.

The mechanism of nitrification in the sterile sediment was probably abiotic oxidation of NH_4^+ that was bound to clay minerals in the sediment. Although minimal concentrations of NO_3^- were introduced through a porous reference electrode placed in the sediment, its input was considered negligible when compared to the high concentrations (up to 97.7 mg/L) observed during the experiment. Abiotic oxidation of NH_4^+ in the presence of oxygen is thermodynamically favorable and was attributed to producing NO_3^- in the column.

Factor II

Factor II (F_{II}^{KLC}) was characterized by strong loadings of FeS_{aq}I (0.808) and FeS_{aq}II (0.805). This factor accounted for 14.3% of the variability of the dataset. There were no other significant loadings in this factor. The process associated with this factor was iron-sulfide mineral dissolution. Similar to LC, both FeS_{aq} measurements were correlated with one another and will be collectively referred to as FeS_{aq}. Although abiotic production of Fe^{2+} was observed (see Factor IV), S^{2-} was not produced (see Factor V) to combine with Fe^{2+} to generate FeS_{aq}. The mean electrical current value (related to concentration) of the FeS_{aq} signal in KLC was 9.1 nA compared to 24.7 nA in LC. A Kruskal-Wallis test ($p < 0.001$) showed that the means were significantly different. Therefore *in situ* generation was unlikely; consequently the FeS_{aq} detected in

the system was probably dissolved from previously formed FeS minerals (Rickard, 2006).

Factor III

Factor III (F_{III}^{KLC}) was characterized by a strong loading of pH (0.825) and a moderate negative loading of Br^- (-0.529). This factor accounted for 12.0% of the variability of the dataset. The process associated with this factor was transport of rainwater through the column. Bromide was used as a conservative tracer in rainwater on two occasions: the first rainfall (11/29) and third rainfall (02/03). Concentrations in the rainwater were approximately 150 mg/L and 250 mg/L Br^- respectively. Thus Br^- can be considered representative of rainwater delivery and flux. Because rainwater was adjusted to a pH of ~5, it would have lowered the pH as water percolated through the sediment. Hence a negative correlation between Br- (in rainwater) and pH is a likely association.

Factor IV

Factor IV (F_{IV}^{KLC}) was characterized by a strong loading of alkalinity (as HCO_3^-) (0.750) and a moderate loading of Fe^{2+} (0.707). This factor accounted for 9.6% of the variability of the dataset. The processes attributed to this factor were carbonate dissolution and abiotic Fe^{2+} production. The correlation between these two variables was likely caused by mineral water interactions within the organic-rich loam material. Because the loam material was more geochemically reactive than the sand, the average alkalinity values were consistently greater in samples located within the loam than in the sand (237.6 mg/L versus 177.6 mg/L).

Similarly, water samples collected from the loam material were colored amber to dark brown which was an indication of the presence of humic substances. Humic substances are divided into two groups (humic and fulvic acids) which are operationally defined by solubility under acidic or alkaline conditions. Both groups describe a range of complex and varying organic molecules that originate from decaying soil organic matter. Both fulvic and humic acids have been shown to abiotically reduce Fe(III) to Fe^{2+} (Deng and Stumm, 1993; Pracht et al., 2001). Thus, these humic substances observed in the loam pore waters were responsible for Fe^{2+} production in the sterilized sediments. The relationship between alkalinity and Fe^{2+} was not cause and effect, but rather stems from geochemical interactions with the loam material.

Factor V

Factor V (F_V^{KLC}) was characterized by moderate loadings of elemental sulfur (S^0) (0.707) and Cl^- (-0.533). This factor accounted for 8.6% of the variability of the dataset. The interpretation of this factor was problematic due to instrument limitations that resulted in the false reading of the S^{2-} peak. Abiotic reduction of SO_4^{2-} only occurs at high temperatures of ~100 ºC or higher (Machel, 2001). Abiotic sulfide production was not possible given the temperature at which the experiment was conducted (~22º C). It has been shown that slow scanning rates during voltammetric analysis will cause peaks of HS^- and (S^0) to merge into one peak (Rozan et al., 2000a). The instrument used in study was not capable of faster scanning rates where the two peaks separate, therefore this peak at -0.6 V probably represents S^0, which has been shown to be an intermediate of pyrite oxidation (Moses et al., 1987).

Despite the aforementioned problems with the isolation of the S^{2-} peak from S^0, there were several indicators that suggested true measurement of S^0. The heights of sulfide peaks from KLC were one to two orders of magnitude lower than those observed in LC. These smaller peak heights suggest S^0 was actually measured because it is a fleeting intermediate and large concentrations should not be observed. Secondly, observations of S^0 were spatially associated with Fe^{2+} within the loam lenses. The exception to this was several observations of ΣS at the lowest sampling location during residence of a sulfate-rich water table. This evidence supports the assignment of voltammetric peaks as S^0. The assignment of this peak to S^0, which represents pyrite oxidation, is more consistent with the other geochemical observations. Secondary electron microscopy has shown pyrite framboids to be abundant in the loam material which helps support the viability of such an interpretation.

Comparison between Active and Killed Control Column

The primary differences between KLC and LC were processes controlled by biological activity. The most important factors in the killed control column (see F_I^{KLC}) were high water content and oxidation of iron-sulfide minerals and dissolution of minerals such as gypsum, anhydrite, or barite, whereas the most important processes in the active column (see F_1^{LC}) were microbial reduction of Fe(III) and SO_4^{2-} and oxidation of iron-sulfur minerals. Loadings of SO_4^{2-}, generated by iron-sulfide oxidation, were significant in each of these factors but measured concentrations differed. (The mean SO_4^{2-} concentrations in KLC and LC were 237.8 and 165.5 mg/L.) The concentrations in

the two columns differed significantly (Wilcoxon Signed Rank-Sum test W (n1 = 200, n2 = 211) = 34,497.5, $p < 0.0001$ two-tailed). The lower concentrations in LC were attributed to removal by bacterial SO_4^{2-} reduction. An absence of active processes removing SO_4^{2-} in KLC resulted in the higher concentrations.

Similarly Fe^{2+} in LC, produced by bacterial Fe(III) reduction, had mean concentrations that were an order of magnitude greater than the mean of abiotically produced Fe^{2+} in KLC. Subsequent oxidation of Fe^{2+} produced H_2O_2 and complexed Fe(III). Although Fe^{2+} oxidation is not necessarily a biological process, concentrations of Fe^{2+} were never high enough for these products of oxidation (H_2O_2 and complexed Fe(III))to be observed in KLC. Thus the observation of H_2O_2 and Fe^{3+}-L can be considered byproducts of microbial activity observed in LC.

Clearly, microbial activity had a significant impact on the actual concentrations of redox sensitive chemical species. The influence of microbial activity also impacted the factor variability as well. The process of Fe(III) reduction assigned to F_1^{LC} accounted for 28.6% of the total variance of LC. This was slightly higher than the variance explained by F_1^{LC} (21.3%). However, there is an even larger difference when F_2^{LC} is compared to F_{IV}^{KLC} (abiotic Fe reduction) which explained 9.6% of the total variance. Moreover, the Fe^{2+} oxidation process in F_1^{LC} which explained 15.4% of the overall variability in LC did not account for any variability in KLC.

There were several abiotic processes, as revealed by factor analysis that were significant in both columns such as oxidation of iron-sulfide minerals, carbonate

dissolution, FeS_{aq} dissolution, and rainwater flow (identified by Br^- tracer). In fact, several of the factors shared the exact same interpretations (i.e. F_{III}^{KLC} and F_5^{LC} ,[rainwater flow] F_{II}^{KLC} and F_3^{LC} [FeS_{aq} dissolution]). However, because each factor accounts for a certain value of variability (i.e. the variability accounted for in Factor 1 is greater than in Factor 5), each factor, or set of processes, are ranked and differentiated as to their level of importance. These differences of importance allow for comparison between the factors in KLC and LC that share the same interpretation.

For example, while, F_{III}^{KLC} and F_5^{LC} were both interpreted as rainwater flow (Br^- tracer with an opposite correlation to pH), F_{III}^{KLC} accounted for 12% of the variability while F_5^{LC} accounted for 8.6% variance. Although these percent differences do not present a compelling case for distinction between the two, the ordering of factors can show the relative importance of a particular factor in comparison to other factors in each column. From the example above, F_{III}^{KLC} was the third most important factor in KLC while the same process, manifest in F_5^{LC}, was least important in LC. Similar observations can be made for F_{II}^{KLC} and F_3^{LC}. The comparison of factor orders demonstrates that although abiotic processes were operating both columns, the degree of importance of these processes was much less in LC than in KLC.

Reduced Flow Rate due to Biogeochemical Activity

The statistical results demonstrated a considerable difference between the

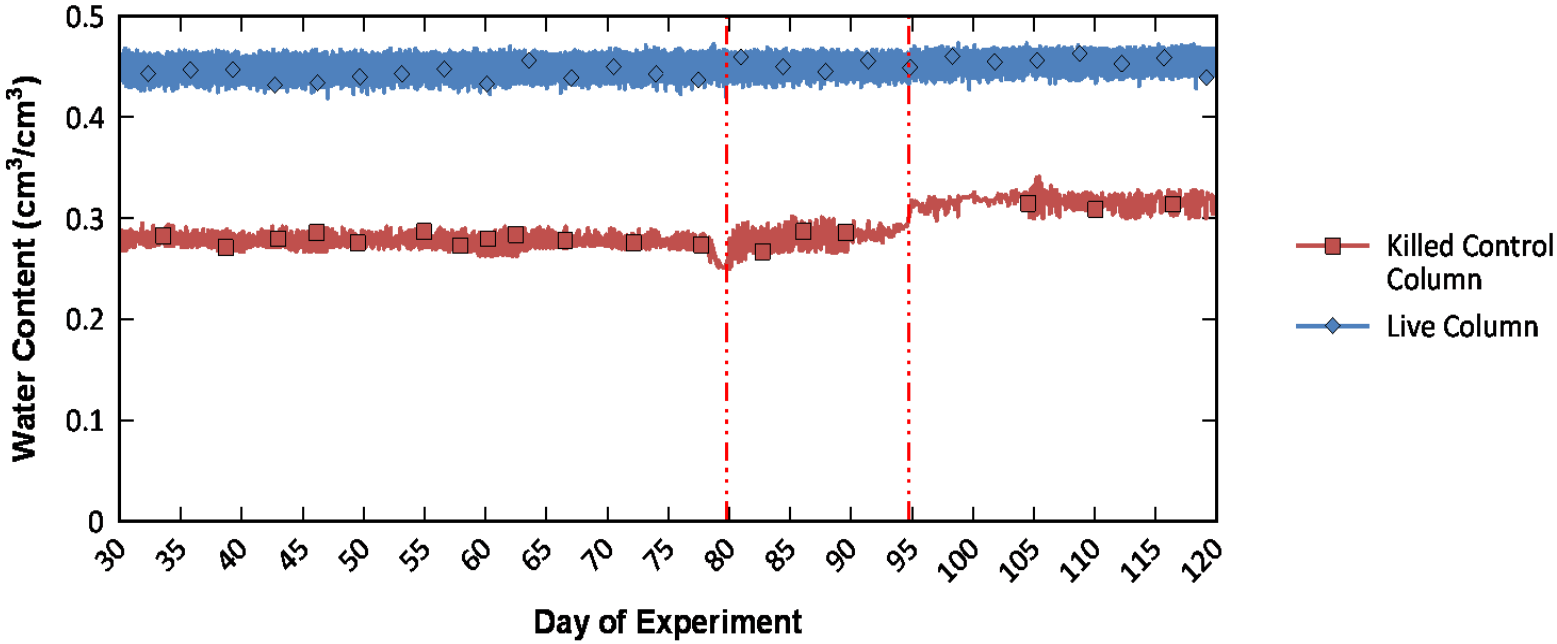

Figure 4.10 - Water content in the upper lenses (-18.7 cm) from the killed control column (KLC) and live column (LC). Dashed-dotted vertical lines indicate times when the water table was raised.

dominant geochemical processes acting in each of the columns; likewise differences in hydrologic behavior were also observed in the two columns. One example of this was the water content in the upper lenses (-18.7 cm) as shown in Figure 4.10. The water content in the lens in KLC during the months of December and January was lower (mean = 0.278) when compared to the water content in the lens in LC (mean = 0.451). The water content data from KLC also show more variability as the water content values respond to the raising and lowering of the water table. In contrast, the water content data from LC show very little variability in response to water table changes.

The near constant water content within the lens column was attributed to the presence of the Fe-oxide bands. Precipitation of Fe-oxides within the pore spaces between sediment grains caused a decrease in porosity and permeability. Undoubtedly, this decrease would have reduced the rate of water flow into or out of the lens. Thus the higher water content in LC stemmed from an impediment to water flow caused by mineralization (i.e. water in the lenses did not evaporate or drain from the lenses). Conversely, the absence of Fe-oxide bands in KLC allowed for water to move in and out of the lens which resulted in lower water content values.

The degree to which water flow through the lenses was decreased after development of the Fe-oxides was unknown. However, a conservative chemical tracer (Br^-) was used to calculate approximate values to compare flow through the lenses in each column. This calculation only takes into consideration hydraulic and geochemical data over a short time period and not the duration of the experiment. The calculation method used Br^- data from the bottom lenses in each column measured before and after

the application of Br^- free rainwater on February 12th. The volume of water that passed through the lens was calculated by comparing the before and after concentrations (dilution) of Br- in the lens.

The concentrations of Br^- in the lenses of LC and KLC before the Nanopure rainfall flushed it out of the lenses were 145.29 mg/L and 142.11 mg/L respectively. After rainfall, the concentrations were 55.36 mg/L and 1.42 mg/L. The bulk volume of the lenses was calculated to be 1119 cm^3. The pore volume was calculated by multiplying the bulk volume of the lens by effective porosity of 62.3% which yielded 697.0 cm^3. The duration of rainfall was approximately 14 hours. An equation generally used for chemical transport and residence time in reservoirs from Thomman and Mueller (1987) was used to solve for flow rate differences.

$$C_{(t)} = C_0 \, e^{\left(-\frac{Q}{V}t\right)} \quad (4)$$

where: $C_{(t)}$ is concentration at time (t), C_0 is concentration at time zero, Q is flow rate (vol/t), V is reservoir volume, and t is time. The equation solved for Q is:

$$Q = -\frac{V \cdot \ln\left(\frac{C(t)}{C_0}\right)}{t} \quad (5)$$

The calculated flow rates for LC and KLC were 0.78 and 3.82 cm^3/min respectively. Converting these to the flow values to velocity by dividing the cross sectional area of the lens yielded values of 0.028 and 0.14 cm/min. When the results were compared to the flow velocity through the lenses from the output of the numerical forward modeling (0.88 -0.104 cm/min), as shown in Figure 4.4, the values obtained in

these calculations were higher for KLC. This was likely due to the underlying assumptions of the calculation that the reservoir was a continuously mixed tank.

Nevertheless, the results of the calculations demonstrated the sizeable difference between water flux rates through the lenses in LC and KLC. Ultimately, the underlying cause behind flow rate differences was microbial activity and the consequential geochemical reactions, such as oxidation and precipitation. These results demonstrate the potential effect of biogeochemical activity on flow in the subsurface. A likely consequence of this retarded flow KLC was a change in flow dynamic near the lenses. At the top of the lenses, ponded water would reside longer at these locations instead of flowing through the lenses after a relatively short period of time.

Environmental Implications

This enhanced potential for ponding is particularly important in systems where the lenses are not strictly composed of fine-grained sediment with low hydraulic conductivity. Although much of the literature focuses on fine grained sediments, the results of this study highlight the need to consider coarser-grained sediment lenses, especially those in biogeochemically active systems. Thus coarser-grained sediment lenses may have the same impact as fine-grained lenses in contaminant fate and transport.

Much of this same literature focuses on the dispersal quality of lenses in contaminant fate, but fails to consider the roles of lenses in remediation. The perched water tables above the lenses create stationary water masses that can be beneficial in

preventing contaminants from entering groundwater. Additionally, there is also potential for biodegradation of many contaminants, including redox sensitive contaminants to occur in these stagnant waters. Microbial metabolism would easily consume O_2 in these immobile waters and force a switch in TEAPs. The progression to different TEAPs creates the potential for anaerobic degradation of contaminants such as chlorinated solvents.

Increased numbers of microorganisms combined with abundant electron acceptors near the fringes of the lenses set these areas apart as zones capable of enhanced biodegradation within the vadose zone. Thus, soil lenses function to do more than spread and dilute contaminants via transport in the vadose zone, but may also significantly add to remediation efforts in nature. This would be especially true in a system where there are many lenses that represent relatively small areal features. As contaminant moves through a comparatively dense distribution of lenses, it would come in contact with the fringes of the lenses. This contact with these biogeochemical reactive portions of the lens would enhance degradation in the vadose zone where it might not otherwise have been considered.

CONCLUSIONS

These study results demonstrate specific linkages between microbial activity geochemistry, and hydrology in the vadose zone. The presence of a capillary barrier at the soil textural interfaces reduced the flow rate into the lenses which created favorable circumstances for reducing conditions caused by microbial activity. In response,

biogeochemical activity created Fe-oxidize band that further retarded the rate of water flow through the lens.

Statistical factor analysis showed that the most important processes in the live column were microbial reduction of Fe(III) and SO_4^{2-}, and oxidation of reduced products. Conversely, factor analysis of data from the sterilized column showed that most important processes were water flux, oxidation, and mineral-water interactions. Iron-oxide bands were not formed in this column and water flux rates did not decrease like they did in the live column.

The impact of biogeochemical activity on water flow in and around soil lenses has implications for contaminant fate and transport. Although fine-grain lenses have been shown to disperse and dilute contaminants, biogeochemical cycling may alter coarser-grained sediment lenses to behave in a similar manner to their fine-grained counterparts. Lenses also need to be considered as they may play a potentially significant role in contaminant remediation in the vadose zone. Perched water tables created by lenses may become reduced which would lead to the remediation of redox sensitive contaminants

In addition, the lenses themselves are likely to be very active biogeochemically and direct contact with contaminants may result in a considerable measure of biodegradation. In general, the impact of soil heterogeneities on contaminant fate and transport need to be further investigated due to their potential to affect hydrologic flow and biogeochemical activity.

CHAPTER V

THE ROLE OF MICROBIAL ACTIVITY AND SOIL HETEROGENEITY IN THE PARTITIONING OF GEOCHEMICALLY DISTINCT WATER MASSES IN THE VADOSE ZONE

INTRODUCTION

A fundamental issue in understanding the biogeochemical transformations that occur in the vadose zone is quantifying the mechanisms controlling linked hydrologic, geochemical, and microbiological processes in variably saturated heterogeneous environments. One property unique to the vadose zone, is that it is confined by two vastly different hydraulic conditions on its lower and upper boundaries. Through either of these boundaries, waters that can affect redox cycling occurring with its sediment, may be introduced. For example, a rising groundwater table may introduce waters with higher chemical concentrations and replace partially-filled pore spaces with anaerobic waters where reducing redox conditions will develop. Conversely, rainwater, which may simultaneously enter the vadose zone from the top boundary may dilute pore-water chemical concentrations and introduce dissolved oxygen to pore waters thus promoting oxidizing redox conditions. Thus the vadose zone serves as a highly dynamic area where vastly different geochemical water masses are juxtaposed. Though these dynamic conditions create difficulty in understanding and characterizing redox geochemistry in the vadose zone, it is critically important as redox conditions control the form and toxicity of many contaminants.

The interaction between geochemically distinct water masses has been documented in the saturated zone on several occasions. Scholl et al. (2006) and McGuire et al. (2005) both observed the segregation of recharge water masses within aquifer groundwaters. These rainwater/recharge water masses were identified by their distinct geochemical signatures (e.g. isotopes, chemical concentrations). Both studies identified these recharge water masses at separate locations where groundwater contaminants were present. The recharge waters were important to redox geochemistry because they provided a fresh supply of higher-energy yielding electron acceptors (O_2, NO_3^-, or SO_4^{2-}) groundwater where low energy-yielding terminal electron accepting processes (TEAPs) were dominant. Although conditions favored segregation of water masses in the saturated zone, it is unclear how the different boundary types and partially-saturated properties of the vadose zone may influence mixing (or lack thereof) of waters in this portion of the subsurface.

For example, in the vadose zone, besides rainwater being introduced at the top boundary, evaporation is also an active process that can affect hydrologic and geochemical conditions in the subsurface. Evaporation is able to remove significant quantities of water from soils and cause waters at depth to rise vertically. This removal of water not only decreases water content, but increases pore-water chemical concentrations. Ultimately, these waters may become over saturated and deposit minerals within sediment pore spaces (Acero et al., 2009). Therefore, evaporation may create waters with much higher concentrations at shallow depths than would be expected from the input of rainwater.

At the bottom boundary, interactions between waters in the vadose and saturated zones vary over time. For example, the height of the water table can change on a daily basis (Loheide et al., 2005) or on a scale of months to years (Rosenberry and Winter, 1997). These fluctuations between groundwater and vadose zone pore waters may cyclically expose sediment to saturated/unsaturated conditions that consequently can lead to rapid cycling between reducing and oxidizing conditions. However, the boundary between the saturated zone and the vadose zone is not a sharp interface, but rather a variably thick interface, generally referred to as the capillary fringe (or zone).

Capillarity in sediment above the saturated zone causes groundwater to rise into the vadose zone, thus connecting groundwaters and vadose zone waters together. The degree to which groundwater is transported upward is dependent on the texture of the overlying sediments, thus the capillary fringe is thicker in fine-grained sediments compared to coarse-grained sediment (Lohman, 1972). Within the capillary fringe, waters have been shown to mix through upward and downward fluxes (Berkowitz et al., 2004) as well as through horizontal flow (Silliman et al., 2002). Waters in the capillary fringe can evolve to become intermediary, possessing characteristics of both groundwater and vadose zone water.

Another factor affecting water distribution in the vadose zone is the presence of soil heterogeneity, such as layers, lenses, or macropores. These heterogeneities have been shown to affect the flow of water (Carrillo et al., 2000; Kohne and Mohanty, 2005). and solute transport (Gachter et al., 1998; Zhou and Selim, 2001) as it is redirected

through or around the heterogeneous feature. Thus heterogeneities have the potential to cause waters to be distributed differently than in homogenous systems.

One final (though certainly not trivial) aspect that needs to be considered in understanding geochemical cycling and water flow in the vadose zone is the linked influence of microbial activity on these other processes. Microbial activity has been shown to alter water flow through sediments by blocking sediment pore spaces by mineral precipitation, biofilm, cell mass accumulation, and biogenic gas production (Baveye et al., 1998). An increase in water content can cause O_2 become limited which causes microorganisms to utilize lower energy yielding electron acceptors in metabolism (Chapelle, 2001; Lovley, 1991; Lovley and Goodwin, 1988; Stumm and Morgan, 1996). This shift in metabolic pathway has implications for not only aqueous chemical concentrations but also for the production of biogenic gases and precipitation/dissolution of minerals which thus affect flow conditions. It is these linked hydrologic, geochemical, and microbiological processes that need better quantification.

The objective of this study was twofold. The first objective was to analyze how soil heterogeneity (in this case, soil lenses) affected aqueous geochemistry under differing hydrologic conditions (rainfall, presence of groundwater, and a fluctuating groundwater table elevation). The second objective was to determine the effect of biological activity in this heterogeneous system by utilizing a sterile control.

MATERIAL AND METHODS

Soil Physical Properties

Soils were collected from a site in close proximity to a closed and capped municipal landfill on the floodplain of the Canadian River in Norman, Oklahoma, USA. The groundwater system beneath the landfill and surrounding areas has been studied comprehensively due to the leachate plume, originating from the landfill, that has developed over years in the aquifer (Cozzarelli et al., 2000). The first soil collected was an alluvial, medium-grained sand taken from the riverside sediments of the Canadian River. The second soil was an organic-rich loam from a wetland adjacent to the landfill whose sediments have been intermittently exposed to the leachate plume. Prior to use, soils were air-dried, ground, and sieved (0.8 mm mesh size). Physical and chemical properties of the soils are listed in Table 5.1.

Soil Chemical Properties

Electrical conductivity and soil pH and were determined in a 1:2 soil:deionized water extract. After the addition of water, samples were stirred and allowed to equilibrate for a minimum of 30 minutes and then pH and conductivity were measured (Rhoades, 1982; Schofield and Taylor, 1955). A 1 N KCl solution was employed for the extraction of nitrate-nitrogen (NO_3^--N) from the soils. Nitrate was reduced to nitrite by a cadmium column before being measured using spectrophotometry (Keeny and Nelson, 1982). Mehlich III extractant was employed to extract P, K, Ca, Mg, Na and S from the

Table 5.1 - Soil textural (USDA classification), organic carbon, bulk density, and hydraulic conductivity values of the two soil types collected from Norman, OK and used in soil columns

	Textural Properties (Percent Weight)								SWRC Van Genuchten Parameters			
Soil	0.5 – 0.2 mm (Medium Sand)	0.2 – 0.05 mm (Fine Sand)	0.05 – 0.002 mm (Silt)	<0.002 mm (Clay)	% Organic Carbon	Bulk Density (g/cm^3)	Porosity (%)	Saturated Hyd. Cond. (cm/min)	θ_r (cm^3/cm^3)	θ_s (cm^3/cm^3)	α (1/cm)	n (unitless)
Sand	33.6	62.9	2.2	1.3	0.02	1.4	43.4 %	0.636	0.027	0.321	0.0318	1.60
Loam	46.5		39.5	12.5	1.5	1.0	58.5 %	0.141	0.015	0.385	0.0202	1.86

Table 5.2 - Chemical analyses results of the two soil types used in the experiments. Concentrations are generally expressed in plant available values.

Soil	pH	Cond (uS/cm)	NO3-N (mg/L)	P (mg/L)	K (mg/L)	Ca (mg/L)	Mg (mg/L)	S (mg/L)	Na (mg/L)	Fe (mg/L)	Mn (mg/L)
Sand	8.5	106	4	4	19	1,688	56	40	154	2.83	1.28
Loam	7.9	1,030	2	5	86	24,833	802	694	374	88.35	19.27

soils and were subsequently measure by inductively coupled plasma (ICP) atomic spectrometry (Mehlich, 1978; Mehlich, 1984). Iron and Mn were extracted by diethylene triamine pentaacetic acid and measured by ICP (Lindsay and Norvell, 1978). The results of these analyses are generally interpreted as plant-available concentrations and are listed in Table 5.2.

Column Setup

Soils columns were constructed from clear acrylic pipes (diameter = 15 cm, height = 60 cm). A densely perforated polyvinyl chloride (PVC) plate, covered with a nylon mesh fabric, was fastened to the bottom of the acrylic pipe to prevent soil loss and allow for water flow. This setup created a seepage face at the bottom boundary of the column wherein water flowed across the nylon mesh after overlaying sediment became saturated. Glues or epoxies (hot melt adhesive, Adhesive Technologies Inc., Hampton, NH and Silvertip Gel Magic Adhesive, System Three, Auburn, WA) that did not exude interfering chemical compounds (e.g. acetate, formaldehyde, etc) after soaking in Nanopure water over a 48 hour time period, were exclusively used in column construction. Rainwater solution was delivered to the column via a rainfall simulator constructed of a PVC reservoir and 18 gauge needles. A digitally controlled peristaltic pump (Cole-Parmer, Vernon Hills, IL) supplied water to the rainfall simulator from a sterilized and sealed nalgene carboy. Fabric drapes were mounted above the columns and were only removed during sampling. These drapes prevented light from entering the column and thus limited the growth of photoautotrophic microorganisms.

Groundwater reservoirs were constructed from 18.9 L polyvinyl chloride (PVC) buckets that were covered with removable lids. Nitrogen gas, introduced through ceramic-stone aquarium gas diffusers placed at the bottom of each bucket, was used to deoxygenate the groundwater before it entered into the columns Buckets were placed on a platform that could be elevated or lowered using hydraulic jacks to simulate changing groundwater table elevations.

The two cylindrical soil columns were constructed and identically packed to create horizontally offset lenses composed of an organic-rich loam within a matrix of sand (Figure 5.1). Using a piston compactor, soils were packed in 3 cm increments to achieve a constant bulk density. The top lens was centered at -19 cm depth and the bottom lens was centered at -42 cm (Figure 5.2a). The thickness of the lenses was approximately 7.5 cm. The two columns were packed in an identical manner and with identical materials, with the exception that sediments for the second column had been previously γ-irradiated to halt microbial activity. Thus the second column acted as a killed-control lens column (KLC) that was used to contrast the other microbial active lens column (LC).

Measurements and Automated Data Collection

Columns were equipped with collocated sets of measurement probes (Figure 5.2b) installed at selected locations (Figure 5.1). Three-pronged time domain reflectometry (TDR) probes (5 and 8 cm long, 1.1 cm spacing between rods) were used

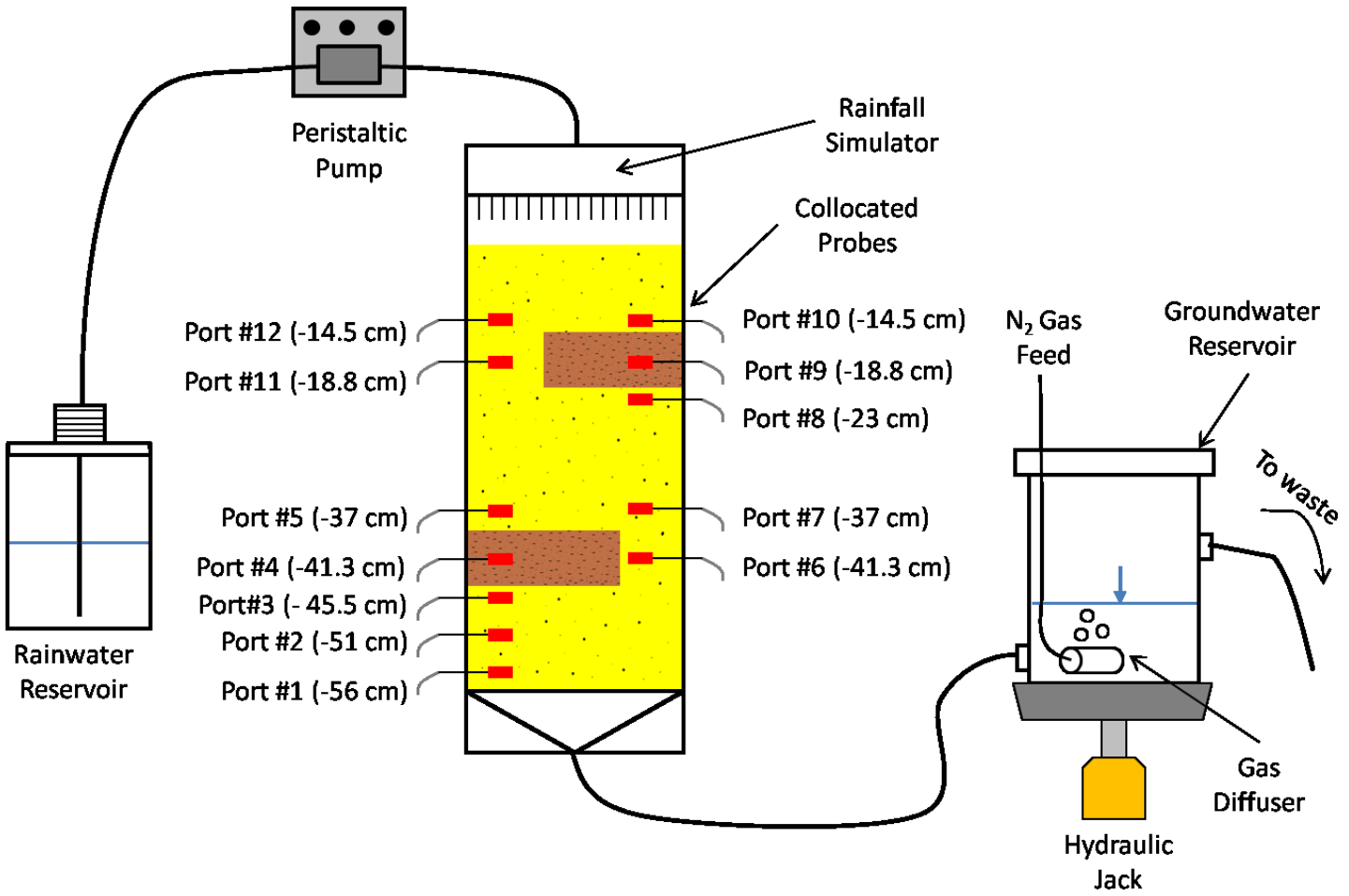

Figure 5.1 - Experimental column setup with rainwater reservoirs, pump, rainfall simulator, and collocated probes (TDR, tensiometers, Eh, and lysimeters).

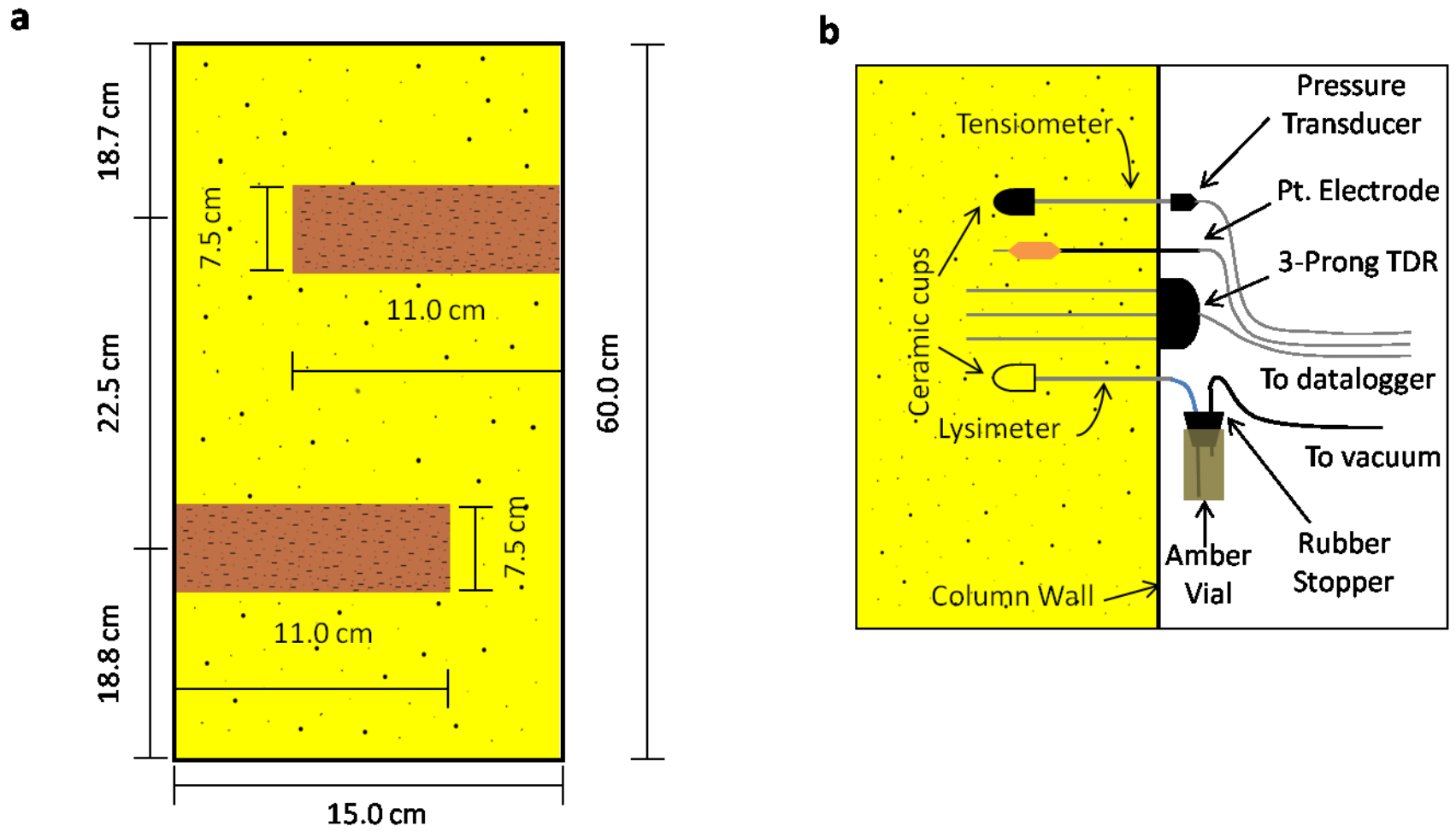

Figure 5.2 - (a) Dimensions of column setup, loam lenses, and sand matrix and (b) expanded view of sampling ports

to measure soil water content. Tensiometers, automated soil-water pressure monitoring, were constructed using 6 mm diameter ceramic cups (SDEC 220, SDEC France) that were connected to pressure transducers (Microswitch, Soil Measurement System, Tucson, AZ) via aluminum tubing. Data from pressure transducers were collected with a CR10X data logger that utilized an AM 16/32A multiplexer (Campbell Scientific, Inc., Logan, UT). Data from TDR probes were collected using a TDR100 connected to SDMX50 multiplexers and a CR10X (Campbell Scientific, Inc., Logan, UT).

To prevent diffusion of oxygen into the sediments through the sampling lysimeters, the sampling ports were flushed with N_2 gas for 5 seconds every 20 minutes when sampling was not taking place. Two-way solenoid valves (Granzow, Charlotte, NC) connected at each sampling location regulated the introduction of N_2 gas or vacuum to lysimeters. All lysimeters were connected to a manifold that was regulated by a master three-way solenoid valve that switched between N_2 gas and vacuum. Solenoid valves were controlled manually while sampling, but were controlled by two relay drivers (SDM-CD16AC) (Campbell Scientific, Inc., Logan, UT) attached to CR10X data logger between sampling events. The lab wherein experiments were conducted had an ambient air temperature of 22º ± 2º C.

Geochemical Analyses

To minimize hydrological disruptions in the soil columns while sampling, less than 7 ml of water was withdrawn at each sample location for all geochemical analyses. Lysimeters constructed from 6-mm diameter ceramic cups (SDEC 220, SDEC France),

aluminum tubing, and amber catchment vials were utilized for *in situ* sampling. Capillary electrophoresis was used, due to low sample volume requirements (Goettlein and Blasek, 1996), to determine the concentrations of major anions (Cl^-, Br^-, SO_4^{2-}, and NO_3^-), and NH_4^+ (Báez-Cazull et al., 2007) Each sample analysis consumed ~1 nL. Sample volumes of 250 µL were collected to ensure sufficient volume for replicate analyses. Anion samples were preserved using formaldehyde while NH_4^+ samples were preserved by flash freezing immediately upon collection. Alkalinity (determined by Gran plot (Gran, 1952)) and pH were measured concurrently. Sulfide and Fe^{2+} were quantified voltammetrically using a hanging drop mercury electrode (Metrohm, Switzerland). The voltage range scanned was from 0 mV to -2100 mV using square wave voltammetry with the following parameters: 15 mV pulse height, 4 mV step increment, 100 mHz frequency, and an 80 mV/S scan rate.

Soil Sterilization

The killed control column (KLC) was packed with sediment that was γ-irradiated at the Nuclear Science Center at Texas A&M University. Before sterilization commenced, soils were dried, ground, and sieved and stored into gallon-sized, freezer, zip-top plastic bags. To ensure the sediments remained sterile, the soil-filled bags were triple bagged. Sediments were irradiated using a 1 MW TRIGA research reactor and received a cumulative dose of 2.687 Mega Rad over a three day period. Sediments were kept in a freezer at a temperature of -15 ºC after irradtion until it was packed into the columns.

Prior to the packing of the column, any column materials (e.g. acrylic pipe, probes, etc) that would come in contact with the sterilized sediments were were exposed to a germocidial lamp (UV-C light) and/or soaked in 3% hydrogen peroxide to kill any microorganism. While the sterile column was packed, it was surrounded by an enclosure composed of plastic sheets to prevent airborne contamination. As an additional precaution, a germocidial lamp was positioned within the enclosure to maintain sterile conditions.

Rainwater and Groundwater

A type I (18.2 MΩ cm^{-1}) Nanopure water (Thermo Fisher Scientific,Waltham, MA) was used throughout the study to emulate the relative purity of rainwater. The Nanopure water was adjusted to a pH of ~5 to simulate the reaction of the rainwater with CO_2 in the atmosphere that forms HCO_3^-, droping the rainwater to a pH of approximately 5. Five liters (which represented 1 pore volume) of water was used for each rainfall event. Bromide was used as a tracer (~250 mg/L Br^- added as sodium salt) in a Nanopure rainwater solution in a rainfall event that occurred on day 78 of the experiment.

Nanopure water was also used for groundwater. Sulfate (as sodium salt) was added to the water to emulate a groundwater having a high concentration (350 mg/L) of SO_4^{2-}. At the bottom of the column, the experimental setup was designed to maintain a constant water table elevation during rainfall, but no attempt to maintain a constant SO_4^{2-} concentration in the groundwater reservoir was made. Thus, SO_4^{2-} concentrations

decrease throughout the experiment as added rainwater dilutes the SO_4^{2-}. Prior to beginning any experimentation, soil columns were wetted up, with Nanopure water, from the bottom, to prevent air from being trapped in the sediment which would alter water flow through the column.

Experimental Timeframe

Experiments took place from 11/18/08 to 03/2/09 for a total of 105 days. The study was designed to analyze the biogeochemical response of the columns to a range of hydrologic conditions, such as rainwater infiltration and a falling and rising water table, that are common to the vadose zone. A frequent and rigorous sampling regimen was implemented to capture geochemical responses to hydrologic variations. A detailed discussion of the entire 105 days of experimentation and sampling are beyond the scope of this paper, instead we will focus on results obtained from the last 28 days (2/3/09-3/2/09) of the experiment to highlight observations of linked hydrologic and biogeochemical processes.

However, to fully understand the geochemical and hydrologic processes occurring during the conclusion of the experiment, a basic knowledge of the experimental conditions and results of the preceding 77 days is needed. Thus, brief portions in the Methods and Materials section and the Results and Discussion section are devoted to a review of this time period. To help distinguish between the two experimental intervals, we refer to the time period covering the first 77 days as the

"Antecedent Experiment" and to the time period covering the concluding 27 days as the "Successive Experiment".

Antecedent Experimental (AE) Conditions

The objective of the first stage of this experiment was to investigate the geochemical response to initial rainfall which would provide baseline geochemical values against which later rainfall events (where a water table was present) were compared.

The second stage examined the response of an introduction of oxygenated Nanopure groundwater to a depth of -55 cm of the columns. A rainfall event occurred while the Nanopure groundwater table was at 55 cm depth on day 22 of the experiment. The elevation of the Nanopure groundwater table was maintained at 55 cm depth over the next 54 days until it was drained before the start of the successive experiment.

Successive Experimental Conditions

Figure 5.3 shows the bottom hydrologic and chemical boundary conditions of KLC and LC. Figure 5.3a shows the depth of the water table elevation over time. Time periods, in which there was no groundwater table present, are indicated by lines that disappear below the horizontal axis. This figure also highlights the duration of each phase of the experiment. Figures 5.3b and 5.3c show the concentrations of SO_4^{2-} and Br^- as measured in the groundwater reservoirs and should not be mistaken for a breakthrough curve.

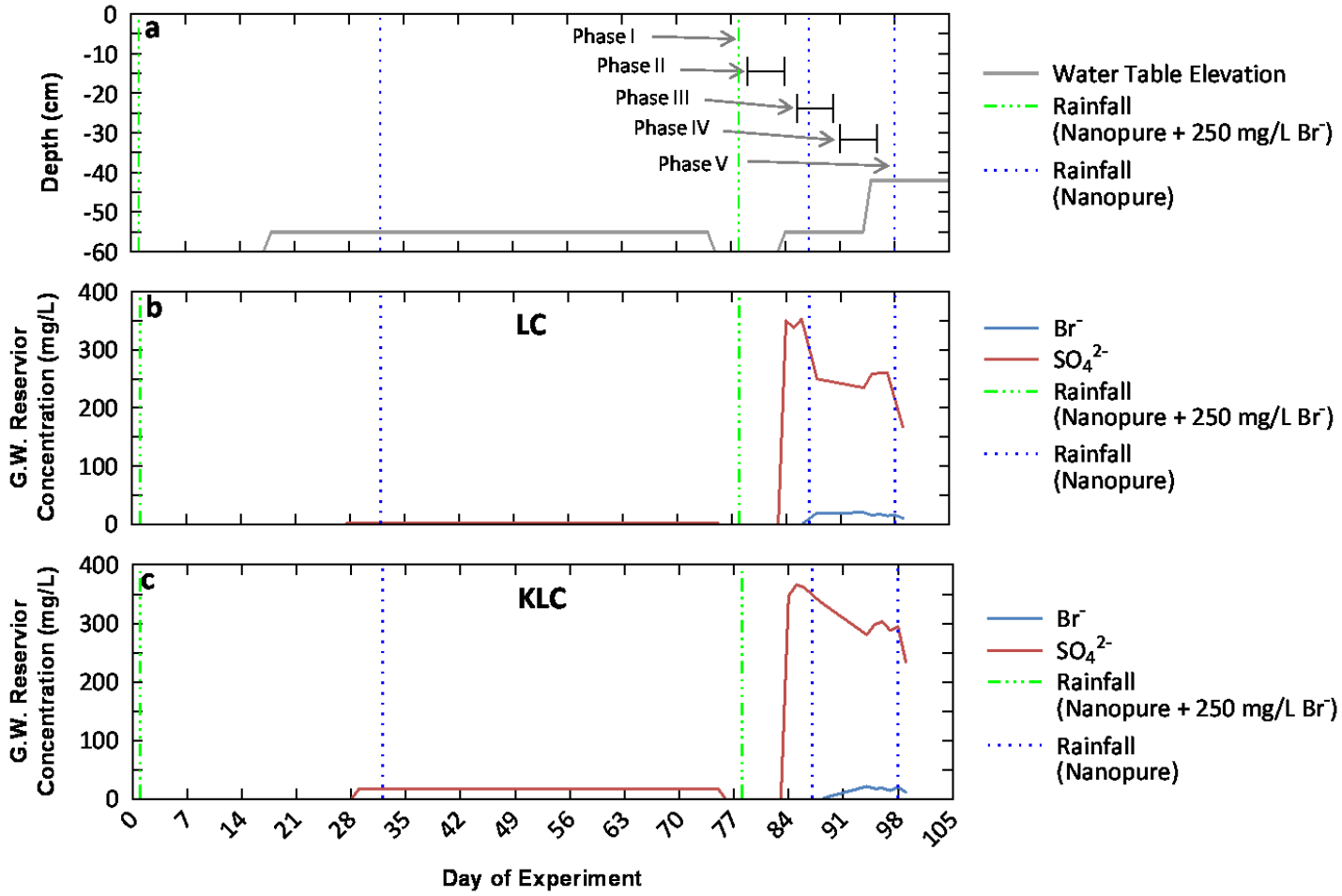

Figure 5.3 – Top and Bottom water and chemical boundary conditions during the experimental period. Note that the groundwater table elevation shown in a is the same for both LC and KLC.

Experimental Phase I - A rainfall event occurred on day 78 of the experiment using an aqueous solution that was augmented with 250 mg/L Br- as a tracer. This tracer was used to distinguish rainwater from groundwater that would be introduced during Phase II. There was no water table applied at the bottom of column during this phase.

Experimental Phase II - Deoxygenated SO_4^{2-} rich (~350 mg/L) groundwater was introduced at the bottom of column to assess the geochemical response to the presence of groundwater. After groundwater introduction, the lower half of the column was sampled each day for three consecutive days (days 84-86 of the experiment) to observe the geochemical impact of a rising water table and the establishment of the capillary fringe.

Experimental Phase III - Following the introduction of the water table, approximately 5 L of rainwater was applied at a rate of 10 mL/min (0.06 cm/min) over approximately 8 hours on day 87 of the experiment. The entire column and water table reservoirs were sampled during rainfall and one and seven days afterwards (days 88 and 94 of the experiment respectively).

Experimental Phase IV - This phase examined the response of the system to the raising of the SO_4^{2-} rich groundwater table by 13 cm, from a depth of 55 cm to a depth of 45 cm, on day 95 of the experiment. The lower half of the column was sampled each day for three consecutive days after the water table was raised (days 95-97 of the experiment).

Experimental Phase V - After the water table was raised, the entire column and water table reservoirs were sampled during rainfall (day 97 of the experiment) and one

Table 5.3 - Column experimental conditions for each sampling round. Abbreviations used in table: B.C. – boundary condition, W.T. – water table.

Sampling Round	Date	General Description	Top Flow B.C.	Top Chemical Transport B.C.	Bottom Flow B.C.	Bottom Chemical Transport B.C.
001	11/18/2008 (1)	Rainfall	39.7 cm^3/min Flux	Nanopure pH ~ 5 125 mg/L Br,	Free Drainage	N/A
002	11/25/2008 (8)	Day 7 response to rainfall	Atmospheric	N/A	Free Drainage	N/A
003	12/02/2008 (15)	Rainfall	10 cm^3/min Flux	Nanopure pH ~ 5	Free Drainage	N/A
004	12/05/2008 (18)	Day 1 after W. T. Intro	Atmospheric	N/A	W.T. @-55 cm	Oxygenated Nanopure
005	12/06/2008 (19)	Day 2 after W. T. Intro	Atmospheric	N/A	W.T. @-55 cm	Oxygenated Nanopure
006	12/07/2008 (20)	Day 3 after W. T. Intro	Atmospheric	N/A	W.T. @-55 cm	Oxygenated Nanopure
007	12/09/2008 (22)	Rainfall w/ water table	20 cm^3/min Flux	Nanopure pH ~ 5	W.T. @-55 cm	Oxygenated Nanopure
008	12/10/2009 (23)	Day 1 response to rainfall	Atmospheric	N/A	W.T. @-55 cm	Oxygenated Nanopure
009	12/16/2008 (29)	Day 7 response to rainfall	Atmospheric	N/A	W.T. @-55 cm	Oxygenated Nanopure
010	2/03/2009 (78)	Rainfall	20 cm^3/min Flux	Nanopure pH ~ 5 250 mg/L Br^-	Free Drainage	N/A
011	2/09/2009 (84)	Day 1 after W. T. Intro	Atmospheric	N/A	W.T. @-55 cm	N_2 purged Nanopure w/ ~ 350 mg/L SO_4^{2-}
012	2/10/2009 (85)	Day 2 after W. T. Intro	Atmospheric	N/A	W.T. @-55 cm	N_2 purged Nanopure w/ ~ 350 mg/L SO_4^{2-}

Table 5.3 – continued

Sampling Round	Date	General Description	Top Flow B.C.	Top Chemical Transport B.C.	Bottom Flow B.C.	Bottom Chemical Transport B.C.
013	2/11/2009 (86)	Day 3 after W. T. Intro	Atmospheric	N/A	W.T. @-55 cm	N_2 purged Nanopure w/ ~ 350 mg/L SO_4^{2-}
014	2/12/2009 (87)	Rainfall with W. T.	10 cm^3/min Flux	Nanopure pH ~ 5	W.T. @-55 cm	N_2 purged Nanopure ~ 350 mg/L SO_4^{2-}
015	2/13/2009 (88)	Day 1 after rainfall	Atmospheric	N/A	W.T. @-55 cm	N_2 purged Nanopure ~ 200-250 mg/L SO_4^{2-}
016	2/19/2009 (94)	Day 7 after rainfall	Atmospheric	N/A	W.T. @-55 cm	N_2 purged Nanopure ~ 200-250 mg/L SO_4^{2-}
017	2/20/2009 (95)	Day 1 - Heightened W. T.	Atmospheric	N/A	W. T. @ -42 cm	N_2 purged Nanopure ~ 200-250 mg/L SO_4^{2-}
018	2/21/2009 (96)	Day 2 - Heightened W. T.	Atmospheric	N/A	W. T. @ -42 cm	N_2 purged Nanopure ~ 200-250 mg/L SO_4^{2-}
019	2/22/2009 (97)	Day 3 - Heightened W. T.	Atmospheric	N/A	W. T. @ -42 cm	N_2 purged Nanopure ~ 200-250 mg/L SO_4^{2-}
020	2/23/2009 (98)	Rainfall with Heightened W. T.	10 cm^3/min Flux	Nanopure pH ~ 5	W. T. @ -42 cm	N_2 purged Nanopure ~ 200-250 mg/L SO_4^{2-}
021	2/24/2009 (99)	Day 1 response to rainfall	Atmospheric	N/A	W. T. @ -42 cm	N_2 purged Nanopure ~ 170-230 mg/L SO_4^{2-}
022	3/2/2009 (105)	Day 7 response to Rainfall	Atmospheric	N/A	W. T. @ -42 cm	N_2 purged Nanopure ~ 170-230 mg/L SO_4^{2-}

and seven days afterwards (days 99 and 105 of the experiment respectively).Table 5.3 shows dates, pumping rates, boundary conditions, and rainwater and water table solution chemistry during each sampling round. A graphical timeline of the bottom and top boundary conditions is also shown in Figure 5.3.

RESULTS AND DISCUSSION

Antecedent Experimental Results

The most significant result observed from the antecedent experiment was the development of Fe-oxide bands that formed near the fringes of the lenses in the live lens column (LC). Figure 5.4 shows the live lens column (LC) and the killed-control lens column (KLC) at the conclusion of the antecedent experiment. The formation of these Fe-oxide bands at the fringes of the lenses in LC are discussed at length in Hansen et al. (submitted). In summary, the Fe-oxide bands were formed in a multiple-step process. This first step began as high water content coupled with microbial metabolism created an O_2 limited environment within the organic-rich loam lenses. This caused microorganisms to utilize other terminal electron acceptors such as NO_3^-, Fe^{2+}, and SO_4^{2-}. These processes produced FeS minerals, derived from iron and sulfate reduction within the core of the organic-rich loam lenses. As O_2 returned (through rainwater or evaporation) to the sediment where the FeS minerals had formed, these minerals were oxidized to Fe-oxide minerals at the interface between the organic-rich loam lens and the surrounding sand matrix material.

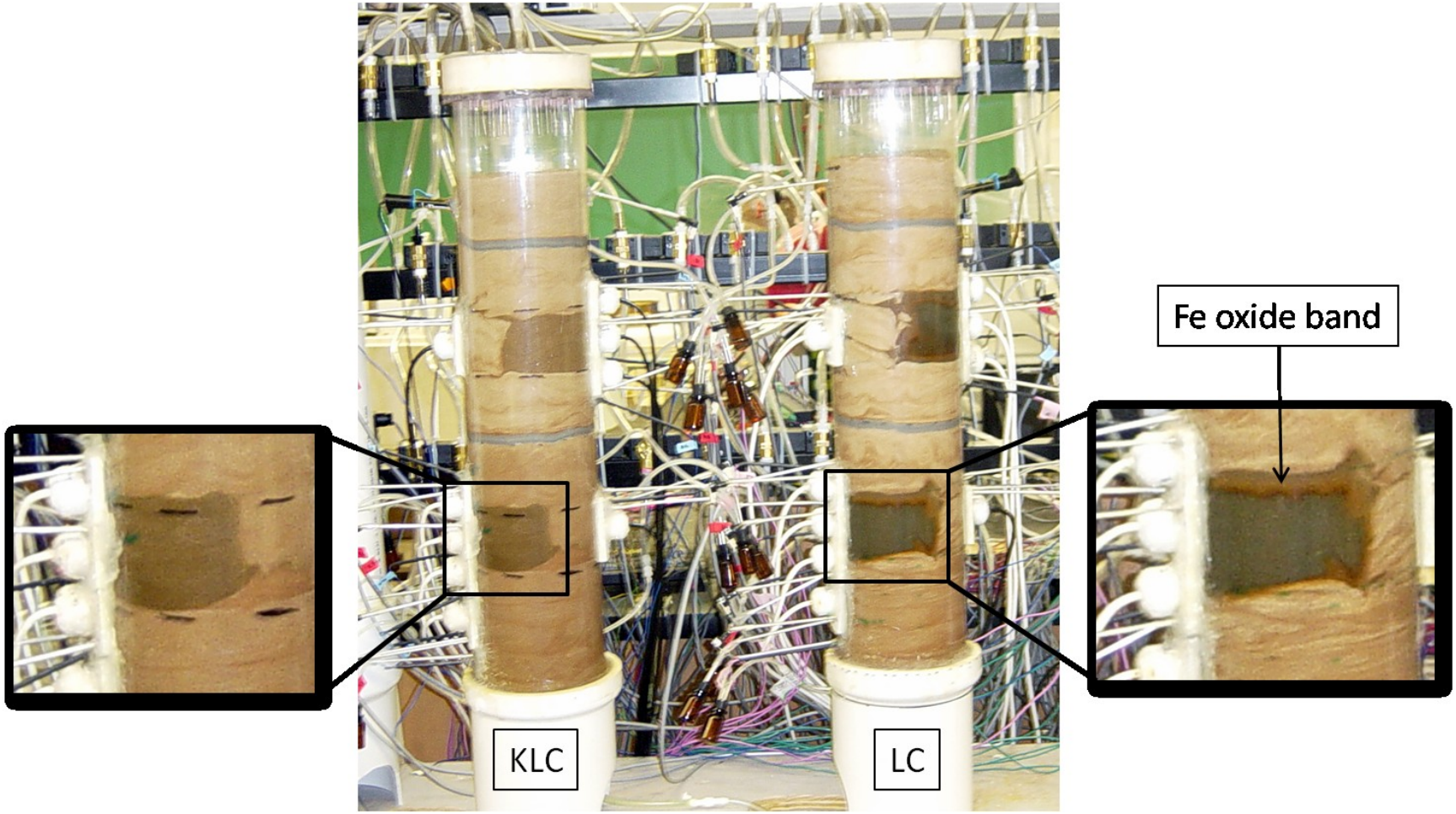

Figure 5.4 - Sterilized [KLC](left) and live [LC] (right) columns after two months of experiments. The lenses in the live column have developed Fe-oxide band near their fringes. The absence of Fe-oxide bands indicated absence of microbial activity in the sterile column.

Ultimately, the oxidized Fe minerals that formed within the sediment pore spaces reduced porosity/permeability and reduced the rate at which water could flow through the lenses. The flow rate through the lenses in KLC, compared to the flow rate through the lenses in LC, was 3.82 cm^3/min and 0.78 cm^3/min respectively (Hansen et al., Submitted, 2011b). The lack of Fe-bands in KLC suggest that sediments remained sterile throughout the experiment.

Experimental Phase I: Bromide Augmented Rainwater

High concentrations of Br^- (up to 199.0 mg/L – data not shown) remained in the sediment porewaters after rainwater passed through the column. These high concentrations of Br- were used in Phase II as an identifier of rainwater.

Experimental Phase II: Introduction of Sulfate-rich Groundwater

The introduction of SO_4^{2-} rich groundwater at the bottom boundary of the columns resulted in separation of distinct water masses into different areas within both LC and KLC. The combination of high SO_4^{2-} concentrations in the groundwater and low background SO_4^{2-} concentrations (3-5 mg/L) in soil porewaters, before the introduction of the groundwater table, allowed for straightforward tracking of groundwater movement in the columns. Additionally, this SO_4^{2-} rich groundwater was devoid of Br^- which allowed us to track the spatial distribution of the rainwater (high Br^- concentrations) and groundwater (high SO_4^{2-} concentrations).

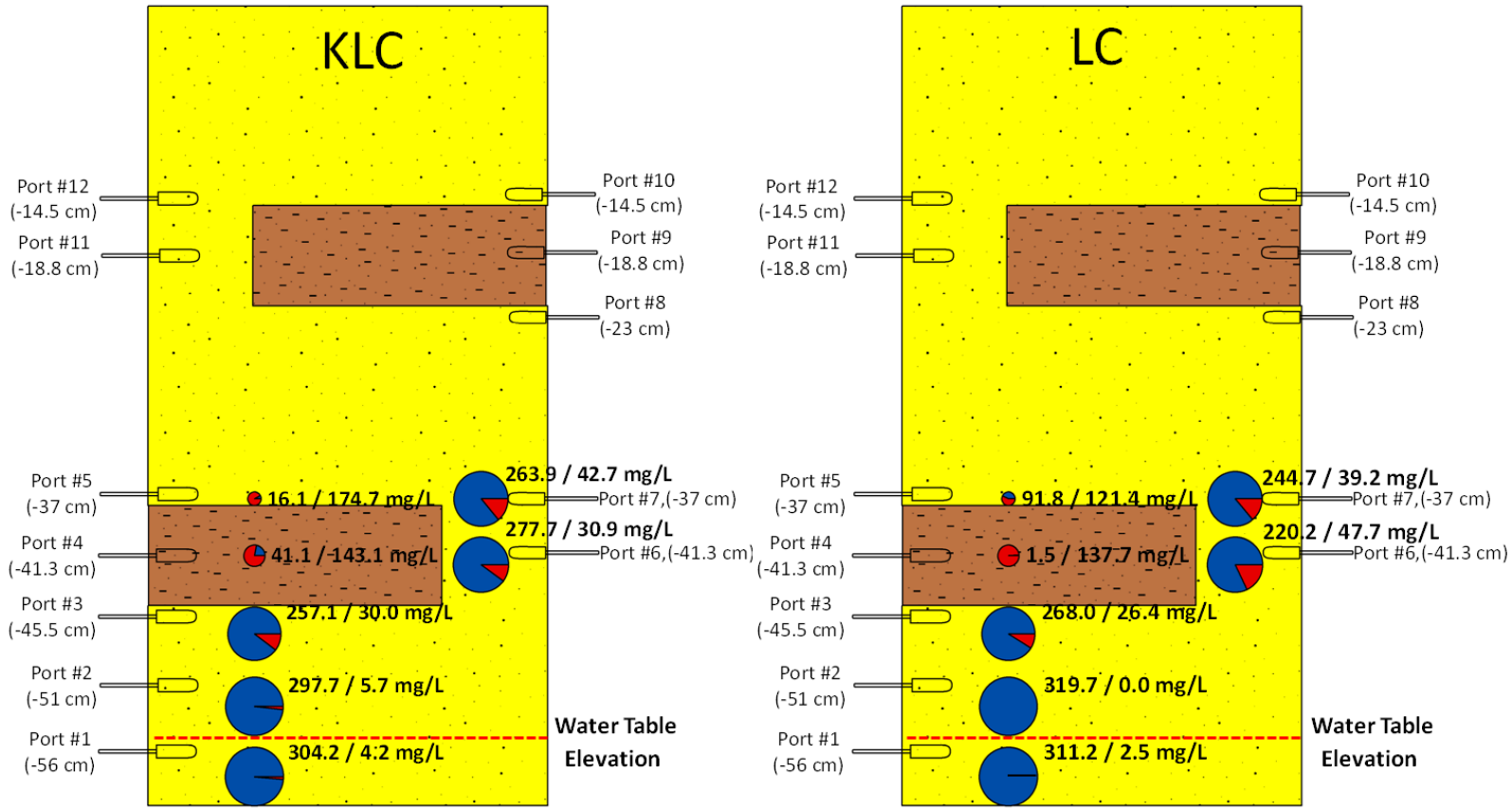

Figure 5.5 – SO_4^{2-} and Br^- concentrations three days after the introduction of a water table (Day 85 of the Experiment). Sulfate concentrations are listed first in labels followed by Br-. Sterilized column [KLC] (left) and live column [LC] (right). Note: data only shown for the lower half of the column because top half was not sampled at this time.

Bromide and SO_4^{2-} concentrations in both the columns 3 days (02/12/2009) after the introduction of groundwater table are shown in Figure 5.5. The SO_4^{2-} concentrations directly below the lower lenses in port 3 were 257.1 mg/L and 268.0 mg/L in KLC and LC respectively which demonstrated that capillary rise was actively transporting groundwater upwards. Similarly, the SO_4^{2-} concentrations in Port #7 (adjacent to the lens) were 263.9 mg/L and 244.7 mg/L in KLC and LC respectively. Compared to Port #4, (within the lower lens) of KLC and LC, the SO_4^{2-} concentrations were much lower at 41.1 mg/L and 1.5 mg/L respectively. This demonstrates that groundwater was prevented from rising up into the lens in LC and to a lesser degree in KLC.

Bromide concentrations, within and above the lens, remain high indicating that these areas were still primarily impacted by rainwater and that groundwater was not entering into or passing through the lens. Within the lens, concentrations in the lens at KLC and LC remained high at 143.1 mg/L. and 145.3 mg/L respectively. Above the lenses Br^- concentrations were also high at174.7 mg/L and 121.4 mg/L in KLC and LC respectively. The Br^- and SO_4^{2-} data demonstrate that Phase I rainwater was retained in the regions in and above the lenses while the sulfate-rich groundwater was transported to the regions below and to the side of the lenses.

The inhibition of capillary rise in KLC was attributed to a capillary barrier created by the contact between the sand and loam materials (Bradford et al., 1998). Capillary barriers are created by either a difference in soil texture, due to abrupt changes in the pore size distribution or by differences in the soil surface wetting characteristics. The capillary barrier created in this system was attributed to the later. In particular,

organic matter (abundant in the loam material) has been shown to be hydrophobic (Chenu et al., 2000; Jouany, 1991). This hydrophobicity increases the contact angle which limits the height of capillary rise. In LC, in addition to the capillary barrier effect, the Fe-oxide bands, which clogged pore spaces, also inhibited the fluid flow rate upwards.

Thus the presence of a soil lens in the capillary fringe led to the partitioning of different (infiltrating and ground) water masses. Furthermore, presence of the lens also prevented groundwater from rising as high as it did in the right-half of column where only sand was present. These findings indicate that contaminants could also be partitioned in different areas of the vadose zone. This also suggests that care should be taken when characterizing the degree of contamination at polluted sites and designing remediation strategies. An underlying lesson from this finding is that sampling of partitioned waters that are relatively less polluted at specific regions, but not necessarily characteristic of the entire subsurface system, may lead to an underestimation of the severity of contamination and vice versa.

Experimental Phase III: Impact of Rainfall on SO_4^{2-} Rich Groundwater Table at -55 cm Depth

This rainfall event occurred on day 87 of the experiment while the SO_4^{2-} rich groundwater was in place at an elevation -55 cm. In both KLC and LC, the rainwater displaced the SO_4^{2-} rich water from the capillary fringe. This replacement of groundwater with rainwater can be demonstrated by comparing the post-rainfall SO_4^{2-}

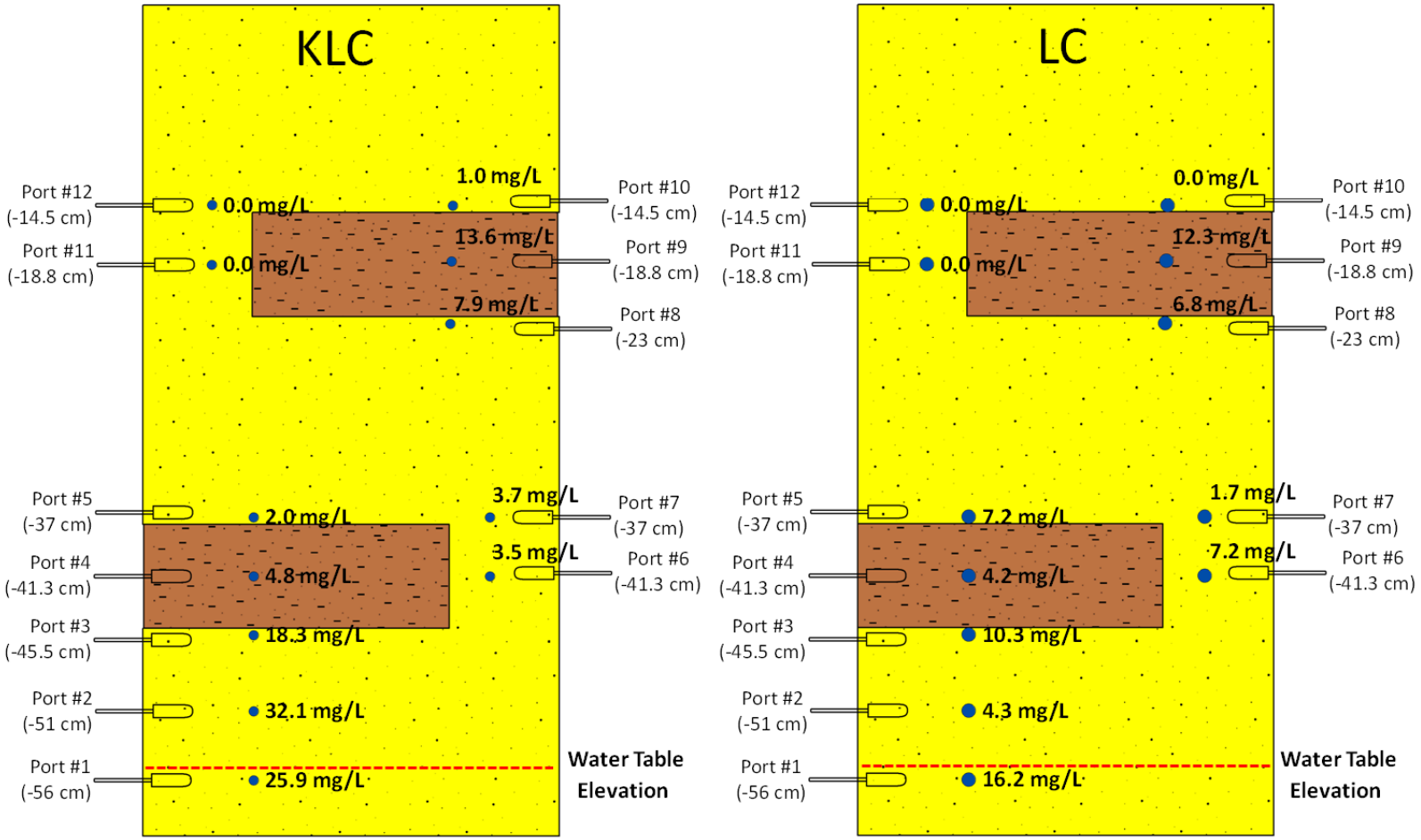

Figure 5.6 – SO_4^{2-} concentrations seven days after rainfall (day 94 of experiment). Sterilized column [KLC](left) and live column [LC] (right)

concentrations to pre-rainfall SO_4^{2-} concentrations at the lowest sampling location (Port #1). Pre-rainfall concentrations in KLC and LC were 304.2 and 311.2 mg/L respectively (Figure 5.3) while post-rainfall concentrations in KLC and LC were 25.9 mg/L and 16.2 respectively (Figure 5.6).

These low concentrations of SO_4^{2-} suggested that there was very little water mixing between the water table and the capillary fringe. It is unclear what the impact of horizontally flowing groundwater (absent in this study) may have had on mixing between the groundwater and capillary fringe. However a study by McGuire et al. (2005) found, unmixed water masses in a natural system where groundwater was actively flowing. They found geochemically distinct water masses had formed in a shallow sandy aquifer and that recharge waters did not mix with groundwater suggesting that horizontal flow did not cause mixing. Consequently, if rainwater transports contaminants through the vadose zone, but does not mix readily with groundwater, then the high concentrations of contaminants may reside in the capillary fringe instead of entering directly into the aquifer. This may have implications for contaminant assessment and remediation design.

Water Flux and Terminal Electron Accepting Processes (TEAPs)

During the infiltration process, the rainwater transported dissolved O_2 to the capillary fringe. Prior to rainfall on day 87 of the experiment, deoxygenated sulfate-rich groundwater resided in the capillary fringe, which caused a shift in terminal electron accepting processes (TEAPs). For instance, before rainfall, low concentrations of S^{2-}

were observed at the lowest sampling location in LC (3.1 – 22.1 μg/L). This was likely produced by bacterial SO_4^{2-} reduction (BSR) (Marschall et al., 1993) shown in the following reaction: $SO_4^{2-} + 2\ CH_2O$ (organic substrate) → $H_2S + 2\ HCO_3^-$. During the rainfall and for 24 hours afterward, S^{2-} was not observed in LC which suggested that the rainfall caused a cessation of BSR. The suspension of BSR was caused by the transport of dissolved O_2 via rainwater to the lower regions of the column that caused the metabolic activity of the anaerobic SO_4^{2-} reducing bacteria to cease. As expected, S^{2-} was not observed in KLC as the sterilization prevented BSR from occurring.

Sulfide was once again observed seven days after the phase III rainfall(day 94 of experiment) and its concentration (213.4 μg/L) was the highest observed up to that point in the experiment (Figure 5.7). The resumption of sulfate reduction demonstrated the relatively rapid removal of O_2 from the capillary fringe. The high degree of microbial activity in the capillary fringe (Konopka and Turco, 1991; Lahvis et al., 1999; Widrig and Manning, 1995), led to the consumption of O_2 by two main processes: (a) abiotic oxidation by dissolved oxygen of reduced minerals (e.g. iron-sulfide minerals) previously formed from biogeochemical activity in Phase II and (b) microbial aerobic respiration. It was unclear, the degree to which each process contributed to the consumption of O_2, however the short duration of time (no more than 5 days) before BSR resumed in the capillary fringe was striking.

Before BSR recommenced, microorganisms would have also consumed terminal electron acceptors such as NO_3^- or Fe(III) that would have yielded more energy. Thus it was expected that NO_3^- concentrations in the capillary fringe would be zero because of

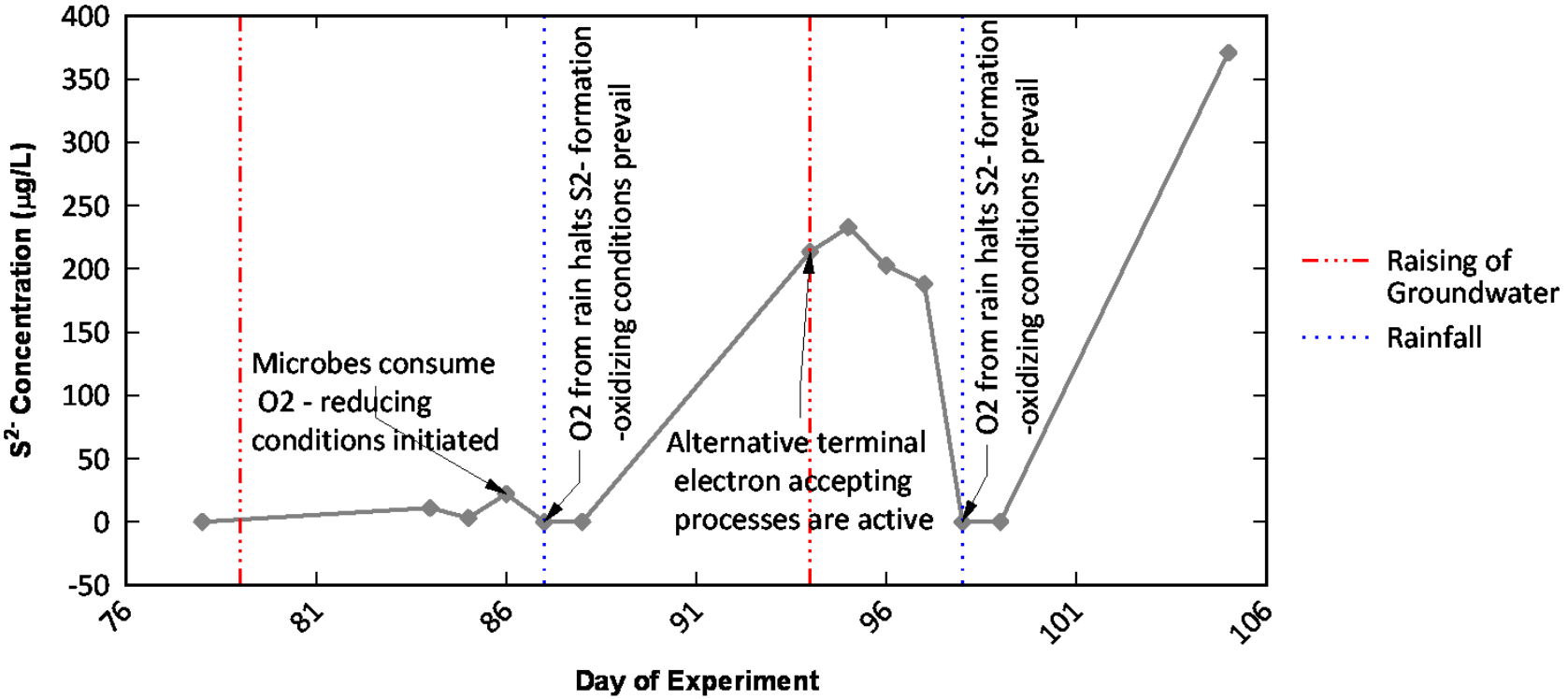

Figure 5.7 - Sulfide concentrations in LC over time at sampling port #1 (-56 cm). Sulfide was not observed in KLC.

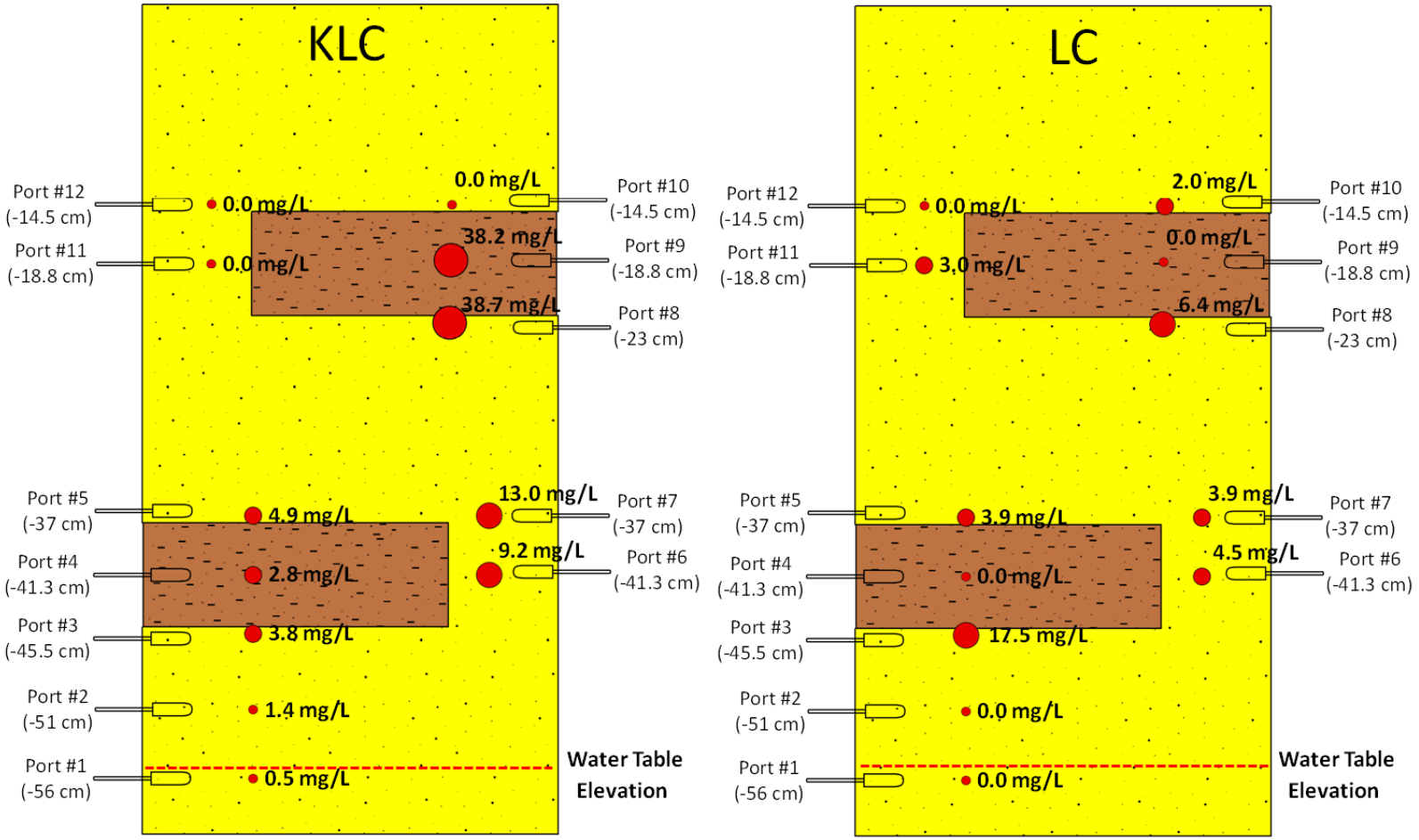

Figure 5.8 - NO_3^- concentrations in the sterile [KLC] (left) and live [LC] (right) columns on day 94 of experiment.

active dentrification. Figure 5.8 show concentrations of NO_3^- in LC as well as KLC. Ports #1 and #2 in the LC column show that NO_3^- had indeed been depleted to zero. Concentrations of 0.5 mg/L and 1.4 mg/L NO_3^- observed in Ports #1 and #2 respectively in KLC demonstate that NO_3^- likely would have been present in LC, if not for dentrification.

Another area where NO_3^- was absent was the inside the lenses. Observations of Fe^{2+} and S^{2-} (data not shown) within the lenses are consistent with the absence of NO_3^-. Nitrogen cycling was active as evidenced by observations of NO_3^- concentration of 17.5 mg/L. This NO_3^- was likely created by oxidation of transported NH_4^+ (Morrill and Dawson, 1967) that originated from microbial cycling of organic matter within the lens (Báez-Cazull et al., 2007).

Observations of highly reducing conditions within the lenses and capillary fringe were accompanied by extraction of gases from the column sediments by the sampling lysimeters. Heretofore, gases had never been observed during sampling. The observation of the greatest volume of gas occurred on (day 94 of the experiment) while sampling port #2 of LC. Normally, this lysimeter container filled with soil pore-water solution in approximately seven minutes. During this sampling, the time it took to fill the lysimeter bottle was tripled because of the relatively large volumes of gas pulled from the column via the lysimeter. Gas volumes, to a lesser extent, were also extracted from Ports #1 and #3. Unfortunately, we were not able to collect the gas or analyze its composition, but because both denitrification and BSR had been active, these sampled gases were likely end products of these processes (e.g. N_2, NO, N_2O or H_2S). Additionally, it was likely

that methanogensis was also actively producing CH_4 as BSR and methanogenesis are not mutually exclusive processes and are frequently observed together (Oremland and Taylor, 1978; Oremland and Polcin, 1982; Senior et al., 1982). The lack of any gas extracted from KLC (where denitrification, BSR, or methanogenesis did not occur) support the supposition that the gases sampled in LC were biogenic in nature.

Experimental Phase IV: Impact of Elevated Sulfate-rich Water Table

After the Phase III rainfall, the SO_4^{2-} rich water table was raised from a depth of -55 cm to a depth of -45 cm. After this event, large differences in distribution and concentration of SO_4^{2-} arose between KLC and LC. Concentrations of SO_4^{2-}, 3 days after the water table was raised, are shown in Figure 5.9. In KLC, concentrations at the lower sampling locations were practically the same as those measured in the groundwater reservoir (average 287.8 mg/L) suggesting groundwater had freely moved into the lower half of the column. Within and above the lens, concentrations were slightly lower, but still show that capillary rise had transported groundwater into these areas.

In contrast to KLC, the concentrations of SO_4^{2-} in LC are considerably lower and don't extend to the heights as observed in case of KLC. The concentration of SO_4^{2-} at the lowest sampling location was ~25% lower than what was observed in the groundwater reservoir. The concentrations decreased rapidly with height to low levels (5.2 - 7.9 mg/L) near the lens. The most striking difference in concentration is between Ports #2 and #3 which are vertically separated by just 5.5 cm. The concentration of SO_4^{2-} at Port #2 is 135.9 mg/L while it is 11.2 mg/L at Port #3. One possible

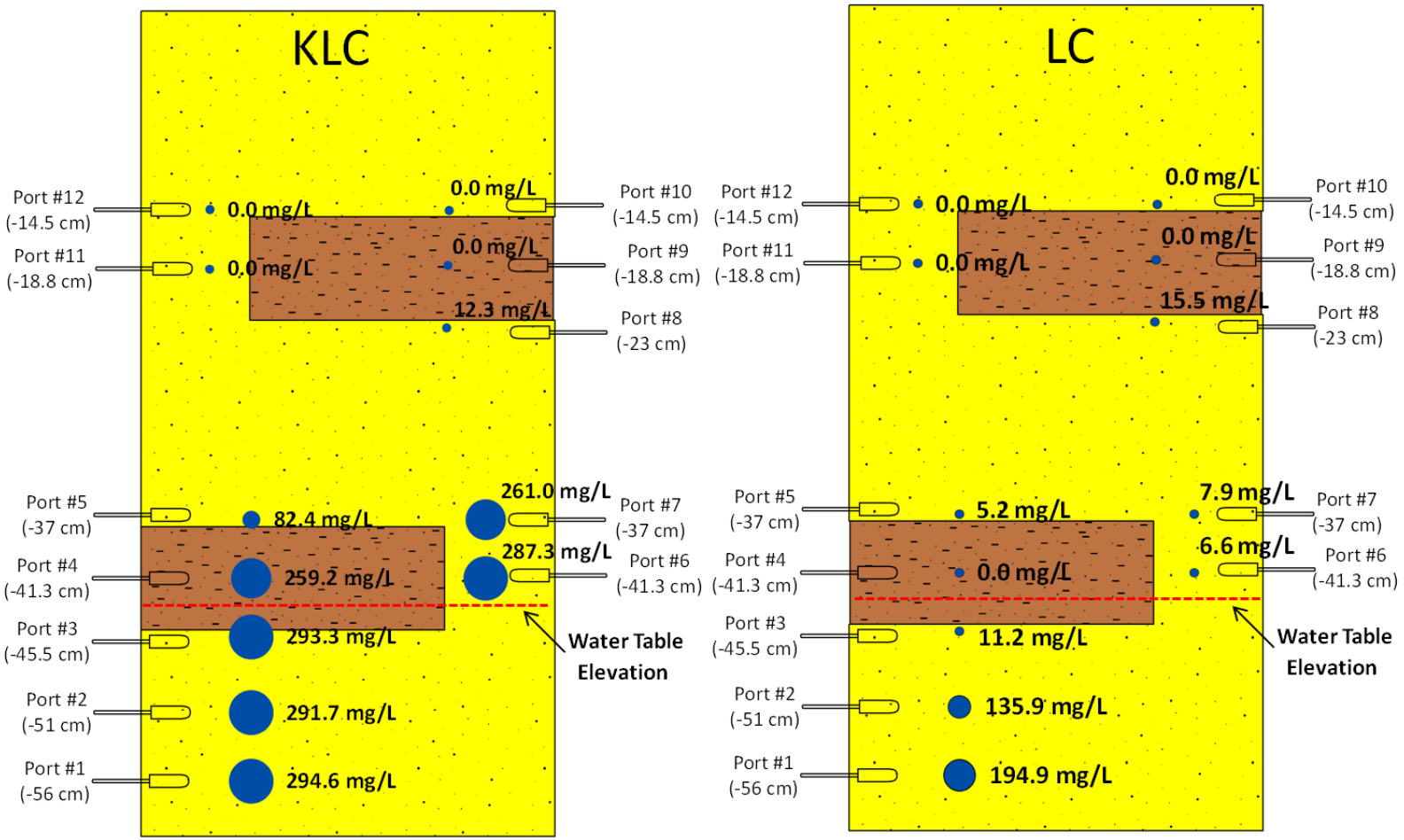

Figure 5.9 – SO_4^{2-} concentrations after the raising of a sulfate-rich water table on day 97 of experiment. Sterilized column [KLC](left) and live column [LC] (right)

explanation for the SO_4^{2-} concentration difference was that BSR was actively removing SO_4^{2-} at Port #3. However, the absence of any S^{2-} at Port #3 during this time demonstrates that BSR was not occurring. Thus the most plausible explanation for the concentration difference is that the upward groundwater flow was being blocked between these two sampling points. Hereafter the area between these two sampling points will be referred to as the flow impedance zone (FIZ). Because the columns were identically constructed, packed, and handled, these concentration differences did not arise from column management. Therefore the variation in concentration and distribution of SO_4^{2-} was attributed to biological activity; the only difference between the two columns.

Biological Impact on Water Flux

While it is not inherently clear what biological mechanism was responsible for the flow impedance, processes that have the potential to decrease the hydraulic conductivity of the sediment were considered. Here, we primarily consider several biological processes whereby hydraulic conductivity is decreased through blockage of pore spaces which in turn leads to a reduction of porosity and/or permeability. Many of these processes are listed and reviewed by Baveye et al.(1998) and Rockhold et al. (2002).

One process, whereby porosity and permeability can be reduced is through mineral precipitation, caused by biogeochemical cycling, within sediment pore spaces. The Fe-oxide bands, near the fringes of the lenses in LC, have already been shown to

limit the flow rate of water through the lenses (Hansen et al., Submitted, 2011b). The development of these types of bands is obvious from a visual analysis standpoint. Thus, the lack any mineral banding in the FLZ suggest that this mineralization process was not responsible for the SO_4^{2-} distribution.

Accumulation of microbial cells in pore spaces has been shown as one of the methods to reduce hydraulic conductivity in porous media (Gupta and Swartzendruber, 1962; Vandevivere and Baveye, 1992a; Vandevivere and Baveye, 1992b). However, these studies utilize substrates that are high in carbon (e.g. glucose, wastewater) that expedite microbial growth and colonization. Organic matter percentage in the sand that occupied the FIZ was a mere 0.02% (for comparision the organic matter percentage in the loam was 2.47%) and thus was not considered to be not enough substrate for substantial cell mass to accumulate in the pore spaces to considerably reduce hydraulic conductivity.

Another manner in which microorganisms can "clog" pore spaces is through excretion of extracellular polysaccharides (Baveye et al., 1998; Vandevivere and Baveye, 1992a) that are frequently referred to as biofilms. The carbon to nitrogen (C:N) ratio of substrate is commonly used as a indicator to predict if biofilms will develop with the minimum threshold being in the 5-12 C:N ratio range. (Huang et al., 1994; Thompson et al., 2006). Carbon and nitrogen combustion analysis revealed that the sand in the FIZ had a 0.56 C:N ratio suggesting that significant biofilm synthesis did not develop and thus retard water flow through the FIZ. Regardless of the exact ratio, an excess of labile carbon will result in microbial fabrication of biofilm and the 0.02%

organic matter in the sand would not support biofilm creation. Therefore, mineral precipitation, accumulation of microbial cells nor biofilms were considered to be responsible for the formation of the FIZ.

Effect of Biogenic Gases on Hydraulic Conductivity

An additional biological mechanism to reduce hydraulic conductivity is through entrapment of metabolic end-product gases such as CO_2, N_2, H_2S, and CH_4. If not dissolved into water, these gases form a distinct gas-phase (bubbles) that can occupy pore space and reduce the pore size. One common method in which this occurs is for gas bubbles to become lodged in the pore throats between soil particles that prevent water from free moving through the pore throats as shown in Figure 5.10 (Seki et al., 1996). Soares et al. (1988) also investigated the influence of gas bubbles on hydraulic conductivity and found that gas bubbles decreased hydraulic conductivity, but that the loss of conductivity could be regained by applying vacuum to the medium.

These biogeochemical end-product gases have a differing potential to affect the hydraulic properties of sediment. The primary control of the establishment of gas bubbles (after biological formation) is the solubility of the gas. If a gas readily dissolves into solution, it will not create bubbles. Predicting the solubility of gases is complex because there are many dynamic environmental conditions such as temperature, pressure, and type of solvent that affects the actual solubility. However, Henry's Law constants can be used to compare the solubility of various gases in water. Lower Henry's Law constant values represent gases that are the least soluble while higher

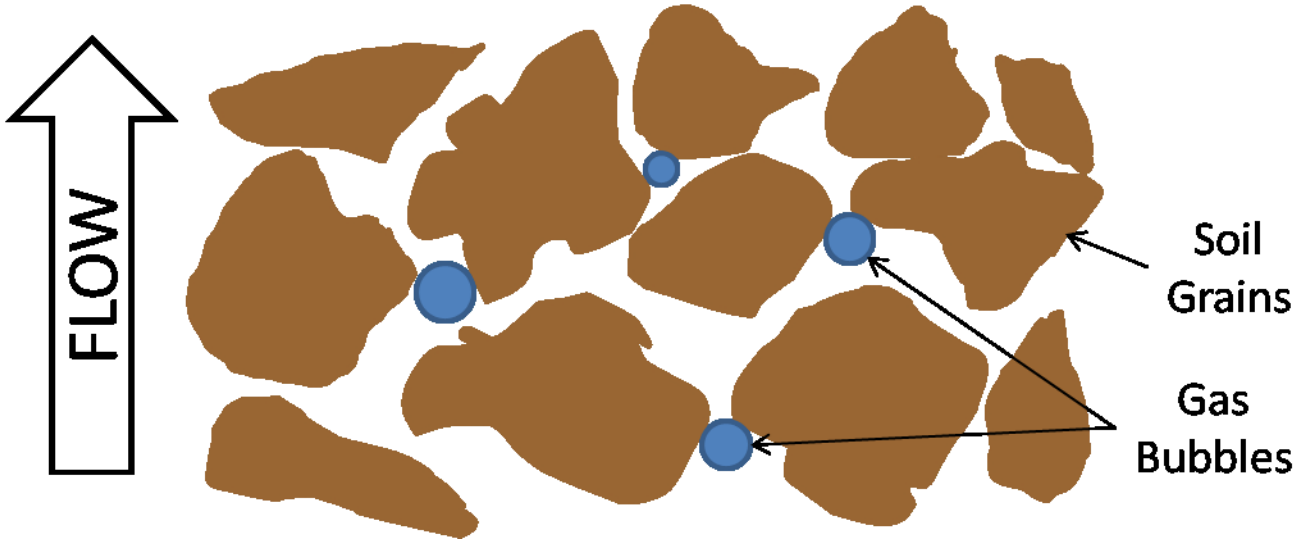

Figure 5.10 – Trapped gas bubbles inhibit water flow by blocking pore throats

values correspond to higher solubility. At standard temperature, the Henry's Law constants (mol × L^{-1} × atm^{-1}) for environmentally pertinent gases, from least to greatest, are: N_2 (6.5×10^{-4}), H_2 (7.8×10^{-4}), O_2 (1.3×10^{-3}), CH_4 (1.4×10^{-3}), NO (1.9×10^{-3}), N_2O (2.4×10^{-2}), CO_2 (3.5×10^{-2}), and H_2S (1.0×10^{-1}) (Lide, 2008; Wilhelm et al., 1977). These constants with the respective biogeochemical processes responsible for gas production are listed in Table 5.4. Although not an end-product of microbial metabolism, O_2 was considered because a significant amount of O_2 bubbles may be introduced into pore spaces via infiltration of rainwater.

The comparatively high solubility of CO_2 in relation to the other gases listed above may limit its contribution to a separate gas phase. Likewise, the high solubility of H_2S also limits its contribution to separate gas phase. In contrast, H_2 has the potential to contribute to a gas phase due to its lower solubility, but it would be consumed in anaerobic microbial metabolism too quickly to accumulate. Also due to its low solubility, CH_4 has a greater potential to contribute to a separate gas phase and has been observed in the vadose zone (Bekins et al., 2005). Methanogenesis is one of the lowest yielding metabolic pathways and generally becomes active only after all other terminal electron acceptors have been exhausted although it is commonly observed along with BSR. Because we observed active BSR, it is likely that CH_4 was also being produced.

In the vadose zone, N_2 has the greatest capability to form an independent gas phase for several reasons. First, N_2 has the lowest solubility of the previously-listed gases and thus the greatest potential to form bubbles that may alter hydraulic

Table 5.4 – Biogenic gas production information.

Gas	Process	Reaction	Henry's Law Const (mol / L • atm)	Depths Where Process Was Likely Active
N_2	Denitrification	Net Reaction $4NO_3^- + 5CH_2O + 4H^+ \rightarrow 2N_2 + 5CO_2 + 7H_2O$ Denitrification sequential reactions $4NO_3^- \rightarrow 4NO_2^- \rightarrow 4NO \rightarrow 2N_2O \rightarrow 2N_2$	6.5×10^{-4}	-60 to -51 cm Within lenses (-41.3 and -18.8)
H_2	Fermentation	$CH_2O + H_2O \rightarrow 2H_2 + CO_2$	7.8×10^{-4}	-60 to -51 cm Within lenses (-41.3 and -18.8)
O_2	Transport via rainwater	N/A	1.3×10^{-3}	Entire Column (0 to -60 cm)
CH_4	Methanogenesis	CO_2 Reduction $CO_2 + 4H_2 \rightarrow CH_4 + 2H_2O$ Aceticlastic Methanogenesis $CH_3COO^-(acetate) + H^+ \rightarrow CH_4 + CO_2$	1.4×10^{-3}	-60 to -51 cm Within lenses (-41.3 and -18.8)
NO	Denitrification	Net Reaction $4NO_3^- + 5CH_2O + 4H^+ \rightarrow 2N_2 + 5CO_2 + 7H_2O$ Denitrification sequential reactions $4NO_3^- \rightarrow 4NO_2^- \rightarrow 4NO \rightarrow 2N_2O \rightarrow 2N_2$	1.9×10^{-3}	-60 to -51 cm Within lenses (-41.3 and -18.8)
N_2O	Denitrification	Net Reaction $4NO_3^- + 5CH_2O + 4H^+ \rightarrow 2N_2 + 5CO_2 + 7H_2O$ Denitrification sequential reactions $4NO_3^- \rightarrow 4NO_2^- \rightarrow 4NO \rightarrow 2N_2O \rightarrow 2N_2$	2.4×10^{-2}	-60 to -51 cm Within lenses (-41.3 and -18.8)

Table 5.4 – continued

Gas	Process	Reaction	Henry's Law Const (mol / L • atm)	Depths Where Process Was Likely Active
CO_2	Aerobic Respiration	$O_2 + CH_2O \rightarrow O_2 + H_2O$	3.5×10^{-2}	Entire Column (0 to -60 cm)
H_2S	Sulfate Reduction	$2CH_2O + SO_4^{2-} \rightarrow HCO_3^- + H_2S$	1.0×10^{-1}	-60 to -51 cm, Within lenses (-41.3 and -18.8)

conductivity. Secondly, microorganism can readily obtain energy from the enzyamatic reduction of NO_3^- to N_2 gas in a multi-step process called denitrification. Denitrification primarily produces N_2 gas, however the small percentage of intermediate gases (N_2O and NO) produced during the reduction process may escape into the sediment pore spaces. These two gases aren't as insoluble as N_2, but nevertheless have the tendency form gas bubbles. Overall, nitrogen gases (primarily N_2) have the greatest potential to affect hydraulic conductivity over other end-product gases.

Recall that, during Phase III, denitrifcation was active; having removed all NO_3^- in the capillary fringe and that gas was observed in Port #2 during sampling. These observations coupled with the solubility characteristics of N_2 gas agree well with a scenario where gas bubbles are blocking water flow in the FIZ. Thus, out of all the biologic processes that could have been responsible for partitioning of SO_4^{2-} in LC, the entrapment of biogenic gases are most consistent with our results.

Supporting Evidence for a Separate Gas Phase

Figure 5.11 shows the soil water pressure data collected at the sampling locations (ports 2, 3, 4, and 6) in LC and KLC. In general, the figure shows that pressures in LC and KLC were roughly equal during Phases I, II, and III (day 78 to day 94 of the experiment). When the water table was raised on day 94 of the experiment, pressure data from both columns showed a sharp increase. After the groundwater table was raised, pressures in KLC begin to steadily decrease over the next three days. This decrease was attributed to the process of groundwater distribution as it spread through

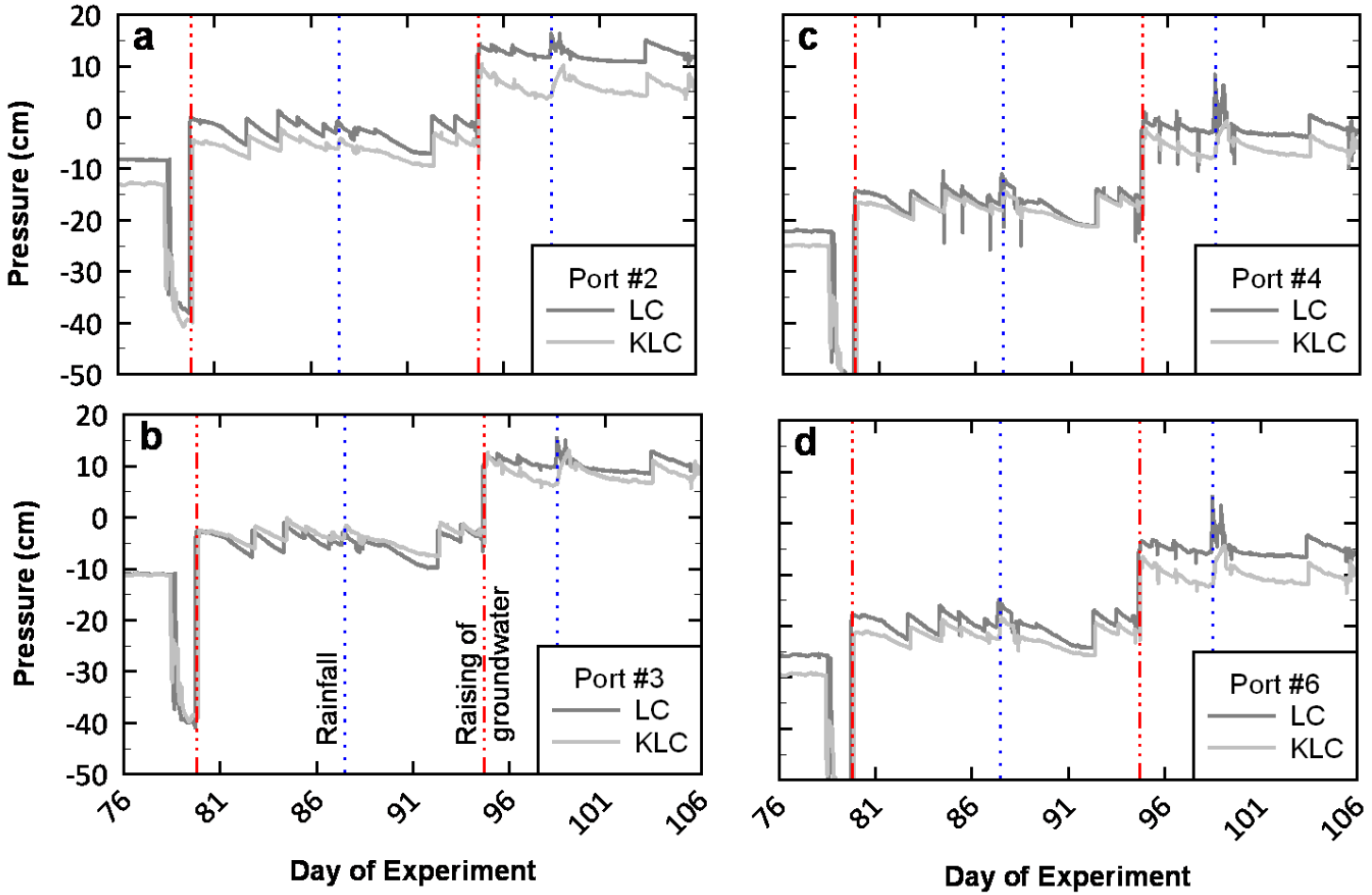

Figure 5.11 – Pore pressure measurements from ports #2 (-51cm), #3 (-45.5 cm), 4 (-41.3 cm, inside lens), and 6 (-41.3 cm, outside of lens) are shown in a, b, c, and d respectively. The dotted lines represent rainfall events and the dashed-dotted lines represent times when the groundwater levels were raised.

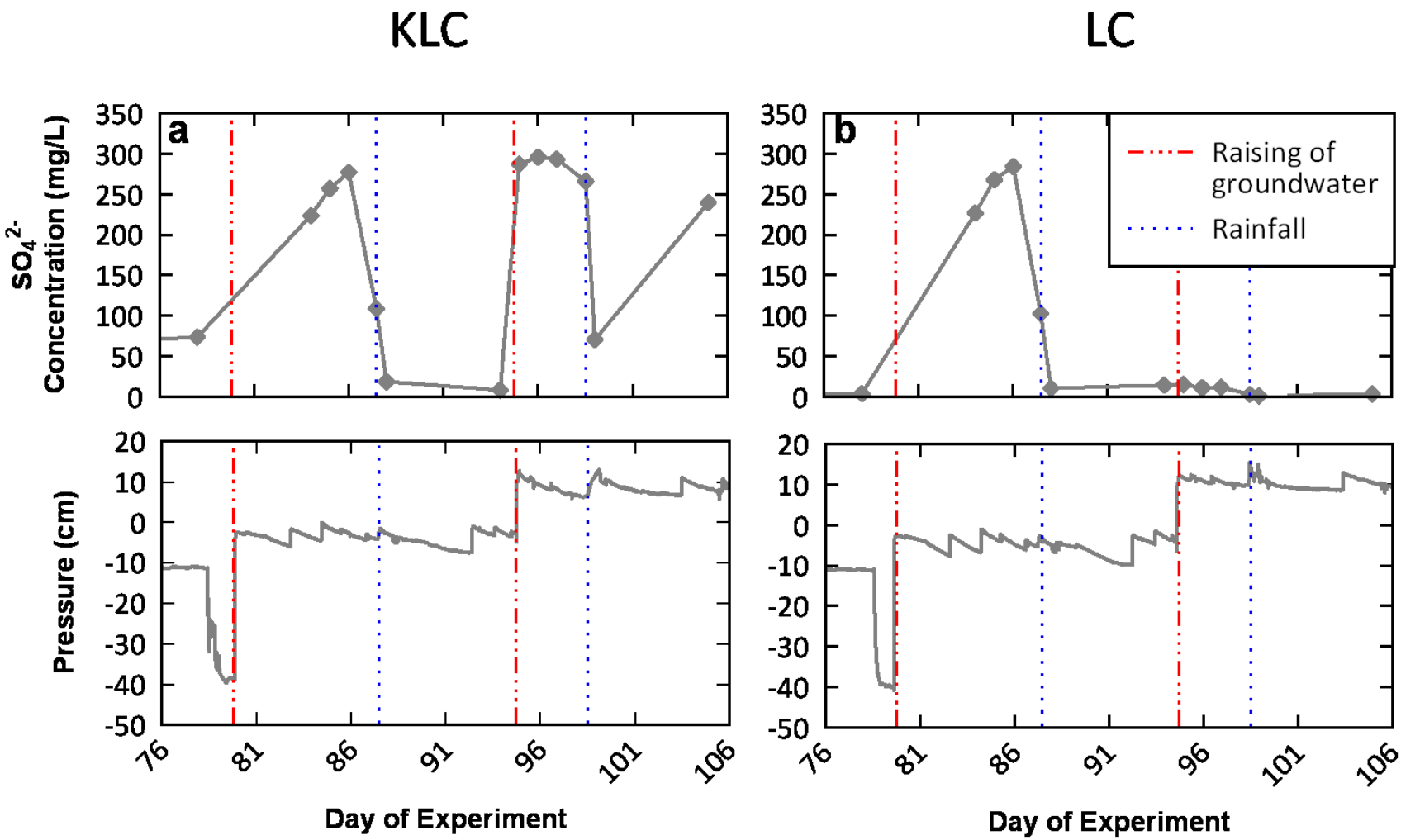

Figure 5.12 – Sulfate concentrations (top) and pore pressure measurements (bottom) from port 3 (-45.5 cm) directly below the lower lenses in KLC (a) and LC (b).

the column, established a capillary fringe and generally equilibrated with unsaturated sediments higher in the column. Figure 5.12a shows the pressure response and SO_4^{2-} to the raising of groundwater at Port #3. Sulfate concentrations increase slightly over the three day period after the groundwater raising suggesting that the groundwater was still being distributed throughout the column; not yet achieving equilibrium.

Conversely, the pressures in LC decreased only slightly during the same three days and remained near the pressure levels observed during the groundwater raising. The higher pressures were sustained because the trapped gas was holding back (much like a dam) groundwater that was being driven by a greater pressure head. In all of the sampling ports, the greatest difference between pressures in the two columns was observed on the third day after the groundwater table was raised (day 97 of the experiment). These higher pressures agree well with results of Dunn and Silliman (2003), who observed that the presence of trapped gases near the water table resulted in higher sediment pore pressures. Figure 5.12b shows pressure data and the near absence of SO_4^{2-} at Port #3 after the groundwater table was raised; further emphasizing the efficiency to which upward groundwater flow was blocked.

Distribution of Water Masses

Results from this study clearly demonstrate that geochemically distinct water masses were partitioned into separate areas of the system. The causes for this partitioning were two fold; the first was heterogeneity (lenses) of the soils. The cause of

the second was gaseous and solid-phase mineral end products, derived from biologic activity, altered water flow through the soils.

The first observation of water mass partitioning occurred during Phase II when SO_4^{2-} groundwater was introduced (Figure 5.5). The presence of a lens limited the extent to which the capillary fringe established and caused pockets of rainwater to develop that were located adjacent to the SO_4^{2-} rich waters of the capillary fringe. The causation of this portioning was not biologic in nature as it was observed in both columns.

The second portioning of water developed due to the presence of biogenic gas phase that caused the concentrations and distribution of SO_4^{2-} in LC and KLC to be substantially different. This led to the development of geochemically distinct water masses to be in close contact with one another. These results were also consistent with a field study by Ronen et al. (2000) who observed that the near stagnant conditions (with respect to water flow and mixing) in the water table were related to air bubbles. Figure 5.13 shows a delineation of water masses into three zones that adjoin one another during the same time period (day 97 of the experiment). These zones were defined by geochemical signatures in each water type that included SO_4^{2-}, alkalinity, NO_3-, and redox sensitive species (Fe^{2+}, S^{2-}).

The lower zone (I), primarily consisting of groundwater, was characterized by lower alkalinity values, high SO_4^{2-} concentrations, and S^{2-} production. The second zone (II), centered around the lens, was characterized by high alkalinity values, an absence of SO_4^{2-}, and Fe^{2+} production. The third zone (III), above and around the lens, was

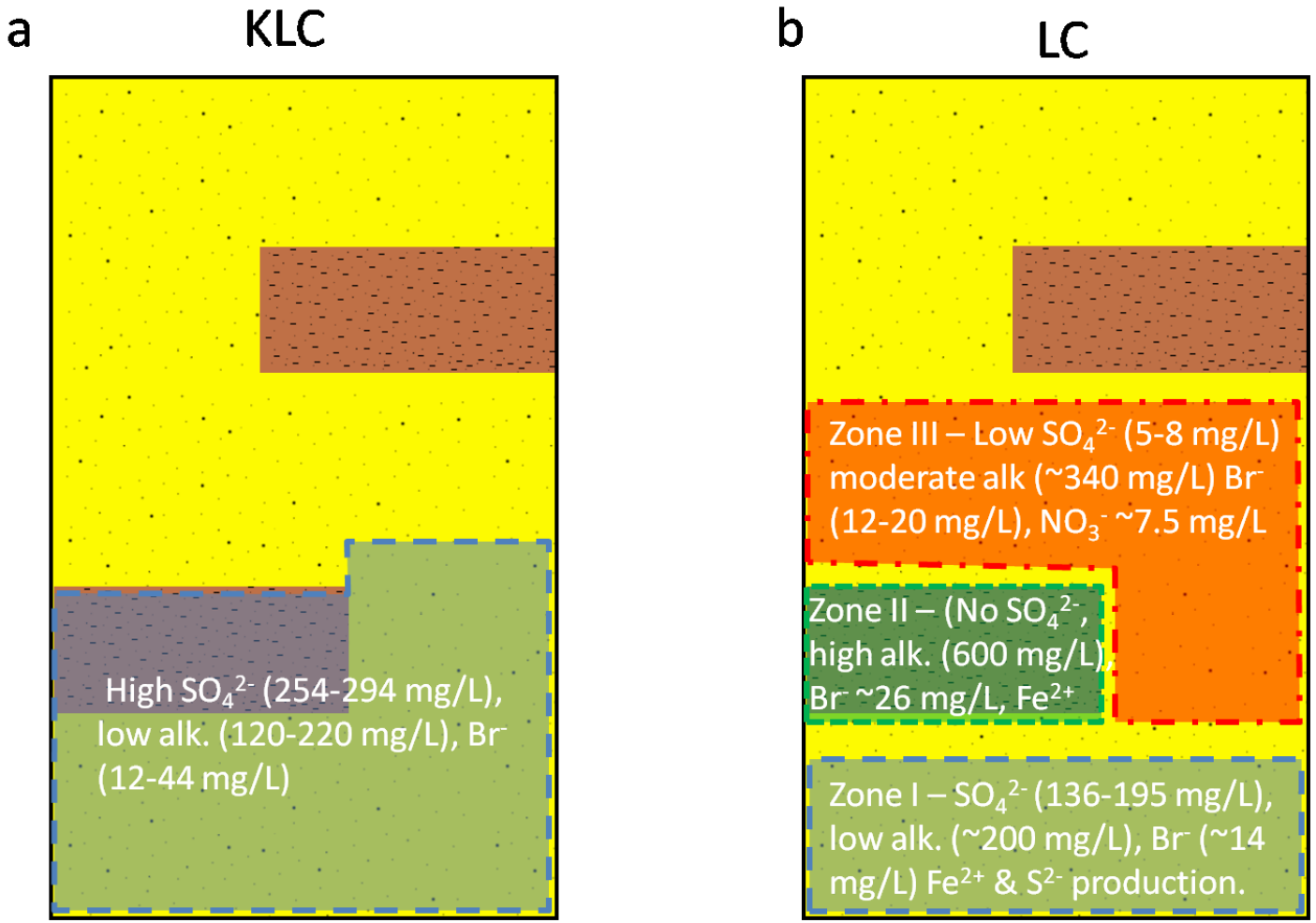

Figure 5.13 – Geochemical water mass in the killed lens column (KLC) versus the distribution of geochemically distinct water masses in the live column (LC) on day 97 of the experiment; after the groundwater table was raised to -42 cm.

characterized by moderate alkalinity values, low SO_4^{2-} concentrations, and low NO_3^- values which suggested that higher energy yield TEAPs were operating in the zone. The different TEAPs in each zone demonstrate the high redox variation that can occur within close proximity in the vadose zone. Because redox potential affects form, toxicity, and mobility of contaminants as well as its degradation pathway and rate, the compact distribution of TEAPs, though controlled by a complex set of processes, is critical to understanding contaminant fate and transport in the vadose zone.

Conceptual Model

Figures 5.14 and 5.15 show simplified conceptual models that highlight the differences in the processes occurring between KLC and LC during Phases I-IV and how geochemically distinct water masses developed in LC. Figure 5.14 shows that aqueous geochemistry is dictated by water movement in the system. In general, when SO_4^{2-} rich groundwater raises, SO_4^{2-} concentrations correspondingly rise. When dilute rainwater infiltrates through the system, low concentrations of all measured anions were low.

Figure 5.15 shows that initially, like KLC, concentrations of SO_4^{2-} increase as the SO_4^{2-} rich groundwater table is introduced. Similar to KLC, dilute rainwater also replaces SO_4^{2-} -rich water in the capillary fringe after rainfall. After this point, the differences between KLC and LC develop as O_2 was consumed which caused the capillary fringe to become anaerobic. The anaerobic conditions allow for denitrification, BSR, and methanogenesis to begin and produce biogenic gases. These biogenic gases accumulate, and as the groundwater table was being raised, the gases block pore throats

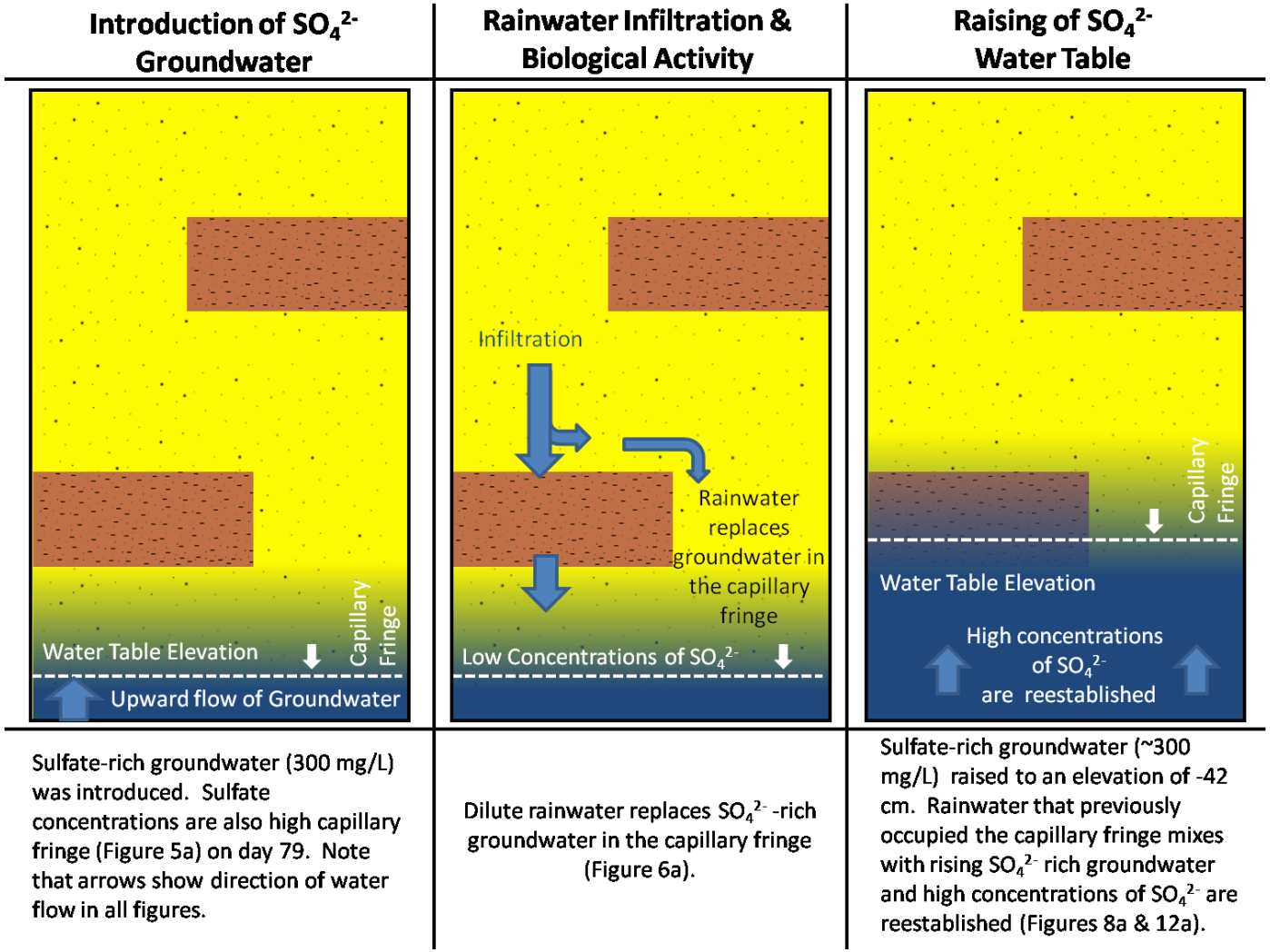

Figure 5.14 - Conceptual model of flow and transport processes occurring in the killed lens column (KLC).

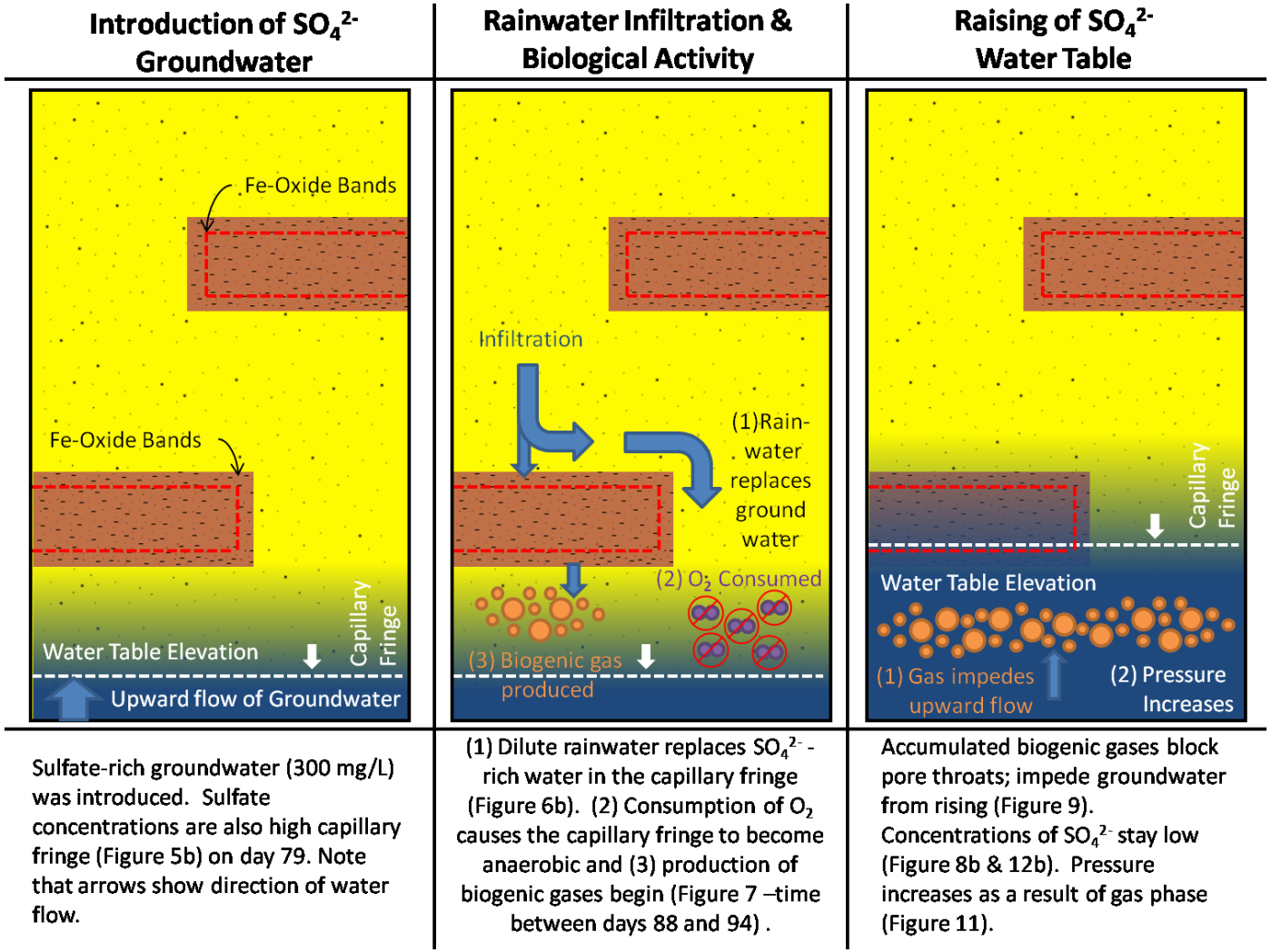

Figure 5.15 - Conceptual model of the processes that led to water mass partitioning in the lens column (LC).

which impede groundwater from rising. Concentrations of SO_4^{2-} stay low above the FIZ and pore pressures increases as a result.

Environmental Implications

The presence of unmixed distinct water masses in the vadose make contaminant monitoring complicated both spatially and temporally. The location where sampling is done is critical to decision making. For example, the lens pore waters that retain contaminants might be sampled and thought to be typical of the system. An observation of unrepresentatively high contaminant concentrations would prompt an unnecessary effort and spending to remediate the area where natural attenuation may have been a satisfactory strategy. Likewise sampling of pore waters in the areas where bypass flow dilutes contaminants to lower levels may be considered safe when in reality much of the contaminant remains in the sediment.

Site characterization of contaminated sites should include characterization of subsurface soil textural and structural heterogeneity that can account for water flow patterns and different water masses. Fortunately, advances are being made, using geophysical methods, to image the subsurface at low cost (Huisman et al., 2003; Snieder et al., 2007). This can ultimately lead to better application of remediation strategies.

The findings of this study also highlight the need to consider the complex hydrologic and biogeochemical interactions near the capillary fringe. The capillary fringe development and chemical distribution in KLC represented the ideal scenario that is likely considered in conceptual or numerical models. However, LC demonstrated the

complex biogeochemical and hydrologic linkages that caused the large variations in the spatial extent and concentrations of groundwater in the sediments. High SO_4^{2-} concentrations did not extend vertically past the lenses, even though the water table should have caused SO_4^{2-} rich groundwater to this point. Mixing between the groundwater and capillary fringe was inhibited as well. These results are particularly important in understanding the fate and transport of contaminants such as NAPLs that strongly interact with the capillary fringe. While LNAPLs have been shown to be dispersed to the upper regions of the capillary fringe, DNAPLs generally continue to travel through the capillary fringe and to the lowest regions of aquifers. This downward flow of DNAPLs could be impeded through the capillary fringe caused by the reduction of hydraulic conductivity due to the biogeochemically produced gas phase. This would ultimately result in a much different distribution of DNAPL in the system than would have been originally predicted. Potentially, DNAPLs and LNAPLs could be distributed relatively close to each other within the capillary fringe.

The formation of separate gas phase also alters hydraulic properties of the sediment as predicted by the soil-water characteristic curve. This is because the gases impact measurement of soil water tension and water content. The gases exert a positive pressure on tensiometers while TDR probes measure lower water content (Dunn and Silliman, 2003). This means that the relationship between pressure and water content can no longer be described by a mathematical function (Brooks and Corey, 1966; van Genuchten, 1980) that neglects the presence of a separate gas phase. Distribution of the gas phase is not likely continuous, but are scattered as “pockets” of gases. This

nonuniform distribution of the gas phase may also limit the use of Richards' equation (Lehmann et al., 1998). Clearly, a separate gas phase formed in the areas of the saturated, capillary fringe, and vadose zone present challenges to numerical simulation of these systems. The findings of this study also suggest that it is critical to consider multiphase flow in the saturated and vadose zones, as well as the capillary fringe.

These findings also indirectly indicate that hydraulic conductivity is a dynamic property that changes over time and with changing boundary conditions. The estimation of hydraulic properties for a particular soil or region reflects a "snapshot" in time of a dynamic property that will change in concert with changing environmental conditions (e.g. flooding, drought, land use change, pollution, etc). Thus, a key to characterizing hydraulic property evolution over time is monitoring environmental changes with an understanding of how these shifting conditions impact biogeochemical cycling. A process-based understanding of linked hydrological and biogeochemical relationships can then be applied to the prediction soil hydraulic properties. Such a process is not trivial and is only made more difficult by the need to account for the presence of heterogeneities in the subsurface that add complexity to the characterization of subsurface properties.

Understanding how the soil heterogeneities and hydraulic properties affect biogeochemical cycling is also important because the cycling is the ultimate kinetic control on long-term biodegradation of contaminants. Thus the findings of this study, which were collected over a relative short period of time, can be viably applied to contaminated systems over the long term.

CONCLUSIONS

This study investigated the effect of changing hydrologic boundary conditions on biogeochemical cycling and water flow in the vadose zone. Sterilized and live sediments were used in identically constructed laboratory columns to determine the impact of microorganisms on geochemistry and hydrology under various experimental conditions. Microorganisms altered the hydrologic behavior of the capillary fringe through addition of metabolically produced gases and precipitation of minerals derived from metabolic end products. This created a separate gas phase, in the form of trapped gas bubbles, which occupied pore spaces and consequently reduced hydraulic conductivity in the sediment.

Reduced hydraulic conductivity limited water flux through sediment which resulted in the separation of geochemically different water masses to specific areas in the vadose zone that were within close proximity to one another. These temporal and hydrologic findings suggest that the capillary fringe is much more complicated than perhaps once thought and that it could have major impact on contaminant fate and transport. For example, because the gas phase impeded groundwater and capillary fringe water from mixing, contaminants like DNAPLs that would normally be transported downward into the aquifer might be retarded in the capillary fringe where it might be easier to remediate.

CHAPTER VI

CONCLUSIONS

The results of this work demonstrate the need to consider the influence of soil structures on linked hydrologic, chemical, and biological processes. The unique combination of linked hydrologic, geologic, and microbial process occurring at soil interfaces created areas of enhanced biogeochemical cycling critical to understanding and predicting water and chemical migration in the unsaturated zone. Consideration of soil interfaces should yield more representative results crucial to the successful application of contaminant fate and transport models to natural systems.

Results from the study of a layered system demonstrate that there is a greater potential for a layered soil system to deliver higher concentrations of terminal electron acceptors (TEAs) to a contaminated aquifer than homogenous soil systems. These higher concentrations can affect rates of degradation as well as cause a shift in the active (dominant) terminal electron acceptor.

In addition to contributing greater concentrations of TEAs to groundwater systems, layered soil systems have greater potential for enhanced biodegradation under unsaturated conditions. Microbial enumerations suggest that contaminants transported through a layered system have a greater chance of being degraded before reaching the saturated zone due to higher activity not only in the system as a whole, but especially near the soil textural interface. This suggests that the majority of biodegradation in the vadose zone may occur in close proximity to soil textural interfaces.

Observations of aqueous iron-sulfide clusters were reported for the first time in the vadose zone. The greatest FeS_{aq} peak heights (semi-quantitative proxy for concentration) were detected near the soil textural interfaces. Though much is still unknown about FeS_{aq}, the intermediary and mobile nature of FeS_{aq} may have immense implications for not only toxicity, but the transport of toxic metals in the vadose zone and other environments. For example, toxic metals may be incorporated into FeS_{aq} clusters which would decrease toxicity in the immediate area, but would also allow for advanced mobility of the metal. Thus the incorporation of an aqueous iron-sulfide specie into current conceptual models should be considered to account for complexities not presently taken into account especially in contaminant fate and transport.

Results from the lens columns also demonstrated the intricate linkages between microbial activity geochemistry, and hydrology in the vadose zone. The presence of a capillary barrier at the soil textural interfaces reduced the flow rate into the lenses which created favorable circumstances for reducing conditions caused by microbial activity. In response, biogeochemical activity created Fe-oxidize band that further retarded the rate of water flow through the lens.

Although fine-grain lenses have been shown to disperse and dilute contaminants, biogeochemical cycling may alter coarser-grained sediment lenses to behave in a similar manner to their fine-grained counterparts. Lenses also need to be considered as they may play a potentially significant role in contaminant remediation in the vadose zone. Perched water tables created by lenses may become reduced which would lead to the remediation of redox sensitive contaminants. In addition, the lenses themselves are likely

to be very active biogeochemically and direct contact with contaminants may result in a considerable measure of biodegradation.

Microorganisms altered the hydrologic behavior of the capillary fringe through addition of biogenic gases. This created a separate gas phase, in the form of trapped gas bubbles, that occupied pore spaces and consequently reduced hydraulic conductivity in the sediment.

Reduced hydraulic conductivity limited the water flux through sediment which resulted in the separation of chemically different water masses to specific areas in the vadose zone that are within close proximity to one another. These temporal and hydrologic findings suggest that the capillary fringe is much more complicated than perhaps once thought and that it could have major impact on contaminant fate and transports. The results highlight the need to consider multiphase flow phenomenon (not just water flow phenomenon) in the vadose and its implication on contaminant fate and transport.

REFERENCES

Acero P., C. Ayora, J. Carrera, M.W. Saaltink and S. Olivella. 2009. Multiphase flow and reactive transport model in vadose tailings. Applied Geochemistry 24:1238-1250.

Achtnich C., F. Bak and R. Conrad. 1995. Competition for electron donors among nitrate reducers, ferric iron reducers, sulfate reducers, and methanogens in anoxic paddy soil. Biology and Fertility of Soils 19:65-72.

Báez-Cazull S., J.T. Mcguire, I.M. Cozzarelli, A. Raymond and L. Welsh. 2007. Centimeter-scale characterization of biogeochemical gradients at a wetland-aquifer interface using capillary electrophoresis. Applied Geochemistry 22:2664-2683.

Baez-Cazull S.E., J.T. Mcguire, I.M. Cozzarelli and M.A. Voytek. 2008. Determination of dominant biogeochemical processes in a contaminated aquifer-wetland system using multivariate statistical analysis. J Environ Qual 37:30-46. DOI: 10.2134/jeq2007.0169.

Bally G., V. Mesnage, J. Deloffre, O. Clarisse, R. Lafite and J.-P. Dupont. 2004. Chemical characterization of porewaters in an intertidal mudflat of the seine estuary: Relationship to erosion-deposition cycles. Marine Pollution Bulletin 49:163-173.

Barry D.A., H. Prommer, C.T. Miller, P. Engesgaard, A. Brun and C. Zheng. 2002. Modelling the fate of oxidisable organic contaminants in groundwater. Advances in Water Resources 25:945-983.

Baveye P., P. Vandevivere, B.L. Hoyle, P.C. Deleo and D.S. De Lozada. 1998. Environmental impact and mechanisms of the biological clogging of saturated soils and aquifer materials. Critical Reviews in Environmental Science and Technology 28:123-191.

Bekins B.A., F.D. Hostettler, W.N. Herkelrath, G.N. Delin, E. Warren and H.I. Essaid. 2005. Progression of methanogenic degradation of crude oil in the subsurface. Environmental Geosciences 12:139-152. DOI: 10.1306/eg.11160404036.

Berkowitz B., S.E. Silliman and A.M. Dunn. 2004. Impact of the capillary fringe on local flow, chemical migration, and microbiology. Vadose Zone J 3:534-548. DOI: 10.2113/3.2.534.

Bosch D.D., C.C. Truman and F.M. Davis. 2001. Vadose zone clay lenses impacts on groundwater loading rates. pp. 69-72. *In*: D. D. Bosch and K. W. King (eds.),

Preferential Flow, Water Movement and Chemical Transport in the Environment, ASAE, Honolulu, Hawaii.

Bradford S.A., L.M. Abriola and K.M. Rathfelder. 1998. Flow and entrapment of dense nonaqueous phase liquids in physically and chemically heterogeneous aquifer formations. Advances in Water Resources 22:117-132.

Bradford S.A., K.M. Rathfelder, J. Lang and L.M. Abriola. 2003. Entrapment and dissolution of dnapls in heterogeneous porous media. Journal of Contaminant Hydrology 67:133-157.

Bradford S.A., M. Bettahar, J. Simunek and M.T. Van Genuchten. 2004. Straining and attachment of colloids in physically heterogeneous porous media. Vadose Zone J 3:384-394. DOI: 10.2113/3.2.384.

Breit G.N., M.L.W. Tuttle, I.M. Cozzarelli, S.C. Christenson, J.B. Jaeschke, D.L. Fey and C.J. Berry. 2005. Results of chemical and isotopic analyses of sediment and water from alluvium of the canadian river near a closed municipal landfill, norman, oklahoma. USGS Open-File Report 2005-1091.

Brockman F.J. and J.S. Selker. 2004. Integrated field, laboratory, and modeling studies to determine the effects of linked microbial and physical spatial heterogeneity on engineered vadose zone bioremediation, in: P. N. N. Laboratory (Ed.), Richaland, WA.

Bronick C.J. and R. Lal. 2005. Soil structure and management: A review. Geoderma 124:3-22.

Brooks R.H. and A.T. Corey. 1966. Properties of porous media affecting fluid flow, American Society of Civil Engineering, Journal of Irrigation Drainage Division, IR2, 61-68. pp. IR2, 61-68.

Buffle J., R.R. De Vitre, D. Perret and G.G. Leppard. 1988. Combining field measurements for speciation in non perturbable waters. pp. 99-124. *In*: J. R. Kramer and H. E. Allen (eds.), Metal speciation: Theory, analysis, and application, Lewis Publishers, Inc., Chelsea, MI.

Bundt M., F. Widmer, M. Pesaro, J. Zeyer and P. Blaser. 2001. Preferential flow paths: Biological 'hot spots' in soils. Soil Biology and Biochemistry 33:729-738.

Bura-Nakic E., D. Krznaric, D. Jurasin, G.R. Helz and I. Ciglenecki. 2007. Voltammetric characterization of metal sulfide particles and nanoparticles in model solutions and natural waters. Analytica Chimica Acta 594:44-51.

Carrillo M.L.K., J. Letey and S.R. Yates. 2000. Unstable water flow in a layered soil: I. Effects of a stable water-repellent layer. Soil Sci Soc Am J 64:450-455.

Chapelle F.H. 2001. Ground-water microbiology and geochemistry. 2nd ed. John Wiley and Sons, Inc., New York.

Chapelle F.H., S.K. Haack, P. Adriaens, M. Henry and P.M. Bradley. 1996. Comparison of eh and h2 measurements for delineating redox processes in a contaminated aquifer. Environmental Science and Technology 30:3565-3569.

Chenu C., Y. Le Bissonnais and D. Arrouays. 2000. Organic matter influence on clay wettability and soil aggregate stability. Soil Sci Soc Am J 64:1479-1486.

Cohn C., R. Laffers, S. Simon, T. O'riordan and M. Schoonen. 2006a. Role of pyrite in formation of hydroxyl radicals in coal: Possible implications for human health. Particle and Fibre Toxicology 3:16.

Cohn C., S. Mueller, E. Wimmer, N. Leifer, S. Greenbaum, D. Strongin and M. Schoonen. 2006b. Pyrite-induced hydroxyl radical formation and its effect on nucleic acids. Geochemical Transactions 7:3.

Cozzarelli I.M., J.M. Suflita, G.A. Ulrich, S.H. Harris, M.A. Scholl, J.L. Schlottmann and S. Christenson. 2000. Geochemical and microbiological methods for evaluating anaerobic processes in an aquifer contaminated by landfill leachate. Environmental Science & Technology 34:4025-4033. DOI: doi:10.1021/es991342b.

Davison W. 1977. The polarographic measurement of o2 fe2+, mn2+, and s2- in hypolimnetic water. Limnology and Oceanography 22:746-753.

Davison W. 1991. The solubility of iron sulphides in synthetic and natural waters at ambient temperature. Aquatic Sciences - Research Across Boundaries 53:309-329.

Davison W., J. Buffle and R. Devitre. 1998. Voltammetric characterization of a dissolved iron sulphide species by laboratory and field studies. Analytica Chimica Acta 377:193-203.

Davison W., N. Phillips and B.J. Tabner. 1999. Soluble iron sulfide species in natural waters: Reappraisal of their stoichiometry and stability constants. Aquatic Sciences - Research Across Boundaries 61:23-43.

De Vitre R.R., J. Buffle, D. Perret and R. Baudat. 1988. A study of iron and manganese transformations at the o2/s(-ii) transition layer in a eutrophic lake (lake bret,

switzerland): A multimethod approach. Geochimica et Cosmochimica Acta 52:1601-1613.

Deng Y. and W. Stumm. 1993. Kinetics of redox cycling of iron coupled with fulvic acid. Aquatic Sciences - Research Across Boundaries 55:103-111.

Dunn A.M. and S.E. Silliman. 2003. Air and water entrapment in the vicinity of the water table. Ground Water 41:729-734.

Emerson W.W. and D.J. Greenland. 1990. Soil aggregates–formation and stability. pp. 485-511. *In*: M. De Boodt, et al. (eds.), Soil colloids and their associations in aggregates, Plenum Press, New York.

Federle T.W., D.C. Dobbins, J.R. Thornton-Manning and D.D. Jones. 1986. Microbial biomass, activity, and community sturcture in subsurface soils. Ground Water 24:365-374.

Fredrickson J.K., J.P. Mckinley, B.N. Bjornstad, P.E. Long, D.B. Ringelberg, D.C. White, L.R. Krumholz, J.M. Suflita, F.S. Colwell and R.M. Lehman. 1997a. Pore-size constraints on the activity and survival of subsurface bacteria in a late cretaceous shale-sandstone sequence, northwestern new mexico. Geomicrobiol J 14:183-202.

Fredrickson J.K., J.P. Mckinley, B.N. Bjornstad, P.E. Long, D.B. Ringelberg, D.C. White, L.R. Krumholz, J.M. Sulfita, F.S. Colwell, R.M. Lehman, T.J. Phelps and T.C. Onstott. 1997b. Pore-size constraints on the activity and survival of subsurface bacteria in a late cretaceous shale-sandstone sequence, northwesteren new mexico. Geomicrobiology Journal 14:183-202.

Gachter R., J.M. Ngatiah and C. Stamm. 1998. Transport of phosphate from soil to surface waters by preferential flow. Environmental Science & Technology 32:1865-1869. DOI: doi:10.1021/es9707825.

Gee G.W. and J.M. Bauder. 1986. Partical-size analysis. pp. 383-411. *In*: A. Klute (ed.), Methods of soil analysis, part 1 - physical and mineralogical methods Agron. Monogr. 9. ASA and SSSA, Madison, WI, USA.

Goettlein A. and R. Blasek. 1996. Analysis of small volumes of soil solution by capillary electrophoresis. Soil Science 161:705-715.

Gran G. 1952. Determination of the equivalence point in potentiometric titrations. Part ii. The Analyst 77:661-671.

Grossman E.L., L.A. Cifuentes and I.M. Cozzarelli. 2002. Anaerobic methane oxidation in a landfill-leachate plume. Environmental Science and Technology 36:2436-2442.

Gulliver J.S. 2007. Introduction to chemical transport in the environment. 1 ed. Cambridge University Press, New York, NY.

Gupta R.P. and D. Swartzendruber. 1962. Flow-associated reduction in the hydraulic conductivity of quartz sand. Soil Sci Soc Am J 26:6-10.

Gwo J.P., L.E. Toran, M.D. Morris and G.V. Wilson. 1996. Subsurface stormflow modeling with sensitivity analysis using a latin-hypercube sampling technique. Ground Water 34:811-818.

Hansen D.J., J.T. Mcguire and B.P. Mohanty. Submitted, 2011a. Enhanced biogeochemical cycling and subsequent reduction of hydraulic conductivity associated with soil-layer interfaces in the vadose zone. Journal of Environmental Quality.

Hansen D.J., J.T. Mcguire and B.P. Mohanty. Submitted, 2011b. Biogeochemical cycling in heterogeneous unsaturated soils: A comparison between live and sterilized sediments.

Hansen D.J., J.T. Mcguire and B.P. Mohanty. Submitted, 2011c. The role of microbial activity and soil heterogeneity in the partitioning of geochemically distinct water masses in the vadose zone. Water Resources Research.

Hillel D. 2004. Introduction to environmental soil physics Academic Press San Diego, USA, San Diego.

Holden P.A. and N. Fierer. 2005. Microbial processes in the vadose zone. Vadose Zone Journal 4:1-21.

Huang C.-T., S.W. Peretti and J.D. Bryers. 1994. Effects of medium carbon-to-nitrogen ratio on biofilm formation and plasmid stability. Biotechnology and Bioengineering 44:329-336.

Huisman J.A., S.S. Hubbard, J.D. Redman and A.P. Annan. 2003. Measuring soil water content with ground penetrating radar: A review. Vadose Zone J. 2:476-491. DOI: 10.2113/2.4.476.

Hunter K.S., Y. Wang and P. Van Cappellen. 1998. Kinertic modeling of microbially-driven redox chemistry of subsurface environments: Coupling transport, microbial metabolism and geochemistry. Journal of Hydrology 209:53-80.

Ines A.V.M. and B.P. Mohanty. 2008. Near-surface soil moisture assimilation for quantifying effective soil hydraulic properties under different hydroclimatic conditions. Vadose Zone J. 7:39-52. DOI: 10.2136/vzj2007.0048.

Iqbal M.Z. 2000. Effects of layered heterogeneity in subsurface geologic materials on solute transport under field conditions: A case study from northeastern iowa, USA. Hydrogeology Journal 8:257-270.

Jouany C. 1991. Surface free energy components of clay-synthetic humic acid complexes from contact-angle measurements. Clays and Clay Minerals 39:43.

Kaiser H.F. 1960. The application of electronic computers to factor analysis. Educational and Psychological Measurement 20:141-151. DOI: 10.1177/001316446002000116.

Keeny D.R. and D.W. Nelson. 1982. Nitrogen -inorganic forms. *In*: A. L. Page (ed.), Methods of soil analysis: Part 2. Agronomy monogr. 9. 2nd ed., ASA and SSSA, Madison, WI.

Klute A. and C. Dirksen. 1986. Hydraulic conductivity and diffusivity: Laboratory methods. pp. 687-734. *In*: A. Klute (ed.), Methods of soil analysis, part 1 - physical and mineralogical methods Agron. Monogr. 9. ASA and SSSA, Madison, WI, USA.

Kneeshaw T.A., J.T. Mcguire, E.W. Smith and I.M. Cozzarelli. 2007. Evaluation of sulfate reduction at experimentally induced mixing interfaces using small-scale push-pull tests in an aquifer-wetland system. Applied Geochemistry 22:2618-2629.

Kock D. and A. Schippers. 2008. Quantitative microbial community analysis of three different sulfidic mine tailing dumps generating acid mine drainage. Appl. Environ. Microbiol. 74:5211-5219. DOI: 10.1128/aem.00649-08.

Kohne J.M. and B.P. Mohanty. 2005. Water flow processes in a soil column with a cylindrical macropore: Experiment and hierchical modeling. Water Resources Research 41.

Konopka A. and R. Turco. 1991. Biodegradation of organic compounds in vadose zone and aquifer sediments. Appl. Environ. Microbiol. 57:2260-2268.

Kuechler R., K. Noack and T. Zorn. 2004. Investigation of gypsum dissolution under saturated and unsaturated water conditions. Ecological Modelling 176:1-14. DOI: DOI: 10.1016/j.ecolmodel.2003.10.025.

Lahvis M.A., A.L. Baehr and R.J. Baker. 1999. Quantification of aerobic biodegradation and volatilization rates of gasoline hydrocarbons near the water table under natural attenuation conditions. Water Resour. Res. 35:753–765.

Lehmann P., F. Stauffer, C. Hinz, O. Dury and H. Flühler. 1998. Effect of hysteresis on water flow in a sand column with a fluctuating capillary fringe. Journal of Contaminant Hydrology 33:81-100.

Li L., Q. Pan, X. Wu, X. Zhou and Z. Li. 1988. Amorphous iron oxide as an electron acceptor for ammonium oxidation under anaerobic condition. acta pedologica sinica 25:184–190.

Lide D.R. 2008. Crc handbook of chemistry and physics: A ready-reference book of chemical and physical data. 89 ed. CRC press.

Lindsay W.L. and W.A. Norvell. 1978. Development of a dtpa soil test for zinc, iron, manganese, and copper. Soil Science Society of America Journal 42:421-428.

Loheide S.P., Ii, J.J. Butler, Jr. and S.M. Gorelick. 2005. Estimation of groundwater consumption by phreatophytes using diurnal water table fluctuations: A saturated-unsaturated flow assessment. Water Resour. Res. 41.

Lohman S.W. 1972. Ground-water hydraulics. U. S. Geological Survery Profesional Paper 708:70.

Lovley D.R. 1991. Dissimilatory fe(iii) and mn (iv) reduction. Microbial Reviews 55:259-287.

Lovley D.R. and E.J.P. Phillips. 1986. Availability of ferric iron for microbial reduction in bottom sediments of the freshwater tidal potomac river. Appl. Environ. Microbiol. 52:751-757.

Lovley D.R. and S. Goodwin. 1988. Hydrogen concentrations as an indicator of the predominant terminal electron-accepting reactions in aquatic sediments. Geochimica et Cosmochimica Acta 52:2993-3003.

Lowson R.T. 1982. Aqueous oxidation of pyrite by molecular oxygen. Chemical Reviews 82:461-497. DOI: doi:10.1021/cr00051a001.

Luther G. and D. Rickard. 2005. Metal sulfide cluster complexes and their biogeochemical importance in the environment. Journal of Nanoparticle Research 7:389-407.

Luther G., B. Glazer, S. Ma, R. Trouwborst, B. Shultz, G. Druschel and C. Kraiya. 2003. Iron and sulfur chemistry in a stratified lake: Evidence for iron-rich sulfide complexes. Aquatic Geochemistry 9:87-110.

Luther G.W., D.T. Rickard, S. Theberge and A. Olroyd. 1996. Determination of metal (bi)sulfide stability constants of mn2+, fe2+, co2+, ni2+, cu2+, and zn2+ by voltammetric methods. Environ. Sci. Technol. 30:671-679.

Luther G.W., C.E. Reimers, D.B. Nuzzio and D. Lovalvo. 1999. In situ deployment of voltammetric, potentiometric, and amperometric microelectrodes from a rov to determine dissolved o2, mn, fe, s(-2), and ph in porewaters. Environ. Sci. Technol. 33:4352-4356.

Luther G.W., P.J. Brendel, B.L. Lewis, B. Sundby, L. Lefrancois, N. Silverberg and D.B. Nuzzio. 1998. Simultaneous measurement of o2, mn, fe, i-, and s(-ii) in marine pore waters with a solid-state voltammetric microelectrode. Limnology and Oceanography 43:325-333.

Luther G.W., B.T. Glazer, L. Hohmann, J.I. Popp, M. Taillefert, T.F. Rozan, P.J. Brendel, S.M. Theberge and D.B. Nuzzio. 2001. Sulfur speciation monitored in situ with solid state gold amalgam voltammetric microelectrodes: Polysulfides as a special case in sediments, microbial mats and hydrothermal vent waters. Journal of Environmental Monitoring 3:61-66.

Machel H.G. 2001. Bacterial and thermochemical sulfate reduction in diagenetic settings -- old and new insights. Sedimentary Geology 140:143-175.

Madigan M.T., J.M. Martinko and J. Parker. 1997a. Brock's biology of microorganisms. 8 ed. Prentice Hall, Upper Saddle River, New Jersey.

Madigan M.T., J.M. Martinko and J. Parker. 1997b. Brock biology of microorganisms. Eight Edition ed. Prentice Hall, Upper Saddle River.

Malecki J. and M. Matyjasik. 2002. Vadose zone - challenges in hydrochemistry. Acta Geologica Polonica 52:449-458.

Marschall C., P. Frenzel and H. Cypionka. 1993. Influence of oxygen on sulfate reduction and growth of sulfate-reducing bacteria. Archives of Microbiology 159:168-173.

Marshall M.J., A.S. Beliaev and J.K. Fredrickson. 2009. Microbiological transformations of radionuclides in the subsurface. pp. 363. *In*: R. Mitchell and J. Gu (eds.), Environmental microbiology, Wiley-Blackwell, Hoboken, New Jersey.

Mayer K.U., E.O. Frind and D.W. Blowes. 2002. Multicomponent reactive transport modeling in variably saturated porous media using a generalized formulation for kinetically controlled reactions. Water Resources Research 38:1174.

Mbonimpa M., M. Aubertin, M. Aachib and B. Bussière. 2003. Diffusion and consumption of oxygen in unsaturated cover materials. Can. Geotech. J 40:916-932.

Mccarthy J.F. and J.M. Zachara. 1989. Subsurface transport of contaminants. Environmental Science & Technology 23:496-502. DOI: 10.1021/es00063a001.

Mccray J.E. and R.W. Falta. 1996. Defining the air sparging radius of influence for groundwater remediation. Journal of Contaminant Hydrology 24:25-52.

Mcguire J.T., D.T. Long and D.W. Hyndman. 2005. Analysis of recharge-induced geochemical change in a contaminated aquifer. Ground Water 43:518-530.

Mcguire J.T., E.W. Smith, D.T. Long, D.W. Hyndman, S.K. Haack, M.J. Klug and M.A. Velbel. 2000. Temporal variations in parameters reflecting terminal-electron-accepting processes in an aquifer contaminated with waste fuel and chlorinated solvents. Chemical Geology 169:471-485.

Mehlich A. 1978. New extractant for soil test evaluation of phosphorus, potassium, magnesium, calcium, sodium, manganese, and zinc. Communications in Soil Science and Plant Analysis 9:477-492.

Mehlich A. 1984. Mehlich-3 soil test extractant: A modification of mehlich-2 extractant. Communications in Soil Science and Plant Analysis 15:1409-1416.

Mikutta R., M. Kleber, K. Kaiser and R. Jahn. 2005. Review: Organic matter removal from soils using hydrogen peroxide, sodium hypochlorite, and disodium peroxodisulfate. Soil Sci Soc Am J 69:120-135.

Morrill L.G. and J.E. Dawson. 1967. Patterns observed for the oxidation of ammonium to nitrate by soil organisms. Soil Sci Soc Am J 31:757-760.

Moses C.O. and J.S. Herman. 1991. Pyrite oxidation at circumneutral ph. Geochimica et Cosmochimica Acta 55:471-482.

Moses C.O., D. Kirk Nordstrom, J.S. Herman and A.L. Mills. 1987. Aqueous pyrite oxidation by dissolved oxygen and by ferric iron. Geochimica et Cosmochimica Acta 51:1561-1571.

Oades J.M. and A.G. Waters. 1991. Aggregate hierarchy in soils. Australian Journal of Soil Research 29:815-828. DOI: doi:10.1071/SR9910815.

Oliver D.S., B. F.J., R.S. Bowman and T.L. Kieft. 2003. Vadose zone processes and chemical transport. Journal of Environmental Quality 32:317-324.

Oremland R.S. and B.F. Taylor. 1978. Sulfate reduction and methanogenesis in marine sediments. Geochimica et Cosmochimica Acta 42:209-214.

Oremland R.S. and S. Polcin. 1982. Methanogenesis and sulfate reduction: Competitive and noncompetitive substrates in estuarine sediments. Applied and Enivornmental Microbiology 44:1270-1276.

Owens P.R., L.P. Wilding, L.M. Lee and B.E. Herbert. 2005. Evaluation of platinum electrodes and three electrode potential standards to determine electrode quality. Soil Science Society of America Journal 69:1541-1550.

Patrick W.H., R.P. Gambrell and S.P. Faulkner. 1996. Redox measurements of soils. pp. 1255–1273. *In*: D. L. Sparks (ed.), Methods of soil analysis part 3, ASA and SSSA, Madison, WI.

Porter L.K., W.D. Kemper, R.D. Jackson and B.A. Stewart. 1960. Chloride diffusion in soils as influenced by moisture content. Soil Sci Soc Am J 24:460-463.

Postgate J.R. 1984. The sulphate-reducing bacteria. 2nd ed. Cambridge University Press, Cambridge.

Pracht J., J. Boenigk, M. Isenbeck-Schröter, F. Keppler and H.F. Schöler. 2001. Abiotic fe(iii) induced mineralization of phenolic substances. Chemosphere 44:613-619.

Prommer H., D.A. Barry and G.B. Davis. 2002. Modelling of physical and reactive processes during biodegradation of a hydrocarbon plume under reducing conditions. Journal of Contaminant Hydrology 59:113-131.

Rhoades J.D. 1982. Soluble salts. *In*: A. L. Page (ed.), Methods of soil analysis: Part 2. Agronomy monogr. 9. 2nd ed., ASA and SSSA, Madision, WI.

Rickard D. 1995. Kinetics of fes precipitation: Part 1. Competing reaction mechanisms. Geochimica et Cosmochimica Acta 59:4367-4379.

Rickard D. 2006. The solubility of fes. Geochimica et Cosmochimica Acta 70:5779-5789.

Rickard D. and G.W. Luther. 1997. Kinetics of pyrite formation by the h2s oxidation of iron (ii) monosulfide in aqueous solutions between 25 and 125°c: The mechanism. Geochimica et Cosmochimica Acta 61:135-147.

Rickard D. and G.W. Luther. 2005. Acid volatile sulfide (avs). Marine Chemistry 97:141–197.

Rickard D. and G.W. Luther. 2007. Chemistry of iron sulfides. Chem. Rev. 107:514-562.

Rickard D., A. Oldroyd and A. Cramp. 1999. Voltammetric evidence for soluble fes complexes in anoxic estuarine muds. Estuaries and Coasts 22:693-701.

Rickard D., I.B. Butler and A. Oldroyd. 2001. A novel iron sulphide mineral switch and its implications for earth and planetary science. Earth and Planetary Science Letters 189:85-91.

Rockhold M.L., R.R. Yarwood, M.R. Niemet, P.J. Bottomley and J.S. Selker. 2002. Considerations for modeling bacterial-induced changes in hydraulic properties of variably saturated porous media. Advances in Water Resources 25:477-495.

Roesler A., C. Gammons, G. Druschel, H. Oduro and S. Poulson. 2007. Geochemistry of flooded underground mine workings influenced by bacterial sulfate reduction. Aquatic Geochemistry 13:211-235.

Ronen D., H. Scher and M. Blunt. 2000. Field observations of a capillary fringe before and after a rainy season. Journal of Contaminant Hydrology 44:103-118.

Rosenberry D.O. and T.C. Winter. 1997. Dynamics of water-table fluctuations in an upland between two prairie-pothole wetlands in north dakota. Journal of Hydrology 191:266-289.

Rosenfeld J.K. 1979. Ammonium adsorption in nearshore anoxic sediments. American Society of Limnology and Oceanography 24:356-364.

Rozan T.F., S.M. Theberge and G. Luther. 2000a. Quantifying elemental sulfur (s0), bisulfide (hs-) and polysulfides (sx2-) using a voltammetric method. Analytica Chimica Acta 415:175-184.

Rozan T.F., M.E. Lassman, D.P. Ridge and G.W. Luther. 2000b. Evidence for iron, copper and zinc complexation as multinuclear sulphide clusters in oxic rivers. Nature 406:879-882.

Salminen J.M., P.J. Hanninen, J. Leveinen, P.T.J. Lintinen and K.S. Jorgensen. 2006. Occurrence and rates of terminal electron-accepting processes and recharge processes in petroleum hydrocarbon-contaminated subsurface. Journal of Environmental Quality 35:2273-2282.

Schofield R.K. and A.W. Taylor. 1955. The measurement of soil ph. Soil Science Society of America Proceedings 19:164-167.

Scholl M.A., I.M. Cozzarelli and S.C. Christenson. 2006. Recharge processes drive sulfate reduction in an alluvial aquifer contaminated with landfill leachate. Journal of Contaminant Hydrology 86:239-261.

Seki T., T. Miyazaki and M. Nakano. 1996. Reduction of hydraulic conductivity due to microbial effects. Transactions of the Japanese Society of Irrigation, Drainage, and Reclamation engineering 181:137-144.

Senior E., B. Lindstrom, I.M. Banat and D.B. Nedwell. 1982. Sulfate reduction and methanogenesis in the sediment of a sulfate reduction and methanogenesis in the sediment of a. Applied and Enivornmental Microbiology 43:987-996.

Silliman S.E., B. Berkowitz, J. Simunek and M.T.V. Genuchten. 2002. Fluid flow and solute migration within the capillary fringe. Ground Water 40:76-84.

Simunek J., M.T. Van Genuchten and M. Sejna. 2008. Development and applications of the hydrus and stanmod software packages and related codes. Vadose Zone J 7:587-600. DOI: 10.2136/vzj2007.0077.

Singh H. and M. Bajwa. 1990. Comparison of different models for describing gypsum dissolution kinetics in different aqueous salt solutions. Soil Research 28:947-953. DOI: doi:10.1071/SR9900947.

Six J., H. Bossuyt, S. Degryze and K. Denef. 2004. A history of research on the link between (micro)aggregates, soil biota, and soil organic matter dynamics. Soil and Tillage Research 79:7-31.

Smith W.A., D.C. Cooper, D.T. Fox, M.A. Plummer and L.C. Hull. 2003. Changes in microbial community structure with depth in a simulated vadose zone environment. American Geophysical Union, Fall Meeting 2003, abstract# B41D-0924.

Snieder R., S. Hubbard, M. Haney, G. Bawden, P. Hatchell, A. Revil and D.O.E. Geophysical Monitoring Working Group. 2007. Advanced noninvasive geophysical monitoring techniques. Annual Review of Earth and Planetary Sciences 35:653-683. DOI: doi:10.1146/annurev.earth.35.092006.145050.

Soares M.I.M., S. Belkin and A. Abeliovich. 1988. Biological groundwater denitrification: Laboratory studies. Water Science & Technology 20:189-195.

Stumm W. and J.J. Morgan. 1996. Aquatic chemistry. third edition ed. John Wiley and Sons, New York.

Suk H.S. and K.-K. Lee. 1999. Characterization of a ground water hydrochemical system through multivariate analysis: Clustering into ground water zones. Ground Water 37:358-366.

Szilas C.P., O.K. Borggaard, H.C.B. Hansen and J. Rauer. 1998. Potential iron and phosphate mobilization during flooding of soil material. Water, Air, & Soil Pollution 106:97-109.

Taillefert M., S. Neuhuber and G. Bristow. 2007. The effect of tidal forcing on biogeochemical processes in intertidal salt marsh sediments. Geochemical Transactions 8:6.

Theberge S.M. and G.W. Luther. 1997. Determination of the electrochemical properties of a soluble aqueous fes species present in sulfidic solutions. Aquatic Geochemistry 3:191-211.

Thomann R.V. and J.A. Mueller. 1987. Principles of surface water quality modeling and control Harper & Row, Publishers.

Thompson L.J., V. Gray, D. Lindsay and A. Von Holy. 2006. Carbon : Nitrogen : Phosphorus ratios influence biofilm formation by enterobacter cloacae and citrobacter freundii. Journal of Applied Microbiology 101:1105-1113.

Tiedje J., A. Sexstone, T. Parkin and N. Revsbech. 1984. Anaerobic processes in soil. Plant and Soil 76:197-212.

Tisdall J.M. and J.M. Oades. 1982. Organic matter and water-stable aggregates in soils. European Journal of Soil Science 33:141-163. DOI: doi:10.1111/j.1365-2389.1982.tb01755.x.

Ulrich G.A., G.N. Breit and I.M. Cozzarelli. 2003. Sources of sulfate supporting anaerobic metabolism in a contaminated aquifer. Environmental Science and Technology 37:1093-1099.

Van Bochove E., S. Beauchemin and G. Theriault. 2002. Continuous multiple measurement of soil redox potential using platinum microelectrodes. Soil Science Society of America Journal 66:1813-1820.

Van Genuchten M.T. 1980. A closed-form equation for predicting the hydraulic conductivity of unsaturated soils. Soil Sci Soc Am J 44:892-898.

Vandevivere P. and P. Baveye. 1992a. Saturated hydraulic conductivity reduction caused by aerobic bacteria in sand columns. Soil Sci Soc Am J 56:1-13.

Vandevivere P. and P. Baveye. 1992b. Relationship between transport of bacteria and their clogging efficiency in sand columns. Appl. Environ. Microbiol. 58:2523-2530.

Vinther F.P., F. Eiland, A.M. Lind and L. Elsgaard. 1999. Microbial biomass and numbers of denitrifiers related to macropore channels in agricultural and forest soils. Soil Biology and Biochemistry 31:603-611.

Wafer C.C., J.B. Richards and D.L. Osmond. 2004. Construction of platinum-tipped redox probes for determining soil redox potential. Journal of Environmental Quality 32:2375-2379.

Walser G.S., T.H. Illangasekare and A.T. Corey. 1999. Retention of liquid contaminants in layered soils. Journal of Contaminant Hydrology 39:91-108.

Ward A.L., G.W. Gee and M.D. White. 1997. A comprehensive analysis of contaminant transport in the vadose zone beneath tank sx-109, Pacific Northwest National Laboratory, Richland, WA. pp. 72.

Wayland K.G., D.T. Long, D.W. Hyndman, B.C. Pijanowski, S.M. Woodhams and S.K. Haack. 2003. Identifying relationships between baseflow geochemistry and land use with synoptic sampling and r-mode factor analysis. J Environ Qual 32:180-190.

Weerts A.H., D. Kandhai, W. Bouten and P.M.A. Sloot. 2001. Tortuosity of an unsaturated sandy soil estimated using gas diffusion and bulk soil electrical conductivity: Comparing analogy-based models and lattice-boltzmann simulations. Soil Sci Soc Am J 65:1577-1584.

Widrig D.L. and J.F. Manning. 1995. Biodegradation of no. 2 diesel fuel in the vadose zone: A soil column study. Environmental Toxicology and Chemistry 14:1813-1822.

Wilhelm E., R. Battino and R.J. Wilcock. 1977. Low-pressure solubility of gases in liquid water. Chemical Reviews 77:219-262. DOI: doi:10.1021/cr60306a003.

Wolthers M., S.J. Van Der Gaast and D. Rickard. 2003. The structure of disordered mackinawite. American Mineralogist 88:2007-2015.

Yanful E.K., S. Morteza Mousavi and M. Yang. 2003. Modeling and measurement of evaporation in moisture-retaining soil covers. Advances in Environmental Research 7:783-801.

Zhou L. and H.M. Selim. 2001. Solute transport in layered soils: Nonlinear and kinetic reactivity. Soil Science Society of America Journal 65:1056-1064.

Zhu J. and B.P. Mohanty. 2002. Spatial averaging of van genuchten hydraulic parameters for steady-state flow in heterogeneous soils: A numerical study. Vadose Zone J. 1:261-272. DOI: 10.2113/1.2.261.

Zhu J. and B.P. Mohanty. 2003. Effective hydraulic parameters for steady state vertical flow in heterogeneous soils. Water Resour. Res. 39:1227. DOI: 10.1029/2002wr001831.

APPENDIX A

Instrument Methods

Capillary Electrophoresis (Agilent Technologies) methods for analysis of cations, NH_4^+, anions, and organic acids in water samples

For all capillary electrophoresis (CE) methods, the following vial positions and designations were used:

Vial 3- inlet home vial (buffer, charge is applied to this vial)

Vial 4-outlet home vial (buffer, charge is applied to this vial)

Vial 5- buffer (for flushing)

Vial 6- waste

Vial 7- water (Nanopure, for flushing)

Vial 47- water (dunk, Nanopure, for rinsing capillary tips)

For CE analyses in which the replenishment system cannot be used due to buffer properties (ex. if buffer is a surfactant) additional methods are created with different home vials. In most cases buffer must be replaced and replenished after six analyses as it becomes degraded with the charge applied during each analysis.

For all analyses standards were made using trace metal grade stock solutions or salts and Nanopure water.

CE method details follow.

Cation/NH_4^+ Capillary Electrophoresis Method

The only difference between Cation runs and NH_4^+ is the run time. For NH_4^+, it can be decreased to 12 minutes

Method uses IonPhor DDP buffer purchased from Dionex (P/N 046071)

Method Information

Cation (DDP Buffer)

Run Time Checklist

Pre-Run Cmd/Macro: off

Data Acquisition: on

Standard Data Analysis: off

Customized Data Analysis: off

Save GLP Data: off

Post-Run Cmd/Macro: off

Save Method with Data: off

CAPILLARY ELECTROPHORESIS

CE mode: CE

Home values:

Lift Offset	4
Cassette Temperature	30.00 °C
Inlet Home Vial	3: Inlet Home
Outlet Home Vial	4: Outlet Home

Replenishment Entries:

Function	Parameter

Preconditioning Entries:

Function	Parameter
1 FLUSH	2.50 min, I:5: Buffer, O:6: waste

Postcondition Entries:

Function	Parameter
1 INLET	47:

Electric:

Electric	On
Polarity	Positive
Voltage	25.00 kV
Current	System Limit
Power	System Limit
Low Current Limit	0.00

Injection Table Entries:

Function	Parameter
1 PRESSURE	50.0 mbar, 2.0 sec, I:3: Inlet Home, O:4: Outlet Home
2 PRESSURE	50.0 mbar, 1.5 sec, I:InjectVial, O:4: Outlet Home
3 PRESSURE	50.0 mbar, 2.0 sec, I:3: Inlet Home, O:4: Outlet Home

Store Data:

Collect voltage	Yes
Collect current	Yes
Collect power	Yes
Collect pressure	Yes
Collect temperature	Yes

Time entries:

Stoptime	16.00 min
Posttime	Off

Time Table is empty.

DIODE ARRAY DETECTOR

Settings:

Stop Time	no Limit
Post Time	Off
Response Time	2.6
Peakwidth	>0.2
Prerun Autobalance	Off
Postrun Autobalance	Off

Spectrum:

Store	None
From	190 nm
To	600 nm
Threshold	100.00 mAu

Signals:

	Store	Signal,Bw	Reference,Bw	[nm]
A:	Yes	310 60	200 20	
B:	Yes	228 10	216 10	
C:	Yes	250 10	216 10	
D:	Yes	250 20	216 20	
E:	Yes	450 80	230 20	

Contacts:

Contact 1	Off
Contact 2	Off

Time Table:

Time [min] Function Contact 1 Contact 2
4.00 Balance

==========

Specify Report

==========

Calculate: Area Percent
Use Multiplier & Dilution Factor with ISTDs

Destination: Screen
Quantitative Results sorted by: Signal
Report Style: Short
Sample info on each page: No
Add Electropherogram Output: Yes
Electropherogram Output: Portrait
Size in Time direction: 100 % of Page
Size in Response direction: 40 % of Page

==========

Signal Options

==========

Include: Axes, Migration Times, Baselines, Tick Marks
Font: Arial, Size: 8

Ranges: Full
Multi Electropherograms: Overlaid, All the same Scale

Cation/NH_4^+ Capillary Electrophoresis Replenishment Method

This is a separate method that is only run every 6-7 samples to prevent sample degradation that reduces reproducibility

Method Information

Cation (DDP Buffer)

Run Time Checklist

Pre-Run Cmd/Macro: off

Data Acquisition: on

Standard Data Analysis: off

Customized Data Analysis: off

Save GLP Data: off

Post-Run Cmd/Macro: off

Save Method with Data: off

CAPILLARY ELECTROPHORESIS

CE mode: CE

Home values:

Lift Offset	4
Cassette Temperature	30.00 °C
Inlet Home Vial	3: Inlet Home
Outlet Home Vial	4: Outlet Home

Replenishment Entries:
Replenishment and Preconditioning:
serial processing

Replenishment Entries:

Function	Parameter
1 REPLENISH	1.6 cm, InHomeVial
2 REPLENISH	1.6 cm, OutHomeVial

Preconditioning Entries:

Function	Parameter
1 FLUSH	2.50 min, I:5: Buffer, O:6: waste

Postcondition Entries:

Function	Parameter
1 INLET	47:

Electric:

Electric	On
Polarity	Positive
Voltage	25.00 kV
Current	System Limit
Power	System Limit
Low Current Limit	0.00

Injection Table Entries:

Function	Parameter
1 PRESSURE	50.0 mbar, 2.0 sec, I:3: Inlet Home, O:4: Outlet Home
2 PRESSURE	50.0 mbar, 1.5 sec, I:InjectVial, O:4: Outlet Home
3 PRESSURE	50.0 mbar, 2.0 sec, I:3: Inlet Home, O:4: Outlet Home

Store Data:

Collect voltage	Yes

Collect current	Yes
Collect power	Yes
Collect pressure	Yes
Collect temperature	Yes

Time entries:

Stoptime	16.00 min
Posttime	Off

Time Table is empty.

DIODE ARRAY DETECTOR

Settings:

Stop Time	no Limit
Post Time	Off
Response Time	2.6
Peakwidth	>0.2
Prerun Autobalance	Off
Postrun Autobalance	Off

Spectrum:

Store	None
From	190 nm
To	600 nm
Threshold	100.00 mAu

Signals:

	Store	Signal,Bw	Reference,Bw	[nm]
A:	Yes	310 60	200 20	
B:	Yes	228 10	216 10	
C:	Yes	250 10	216 10	
D:	Yes	250 20	216 20	
E:	Yes	450 80	230 20	

Contacts:

Contact 1 Off
Contact 2 Off

Time Table:

Time [min]	Function	Contact 1	Contact 2
4.00	Balance		

==========

Specify Report

==========

Calculate: Area Percent
Use Multiplier & Dilution Factor with ISTDs

Destination: Screen
Quantitative Results sorted by: Signal
Report Style: Short
Sample info on each page: No
Add Electropherogram Output: Yes
Electropherogram Output: Portrait
Size in Time direction: 100 % of Page
Size in Response direction: 40 % of Page

==========

Signal Options

==========

Include: Axes, Migration Times, Baselines, Tick Marks
Font: Arial, Size: 8

Ranges: Full
Multi Electropherograms: Overlaid, All the same Scale

Anion/Organic Acids Capillary Electrophoresis Method

The only difference between Anion method and the Organic Acid method is the run time. For the Organic Acid method, it can be decreased to 30 minutes

Method uses IonSelect High Mobility Anion purchased from Waters (P/N WAT049385)

Method Information

anion chromate buffer

Run Time Checklist

Pre-Run Cmd/Macro: off

Data Acquisition: on

Standard Data Analysis: on

Customized Data Analysis: off

Save GLP Data: off

Post-Run Cmd/Macro: off

Save Method with Data: skipped - no ACQ running

CAPILLARY ELECTROPHORESIS

CE mode: CE

Home values:

Lift Offset	4
Cassette Temperature	25.00 °C
Inlet Home Vial	3: Inlet Home
Outlet Home Vial	4: Outlet Home

Replenishment and Preconditioning:
serial processing

Replenishment Entries:
No Replenishment used

Preconditioning Entries:

	Function	Parameter
1	INLET	47: nanowater
2	FLUSH	5.00 min, I:5: Buffer, O:6: waste

Postcondition Entries:

	Function	Parameter
1	INLET	47: nanowater
2	FLUSH	5.00 min, I:7: blank (nanowater, O:6: waste

Electric:

Electric	On
Polarity	Negative
Voltage	15.00 kV
Current	14.00 µA
Power	System Limit
Low Current Limit	0.00 µA

Injection Table Entries:

	Function	Parameter
1	PRESSURE	50.0 mbar, 2.0 sec, I:5: Buffer, O:6: waste
2	PRESSURE	50.0 mbar, 9.0 sec, I:InjectVial, O:6: waste
3	PRESSURE	50.0 mbar, 2.0 sec, I:5: Buffer, O:6: waste

Store Data:

Collect voltage	Yes
Collect current	Yes

Collect power	Yes
Collect pressure	Yes
Collect temperature	Yes

Time entries:

Stoptime	22.00 min
Posttime	Off

Time Table is empty.

DIODE ARRAY DETECTOR

Settings:

Stop Time	as CE: 22.00 min
Post Time	Off
Response Time	2.6
Peakwidth	>0.2
Prerun Autobalance	On
Postrun Autobalance	Off

Spectrum:

Store	None
From	200 nm
To	350 nm
Threshold	40.00 mAu

Signals:

	Store	Signal,Bw	Reference,Bw	[nm]
A:	Yes	315 5	375 30	
B:	Yes	510 10	375 30	
C:	Yes	325 10	280 40	
D:	Yes	325 10	375 40	
E:	Yes	315 20	375 40	

Contacts:

Contact 1	Off

Contact 2 Off

Time Table is empty.

==========

Specify Report

==========

Calculate: Area Percent
Use Multiplier & Dilution Factor with ISTDs

Destination: Screen, File (Prefix: Report)
Destination File Types: .TXT, .PDF
Quantitative Results sorted by: Signal
Report Style: Short
Sample info on each page: Yes
Add Electropherogram Output: Yes
Electropherogram Output: Portrait
Size in Time direction: 100 % of Page
Size in Response direction: 20 % of Page

==========

Signal Options

==========

Include: Axes, Compound Names, Migration Times, Baselines, Tick Marks
Font: Arial, Size: 8

Ranges: Use Ranges | Min Value | Max Value |

Time	0.000	8.000
Response	-20.000	5.000

Multi Electropherograms: Separated, All the same Scale

Polarography Methods to Determine Reduced S, Fe, and Mn

```
================== METROHM 746 VA TRACE ANALYZER (5.746.0101)
==================
 Method: Luthe5  .mth        OPERATION SEQUENCE
 Title : determine sulfide, mn, fe2+
--------------------------------------------------------------------------------

    Instructions   t/s   Main parameters          Auxiliary parameters
    ------------ -----  ------------------------  ------------------------
 1   STIR              Rot.speed      1600 /min
 2   TPURGE       240.0
** Purging is only needed for standards when calibrating – Change TPURGE to 0 for
sample determination**
 3   0STIR
 4   (REP
 5    SEGMENT          Segm.name   swv
 6   REP)3
 7   END

 Method: Luthe5              SEGMENT
                           swv
--------------------------------------------------------------------------------

    Instructions   t/s   Main parameters          Auxiliary parameters
    ------------ -----  ------------------------  ------------------------
 1   0STIR        10.0
 2   HMDE              Drop size        4       Meas.cell   normal
 3   SQWMODE           U.ampl          15 mV     Modul.freq.     100 Hz
                   t.step        0.05 s      Prep.cycles       0
                   t.meas         1.0 ms     Meas.cycles       2
 4   FSWEEP       22.6   U.start          0 mV     U.step          4 mV
                   U.end        -1800 mV     Sweep rate       80 mV/s
 5   END
Method: Luthe5              SEGMENT
                           oxy
--------------------------------------------------------------------------------

    Instructions   t/s   Main parameters          Auxiliary parameters
    ------------ -----  ------------------------  ------------------------
 1   0STIR        10.0
 2   HMDE              Drop size        4       Meas.cell   normal
 3   DCTMODE           t.step        0.05 s      t.meas         1.0 ms
```

4 SWEEP 4.6 U.start -100 mV U.step 8 mV
U.end -800 mV Sweep rate 160 mV/s
5 END

Method: Luthe5 DOCUMENTATION

Auto form feed no Auto error printing no

COPY Reports, Curves	TO Destination
Report ActDetm	RSIfc.1

Method: Luthe5 SUBSTANCES
Manganes - swv

Recognition		Display / Plot	
U.verify	-1500 mV	I.scale	auto
U.tol (+/-)	75 mV	U.div	50.00 mV/cm
U.width min	10 mV	U.begin	-1800 mV
U.width max	400 mV	U.end	-1200 mV
I.threshold	200 pA		

Baseline		Evaluation	
Type	linear	Mode	VA
Scope	whole	Quantity	I.peak
dU.front	auto	Sign. digits	5
S.front	auto		
dU.rear	auto		
S.rear	auto		

Calibration 1900-01-00 00:00:00

Technique none

Method: Luthe5 SUBSTANCES
Sulfide - swv

Recognition		Display / Plot	
U.verify	-620 mV	I.scale	auto
U.tol (+/-)	50 mV	U.div	50.00 mV/cm
U.width min	20 mV	U.begin	-800 mV
U.width max	300 mV	U.end	-100 mV
I.threshold	200 pA		

Baseline		Evaluation	
Type	linear	Mode	VA
Scope	whole	Quantity	I.peak
dU.front	auto	Sign. digits	5
S.front	auto		
dU.rear	auto		
S.rear	auto		

Calibration 2007-07-12 11:07:30

Technique none

Method: Luthe5 SUBSTANCES
Iron(II) - swv

Recognition		Display / Plot	
U.verify	-1400 mV	I.scale	auto
U.tol (+/-)	75 mV	U.div	25.00 mV/cm
U.width min	10 mV	U.begin	-900 mV
U.width max	400 mV	U.end	-1800 mV
I.threshold	200 pA		

Baseline		Evaluation	
Type	linear	Mode	VA
Scope	whole	Quantity	I.peak
dU.front	auto	Sign. digits	5

S.front auto
dU.rear auto
S.rear auto

Calibration 2007-03-01 15:47:51

Technique none

Sand Column Program for TDR, Tensiometer, and Pt electrodes

```
;{CR10X}
;
*Table 1 Program
  01: 600       Execution Interval (seconds)


1:  Internal Temperature (P17)
 1: 1        Loc [ TEMP      ]

;Measure Coil TDR Probe and EC


2:  Do (P86)
 1: 44       Set Port 4 High


3:  TDR100 Measurement (P119)
 1: 0        SDM Address
 2: 0        La/L for Water Content
 3: 1001     MMMP Mux & Probe Selection
 4: 4        Waveform Averaging
 5: 1        Vp
 6: 251      Points
 7: 5.4      Cable Length (meters)
 8: 1.5      Window Length (meters)
 9: .22      Probe Length (meters)
10: 0        Probe Offset (meters)
11: 2        Loc [ CTDR_SSB  ]
12: .1138    Mult
13: -.1758   Offset

4:  TDR100 Measurement (P119)
 1: 0        SDM Address
 2: 3        Electrical Conductivity
 3: 1001     MMMP Mux & Probe Selection
 4: 4        Waveform Averaging
 5: 1        Vp
 6: 251      Points
 7: 5.4      Cable Length (meters)
 8: 1.5      Window Length (meters)
 9: .22      Probe Length (meters)
10: 0        Probe Offset (meters)
```

```
11: 3        Loc [ CEC_SSB   ]
12: 1000     Mult
13: 0        Offset

;Measure 3-Prong TDR probes and EC

5:  TDR100 Measurement (P119)
 1: 0        SDM Address
 2: 0        La/L for Water Content
 3: 2004     MMMP Mux & Probe Selection
 4: 4        Waveform Averaging
 5: 1        Vp
 6: 251      Points
 7: 4.4      Cable Length (meters)
 8: 1        Window Length (meters)
 9: .078     Probe Length (meters)
10: .0481    Probe Offset (meters)
11: 4        Loc [ TDR_SSA   ]
12: .1138    Mult
13: -.1758   Offset

6:  TDR100 Measurement (P119)
 1: 0        SDM Address
 2: 3        Electrical Conductivity
 3: 2004     MMMP Mux & Probe Selection
 4: 4        Waveform Averaging
 5: 1        Vp
 6: 251      Points
 7: 4.4      Cable Length (meters)
 8: 1        Window Length (meters)
 9: .078     Probe Length (meters)
10: .0481    Probe Offset (meters)
11: 7        Loc [ EC_SSA    ]
12: 1000     Mult
13: 0        Offset


7:  Do (P86)
 1: 54       Set Port 4 Low


;Measure Tensiometers and Pt Electrodes

8:  Do (P86)
```

```
 1: 45       Set Port 5 High

9:  Beginning of Loop (P87)
 1: 0        Delay
 2: 08       Loop Count

10:  Do (P86)
 1: 76       Pulse Port 6

11:  Volt (Diff) (P2)
 1: 1        Reps
 2: 0        Auto Slow Range (OS>1.9)
 3: 1        DIFF Channel
 4: 10    -- Loc [ TENS_SSA  ]
 5: 1        Mult
 6: 0        Offset

12:  End (P95)


13:  Do (P86)
 1: 55       Set Port 5 Low

14:  Do (P86)
 1: 10       Set Output Flag High (Flag 0)

15:  Real Time (P77)
 1: 120      (Same as 220) D,Hr/Mn

16:  Sample (P70)
 1: 18       Reps
 2: 1        Loc [ TEMP      ]


*Table 2 Program
  02: 0.0000    Execution Interval (seconds)

*Table 3 Subroutines

End Program

1      [ TEMP      ]  RW--   1       1      Start ------ ---
2      [ CTDR_SSB  ]  RW--   1       1      ----- Member ---
3      [ CEC_SSB   ]  RW--   1       1      ----- Member ---
```

```
4     [ TDR_SSA   ]  RW--   1       1      ----- Member ---
5     [ TDR_SSC   ]  R---   1       0      ----- Member ---
6     [ TDR_SSD   ]  R---   1       0      ----- Member ---
7     [ EC_SSA    ]  RW--   1       1      ----- Member ---
8     [ EC_SSC    ]  R---   1       0      ----- Member ---
9     [ EC_SSD    ]  R---   1       0      ----- Member ---
10    [ TENS_SSA  ]  RW--   1       1      ----- Member ---
11    [ TENS_SSB  ]  R---   1       0      ----- Member ---
12    [ TENS_SSC  ]  R---   1       0      ----- Member ---
13    [ TENS_SSD  ]  R---   1       0      ----- Member ---
14    [ PT_SSA    ]  R---   1       0      ----- Member ---
15    [ PT_SSB    ]  R---   1       0      ----- Member ---
16    [ PT_SSC    ]  R---   1       0      ----- Member ---
17    [ PT_SSD    ]  R---   1       0      ----- Member ---
18    [ TENS_SCA  ]  R---   1       0      ----- ------ End
```

TDR Program (layered columns)

```
;{CR10X}
;
*Table 1 Program
  01: 300.0000  Execution Interval (seconds)

1:  Internal Temperature (P17)
 1: 1        Loc [ TEMP_____ ]

2:  Do (P86)
 1: 44       Set Port 4 High

3:  TDR100 Measurement (P119)
 1: 0        SDM Address
 2: 0        La/L for Water Content
 3: 1004     MMMP Mux & Probe Selection
 4: 4        Waveform Averaging
 5: 1        Vp
 6: 251      Points
 7: 4.4      Cable Length (meters)
 8: 1        Window Length (meters)
 9: .078     Probe Length (meters)
10: .0481    Probe Offset (meters)
11: 2        Loc [ TDR_SCA   ]
12: .1138    Mult
13: -.1758   Offset

4:  TDR100 Measurement (P119)
 1: 0        SDM Address
 2: 3        Electrical Conductivity
 3: 1004     MMMP Mux & Probe Selection
 4: 4        Waveform Averaging
 5: 1        Vp
 6: 251      Points
 7: 4.4      Cable Length (meters)
 8: 1        Window Length (meters)
 9: .078     Probe Length (meters)
10: .0481    Probe Offset (meters)
11: 6        Loc [ EC_SCA    ]
12: 1000     Mult
13: 0        Offset

5:  TDR100 Measurement (P119)
```

```
 1: 0       SDM Address
 2: 0       La/L for Water Content
 3: 5001    MMMP Mux & Probe Selection
 4: 4       Waveform Averaging
 5: 1       Vp
 6: 251     Points
 7: 5.4     Cable Length (meters)
 8: 1.5     Window Length (meters)
 9: .22     Probe Length (meters)
10: 0       Probe Offset (meters)
11: 10      Loc [ CTDR_SCC  ]
12: .1138   Mult
13: -.1758  Offset

6:  TDR100 Measurement (P119)
 1: 0       SDM Address
 2: 3       Electrical Conductivity
 3: 5001    MMMP Mux & Probe Selection
 4: 4       Waveform Averaging
 5: 1       Vp
 6: 251     Points
 7: 5.4     Cable Length (meters)
 8: 1.5     Window Length (meters)
 9: .22     Probe Length (meters)
10: 0       Probe Offset (meters)
11: 11      Loc [ CEC_SCC   ]
12: 1000    Mult
13: 0       Offset

7:  TDR100 Measurement (P119)
 1: 0       SDM Address
 2: 0       La/L for Water Content
 3: 8106    MMMP Mux & Probe Selection
 4: 4       Waveform Averaging
 5: 1       Vp
 6: 251     Points
 7: 5.7     Cable Length (meters)
 8: 1       Window Length (meters)
 9: .078    Probe Length (meters)
10: .0481   Probe Offset (meters)
11: 12      Loc [ TDR_S2A   ]
12: .1138   Mult
13: -.1758  Offset
```

```
8:  TDR100 Measurement (P119)
 1: 0        SDM Address
 2: 3        Electrical Conductivity
 3: 8106     MMMP Mux & Probe Selection
 4: 4        Waveform Averaging
 5: 1        Vp
 6: 251      Points
 7: 5.7      Cable Length (meters)
 8: 1        Window Length (meters)
 9: .078     Probe Length (meters)
10: .0481    Probe Offset (meters)
11: 18       Loc [ EC_S2A    ]
12: 1000     Mult
13: 0        Offset

9:  TDR100 Measurement (P119)
 1: 0        SDM Address
 2: 0        La/L for Water Content
 3: 8702     MMMP Mux & Probe Selection
 4: 4        Waveform Averaging
 5: 1        Vp
 6: 251      Points
 7: 6.6      Cable Length (meters)
 8: 1.5      Window Length (meters)
 9: .22      Probe Length (meters)
10: 0        Probe Offset (meters)
11: 24       Loc [ CTDR_S2C  ]
12: .1138    Mult
13: -.1758   Offset

10:  TDR100 Measurement (P119)
 1: 0        SDM Address
 2: 3        Electrical Conductivity
 3: 8702     MMMP Mux & Probe Selection
 4: 4        Waveform Averaging
 5: 1        Vp
 6: 251      Points
 7: 6.6      Cable Length (meters)
 8: 1.5      Window Length (meters)
 9: .22      Probe Length (meters)
10: 0        Probe Offset (meters)
11: 26       Loc [ CEC_S2C   ]
12: 1000     Mult
13: 0        Offset
```

```
11:  Do (P86)
 1: 54       Set Port 4 Low

12:  Do (P86)
 1: 10       Set Output Flag High (Flag 0)

13:  Real Time (P77)
 1: 120      (Same as 220) D,Hr/Mn

14:  Sample (P70)
 1: 27       Reps
 2: 1        Loc [ TEMP_____ ]


*Table 2 Program
  01: 0.0000    Execution Interval (seconds)


*Table 3 Subroutines


End Program

1     [ TEMP_____ ]  RW--   1       1      ----- ------ ---
2     [ TDR_SCA   ]  RW--   1       1      ----- ------ ---
3     [ TDR_SCB   ]  R---   1       0      ----- ------ ---
4     [ TDR_SCD   ]  R---   1       0      ----- ------ ---
5     [ TDR_SCE   ]  R---   1       0      ----- ------ ---
6     [ EC_SCA    ]  RW--   1       1      ----- ------ ---
7     [ EC_SCB    ]  R---   1       0      ----- ------ ---
8     [ EC_SCD    ]  R---   1       0      ----- ------ ---
9     [ EC_SCE    ]  R---   1       0      ----- ------ ---
10    [ CTDR_SCC  ]  RW--   1       1      ----- ------ ---
11    [ CEC_SCC   ]  RW--   1       1      ----- ------ ---
12    [ TDR_S2A   ]  RW--   1       1      ----- ------ ---
13    [ TDR_S2B   ]  R---   1       0      ----- ------ ---
14    [ TDR_S2C   ]  R---   1       0      ----- ------ ---
15    [ TDR_S2D   ]  R---   1       0      ----- ------ ---
16    [ TDR_S2E   ]  R---   1       0      ----- ------ ---
17    [ TDR_S2F   ]  R---   1       0      ----- ------ ---
18    [ EC_S2A    ]  RW--   1       1      ----- ------ ---
19    [ EC_S2B    ]  R---   1       0      ----- ------ ---
20    [ EC_S2C    ]  R---   1       0      ----- ------ ---
```

```
21    [ EC_S2D    ] R---   1       0      ----- ------ ---
22    [ EC_S2E    ] R---   1       0      ----- ------ ---
23    [ EC_S2F    ] R---   1       0      ----- ------ ---
24    [ CTDR_S2C  ] RW--   1       1      ----- ------ ---
25    [ CTDR_S2D  ] R---   1       0      ----- ------ ---
26    [ CEC_S2C   ] RW--   1       1      ----- ------ ---
27    [ CEC_S2D   ] R---   1       0      ----- ------ ---
```

Tensiometers and Platinum Electrode Datalogger Program

```
;{CR10X}
:
*Table 1 Program
  01: 300.0000  Execution Interval (seconds)

1:  Do (P86)
 1: 45       Set Port 5 High

2:  Beginning of Loop (P87)
 1: 0        Delay
 2: 11       Loop Count

3:  Do (P86)
 1: 76       Pulse Port 6

4:  Volt (Diff) (P2)
 1: 1        Reps
 2: 0        Auto Slow Range (OS>1.9)
 3: 1        DIFF Channel
 4: 1     -- Loc [ TENS_SCA  ]
 5: 1        Mult
 6: 0        Offset

5:  End (P95)

6:  Beginning of Loop (P87)
 1: 0        Delay
 2: 11       Loop Count

7:  Do (P86)
 1: 76       Pulse Port 6

8:  Volt (Diff) (P2)
 1: 1        Reps
 2: 0        Auto Slow Range (OS>1.9)
 3: 1        DIFF Channel
 4: 12    -- Loc [ PT_SCA    ]
 5: 1        Mult
 6: 0        Offset

9:  End (P95)
```

```
10:  Do (P86)
 1: 55       Set Port 5 Low

11:  Internal Temperature (P17)
 1: 23       Loc [ TEMP      ]

12:  Do (P86)
 1: 10       Set Output Flag High (Flag 0)

13:  Real Time (P77)
 1: 120      (Same as 220) D,Hr/Mn

14:  Sample (P70)
 1: 23       Reps
 2: 1        Loc [ TENS_SCA  ]


*Table 2 Program
  01: 0.0000    Execution Interval (seconds)


*Table 3 Subroutines


End Program


1     [ TENS_SCA  ]  RW--   1       1      ----- ------ ---
2     [ TENS_SCB  ]  R---   1       0      ----- ------ ---
3     [ TENS_SCC  ]  R---   1       0      ----- ------ ---
4     [ TENS_SCD  ]  R---   1       0      ----- ------ ---
5     [ TENS_SCE  ]  R---   1       0      ----- ------ ---
6     [ TENS_S2A  ]  R---   1       0      ----- ------ ---
7     [ TENS_S2B  ]  R---   1       0      ----- ------ ---
8     [ TENS_S2C  ]  R---   1       0      ----- ------ ---
9     [ TENS_S2D  ]  R---   1       0      ----- ------ ---
10    [ TENS_S2E  ]  R---   1       0      ----- ------ ---
11    [ TENS_S2F  ]  R---   1       0      ----- ------ ---
12    [ PT_SCA    ]  RW--   1       1      ----- ------ ---
13    [ PT_SCB    ]  R---   1       0      ----- ------ ---
14    [ PT_SCC    ]  R---   1       0      ----- ------ ---
15    [ PT_SCD    ]  R---   1       0      ----- ------ ---
16    [ PT_SCE    ]  R---   1       0      ----- ------ ---
17    [ PT_S2A    ]  R---   1       0      ----- ------ ---
```

```
18    [ PT_S2B    ] R---   1       0      ----- ------ ---
19    [ PT_S2C    ] R---   1       0      ----- ------ ---
20    [ PT_S2D    ] R---   1       0      ----- ------ ---
21    [ PT_S2E    ] R---   1       0      ----- ------ ---
22    [ PT_S2F    ] R---   1       0      ----- ------ ---
23    [ TEMP      ] RW--   1       1      ----- ------ ---
```

Flow Meter Datalogger Program

```
;{CR10X}
;
*Table 1 Program
  01: 1        Execution Interval (seconds)

;Measure Flow from SM Colum (Serial Number 15595)

1:  Volt (SE) (P1)
 1: 1        Reps
 2: 00       Range Option
 3: 1        SE Channel
 4: 1        Loc [ SM_Flow   ]
 5: .019858  Mult
 6: .667005  Offset

;Measure Flow from SL Colum (Serial Number 15594)

2:  Volt (SE) (P1)
 1: 1        Reps
 2: 00       Range Option
 3: 2        SE Channel
 4: 2        Loc [ SL_Flow   ]
 5: .020303  Mult
 6: -.858405 Offset


;Measure Flow from SLK Colum (Serial Number 15596)

3:  Volt (SE) (P1)
 1: 1        Reps
 2: 00       Range Option
 3: 3        SE Channel
 4: 3        Loc [ SLK_Flow  ]
 5: .019865  Mult
 6: .579298  Offset

;

4:  Volt (Diff) (P2)
 1: 1        Reps
 2: 00       Range Option
 3: 4        DIFF Channel
```

4: 4 Loc [Br_SM]
5: 1.0 Mult
6: 0.0 Offset

5: Volt (Diff) (P2)
1: 1 Reps
2: 00 Range Option
3: 5 DIFF Channel
4: 5 Loc [Br_SL]
5: 1.0 Mult
6: 0.0 Offset

6: Volt (Diff) (P2)
1: 1 Reps
2: 00 Range Option
3: 06 DIFF Channel
4: 6 Loc [Br_SLK]
5: 1.0 Mult
6: 0.0 Offset

7: Running Average (P52)
1: 1 Reps
2: 4 First Source Loc [Br_SM]
3: 7 First Destination Loc [Br_SM_Run]
4: 6 Number of Values in Avg Window

8: Running Average (P52)
1: 1 Reps
2: 5 First Source Loc [Br_SL]
3: 8 First Destination Loc [Br_SL_Run]
4: 6 Number of Values in Avg Window

9: Running Average (P52)
1: 1 Reps
2: 6 First Source Loc [Br_SLK]
3: 9 First Destination Loc [Br_SLK_Ru]
4: 6 Number of Values in Avg Window

```
10:  Do (P86)
 1: 10       Set Output Flag High (Flag 0)


11:  Real Time (P77)
 1: 110      Day,Hour/Minute (midnight = 0000)



12:  Sample (P70)
 1: 3        Reps
 2: 1        Loc [ SM_Flow    ]


13:  Sample (P70)
 1: 3        Reps
 2: 7        Loc [ Br_SM_Run ]

*Table 2 Program
  02: 0.0000    Execution Interval (seconds)

*Table 3 Subroutines

End Program

1      [ SM_Flow   ]  RW--   1       1      Start ------ ---
2      [ SL_Flow   ]  RW--   1       1      ----- Member ---
3      [ SLK_Flow  ]  RW--   1       1      ----- ------ End
4      [ Br_SM     ]  RW--   1       1      Start ------ ---
5      [ Br_SL     ]  RW--   1       1      ----- ------ ---
6      [ Br_SLK    ]  RW--   1       1      ----- ------ ---
7      [ Br_SM_Run ]  RW--   1       1      Start ------ ---
8      [ Br_SL_Run ]  RW--   1       1      ----- ------ ---
9      [ Br_SLK_Ru ]  RW--   1       1      ----- ------ ---
```

TDR Measurement Datalogger Program (Lens Column Experiments)

```
;{CR10X}
;
*Table 1 Program
  01: 300       Execution Interval (seconds)


1:  Do (P86)
 1: 44       Set Port 4 High

;SMB - D11

2:  TDR100 Measurement (P119)
 1: 00       SDM Address
 2: 0        La/L for Water Content
 3: 1101     MMMP Mux & Probe Selection
 4: 4        Waveform Averaging
 5: 1        Vp
 6: 251      Points
 7: 5.75     Cable Length (meters)
 8: 1.0      Window Length (meters)
 9: .081     Probe Length (meters)
10: .041726  Probe Offset (meters)
11: 1        Loc [ SMB_LAL   ]
12: 1        Mult
13: 0        Offset

;SMC - CT2

3:  TDR100 Measurement (P119)
 1: 00       SDM Address
 2: 0        La/L for Water Content
 3: 1102     MMMP Mux & Probe Selection
 4: 4        Waveform Averaging
 5: 1        Vp
 6: 1201     Points
 7: 5.75     Cable Length (meters)
 8: 1.5      Window Length (meters)
 9: .230     Probe Length (meters)
10: 0.0      Probe Offset (meters)
11: 2        Loc [ SMC_LAL   ]
```

```
12: 1.0      Mult
13: 0.0      Offset

;SMD - CT4

4:  TDR100 Measurement (P119)
 1: 00       SDM Address
 2: 0        La/L for Water Content
 3: 1301     MMMP Mux & Probe Selection
 4: 4        Waveform Averaging
 5: 1        Vp
 6: 251      Points
 7: 5.75     Cable Length (meters)
 8: 1.5      Window Length (meters)
 9: .230     Probe Length (meters)
10: 0.0      Probe Offset (meters)
11: 3        Loc [ SMD_LAL   ]
12: 1.0      Mult
13: 0.0      Offset

;SME - D14

5:  TDR100 Measurement (P119)
 1: 00       SDM Address
 2: 0        La/L for Water Content
 3: 1401     MMMP Mux & Probe Selection
 4: 4        Waveform Averaging
 5: 1        Vp
 6: 251      Points
 7: 5.75     Cable Length (meters)
 8: .75      Window Length (meters)
 9: .048     Probe Length (meters)
10: .039217  Probe Offset (meters)
11: 4        Loc [ SME_LAL   ]
12: 1.0      Mult
13: 0.0      Offset

;SMF - CT5

6:  TDR100 Measurement (P119)
 1: 00       SDM Address
 2: 0        La/L for Water Content
 3: 1501     MMMP Mux & Probe Selection
 4: 4        Waveform Averaging
```

```
 5: 1        Vp
 6: 251      Points
 7: 5.75     Cable Length (meters)
 8: 1.5      Window Length (meters)
 9: .230     Probe Length (meters)
10: 0.0      Probe Offset (meters)
11: 5        Loc [ SMF_LAL   ]
12: 1.0      Mult
13: 0.0      Offset

;SMG - CT7

7:  TDR100 Measurement (P119)
 1: 00       SDM Address
 2: 0        La/L for Water Content
 3: 1601     MMMP Mux & Probe Selection
 4: 4        Waveform Averaging
 5: 1        Vp
 6: 251      Points
 7: 5.75     Cable Length (meters)
 8: 1.5      Window Length (meters)
 9: .230     Probe Length (meters)
10: 0.0      Probe Offset (meters)
11: 6        Loc [ SMG_LAL   ]
12: 1.0      Mult
13: 0.0      Offset

;SMH - D15

8:  TDR100 Measurement (P119)
 1: 00       SDM Address
 2: 0        La/L for Water Content
 3: 1701     MMMP Mux & Probe Selection
 4: 4        Waveform Averaging
 5: 1        Vp
 6: 251      Points
 7: 5.75     Cable Length (meters)
 8: 1.0      Window Length (meters)
 9: .048     Probe Length (meters)
10: .047217  Probe Offset (meters)
11: 7        Loc [ SMH_LAL   ]
12: 1.0      Mult
13: 0.0      Offset
```

```
;SMI - CT8

9:  TDR100 Measurement (P119)
 1: 00       SDM Address
 2: 0        La/L for Water Content
 3: 1801     MMMP Mux & Probe Selection
 4: 4        Waveform Averaging
 5: 1        Vp
 6: 251      Points
 7: 5.75     Cable Length (meters)
 8: 1.5      Window Length (meters)
 9: .230     Probe Length (meters)
10: 0.0      Probe Offset (meters)
11: 8        Loc [ SMI_LAL   ]
12: 1.0      Mult
13: 0.0      Offset

;SMJ - M2

10:  TDR100 Measurement (P119)
 1: 00       SDM Address
 2: 0        La/L for Water Content
 3: 2101     MMMP Mux & Probe Selection
 4: 4        Waveform Averaging
 5: 1        Vp
 6: 251      Points
 7: 6.5      Cable Length (meters)
 8: 1.5      Window Length (meters)
 9: .230     Probe Length (meters)
10: 0.0      Probe Offset (meters)
11: 9        Loc [ SMJ_LAL   ]
12: 1.0      Mult
13: 0.0      Offset

;SMK - D16

11:  TDR100 Measurement (P119)
 1: 00       SDM Address
 2: 0        La/L for Water Content
 3: 2201     MMMP Mux & Probe Selection
 4: 4        Waveform Averaging
 5: 1        Vp
 6: 251      Points
 7: 5.75     Cable Length (meters)
```

```
 8: 1.0      Window Length (meters)
 9: .05      Probe Length (meters)
10: .033278  Probe Offset (meters)
11: 10       Loc [ SMK_LAL   ]
12: 1.0      Mult
13: 0.0      Offset

;SLB - D1

12:  TDR100 Measurement (P119)
 1: 00       SDM Address
 2: 0        La/L for Water Content
 3: 2301     MMMP Mux & Probe Selection
 4: 4        Waveform Averaging
 5: 1        Vp
 6: 251      Points
 7: 5.75     Cable Length (meters)
 8: 1.0      Window Length (meters)
 9: 7.4      Probe Length (meters)
10: .038512  Probe Offset (meters)
11: 11       Loc [ SLB_LAL   ]
12: 1.0      Mult
13: 0.0      Offset

;SLC - D2

13:  TDR100 Measurement (P119)
 1: 00       SDM Address
 2: 0        La/L for Water Content
 3: 2401     MMMP Mux & Probe Selection
 4: 4        Waveform Averaging
 5: 1        Vp
 6: 2401     Points
 7: 5.75     Cable Length (meters)
 8: 1.0      Window Length (meters)
 9: 7.6      Probe Length (meters)
10: .031573  Probe Offset (meters)
11: 12       Loc [ SLC_LAL   ]
12: 1.0      Mult
13: 0.0      Offset

;SLD - D3

14:  TDR100 Measurement (P119)
```

```
 1: 00       SDM Address
 2: 0        La/L for Water Content
 3: 2501     MMMP Mux & Probe Selection
 4: 4        Waveform Averaging
 5: 1        Vp
 6: 251      Points
 7: 5.75     Cable Length (meters)
 8: 1.0      Window Length (meters)
 9: .077     Probe Length (meters)
10: .033854  Probe Offset (meters)
11: 13       Loc [ SLD_LAL   ]
12: 1.0      Mult
13: 0.0      Offset

;SLE - D4

15:  TDR100 Measurement (P119)
 1: 00       SDM Address
 2: 0        La/L for Water Content
 3: 2601     MMMP Mux & Probe Selection
 4: 4        Waveform Averaging
 5: 1        Vp
 6: 251      Points
 7: 5.75     Cable Length (meters)
 8: 1.0      Window Length (meters)
 9: .077     Probe Length (meters)
10: .023604  Probe Offset (meters)
11: 14       Loc [ SLE_LAL   ]
12: 1.0      Mult
13: 0.0      Offset

;SLF - D17

16:  TDR100 Measurement (P119)
 1: 00       SDM Address
 2: 0        La/L for Water Content
 3: 2701     MMMP Mux & Probe Selection
 4: 4        Waveform Averaging
 5: 1        Vp
 6: 251      Points
 7: 5.75     Cable Length (meters)
 8: 1        Window Length (meters)
 9: .033     Probe Length (meters)
10: .0481    Probe Offset (meters)
```

```
11: 15       Loc [ SLF_LAL   ]
12: 1.0      Mult
13: 0.0      Offset

;SLH - D5

17:  TDR100 Measurement (P119)
 1: 00       SDM Address
 2: 0        La/L for Water Content
 3: 2801     MMMP Mux & Probe Selection
 4: 4        Waveform Averaging
 5: 1        Vp
 6: 251      Points
 7: 5.75     Cable Length (meters)
 8: 1        Window Length (meters)
 9: .073     Probe Length (meters)
10: .042231  Probe Offset (meters)
11: 16       Loc [ SLH_LAL   ]
12: 1.0      Mult
13: 0.0      Offset

;SLI - D6

18:  TDR100 Measurement (P119)
 1: 00       SDM Address
 2: 0        La/L for Water Content
 3: 3101     MMMP Mux & Probe Selection
 4: 4        Waveform Averaging
 5: 1        Vp
 6: 251      Points
 7: 5.5      Cable Length (meters)
 8: 1        Window Length (meters)
 9: .074     Probe Length (meters)
10: .0481    Probe Offset (meters)
11: 17       Loc [ SLI_LAL   ]
12: 1.0      Mult
13: 0.0      Offset

;SLJ - D8

19:  TDR100 Measurement (P119)
 1: 00       SDM Address
 2: 0        La/L for Water Content
 3: 3201     MMMP Mux & Probe Selection
```

```
 4: 4        Waveform Averaging
 5: 1        Vp
 6: 251      Points
 7: 5.5      Cable Length (meters)
 8: 1        Window Length (meters)
 9: .073     Probe Length (meters)
10: .047731  Probe Offset (meters)
11: 18       Loc [ SLJ_LAL   ]
12: 1.0      Mult
13: 0.0      Offset

;SLK - R2

20:  TDR100 Measurement (P119)
 1: 00       SDM Address
 2: 0        La/L for Water Content
 3: 3301     MMMP Mux & Probe Selection
 4: 4        Waveform Averaging
 5: 1        Vp
 6: 251      Points
 7: 5.5      Cable Length (meters)
 8: 1.0      Window Length (meters)
 9: .04      Probe Length (meters)
10: .045723  Probe Offset (meters)
11: 19       Loc [ SLK_LAL   ]
12: 1.0      Mult
13: 0.0      Offset

;SLKB - M4

21:  TDR100 Measurement (P119)
 1: 00       SDM Address
 2: 0        La/L for Water Content
 3: 3401     MMMP Mux & Probe Selection
 4: 4        Waveform Averaging
 5: 1        Vp
 6: 251      Points
 7: 5.5      Cable Length (meters)
 8: 1        Window Length (meters)
 9: .076     Probe Length (meters)
10: .064232  Probe Offset (meters)
11: 20       Loc [ SLKB_LAL  ]
12: 1.0      Mult
13: 0.0      Offset
```

```
;SLKC - M5

22:  TDR100 Measurement (P119)
 1: 00       SDM Address
 2: 0        La/L for Water Content
 3: 3501     MMMP Mux & Probe Selection
 4: 4        Waveform Averaging
 5: 1        Vp
 6: 251      Points
 7: 5.5      Cable Length (meters)
 8: 1.0      Window Length (meters)
 9: .076     Probe Length (meters)
10: .056232  Probe Offset (meters)
11: 21       Loc [ SLKC_LAL  ]
12: 1.0      Mult
13: 0.0      Offset

;SLKD - M6

23:  TDR100 Measurement (P119)
 1: 00       SDM Address
 2: 0        La/L for Water Content
 3: 3601     MMMP Mux & Probe Selection
 4: 4        Waveform Averaging
 5: 1        Vp
 6: 251      Points
 7: 5.5      Cable Length (meters)
 8: 1.0      Window Length (meters)
 9: .076     Probe Length (meters)
10: .056232  Probe Offset (meters)
11: 22       Loc [ SLKD_LAL  ]
12: 1.0      Mult
13: 0.0      Offset

;SLKE - D7

24:  TDR100 Measurement (P119)
 1: 00       SDM Address
 2: 0        La/L for Water Content
 3: 3701     MMMP Mux & Probe Selection
 4: 4        Waveform Averaging
 5: 1        Vp
 6: 251      Points
```

```
 7: 5.5      Cable Length (meters)
 8: 1.0      Window Length (meters)
 9: .075     Probe Length (meters)
10: .039792  Probe Offset (meters)
11: 23       Loc [ SLKE_LAL  ]
12: 1.0      Mult
13: 0.0      Offset

;SLKF - D19

25:  TDR100 Measurement (P119)
 1: 00       SDM Address
 2: 0        La/L for Water Content
 3: 3801     MMMP Mux & Probe Selection
 4: 4        Waveform Averaging
 5: 1        Vp
 6: 251      Points
 7: 5.5      Cable Length (meters)
 8: 1.0      Window Length (meters)
 9: .039     Probe Length (meters)
10: .051447  Probe Offset (meters)
11: 24       Loc [ SLKF_LAL  ]
12: 1.0      Mult
13: 0.0      Offset

;SLKH - UNK

26:  TDR100 Measurement (P119)
 1: 00       SDM Address
 2: 0        La/L for Water Content
 3: 4101     MMMP Mux & Probe Selection
 4: 4        Waveform Averaging
 5: 1        Vp
 6: 251      Points
 7: 5.5      Cable Length (meters)
 8: 1        Window Length (meters)
 9: .077     Probe Length (meters)
10: .0481    Probe Offset (meters)
11: 25       Loc [ SLKH_LAL  ]
12: 1.0      Mult
13: 0.0      Offset

;SLKI - D12
```

```
27:  TDR100 Measurement (P119)
 1: 00       SDM Address
 2: 0        La/L for Water Content
 3: 4201     MMMP Mux & Probe Selection
 4: 4        Waveform Averaging
 5: 1        Vp
 6: 251      Points
 7: 5.5      Cable Length (meters)
 8: 1.0      Window Length (meters)
 9: .073     Probe Length (meters)
10: .041981  Probe Offset (meters)
11: 26       Loc [ SLKI_LAL  ]
12: 1.0      Mult
13: 0.0      Offset

;SLKJ - D13

28:  TDR100 Measurement (P119)
 1: 00       SDM Address
 2: 0        La/L for Water Content
 3: 4301     MMMP Mux & Probe Selection
 4: 4        Waveform Averaging
 5: 1        Vp
 6: 251      Points
 7: 5.5      Cable Length (meters)
 8: 1        Window Length (meters)
 9: .076     Probe Length (meters)
10: 0.0      Probe Offset (meters)
11: 27       Loc [ SLKJ_LAL  ]
12: 1.0      Mult
13: 0.0      Offset

;SLKK - D18

29:  TDR100 Measurement (P119)
 1: 00       SDM Address
 2: 0        La/L for Water Content
 3: 4401     MMMP Mux & Probe Selection
 4: 4        Waveform Averaging
 5: 1        Vp
 6: 251      Points
 7: 5.5      Cable Length (meters)
 8: 1.0      Window Length (meters)
 9: .038     Probe Length (meters)
```

```
10: .045673  Probe Offset (meters)
11: 28       Loc [ SLKK_LAL  ]
12: 1.0      Mult
13: 0.0      Offset


30:  Beginning of Loop (P87)
 1: 0        Delay
 2: 28       Loop Count

;SQUARE La/L TO CONVERT TO DIELECTRIC CONSTANT

31:  Z=X*Y (P36)
 1: 1     -- X Loc [ SMB_LAL   ]
 2: 1     -- Y Loc [ SMB_LAL   ]
 3: 29    -- Z Loc [ SMB_WC    ]

;MULTIPLY BY 0.1 TO PREPARE FOR THE 3RD ORDER POLYNOMIAL

32:  Z=X*F (P37)
 1: 29    -- X Loc [ SMB_WC    ]
 2: .1       F
 3: 29    -- Z Loc [ SMB_WC    ]

;APPLY TOPP'S 3RD ORDER POLYNOMIAL

33:  Polynomial (P55)
 1: 1        Reps
 2: 29    -- X Loc [ SMB_WC    ]
 3: 29    -- F(X) Loc [ SMB_WC    ]
 4: -.053    C0
 5: .292     C1
 6: -.055    C2
 7: .0043    C3
 8: 0.0      C4
 9: 0.0      C5


34:  End (P95)


35:  Do (P86)
 1: 54       Set Port 4 Low
```

36: Do (P86)
 1: 10   Set Output Flag High (Flag 0)

37: Real Time (P77)
 1: 110   Day,Hour/Minute (midnight = 0000)

38: Sample (P70)
 1: 28   Reps
 2: 29   Loc [SMB_WC   ]

*Table 2 Program
  02: 0.0000   Execution Interval (seconds)

*Table 3 Subroutines

End Program

1   [SMB_LAL   ] RW--   2   1   ----- ------ ---
2   [SMC_LAL   ] -W--   0   1   ----- ------ ---
3   [SMD_LAL   ] -W--   0   1   ----- ------ ---
4   [SME_LAL   ] -W--   0   1   ----- ------ ---
5   [SMF_LAL   ] -W--   0   1   ----- ------ ---
6   [SMG_LAL   ] -W--   0   1   ----- ------ ---
7   [SMH_LAL   ] -W--   0   1   ----- ------ ---
8   [SMI_LAL   ] -W--   0   1   ----- ------ ---
9   [SMJ_LAL   ] -W--   0   1   ----- ------ ---
10   [SMK_LAL   ] -W--   0   1   ----- ------ ---
11   [SLB_LAL   ] -W--   0   1   ----- ------ ---
12   [SLC_LAL   ] -W--   0   1   ----- ------ ---
13   [SLD_LAL   ] -W--   0   1   ----- ------ ---
14   [SLE_LAL   ] -W--   0   1   ----- ------ ---
15   [SLF_LAL   ] -W--   0   1   ----- ------ ---
16   [SLH_LAL   ] -W--   0   1   ----- ------ ---
17   [SLI_LAL   ] -W--   0   1   ----- ------ ---
18   [SLJ_LAL   ] -W--   0   1   ----- ------ ---
19   [SLK_LAL   ] -W--   0   1   ----- ------ ---
20   [SLKB_LAL] -W--   0   1   ----- ------ ---
21   [SLKC_LAL] -W--   0   1   ----- ------ ---
22   [SLKD_LAL] -W--   0   1   ----- ------ ---
23   [SLKE_LAL] -W--   0   1   ----- ------ ---
24   [SLKF_LAL] -W--   0   1   ----- ------ ---
25   [SLKH_LAL] -W--   0   1   ----- ------ ---
26   [SLKI_LAL] -W--   0   1   ----- ------ ---
27   [SLKJ_LAL] -W--   0   1   ----- ------ ---

```
28   [ SLKK_LAL  ] -W--  0     1     ----- ------ ---
29   [ SMB_WC    ] RW--  3     3     ----- ------ ---
30   [ SMC_WC    ] ----  0     0     ----- ------ ---
31   [ SMD_WC    ] ----  0     0     ----- ------ ---
32   [ SME_WC    ] ----  0     0     ----- ------ ---
33   [ SMF_WC    ] ----  0     0     ----- ------ ---
34   [ SMG_WC    ] ----  0     0     ----- ------ ---
35   [ SMH_WC    ] ----  0     0     ----- ------ ---
36   [ SMI_WC    ] ----  0     0     ----- ------ ---
37   [ SMJ_WC    ] ----  0     0     ----- ------ ---
38   [ SMK_WC    ] ----  0     0     ----- ------ ---
39   [ SLB_WC    ] ----  0     0     ----- ------ ---
40   [ SLC_WC    ] ----  0     0     ----- ------ ---
41   [ SLD_WC    ] ----  0     0     ----- ------ ---
42   [ SLE_WC    ] ----  0     0     ----- ------ ---
43   [ SLF_WC    ] ----  0     0     ----- ------ ---
44   [ SLH_WC    ] ----  0     0     ----- ------ ---
45   [ SLI_WC    ] ----  0     0     ----- ------ ---
46   [ SLJ_WC    ] ----  0     0     ----- ------ ---
47   [ SLK_WC    ] ----  0     0     ----- ------ ---
48   [ SLKB_WC   ] ----  0     0     ----- ------ ---
49   [ SLKC_WC   ] ----  0     0     ----- ------ ---
50   [ SLKD_WC   ] ----  0     0     ----- ------ ---
51   [ SLKE_WC   ] ----  0     0     ----- ------ ---
52   [ SLKF_WC   ] ----  0     0     ----- ------ ---
53   [ SLKH_WC   ] ----  0     0     ----- ------ ---
54   [ SLKI_WC   ] ----  0     0     ----- ------ ---
55   [ SLKJ_WC   ] ----  0     0     ----- ------ ---
56   [ SLKK_WC   ] ----  0     0     ----- ------ ---
```

Tensiometers and Platinum Electrode Datalogger Program

```
;{CR10X}

*Table 1 Program
  01: 300       Execution Interval (seconds)


1:  Do (P86)
 1: 41       Set Port 1 High


2:  Beginning of Loop (P87)
 1: 0        Delay
 2: 32       Loop Count


3:  Do (P86)
 1: 72       Pulse Port 2


4:  Volt (Diff) (P2)
 1: 1        Reps
 2: 00       Range Option
 3: 1        DIFF Channel
 4: 1     -- Loc [ TENS_SMB  ]
 5: 1.0      Mult
 6: 0.0      Offset

5:  End (P95)


6:  Do (P86)
 1: 51       Set Port 1 Low



7:  Do (P86)
 1: 43       Set Port 3 High


8:  Beginning of Loop (P87)
 1: 0        Delay
 2: 31       Loop Count
```

```
9:  Do (P86)
 1: 72       Pulse Port 2


10:  Volt (Diff) (P2)
 1: 1        Reps
 2: 00       Range Option
 3: 1        DIFF Channel
 4: 33    -- Loc [ PT_SMA    ]
 5: 1.0      Mult
 6: 0.0      Offset

11:  End (P95)


12:  Do (P86)
 1: 53       Set Port 3 Low


13:  Do (P86)
 1: 10       Set Output Flag High (Flag 0)



14:  Real Time (P77)
 1: 110      Day,Hour/Minute (midnight = 0000)


15:  Sample (P70)
 1: 63       Reps
 2: 1        Loc [ TENS_SMB  ]


*Table 2 Program
  02: 0.0000    Execution Interval (seconds)

*Table 3 Subroutines

End Program

1      [ TENS_SMB  ]  RW--   1       1      Start ------ ---
2      [ TENS_SMC  ]  R---   1       0      ----- Member ---
```

```
3     [ TENS_SMD  ] R---   1       0      ----- Member ---
4     [ TENS_SME  ] R---   1       0      ----- Member ---
5     [ TENS_SMF  ] R---   1       0      ----- Member ---
6     [ TENS_SMG  ] R---   1       0      ----- Member ---
7     [ TENS_SMH  ] R---   1       0      ----- Member ---
8     [ TENS_SMI  ] R---   1       0      ----- Member ---
9     [ TENS_SMJ  ] R---   1       0      ----- Member ---
10    [ TENS_SMK  ] R---   1       0      ----- Member ---
11    [ TENS_SML  ] R---   1       0      ----- Member ---
12    [ TENS_SMM  ] R---   1       0      ----- Member ---
13    [ TENS_SLB  ] R---   1       0      ----- Member ---
14    [ TENS_SLC  ] R---   1       0      ----- Member ---
15    [ TENS_SLD  ] R---   1       0      ----- Member ---
16    [ TENS_SLE  ] R---   1       0      ----- Member ---
17    [ TENS_SLF  ] R---   1       0      ----- Member ---
18    [ TENS_SLH  ] R---   1       0      ----- Member ---
19    [ TENS_SLI  ] R---   1       0      ----- Member ---
20    [ TENS_SLJ  ] R---   1       0      ----- Member ---
21    [ TENS_SLK  ] R---   1       0      ----- Member ---
22    [ TENS_SLM  ] R---   1       0      ----- Member ---
23    [ TENS_SLKB ] R---   1       0      ----- Member ---
24    [ TENS_SLKC ] R---   1       0      ----- Member ---
25    [ TENS_SLKD ] R---   1       0      ----- Member ---
26    [ TENS_SLKE ] R---   1       0      ----- Member ---
27    [ TENS_SLKF ] R---   1       0      ----- Member ---
28    [ TENS_SLKH ] R---   1       0      ----- Member ---
29    [ TENS_SLKI ] R---   1       0      ----- Member ---
30    [ TENS_SLKJ ] R---   1       0      ----- Member ---
31    [ TENS_SLKK ] R---   1       0      ----- ------ ---
32    [ TENS_SLKM ] R---   1       0      ----- ------ ---
33    [ PT_SMA    ] RW--   1       1      ----- Member ---
34    [ PT_SMB    ] R---   1       0      ----- Member ---
35    [ PT_SMC    ] R---   1       0      ----- Member ---
36    [ PT_SMD    ] R---   1       0      ----- Member ---
37    [ PT_SME    ] R---   1       0      ----- Member ---
38    [ PT_SMF    ] R---   1       0      ----- Member ---
39    [ PT_SMG    ] R---   1       0      ----- Member ---
40    [ PT_SMH    ] R---   1       0      ----- Member ---
41    [ PT_SMI    ] R---   1       0      ----- Member ---
42    [ PT_SMJ    ] R---   1       0      ----- Member ---
43    [ PT_SMK    ] R---   1       0      ----- Member ---
44    [ PT_SLA    ] R---   1       0      ----- Member ---
45    [ PT_SLB    ] R---   1       0      ----- Member ---
46    [ PT_SLC    ] R---   1       0      ----- Member ---
```

47 [PT_SLD] R--- 1 0 ----- Member ---
48 [PT_SLE] R--- 1 0 ----- Member ---
49 [PT_SLF] R--- 1 0 ----- Member ---
50 [PT_SLH] R--- 1 0 ----- Member ---
51 [PT_SLI] R--- 1 0 ----- Member ---
52 [PT_SLJ] R--- 1 0 ----- Member ---
53 [PT_SLK] R--- 1 0 ----- Member ---
54 [PT_SLKA] R--- 1 0 ----- Member ---
55 [PT_SLKB] R--- 1 0 ----- Member ---
56 [PT_SLKC] R--- 1 0 ----- Member ---
57 [PT_SLKD] R--- 1 0 ----- Member ---
58 [PT_SLKE] R--- 1 0 ----- Member ---
59 [PT_SLKF] R--- 1 0 ----- Member ---
60 [PT_SLKH] R--- 1 0 ----- Member ---
61 [PT_SLKI] R--- 1 0 ----- Member ---
62 [PT_SLKJ] R--- 1 0 ----- Member ---
63 [PT_SLKK] R--- 1 0 ----- ------ End

Vacuum/Nitrogen Gas Solenoid Valve Control Program

```
;{CR10X}
;
*Table 1 Program
  01: 1        Execution Interval (seconds)

;Valve 1 & 2 - Vacuum

1:  If time is (P92)
 1: 0        Minutes (Seconds --) into a
 2: 120      Interval (same units as above)
 3: 30       Then Do

2:  Z=F (P30)
 1: 1        F
 2: 00       Exponent of 10
 3: 1        Z Loc [ Valve1    ]

3:  Z=F (P30)
 1: 1        F
 2: 00       Exponent of 10
 3: 2        Z Loc [ Valve2    ]

4:  End (P95)

;Valve 3 & 4 - Vacuum

5:  If time is (P92)
 1: 1        Minutes (Seconds --) into a
 2: 120      Interval (same units as above)
 3: 30       Then Do

6:  Z=F (P30)
 1: 1        F
 2: 00       Exponent of 10
 3: 3        Z Loc [ Valve3    ]

7:  Z=F (P30)
 1: 1        F
 2: 00       Exponent of 10
 3: 4        Z Loc [ Valve4    ]
```

```
8:  End (P95)

;Valve 5 & 6 - Vacuum

9:  If time is (P92)
 1: 2        Minutes (Seconds --) into a
 2: 120      Interval (same units as above)
 3: 30       Then Do

10:  Z=F (P30)
 1: 1        F
 2: 00       Exponent of 10
 3: 5        Z Loc [ Valve5    ]

11:  Z=F (P30)
 1: 1        F
 2: 00       Exponent of 10
 3: 6        Z Loc [ Valve6    ]

12:  End (P95)

;Valve 7 & 8 - Vacuum

13:  If time is (P92)
 1: 3        Minutes (Seconds --) into a
 2: 120      Interval (same units as above)
 3: 30       Then Do

14:  Z=F (P30)
 1: 1        F
 2: 00       Exponent of 10
 3: 7        Z Loc [ Valve7    ]

15:  Z=F (P30)
 1: 1        F
 2: 00       Exponent of 10
 3: 8        Z Loc [ Valve8    ]

16:  End (P95)

;Valve 9 & 10 - Vacuum

17:  If time is (P92)
 1: 4        Minutes (Seconds --) into a
```

```
 2: 120      Interval (same units as above)
 3: 30       Then Do

18:  Z=F (P30)
 1: 1        F
 2: 00       Exponent of 10
 3: 9        Z Loc [ Valve9    ]

19:  Z=F (P30)
 1: 1        F
 2: 00       Exponent of 10
 3: 10       Z Loc [ Valve10   ]

20:  End (P95)

;Valve 11 & 12 - Vacuum

21:  If time is (P92)
 1: 5        Minutes (Seconds --) into a
 2: 120      Interval (same units as above)
 3: 30       Then Do

22:  Z=F (P30)
 1: 1        F
 2: 00       Exponent of 10
 3: 11       Z Loc [ Valve11   ]

23:  Z=F (P30)
 1: 1        F
 2: 00       Exponent of 10
 3: 12       Z Loc [ Valve12   ]

24:  End (P95)

;Valve 13 & 14 - Vacuum

25:  If time is (P92)
 1: 6        Minutes (Seconds --) into a
 2: 120      Interval (same units as above)
 3: 30       Then Do

26:  Z=F (P30)
 1: 1        F
 2: 00       Exponent of 10
```

```
 3: 13       Z Loc [ Valve13   ]

27:  Z=F (P30)
 1: 1        F
 2: 00       Exponent of 10
 3: 14       Z Loc [ Valve14   ]

28:  End (P95)

;Valve 15 & 16 - Vacuum

29:  If time is (P92)
 1: 7        Minutes (Seconds --) into a
 2: 120      Interval (same units as above)
 3: 30       Then Do

30:  Z=F (P30)
 1: 1        F
 2: 00       Exponent of 10
 3: 15       Z Loc [ Valve15   ]

31:  Z=F (P30)
 1: 1        F
 2: 00       Exponent of 10
 3: 16       Z Loc [ Valve16   ]

32:  End (P95)

;Valve 17 & 18 - Vacuum

33:  If time is (P92)
 1: 8        Minutes (Seconds --) into a
 2: 120      Interval (same units as above)
 3: 30       Then Do

34:  Z=F (P30)
 1: 1        F
 2: 00       Exponent of 10
 3: 17       Z Loc [ Valve17   ]

35:  Z=F (P30)
 1: 1        F
 2: 00       Exponent of 10
 3: 18       Z Loc [ Valve18   ]
```

```
36:  End (P95)

;Valve 19 & 20 - Vacuum

37:  If time is (P92)
 1: 9        Minutes (Seconds --) into a
 2: 120      Interval (same units as above)
 3: 30       Then Do

38:  Z=F (P30)
 1: 1        F
 2: 00       Exponent of 10
 3: 19       Z Loc [ Valve19   ]

39:  Z=F (P30)
 1: 1        F
 2: 00       Exponent of 10
 3: 20       Z Loc [ Valve20   ]

40:  End (P95)

;Valve 21 & 22 - Vacuum

41:  If time is (P92)
 1: 10       Minutes (Seconds --) into a
 2: 120      Interval (same units as above)
 3: 30       Then Do

42:  Z=F (P30)
 1: 1        F
 2: 00       Exponent of 10
 3: 21       Z Loc [ Valve21   ]

43:  Z=F (P30)
 1: 1        F
 2: 00       Exponent of 10
 3: 22       Z Loc [ Valve22   ]

44:  End (P95)

;Valve 23 & 24 - Vacuum

45:  If time is (P92)
```

```
 1: 11       Minutes (Seconds --) into a
 2: 120      Interval (same units as above)
 3: 30       Then Do

46:  Z=F (P30)
 1: 1        F
 2: 00       Exponent of 10
 3: 23       Z Loc [ Valve23   ]

47:  Z=F (P30)
 1: 1        F
 2: 00       Exponent of 10
 3: 24       Z Loc [ Valve24   ]

48:  End (P95)

;Valve 25 & 26 - Vacuum

49:  If time is (P92)
 1: 12       Minutes (Seconds --) into a
 2: 120      Interval (same units as above)
 3: 30       Then Do

50:  Z=F (P30)
 1: 1        F
 2: 00       Exponent of 10
 3: 25       Z Loc [ Valve25   ]

51:  Z=F (P30)
 1: 1        F
 2: 00       Exponent of 10
 3: 26       Z Loc [ Valve26   ]

52:  End (P95)

;Valve 27 & 28 - Vacuum

53:  If time is (P92)
 1: 13       Minutes (Seconds --) into a
 2: 120      Interval (same units as above)
 3: 30       Then Do

54:  Z=F (P30)
 1: 1        F
```

```
 2: 00       Exponent of 10
 3: 27       Z Loc [ Valve27   ]

55:  Z=F (P30)
 1: 1        F
 2: 00       Exponent of 10
 3: 28       Z Loc [ Valve28   ]

56:  End (P95)

;Valve 29 & 30 - Vacuum

57:  If time is (P92)
 1: 14       Minutes (Seconds --) into a
 2: 120      Interval (same units as above)
 3: 30       Then Do

58:  Z=F (P30)
 1: 1        F
 2: 00       Exponent of 10
 3: 29       Z Loc [ Valve29   ]

59:  Z=F (P30)
 1: 1        F
 2: 00       Exponent of 10
 3: 30       Z Loc [ Valve30   ]

60:  End (P95)

;Valve 31 & 32 - Vacuum

61:  If time is (P92)
 1: 15       Minutes (Seconds --) into a
 2: 120      Interval (same units as above)
 3: 30       Then Do

62:  Z=F (P30)
 1: 1        F
 2: 00       Exponent of 10
 3: 31       Z Loc [ Valve31   ]

63:  Z=F (P30)
 1: 1        F
 2: 00       Exponent of 10
```

```
 3: 32       Z Loc [ Valve32   ]

64:  End (P95)

;Open Valve 33 - Vacuum

65:  If time is (P92)
 1: 16       Minutes (Seconds --) into a
 2: 120      Interval (same units as above)
 3: 30       Then Do

66:  Do (P86)
 1: 44       Set Port 4 High

67:  End (P95)

;Open Valve 34 - Vacuum

68:  If time is (P92)
 1: 17       Minutes (Seconds --) into a
 2: 120      Interval (same units as above)
 3: 30       Then Do

69:  Do (P86)
 1: 45       Set Port 5 High

70:  End (P95)


;Open Valve 35 - Vacuum

71:  If time is (P92)
 1: 18       Minutes (Seconds --) into a
 2: 120      Interval (same units as above)
 3: 30       Then Do

72:  Do (P86)
 1: 46       Set Port 6 High

73:  End (P95)


;Switch to N2 Gas
```

```
74:  If time is (P92)
 1: 19       Minutes (Seconds --) into a
 2: 120      Interval (same units as above)
 3: 30       Then Do

75:  Do (P86)
 1: 47       Set Port 7 High

76:  End (P95)

;Flush each valve with N2 gas

;Valve 1 & 2 - Gas

77:  If time is (P92)
 1: 20       Minutes (Seconds --) into a
 2: 120      Interval (same units as above)
 3: 30       Then Do

78:  Z=F (P30)
 1: 1        F
 2: 00       Exponent of 10
 3: 1        Z Loc [ Valve1    ]

79:  Z=F (P30)
 1: 1        F
 2: 00       Exponent of 10
 3: 2        Z Loc [ Valve2    ]

80:  End (P95)

;Valve 3 & 4 - Gas

81:  If time is (P92)
 1: 21       Minutes (Seconds --) into a
 2: 120      Interval (same units as above)
 3: 30       Then Do

82:  Z=F (P30)
 1: 1        F
 2: 00       Exponent of 10
 3: 3        Z Loc [ Valve3    ]

83:  Z=F (P30)
```

```
 1: 1        F
 2: 00       Exponent of 10
 3: 4        Z Loc [ Valve4    ]

84:  End (P95)

;Valve 5 & 6 - Gas

85:  If time is (P92)
 1: 22       Minutes (Seconds --) into a
 2: 120      Interval (same units as above)
 3: 30       Then Do

86:  Z=F (P30)
 1: 1        F
 2: 00       Exponent of 10
 3: 5        Z Loc [ Valve5    ]

87:  Z=F (P30)
 1: 1        F
 2: 00       Exponent of 10
 3: 6        Z Loc [ Valve6    ]

88:  End (P95)

;Valve 7 & 8 - Gas

89:  If time is (P92)
 1: 23       Minutes (Seconds --) into a
 2: 120      Interval (same units as above)
 3: 30       Then Do

90:  Z=F (P30)
 1: 1        F
 2: 00       Exponent of 10
 3: 7        Z Loc [ Valve7    ]

91:  Z=F (P30)
 1: 1        F
 2: 00       Exponent of 10
 3: 8        Z Loc [ Valve8    ]

92:  End (P95)
```

```
;Valve 9 & 10 - Gas

93:  If time is (P92)
 1: 24       Minutes (Seconds --) into a
 2: 120      Interval (same units as above)
 3: 30       Then Do

94:  Z=F (P30)
 1: 1        F
 2: 00       Exponent of 10
 3: 9        Z Loc [ Valve9    ]

95:  Z=F (P30)
 1: 1        F
 2: 00       Exponent of 10
 3: 10       Z Loc [ Valve10   ]

96:  End (P95)

;Valve 11 & 12 - Gas

97:  If time is (P92)
 1: 25       Minutes (Seconds --) into a
 2: 120      Interval (same units as above)
 3: 30       Then Do

98:  Z=F (P30)
 1: 1        F
 2: 00       Exponent of 10
 3: 11       Z Loc [ Valve11   ]

99:  Z=F (P30)
 1: 1        F
 2: 00       Exponent of 10
 3: 12       Z Loc [ Valve12   ]

100:  End (P95)

;Valve 13 & 14 - Gas

101:  If time is (P92)
 1: 26       Minutes (Seconds --) into a
 2: 120      Interval (same units as above)
 3: 30       Then Do
```

```
102:  Z=F (P30)
 1: 1        F
 2: 00       Exponent of 10
 3: 13       Z Loc [ Valve13   ]

103:  Z=F (P30)
 1: 1        F
 2: 00       Exponent of 10
 3: 14       Z Loc [ Valve14   ]

104:  End (P95)

;Valve 15 & 16 - Gas

105:  If time is (P92)
 1: 27       Minutes (Seconds --) into a
 2: 120      Interval (same units as above)
 3: 30       Then Do

106:  Z=F (P30)
 1: 1        F
 2: 00       Exponent of 10
 3: 15       Z Loc [ Valve15   ]

107:  Z=F (P30)
 1: 1        F
 2: 00       Exponent of 10
 3: 16       Z Loc [ Valve16   ]

108:  End (P95)

;Valve 17 & 18 - Gas

109:  If time is (P92)
 1: 28       Minutes (Seconds --) into a
 2: 120      Interval (same units as above)
 3: 30       Then Do

110:  Z=F (P30)
 1: 1        F
 2: 00       Exponent of 10
 3: 17       Z Loc [ Valve17   ]
```

```
111:  Z=F (P30)
 1: 1        F
 2: 00       Exponent of 10
 3: 18       Z Loc [ Valve18   ]

112:  End (P95)

;Valve 19 & 20 - Gas

113:  If time is (P92)
 1: 29       Minutes (Seconds --) into a
 2: 120      Interval (same units as above)
 3: 30       Then Do

114:  Z=F (P30)
 1: 1        F
 2: 00       Exponent of 10
 3: 19       Z Loc [ Valve19   ]

115:  Z=F (P30)
 1: 1        F
 2: 00       Exponent of 10
 3: 20       Z Loc [ Valve20   ]

116:  End (P95)

;Valve 21 & 22 - Gas

117:  If time is (P92)
 1: 30       Minutes (Seconds --) into a
 2: 120      Interval (same units as above)
 3: 30       Then Do

118:  Z=F (P30)
 1: 1        F
 2: 00       Exponent of 10
 3: 21       Z Loc [ Valve21   ]

119:  Z=F (P30)
 1: 1        F
 2: 00       Exponent of 10
 3: 22       Z Loc [ Valve22   ]

120:  End (P95)
```

```
;Valve 23 & 24 - Gas

121:  If time is (P92)
 1: 31       Minutes (Seconds --) into a
 2: 120      Interval (same units as above)
 3: 30       Then Do

122:  Z=F (P30)
 1: 1        F
 2: 00       Exponent of 10
 3: 23       Z Loc [ Valve23   ]

123:  Z=F (P30)
 1: 1        F
 2: 00       Exponent of 10
 3: 24       Z Loc [ Valve24   ]

124:  End (P95)

;Valve 25 & 26 - Gas

125:  If time is (P92)
 1: 32       Minutes (Seconds --) into a
 2: 120      Interval (same units as above)
 3: 30       Then Do

126:  Z=F (P30)
 1: 1        F
 2: 00       Exponent of 10
 3: 25       Z Loc [ Valve25   ]

127:  Z=F (P30)
 1: 1        F
 2: 00       Exponent of 10
 3: 26       Z Loc [ Valve26   ]

128:  End (P95)

;Valve 27 & 28 - Gas

129:  If time is (P92)
 1: 33       Minutes (Seconds --) into a
 2: 120      Interval (same units as above)
```

```
 3: 30       Then Do

130:  Z=F (P30)
 1: 1        F
 2: 00       Exponent of 10
 3: 27       Z Loc [ Valve27   ]

131:  Z=F (P30)
 1: 1        F
 2: 00       Exponent of 10
 3: 28       Z Loc [ Valve28   ]

132:  End (P95)

;Valve 29 & 30 - Gas

133:  If time is (P92)
 1: 34       Minutes (Seconds --) into a
 2: 120      Interval (same units as above)
 3: 30       Then Do

134:  Z=F (P30)
 1: 1        F
 2: 00       Exponent of 10
 3: 29       Z Loc [ Valve29   ]

135:  Z=F (P30)
 1: 1        F
 2: 00       Exponent of 10
 3: 30       Z Loc [ Valve30   ]

136:  End (P95)

;Valve 31 & 32 - Gas

137:  If time is (P92)
 1: 35       Minutes (Seconds --) into a
 2: 120      Interval (same units as above)
 3: 30       Then Do

138:  Z=F (P30)
 1: 1        F
 2: 00       Exponent of 10
 3: 31       Z Loc [ Valve31   ]
```

```
139:  Z=F (P30)
 1: 1        F
 2: 00       Exponent of 10
 3: 32       Z Loc [ Valve32    ]

140:  End (P95)

;Open Valve 33 - Gas

141:  If time is (P92)
 1: 34       Minutes (Seconds --) into a
 2: 120      Interval (same units as above)
 3: 30       Then Do

142:  Do (P86)
 1: 44       Set Port 4 High


143:  Do (P86)
 1: 45       Set Port 5 High


144:  End (P95)

145:  If time is (P92)
 1: 35       Minutes (Seconds --) into a
 2: 120      Interval (same units as above)
 3: 30       Then Do

146:  Do (P86)
 1: 46       Set Port 6 High

147:  End (P95)

;Switch from N2 to vacuum

148:  If time is (P92)
 1: 36       Minutes (Seconds --) into a
 2: 120      Interval (same units as above)
 3: 30       Then Do

149:  Do (P86)
 1: 57       Set Port 7 Low
```

```
150:  End (P95)

;Shuts off all valves at 5 seconds after the minute

151:  If time is (P92)
 1: 5     -- Minutes (Seconds --) into a
 2: 60       Interval (same units as above)
 3: 30       Then Do

152:  Z=F (P30)
 1: 0.0      F
 2: 00       Exponent of 10
 3: 1        Z Loc [ Valve1    ]

153:  Z=F (P30)
 1: 0.0      F
 2: 00       Exponent of 10
 3: 2        Z Loc [ Valve2    ]

154:  Z=F (P30)
 1: 0.0      F
 2: 00       Exponent of 10
 3: 3        Z Loc [ Valve3    ]

155:  Z=F (P30)
 1: 0.0      F
 2: 00       Exponent of 10
 3: 4        Z Loc [ Valve4    ]

156:  Z=F (P30)
 1: 0.0      F
 2: 00       Exponent of 10
 3: 5        Z Loc [ Valve5    ]

157:  Z=F (P30)
 1: 0.0      F
 2: 00       Exponent of 10
 3: 6        Z Loc [ Valve6    ]

158:  Z=F (P30)
 1: 0.0      F
 2: 00       Exponent of 10
 3: 7        Z Loc [ Valve7    ]
```

159: Z=F (P30)
1: 0.0 F
2: 00 Exponent of 10
3: 8 Z Loc [Valve8]

160: Z=F (P30)
1: 0.0 F
2: 00 Exponent of 10
3: 9 Z Loc [Valve9]

161: Z=F (P30)
1: 0.0 F
2: 00 Exponent of 10
3: 10 Z Loc [Valve10]

162: Z=F (P30)
1: 0.0 F
2: 00 Exponent of 10
3: 11 Z Loc [Valve11]

163: Z=F (P30)
1: 0.0 F
2: 00 Exponent of 10
3: 12 Z Loc [Valve12]

164: Z=F (P30)
1: 0.0 F
2: 00 Exponent of 10
3: 13 Z Loc [Valve13]

165: Z=F (P30)
1: 0.0 F
2: 00 Exponent of 10
3: 14 Z Loc [Valve14]

166: Z=F (P30)
1: 0 F
2: 00 Exponent of 10
3: 15 Z Loc [Valve15]

167: Z=F (P30)
1: 0 F
2: 00 Exponent of 10

```
 3: 16      Z Loc [ Valve16   ]


168:  Z=F (P30)
 1: 0.0     F
 2: 00      Exponent of 10
 3: 17      Z Loc [ Valve17   ]

169:  Z=F (P30)
 1: 0.0     F
 2: 00      Exponent of 10
 3: 18      Z Loc [ Valve18   ]

170:  Z=F (P30)
 1: 0.0     F
 2: 00      Exponent of 10
 3: 19      Z Loc [ Valve19   ]

171:  Z=F (P30)
 1: 0.0     F
 2: 00      Exponent of 10
 3: 20      Z Loc [ Valve20   ]

172:  Z=F (P30)
 1: 0.0     F
 2: 00      Exponent of 10
 3: 21      Z Loc [ Valve21   ]

173:  Z=F (P30)
 1: 0.0     F
 2: 00      Exponent of 10
 3: 22      Z Loc [ Valve22   ]

174:  Z=F (P30)
 1: 0.0     F
 2: 00      Exponent of 10
 3: 23      Z Loc [ Valve23   ]

175:  Z=F (P30)
 1: 0.0     F
 2: 00      Exponent of 10
 3: 24      Z Loc [ Valve24   ]

176:  Z=F (P30)
```

```
 1: 0.0      F
 2: 00       Exponent of 10
 3: 25       Z Loc [ Valve25   ]

177:  Z=F (P30)
 1: 0.0      F
 2: 00       Exponent of 10
 3: 26       Z Loc [ Valve26   ]

178:  Z=F (P30)
 1: 0.0      F
 2: 00       Exponent of 10
 3: 27       Z Loc [ Valve27   ]

179:  Z=F (P30)
 1: 0.0      F
 2: 00       Exponent of 10
 3: 28       Z Loc [ Valve28   ]

180:  Z=F (P30)
 1: 0.0      F
 2: 00       Exponent of 10
 3: 29       Z Loc [ Valve29   ]

181:  Z=F (P30)
 1: 0.0      F
 2: 00       Exponent of 10
 3: 30       Z Loc [ Valve30   ]

182:  Z=F (P30)
 1: 0.0      F
 2: 00       Exponent of 10
 3: 31       Z Loc [ Valve31   ]

183:  Z=F (P30)
 1: 0.0      F
 2: 00       Exponent of 10
 3: 32       Z Loc [ Valve32   ]

;Turns off Port 4 after 5 seconds on the minute

184:  Do (P86)
 1: 54       Set Port 4 Low
```

185: Do (P86)
1: 55 Set Port 5 Low

186: Do (P86)
1: 56 Set Port 6 Low

187: End (P95)

188: SDM-CD16 / SDM-CD16AC (P104)
1: 2 Reps
2: 00 SDM Address
3: 1 Loc [Valve1]

189: Do (P86)
1: 10 Set Output Flag High (Flag 0)

*Table 2 Program
02: 0.0000 Execution Interval (seconds)

*Table 3 Subroutines

End Program

1	[Valve1]	RW--	1	3	----- ------ ---
2	[Valve2]	RW--	1	3	----- ------ ---
3	[Valve3]	RW--	1	3	----- ------ ---
4	[Valve4]	RW--	1	3	----- ------ ---
5	[Valve5]	RW--	1	3	----- ------ ---
6	[Valve6]	RW--	1	3	----- ------ ---
7	[Valve7]	RW--	1	3	----- ------ ---
8	[Valve8]	RW--	1	3	----- ------ ---
9	[Valve9]	RW--	1	3	----- ------ ---
10	[Valve10]	RW--	1	3	----- ------ ---
11	[Valve11]	RW--	1	3	----- ------ ---
12	[Valve12]	RW--	1	3	----- ------ ---
13	[Valve13]	RW--	1	3	----- ------ ---
14	[Valve14]	RW--	1	3	----- ------ ---
15	[Valve15]	RW--	1	3	----- ------ ---
16	[Valve16]	RW--	1	3	----- ------ ---
17	[Valve17]	-W--	0	3	----- ------ ---
18	[Valve18]	-W--	0	3	----- ------ ---

```
19    [ Valve19  ] -W--  0     3     ----- ------ ---
20    [ Valve20  ] -W--  0     3     ----- ------ ---
21    [ Valve21  ] -W--  0     3     ----- ------ ---
22    [ Valve22  ] -W--  0     3     ----- ------ ---
23    [ Valve23  ] -W--  0     3     ----- ------ ---
24    [ Valve24  ] -W--  0     3     ----- ------ ---
25    [ Valve25  ] -W--  0     3     ----- ------ ---
26    [ Valve26  ] -W--  0     3     ----- ------ ---
27    [ Valve27  ] -W--  0     3     ----- ------ ---
28    [ Valve28  ] -W--  0     3     ----- ------ ---
29    [ Valve29  ] -W--  0     3     ----- ------ ---
30    [ Valve30  ] -W--  0     3     ----- ------ ---
31    [ Valve31  ] -W--  0     3     ----- ------ ---
32    [ Valve32  ] -W--  0     3     ----- ------ ---
```

APPENDIX B

The following is a listing of all datasets used in each chapter and their location on a DVD disc. To request the accompanying DVD, please contact Dr. Jennifer McGuire or Dr. Binayak Mohanty.

Chapter 1 Data Locations

Description	**Location on DVD**
Photographs of Columns	\Chapter 1\Pictures\Columns
Photographs of Columns on Experimental Bench	\Chapter 1\Pictures\Columns on Experiment Bench
Photographs of Core Taken From the Column	\Chapter 1\Pictures\Core
Photographs of Most Probable Number Results	\Chapter 1\Pictures\Most Probable Number
Photographs of Drained Columns (Post Experiment)	\Chapter 1\Pictures\Drained Columns
High Resolutions of Thin Section Scans	\Chapter 1\Pictures\High Resolution Thin Section Scans
Electron Microprobe Images	\Chapter 1\Pictures\Electron Microprobe Images
Raw High Resolution Data	\Chapter 1\Pictures\High Resolution Raw Data
Layered Column Anion Data	\Chapter 1\Layered Column Data (S2)\Chemical Data\Anions\S2_anions_Spring2007.xlsx
Layered Alkalinity Data	\Chapter 1\Layered Column Data (S2)\Chemical Data\Alkalinity
Layered pH Data	\Chapter 1\Layered Column Data (S2)\Chemical Data\pH\pH_Fall2007.xlsx
Layered Voltammetric Data	\Chapter 1\Layered Column Data (S2)\Chemical Data\Hg Drop Data
Layered Cation and NH_4^+ Data	\Chapter 1\Layered Column Data (S2)\Chemical Data\Cations_NH4
Layered Eh Data	\Chapter 1\Layered Column Data (S2)\Chemical Data\Eh
Layered Pressure Data	\Chapter 1\Layered Column Data (S2)\Hydraulic Data\Tensiometer\All Pt Electrode_Tensiometer data_Fall2007.xlsx
Layered Water Content Data	\Chapter 1\Layered Column Data (S2)\Hydraulic Data\TDR
Homogenous Loam Column Anion Data	\Chapter 1\Homogenous Loam Column (SC)\Chemical

	Data\Anions\S2_anions_Spring2007.xlsx
Homogenous Loam Alkalinity Data	\Chapter 1\Homogenous Loam Column (SC)\Chemical Data\Alkalinity
Homogenous Loam pH Data	\Chapter 1\Homogenous Loam Column (SC)\Chemical Data\pH\pH_Fall2007.xlsx
Homogenous Loam Voltammetric Data	\Chapter 1\Homogenous Loam Column (SC)\Chemical Data\Hg Drop Data
Homogenous Loam Cation and NH_4^+ Data	\Chapter 1\Homogenous Loam Column (SC)\Chemical Data\Cations_NH4
Homogenous Loam Eh Data	\Chapter 1\Homogenous Loam Column (SC)\Chemical Data\Eh
Homogenous Loam Pressure Data	\Chapter 1\Homogenous Loam Column (SC)\Hydraulic Data\Tensiometer\All Pt Electrode_Tensiometer data_Fall2007.xlsx
Homogenous Loam Water Content Data	\Chapter 1\Homogenous Loam Column (SC)\Hydraulic Data\TDR
Homogenous Sand Column Anion Data	\Chapter 1\Homogenous Sand Column (SS)\Chemical Data\Anions\SS-anions.xlsx
Homogenous Sand Eh Data	\Chapter 1\Homogenous Sand Column (SS)\Chemical Data\Eh\SS_Pt_Electrode_Data.xlsx
Homogenous Sand Pressure Data	\Chapter 1\Homogenous Sand Column (SS)\Hydraulic Data\Tensiometer\
Homogenous Sand Water Content Data	\Chapter 1\Homogenous Sand Column (SS)\Hydraulic Data\TDR
Homogenous Sand Inverse Modeling Files	\Chapter 1\Models\Inverse Modeling Files\Sand Column Files
Homogenous Sand Inverse Modeling Files	\Chapter 1\Models\Inverse Modeling Files\Sand Column Files
Layered Column Inverse Modeling Files	\Chapter 1\Models\Inverse Modeling Files\Sand Column Files
Loam and Layered Column Inverse Modeling Results	\Chapter 1\Models\Inverse Modeling Results
Inverse Modeling Input Files	\Chapter 1\Models\Inverse Modeling Input Data
Microbiology Methods	\Chapter 1\Microbiology\Microbiology Methods
Most Probable Number (MPN) Results	\Chapter 1\Microbiology
MPN Software	\Chapter 1\Microbiology\Software for calculating MPN
Saturated Hydraulic Conductivity of Soils	\Chapter 1\Soil Properties\Saturated Hydraulic Conductivity\Sat Hydro Cond of sand and loam.xlsx

Soil Water Retention Curve of Soils	Chapter 1\Soil Properties\Unsaturated Hydraulic Conductivity\SWRC.xlsx
Fitting Models of SWRC	\Chapter 1\Soil Properties\Unsaturated Hydraulic Conductivity\SWRC Modeling to Fit Parameters
Plant Available Chemical Extraction Data	\Chapter 1\Soil Properties\Plant Available Chemical Extractions\Soil Analysis Reports.xlsx
Soil Iron Extraction Data	\Chapter 1\Soil Properties\Iron Extractions\
Carbon Nitrogen Sulfur Combustion Results	\Chapter 1\Soil Properties\Carbon Nitrogen Sulfur\CNS analysis of sand and loam.xlsx
Bottom Hole Spacings	\Chapter 1\Calculations\bottomcolumnholespacing.pptx
Decreased Hydraulic Conductivity Values	\Chapter 1\Calculations\Decreased hydraulic conductivity values.xlsx
Summary of Boundary Conditions for Homogenous Sand Column	\Chapter 1\Boundary Conditions\Hom Sand Boundary Conditions.docx
Summary of Boundary Conditions for Homogenous Loam and Layered Columns	\Chapter 1\Boundary Conditions\Loam and Layered boundary condtions.docx
Homogenous Loam and Layered Experimental Overview	\Chapter 1\Loam and Layered Experimental Overview.docx
Hom Sand Column Experiment Overview	\Chapter 1\Hom Sand Column Experiment Overview.doc
List of Probes Used in Experiments	\Chapter 1\Resources\Probes Used in Experiment\Probes Use in Layered Columns.xlsx
Figure of Locations of Probes Used in Experiments	\Chapter 1\Resources\Probes Used in Experiment\Experiment_probe_legend.ppt
Datalogger Programs Used During Experiment	\Chapter 1\Analytical Methods\CS Datalogger
Mercury Drop Electrode Methods	\Chapter 1\Analytical Methods\Hg Drop Electrode
Final Plot Files – X-axis “Date” (Dplot format)	\Chapter 1\Raw Figures\Dplot Files
Excel Plot Files (Files That Preceded Dplot Files)	\Chapter 1\Raw Figures\Excel Graphs
Powerpoint Figures (Drawings)	\Chapter 1\Raw Figures\Powerpoint Figures

Chapter 2 Appendix

Description	**Location on DVD**
Photographs of Columns	\Chapter 2\Pictures\Columns
Photographs of Columns on	\Chapter 2\Pictures\Columns on Experiment

Experimental Bench	Bench
Photographs of Core Taken From the Column	\Chapter 2\Pictures\Core
Photographs of Most Probable Number Results	\Chapter 2\Pictures\Most Probable Number
Photographs of Drained Columns (Post Experiment)	\Chapter 2\Pictures\Drained Columns
High Resolutions of Thin Section Scans	\Chapter 2\Pictures\High Resolution Thin Section Scans
Electron Microprobe Images	\Chapter 2\Pictures\Electron Microprobe Images
Raw High Resolution Data	\Chapter 2\Pictures\High Resolution Raw Data
Layered Column Anion Data	\Chapter 2\Layered Column Data (S2)\Chemical Data\Anions\S2_anions_Spring2007.xlsx
Layered Alkalinity Data	\Chapter 2\Layered Column Data (S2)\Chemical Data\Alkalinity
Layered pH Data	\Chapter 2\Layered Column Data (S2)\Chemical Data\pH\pH_Fall2007.xlsx
Layered Voltammetric Data	\Chapter 2\Layered Column Data (S2)\Chemical Data\Hg Drop Data
Layered Cation and NH_4^+ Data	\Chapter 2\Layered Column Data (S2)\Chemical Data\Cations_NH4
Layered Eh Data	\Chapter 2\Layered Column Data (S2)\Chemical Data\Eh
Layered Pressure Data	\Chapter 2\Layered Column Data (S2)\Hydraulic Data\Tensiometer\All Pt Electrode_Tensiometer data_Fall2007.xlsx
Layered Water Content Data	\Chapter 2\Layered Column Data (S2)\Hydraulic Data\TDR
Homogenous Loam Column Anion Data	\Chapter 2\Homogenous Loam Column (SC)\Chemical Data\Anions\S2_anions_Spring2007.xlsx
Homogenous Loam Alkalinity Data	\Chapter 2\Homogenous Loam Column (SC)\Chemical Data\Alkalinity
Homogenous Loam pH Data	\Chapter 2\Homogenous Loam Column (SC)\Chemical Data\pH\pH_Fall2007.xlsx
Homogenous Loam Voltammetric Data	\Chapter 2\Homogenous Loam Column (SC)\Chemical Data\Hg Drop Data
Homogenous Loam Cation and NH_4^+ Data	\Chapter 2\Homogenous Loam Column (SC)\Chemical Data\Cations_NH4
Homogenous Loam Eh Data	\Chapter 2\Homogenous Loam Column

	(SC)\Chemical Data\Eh
Homogenous Loam Pressure Data	\Chapter 2\Homogenous Loam Column (SC)\Hydraulic Data\Tensiometer\All Pt Electrode_Tensiometer data_Fall2007.xlsx
Homogenous Loam Water Content Data	\Chapter 2\Homogenous Loam Column (SC)\Hydraulic Data\TDR
Homogenous Sand Column Anion Data	\Chapter 2\Homogenous Sand Column (SS)\Chemical Data\Anions\SS-anions.xlsx
Homogenous Sand Eh Data	\Chapter 2\Homogenous Sand Column (SS)\Chemical Data\Eh\SS_Pt_Electrode_Data.xlsx
Homogenous Sand Pressure Data	\Chapter 2\Homogenous Sand Column (SS)\Hydraulic Data\Tensiometer\
Homogenous Sand Water Content Data	\Chapter 2\Homogenous Sand Column (SS)\Hydraulic Data\TDR
Saturated Hydraulic Conductivity of Soils	\Chapter 2\Soil Properties\Saturated Hydraulic Conductivity\Sat Hydro Cond of sand and loam.xlsx
Soil Water Retention Curve of Soils	Chapter 2\Soil Properties\Unsaturated Hydraulic Conductivity\SWRC.xlsx
Fitting Models of SWRC	\Chapter 2\Soil Properties\Unsaturated Hydraulic Conductivity\SWRC Modeling to Fit Parameters
Plant Available Chemical Extraction Data	\Chapter 2\Soil Properties\Plant Available Chemical Extractions\Soil Analysis Reports.xlsx
Soil Iron Extraction Data	\Chapter 2\Soil Properties\Iron Extractions\
Carbon Nitrogen Sulfur Combustion Results	\Chapter 2\Soil Properties\Carbon Nitrogen Sulfur\CNS analysis of sand and loam.xlsx
Bottom Hole Spacings	\Chapter 2\Calculations\bottomcolumnholespacing.pptx
Decreased Hydraulic Conductivity Values	\Chapter 2\Calculations\Decreased hydraulic conductivity values.xlsx
Summary of Boundary Conditions for Homogenous Sand Column	\Chapter 2\Boundary Conditions\Hom Sand Boundary Conditions.docx
Summary of Boundary Conditions for Homogenous Loam and Layered Columns	\Chapter 2\Boundary Conditions\Loam and Layered boundary condtions.docx
Homogenous Loam and Layered Experimental Overview	\Chapter 2\Loam and Layered Experimental Overview.docx
Hom Sand Column Experiment Overview	\Chapter 2\Hom Sand Column Experiment Overview.doc
List of Probes Used in Experiments	\Chapter 2\Resources\Probes Used in

	Experiment\Probes Use in Layered Columns.xlsx
Figure of Locations of Probes Used in Experiments	\Chapter 2\Resources\Probes Used in Experiment\Experiment_probe_legend.ppt
Datalogger Programs Used During Experiment	\Chapter 2\Analytical Methods\CS Datalogger
Mercury Drop Electrode Methods	\Chapter 2\Analytical Methods\Hg Drop Electrode
Final Plot Files – X-axis "Date" (Dplot format)	\Chapter 2\Raw Figures\Dplot Files
Excel Plot Files (Files That Preceded Dplot Files)	\Chapter 2\Raw Figures\Excel Graphs
Powerpoint Figures (Drawings)	\Chapter 2\Raw Figures\Powerpoint Figures

Chapter 3 Appendix

Description	**Location on DVD**
Photographs of Columns	\Chapter 3\Pictures
Anion Data	\Chapter 3\Lens Column Data\Chemical Data\Anions\Anion Data Compiled and Sorted by Sampling Round.xlsm
Alkalinity and pH Data	\Chapter 3\Lens Column Data\Chemical Data\Alkalinity\Alkalinity and pH sorted by Sampling Round.xlsx
Voltammetric Data	\Chapter 3\Lens Column Data\Chemical Data\Voltammetric\Voltammetric Data Sorted by Sampling Round.xlsx
NH4+ Data	\Chapter 3\Lens Column Data\Chemical Data\Ammonium\NH4 Sorted by Sampling Round.xslx
Eh Data	\Chapter 3\Lens Column Data\Chemical Data\Eh
Pressure Data	\Chapter 3\Lens Column Data\Hydraulic Data\Tensiometer\
Water Content Data	\Chapter 3\Lens Column Data\Hydraulic Data\TDR\TDR Data All.xlsx
Saturated Hydraulic Conductivity of Soils	\Chapter 3\Soil Properties\Saturated Hydraulic Conductivity\Saturated Hydraulic Conductivity of Soils.xlsx
Soil Water Retention Curve of Soils	Chapter 3\Soil Properties\Unsaturated Hydraulic Conductivity\SWRC.xlsx
Plant Available Chemical Extraction Data	\Chapter 3\Soil Properties\Plant Available Chemical Extractions\Chemical Extractions.xlsx

Soil Iron Extraction Data	\Chapter 3\Soil Properties\Iron Extractions\Iron Extraction Results.ppt
Carbon Nitrogen Sulfur Combustion Results	\Chapter 3\Soil Properties\Carbon Nitrogen Sulfur\CNS Combustion Results.xlsx
Flow Velocity HYDRUS 2D Model	\Chapter 3\Models\Flow Velocity Forward Model\Forward Velocity.h3d
Sulfide Statistical Wilcoxon Test (JMP Format)	\Chapter 3\Statistical Analysis\Non Param Tests – JMP\wilcoxon_SULFIDE.jrp
Lens Column (LC) PCA Analysis	\Chapter 3\Statistical Analysis\PCA - JMP
Lens Column (LC) PCA Analysis Results	\Chapter 3\Statistical Analysis\PCA - JMP\Reports\
Killed-Control Lens Column (KLC) PCA Anaylsis	\Chapter 3\Statistical Analysis\PCA - JMP\Data Tables
Killed-Control Lens Column (KLC) PCA Anaylsis Results	\Chapter 3\Statistical Analysis\PCA - JMP\Reports
Summary of Boundary Conditions	\Chapter 3\Boundary Conditions\Experiment Table.docx
List of Probes Used in Experiments	\Chapter 3\Resources\Probes Used in Experiment\Probes Use in Layered Columns.xlsx
Figure of Locations of Probes Used in Experiments	\Chapter 3\Resources\Probes Used in Experiment\Experiment_probe_legend.ppt
Time between Samplings	\Chapter 3\Resources\Time Between Sampling\gasbubble_lysimeter sampling times.xlsx
Datalogger Programs Used During Experiment	\Chapter 3\Analytical Methods\CS Datalogger
Mercury Drop Electrode Methods	\Chapter 3\Analytical Methods\Hg Drop Electrode
Final Plot Files – X-axis “Day of Experiment” (Dplot format)	\Chapter 3\Raw Figures\Dplot Day of Experiment Figures
Final Plot Files – X-axis “Date” (Dplot format)	\Chapter 3\Raw Figures\Dplot Files
Excel Plot Files (Files That Preceded Dplot Files)	\Chapter 3\Raw Figures\Excel Graphs
Powerpoint Figures (Drawings)	\Chapter 3\Raw Figures\Powerpoint Figures

Chapter 4 Appendix

Description	**Location on DVD**
Photographs of Columns	\Chapter 4\Pictures
Anion Data	\Chapter 4\Lens Column Data\Chemical Data\Anions\Anion Data Compiled and Sorted by Sampling Round.xlsm

Alkalinity and pH Data	\Chapter 4\Lens Column Data\Chemical Data\Alkalinity\Alkalinity and pH sorted by Sampling Round.xlsx
Voltammetric Data	\Chapter 4\Lens Column Data\Chemical Data\Voltammetric\Voltammetric Data Sorted by Sampling Round.xlsx
NH_4^+ Data	\Chapter 4\Lens Column Data\Chemical Data\Ammonium\NH4 Sorted by Sampling Round.xslx
Eh Data	\Chapter 4\Lens Column Data\Chemical Data\Eh
Pressure Data	\Chapter 4\Lens Column Data\Hydraulic Data\Tensiometer\Tensiometer Data All.xlsx
Water Content Data	\Chapter 4\Lens Column Data\Hydraulic Data\TDR\TDR Data All.xlsx
Saturated Hydraulic Conductivity of Soils	\Chapter 4\Soil Properties\Saturated Hydraulic Conductivity\Saturated Hydraulic Conductivity of Soils.xlsx
Soil Water Retention Curve of Soils	Chapter 4\Soil Properties\Unsaturated Hydraulic Conductivity\SWRC.xlsx
Plant Available Chemical Extraction Data	\Chapter 4\Soil Properties\Plant Available Chemical Extractions\Chemical Extractions.xlsx
Soil Iron Extraction Data	\Chapter 4\Soil Properties\Iron Extractions\Iron Extraction Results.ppt
Carbon Nitrogen Sulfur Combustion Results	\Chapter 4\Soil Properties\Carbon Nitrogen Sulfur\CNS Combustion Results.xlsx
Summary of Boundary Conditions	\Chapter 4\Boundary Conditions\Experiment Table.docx
List of Probes Used in Experiments	\Chapter 4\Resources\Probes Used in Experiment\Probes Use in Layered Columns.xlsx
Figure of Locations of Probes Used in Experiments	\Chapter 4\Resources\Probes Used in Experiment\Experiment_probe_legend.ppt
Time between Samplings	\Chapter 4\Resources\Time Between Sampling\gasbubble_lysimeter sampling times.xlsx
Datalogger Programs Used During Experiment	\Chapter 4\Analytical Methods\CS Datalogger
Mercury Drop Electrode Methods	\Chapter 4\Analytical Methods\Hg Drop Electrode
Final Plot Files – X-axis “Day of Experiment” (Dplot format)	\Chapter 4\Raw Figures\Dplot Day of Experiment Figures

Final Plot Files – X-axis "Date" (Dplot format)	\Chapter 4\Raw Figures\Dplot Files
Excel Plot Files (Files That Preceded Dplot Files)	\Chapter 4\Raw Figures\Excel Graphs
GIS Data Graphing Files	\Chapter 4\Raw Figures\ArcGIS Files
Powerpoint Figures (Drawings)	\Chapter 4\Raw Figures\Powerpoint Figures

VITA

Name:	David Joseph Hansen
Address:	ConocoPhillips 600 N. Dairy Ashford, Houston, TX 77084
Email Address:	davidjoshansen@gmail.com
Education:	B.S., Geology, Brigham Young University - Idaho, 2004
Honors and Awards:	Aggie Honor Council Member (2006 - 2009) ConocoPhilips SPIRIT Scholar (2006 - 2009) D Port Smythe Scholarship (2008) East Texas Communties Foundation Scholarship (2008) American Geophysical Union - Best Student Paper Award (2007) Noble Energy Scholarship (2007) Recognition for role in NST_{LLC} Outstanding Performance Award (2007) Association of Former Students Scholarship (2007) CR "Smilo" Mallison Scholarship (2006) SIPES Foundation Scholarship (2006) TWRI Mills Scholarship (2005)